Universidad de Valladolid

Escuela de Doctorado Universidad de Valladolid

PROGRAMA DE DOCTORADO EN INGENIERÍA INDUSTRIAL

TESIS DOCTORAL:

EXPLOSIVE VAPOR DETECTION TECHNOLOGY IN THE ATMOSPHERE AT CONCENTRATIONS OF PARTS PER QUADRILLION AND BELOW

Presentada por Mario Amo González para optar al grado de
Doctor por la Universidad de Valladolid

Dirigida por:
Juan Fernández de la Mora

ABSTRACT

This doctoral thesis is aimed at the development of new analytical instrumentation for the detection of trace vapor species in the atmosphere at concentrations of parts per quadrillion (ppq = $1x10^{-15}$ atmospheres of partial pressure) and below. The work is structured around three overall objectives:

- To optimize the analytical performance of the planar differential mobility analyzer (DMA) and the secondary electrospray ionization source (SESI), so as to bring their performance closer to the ideal one.
- To develop an explosive vapor detector, based on DMA-triple quadrupole mass spectrometry technology (DMA-MS/MS), capable of detecting explosive vapors at sub-ppq concentrations.
- To develop an explosive vapor detector based on analyzers and detectors far simpler and more economical than mass spectrometry, yet still capable of detecting explosive vapors at concentrations of a few ppq.

The SESI ionization source was redesigned to achieve successful desolvation of the electrospray cloud, preventing droplets and neutral vapors from reaching the DMA. This improvement yielded ideal tail-free mobility peaks with a tailing ratio (*TR*) much larger than previously observed (100-1000 times better), reaching the theoretical limit ~10^5 (Gaussian peaks). Furthermore, the ionization efficiency was also improved, delivering an unprecedented value for TNT of one ion out of 140 neutral molecules. The planar DMA was adapted to minimize vapor emissions which, combined with the desolvation in the SESI ion source, allowed eliminating a previously existing mobility peak tailing problem phenomenon. The laminarization in the DMA was also improved, allowing to achieve resolutions of 110, practically matching the theoretical limit of the planar DMA at the operating conditions.

The improvements in the DMA and the SESI ion source significantly enhanced the analytical performance of the planar DMA, enabling the development of an explosive vapor detector, based on DMA-MS/MS technology with unprecedented sensitivity, capable of detecting explosive vapors at sub-ppq concentrations. The method of detection was patented and, through the analysis of hundreds of blank and loaded air samples, has demonstrated the capacity to detect explosive vapors at unmatched concentrations of only 0.01 ppq for RDX and 0.1 ppq for TNT.

Despite the unique performance of the DMA-MS/MS technology, the use of mass spectrometry involves a higher cost (also volume and complexity) of the analyzer, limiting the number of potential customers. This fact motivated the development of a radically new technology, called tandem differential mobility analysis with ambient pressure ion fragmentation in between (henceforth DMA-F-DMA), which emulates the operation principle of the triple quadrupole mass spectrometer, at a substantially reduced level of complexity and price thanks to the operation at ambient pressure instead of under vacuum conditions. The traditional approach of ion mobility spectrometry has been used in airport security for several decades; however, its limited selectivity has limited its operativity, precluding vapor detection of most explosives. The radically new method presented here has the capacity to detect explosive vapors at concentrations of a few ppq. A first DMA-F-DMA prototype was used as a proof of concept to demonstrate the fragmentation feasibility of five explosives (RDX, PETN, NG, EGDN and TNT) at ambient pressure by thermal means exclusively. A second prototype was built, including a new fragmenter with better fragmentation ability and combining multicapillary gas chromatography in series with the DMA-F-DMA technology, which improved selectivity. The analyzer background was evaluated for the five explosives studied, using air samples of 500 L volume. An atmospheric background of only 5 ppq (2.5 pg in 500 L) was found for TNT, being somewhat higher for the rest of the explosives studied. The GC-DMA-F-DMA technology was also tested with commercial explosives hidden in cargo pallets at the Spain's National Institute of Aerospace Technology (INTA), achieving successful detection of four (EGDN, NG, TNT and PETN) out of the five explosives. The DMA-F-DMA development has been funded by the United Kingdom Government by three consecutive projects (EffeX, EffeX II and HITEX) and also by the Horizon 2020 Research and Innovation Programme (COSMIC), highlighting the potential of this technology. The tandem mobility analysis with intermediate ion fragmentation at ambient pressure has

recently been demonstrated (results published in 2019) by only one other research group worldwide, illustrating the degree of novelty of this technology.

RESUMEN

Esta tesis doctoral tiene como propósito el desarrollo de nueva instrumentación analítica para la detección de trazas de vapor en la atmósfera en concentraciones de partes por cuatrillón americano e incluso inferiores (ppq = $1x10^{-15}$ atmósferas de presión de vapor). El trabajo se ha estructurado en base a tres objetivos globales:

- Optimización del rendimiento analítico del analizador diferencial de movilidad (DMA) y de la fuente de ionización secundaria por electrospray (SESI), de manera que sus rendimientos se aproximen al ideal.
- Desarrollo de un detector de vapores de explosivo basado en la combinación del DMA y de la espectrometría de masas de triple cuadrupolo (DMA-MS/MS), con capacidad para detectar vapores de explosivo en concentraciones inferiores a 1 ppq.
- Desarrollo de un detector de vapores de explosivo basado en analizadores y detectores más simples y económicos que los usados en espectrometría de masas, con capacidad para detectar vapores de explosivo en concentraciones de unas pocas ppq.

Se llevó a cabo un rediseño de la fuente de ionización SESI que permitió lograr una desolvatación eficiente de la pluma de electrospray, evitando la penetración de gotas y vapores neutros en el DMA, y reduciendo las colas de movilidad en un factor comprendido entre 100 y 1.000 con respecto a la tecnología previa. Además, también se mejoró la eficiencia de ionización, alcanzando el valor sin precedentes de un ión de TNT por cada 140 moléculas neutras. Las mejoras en la desolvatación de la fuente de ionización SESI, en combinación con las adaptaciones del DMA plano para minimizar su emisión de vapores, permitieron la eliminación del problema de colas de movilidad previamente existente en el DMA. La laminarización en el DMA también se mejoró, permitiéndole alcanzar resoluciones de 110, un valor prácticamente coincidente con el límite teórico en las condiciones de operación.

Las mejoras llevadas a cabo en el DMA y en su fuente de ionización SESI mejoraron de manera muy significativa su rendimiento analítico, haciendo posible el desarrollo de un detector de vapores de explosivo basado en la tecnología DMA-MS/MS con una sensibilidad sin precedentes. A través del análisis de cientos de muestras atmosféricas, con y sin carga de vapores de explosivo, el analizador demostró su capacidad para detectar dichos vapores en concentraciones de 0,01 ppq para el explosivo RDX y de 0,1 ppq para el TNT. El método de detección fue patentado.

A pesar del excepcional rendimiento de la tecnología DMA-MS/MS, el uso de la espectrometría de masas supone un incremento significativo del coste final del analizador (también de su volumen y complejidad), limitando el número de potenciales clientes. Este hecho motivó el desarrollo de una tecnología radicalmente nueva, denominada análisis diferencial de movilidad en tándem con fragmentación intermedia de iones a presión ambiente (en adelante DMA-F-DMA), que emula el principio de operación del espectrómetro de masas de triple cuadrupolo, con un nivel de complejidad y precio reducido, gracias a la operación en condiciones de presión ambiente en vez de vacío. El planteamiento tradicional de la espectrometría de movilidad iónica, se viene utilizando en la seguridad de los aeropuertos desde hace varias décadas; sin embargo su escasa selectividad ha limitado su funcionalidad, impidiendo la detección de vapores de la mayor parte de explosivos. El nuevo método aquí presentado permite, sin embargo, detectar vapores de explosivo en concentraciones de unas pocas ppq. El primer prototipo DMA-F-DMA permitió demostrar la factibilidad de la fragmentación de cinco explosivos (RDX, PETN, NG, EGDN y TNT) a través del uso de elevadas temperaturas en condiciones de presión ambiente. Posteriormente se fabricó un segundo prototipo con mayor capacidad de fragmentación, que combinó eficazmente la tecnología DMA-F-DMA con la cromatografía de gases multicapilar, lo que contribuyó a mejorar su selectividad. A través de muestras atmosféricas de 500 L de volumen se evaluó el fondo del analizador para cinco canales de explosivo. Para el TNT se registró un fondo de tan solo 5 ppq (2,5 pg en 500 L), siendo algo mayor para el resto de los explosivos estudiados. La tecnología GC-DMA-F-DMA fue

posteriormente evaluada en el INTA (Instituto Nacional de Técnica Aeroespacial) utilizando explosivos comerciales ocultos en palés de carga, consiguiendo detectar con éxito cuatro (EGDN, NG, TNT y PETN) de los cinco explosivos ensayados. El desarrollo del DMA-F-DMA ha sido financiado por el Gobierno del Reino Unido a través de tres proyectos consecutivos (EffeX, EffeX II and HITEX) y a través del Programa de Innovación e Investigación Horizonte 2020 (COSMIC), demostrando el potencial de esta tecnología. El análisis de movilidad en tándem con fragmentación intermedia de iones ha sido recientemente demostrado (resultados publicados en 2019), por tan sólo otro grupo de investigación a escala global, ilustrando el grado de novedad de esta tecnología.

ACKNOWLEDGEMENT

I would first like to express my sincere gratitude to my Dissertation Advisor Professor Juan Fernández de la Mora of the School of Engineering & Applied Science at Yale University, whose expertise and guidance were invaluable during all the time of research and writing of this thesis.

I am also grateful to my colleagues at SEADM laboratories for their wonderful collaboration and support.

I would also like to extend thanks to SEADM and the funding agencies which supported the research projects related to this thesis.

I would like to thank my tutor, Gregorio Antolín Professor of the School of Industrial Engineering at Valladolid University, for his valuable guidance in this thesis process.

I am indebted to my colleague Guillermo Vidal, who encouraged me to start with the doctoral studies.

I would also thank Gonzalo Fernández de la Mora and Lloyd Harrison for their wise advice and their complete willingness to help.

Last but not the least, I would like to thank my family for providing me with unfailing support throughout my years of researching. I wish to thank my parents, my loving and supporting wife, Cristina, and my three wonderful children, Lucas, Pablo and María.

INDEX

INTRODUCTION

Ion mobility spectrometry (IMS) is a widely used analytical technique employed to separate gas-phase ions based on their mobilities in a carrier buffer gas under the influence of an electric field.

Several analyzers have been developed in the last two decades within the ion mobility spectrometry family, making it possible to distinguish between narrow-band mobility-filters, which separate ions in space and the rest of the analyzers that usually separate ions in time. Within the second family, the most widespread technologies are the drift-tube IMS (DT-IMS),[1,2,3] high-resolution ion-cyclotron-mobility spectrometry (HR-ICMS),[4] and trapped-ion-mobility spectrometry (TIMS),[5] offering a pulsed stream of ions. In contrast, the narrow-band mobility-filters offer a continuous flux of selected mobility ions in a similar way as the triple quadrupole extracts a single ion mass-to-charge ratio out of a complex mix for subsequent study or manipulation. Examples of narrow-band mobility-filters include the field asymmetric ion-mobility spectrometry (FAIMS, also referred to as differential-mobility spectrometry, DMS),[6,7,8,9] transversal-modulation IMS (TMIMS),[10,11] the periodic-focusing differential-mobility analyzer (PFDMA),[12] overtone mobility spectrometry (OMS),[13] and the differential mobility analyzer (DMA).[14,15,16]

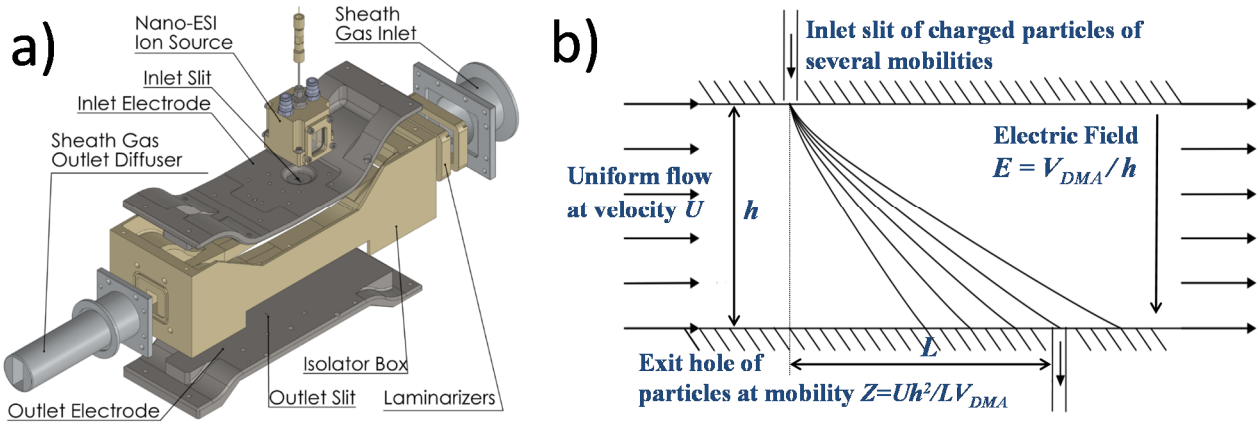

Figure 1. a) Planar differential mobility analyzer (DMA) architecture. B) DMA principle of operation (after Rus et al.).[16]

The DMA operation principle, shown in Figure 1, combines a laminar flow of sheath gas with an orthogonal electric field between two parallel plates, such that ions of different mobilities penetrating through a slit in the inlet plate open up in a fan as they drift toward the outlet plate. Accordingly, only a small range of mobilities is sampled through the slit in the outlet plate. The selected mobility ions can be either detected and quantified by a Faraday cup electrometer[17] or directed to a second analyzer for tandem analysis, which offers extended analytical selectivity thanks to the separation based on unrelated properties of the compounds (also known as orthogonal separation). Among the tandem analysis options, the most popular is the combination of the DMA with a mass spectrometer (Chapters 3 and 4), allowing simultaneous classification of ions based on their ion mobility and mass-to-charge ratio (*m/z*). Another option, also addressed in this thesis, is the tandem DMA configuration (Chapters 5 and 6), generally known as tandem IMS, which enables to benefit from the chemical orthogonality[18] provided by selective ion transformations taking place between the mobility analysis regions:

mobility-selected ions from a first DMA are modified in an intermediate reaction region and the resultant products are analyzed again in a second DMA.

The planar DMA is particularly suitable to be coupled in the interface region of an atmospheric pressure mass spectrometer, as noted by Rus and colleagues,[16] due to the following characteristics:

1. Atmospheric pressure operation in the mobility classification region, which minimizes ion fragmentation
2. High transmission > 50 %
3. High resolving power > 50
4. Narrow-band mobility filter capacity and extremely low ion residence time, lower than 1 ms, hence not generating delays in the mass spectrometers acquisition methods (either multiple ion monitoring or multiple reaction monitoring).

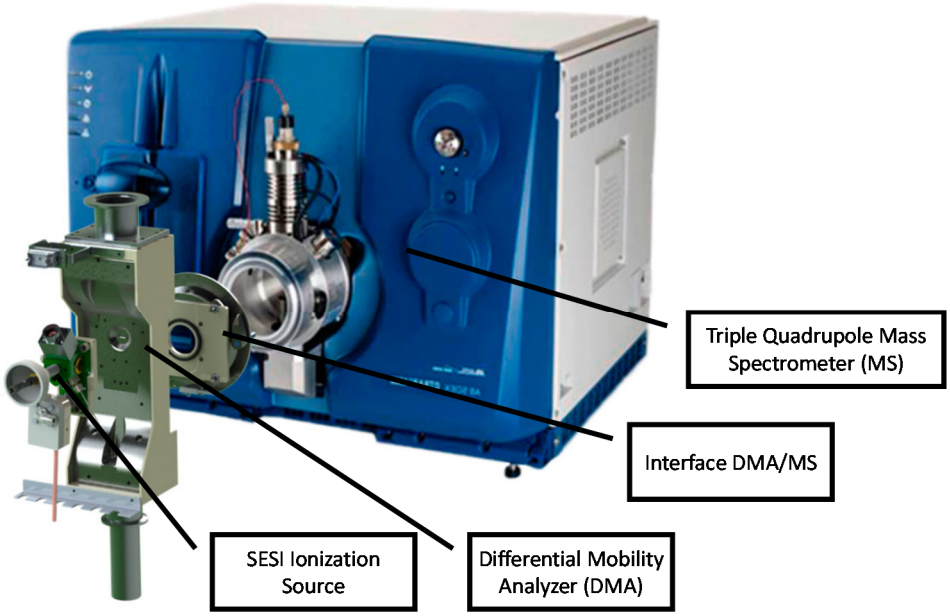

Figure 2. Coupling of a SESI ionization source + a Differential Mobility Analyzer (DMA) + a Triple Quad Mass Spectrometer (MS).

The combination DMA-MS/MS (Figure 2) has demonstrated excellent performance in a variety of analytical and basic applications.[19,20,21,22] From the analytical perspective, the DMA can be viewed as a chromatography of sorts, removing 98%–99% of the ion mobilities in a complex mix[23] while being able to shift from one mobility to another in a few milliseconds. The background suppression capability of the DMA allows to significantly increase the sensitivity attainable by modern mass spectrometers in the analysis of complex samples.

Figure 3, extracted from Chapter 2, shows a DMA-MS analysis of a complex sample consisting of an extra virgin olive oil sample, 1,000-fold diluted in the electrospray liquid. It properly illustrates the additional information provided by a high-resolution DMA to a mass spectrometry analysis, enabling the quantification of many isobar/isomer species completely resolved in mobility.

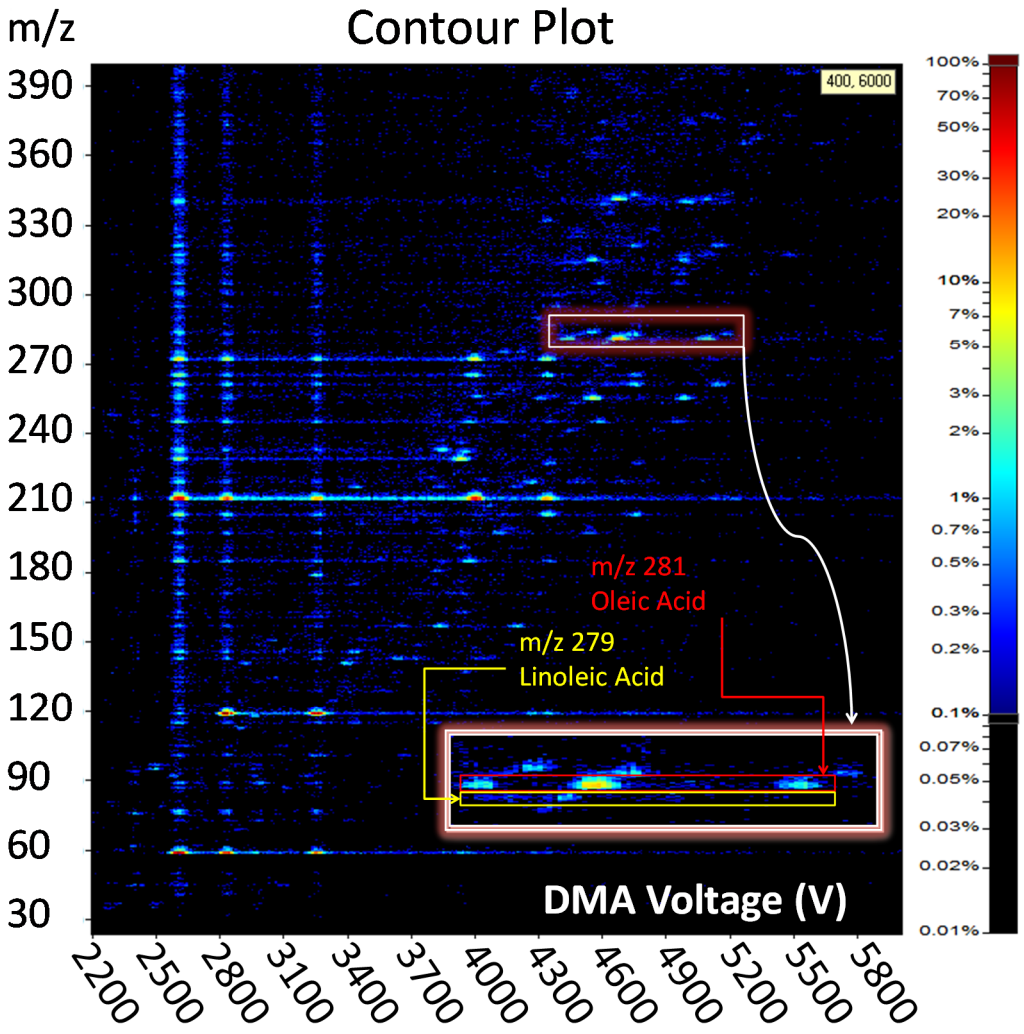

Figure 3. Electrospray DMA-MS contour plot of the extra virgin olive oil solution, including a magnified version in the mass region for oleic and linoleic acids. Graph extracted from the scientific article presented in Chapter 2.

The aforementioned DMA's unique characteristics make it also suitable to be used in tandem DMA configuration. Especially critical is the feature of the low ion residence time within the DMA, decreasing ion transformations within the mobility analysis regions, which would produce tails in the tandem mobility spectra and ultimately a loss of analytical performance.

To a great extent, this thesis revolves around the improvement of the analysis performance of the planar DMA and its application to explosive vapor detection. IMS has been the most widespread technology for explosive trace detection since the 1970s. Explosive trace detection based on IMS has been the main technology used at security checkpoints in airports worldwide from the 1990s to the present day.[24] However, given the extremely low vapor pressures of military explosives and the limited selectivity of standalone drift tube IMS analyzers, the available vapor concentration for most of the explosives was well below the sensitivity of IMS explosive trace detectors, restricting their detection capability to solid particles rather than vapors.[25,26]

In 2009 Martínez-Lozano and colleagues laid the groundwork for explosive detection based entirely on vapors, at concentrations below parts per trillion (ppt), using a secondary electrospray (SESI)

charger and several mass spectrometers (MS).[27] The key to that achievement was the SESI ionization of vapors, discovered some years before by Fenn and colleagues, who noted that an electrospray cloud had the singular ability to produce ions from ambient vapors present in its surroundings at very low concentrations.[28,29]

Fernandez de la Mora studied the ionization probability of a standard SESI, similar to the one used by Martínez-Lozano and colleagues,[27,30] in which the ionized vapor molecules are drawn to the analyzer by means of a gas current. He found that given enough time of exposure of the vapors to the spray, an equilibrium condition was reached where the rate of ion production was balanced by the rate of dilution by space charge. In this limit, the estimated equilibrium ratio between ionized and neutral vapors for a unipolar charger is of the order of $n_i/n_v \sim 10^{-4}$, being n_i the concentration of ionized vapor molecules and n_v the concentration of neutral vapor molecules, and n_i/n_v the ionization probability (p_i).[31] In 2012, Vidal-de-Miguel and colleagues refined the design of the standard SESI improving p_i by reducing the sample flow and transmitting the generated sample ions to the analyzer by electric fields.[32] The reduction of the sample flow increases the exposure time of the sample molecules to the electrospray cloud, increasing p_i. The transmission of the generated sample ions by electric fields instead of by a gas current, noticeably reduces the ion residence time from the ionization region to the DMA inlet, thus considerably reducing the dilution produced by the space charge in that region. The new ionizer was termed Low-Flow SESI (LFSESI) and was first designed to be coupled with a DMA-MS instrument devoted to the analysis of explosive vapors. This new SESI charger increased the ionization probability to 1/700 (one ion for every 700 vapor molecules). The sample background of the explosive analyzer was also reduced by maintaining the ionization source walls at 170 – 200 ºC, minimizing sample adsorption and memory effect issues. Most of the common electrospray solvents are not a liquid at such high temperatures, so following Fernandez de la Mora's recommendations, new high boiling point electrospray solvents were selected for the electrospray in order to continuously operate it at temperatures between 170 – 200 ºC.

This early version of SEADM´s explosive vapor detector, named ACES E1 (ACES stands for Air Cargo Explosive Screener), benefited from two improvements with respect to the SESI-MS used by Martínez-Lozano and colleagues: the addition of the DMA to the triple quadrupole mass spectrometer (Sciex´s API 5000) and the improved ionization probability achieved by the LFSESI ion source.

Table 1. Most relevant properties, from the detection perspective, of the explosives studied in this thesis.

Explosive	EGDN[a]	NG[b]	PETN[c]	RDX[d]	TNT[e]
Precursor ion m_1 (Da)	187	262	351	257	226
Product ions m_2 (Da)	62[f]	46[f] or 62[g]	46[f] or 62[g]	46[f]	46[f] or 196[h]
Ionization mechanism	EGDN-Cl^-	NG-Cl^-	PETN-Cl^-	RDX-Cl^-	TNT^-
Structure	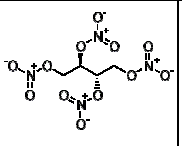	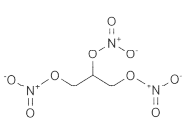	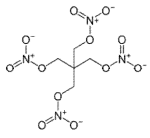	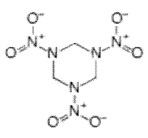	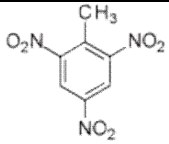
Vapor Pressure (ppb_v)[i]	1.02×10^5	645	9.15	1.07×10^{-2}	4.85×10^{-3}

[a] Ethylene glycol dinitrate [b] Nitroglycerin. [c]Pentaerythritol tetranitrate. [d]1,3,5-Trinitroperhydro-1,3,5-triazine. [e]Trinitrotoluene. [f] NO_2^-. [g] NO_3^-. [h] $C_6H_2N_2O_5CH_2^-$. [i]Vapor pressures obtained from Ewing et al. 2012.[33]

The explosives evaluated with this explosive vapor detector are detailed in Table 1, whereas their detection thresholds in the ACES E1 explosive vapor detector are summarized in Table 2.

Table 2. ACES E1 thresholds (ppq) in atmospheric air samples (~ 600 L).

	EGDN	NG	PETN	TNT	RDX
ACES E1 thresholds (ppq)	30,000	40	12	6.5	5.5

* Data extracted from an internal report property of the company SEDET (year 2012).

The thresholds were calculated through atmospheric samples pre-concentrated in a Tenax adsorbent filter. It should be noted that sample pre-concentration enables to increase the analysis sensitivity, only in the event that the analyzer is able to filter all the atmospheric analyte interference vapors which are also pre-concentrated in the adsorption filter. The results of the ACES E1 explosive vapor detector were not published in order not to disclose sensitive information to possible commercial competitors.

Despite the significant increase in the ionization probability and the important improvement achieved in the analyzer background, the LFSESI-DMA configuration promoted the presence of small tails in the DMA mobility peaks, generated in part by the inability of the DMA counterflow to prevent neutral vapors and high-boiling point droplets from entering the DMA. The presence of small tails in the mobility peaks is particularly critical, since it may obscure the presence of traces of analytes of interest, hence limiting the utility of the DMA for explosive vapor trace detection. The causes of this problem are further described below.

As shown in Figure 4, the drying gas originates from inside the DMA, where it moves leftwards at speeds of many tens of m/s. Therefore, the drying gas jet emerging outwards through the slit impacts the ES cloud at a substantial angle, being unable to fully avoid the diffusion of vapors from the spray into the DMA. Furthermore, the drying capacity of the jet at a temperature < 70 ºC, is insufficient to evaporate the high-boiling point electrospray droplets generated by the electrospray.

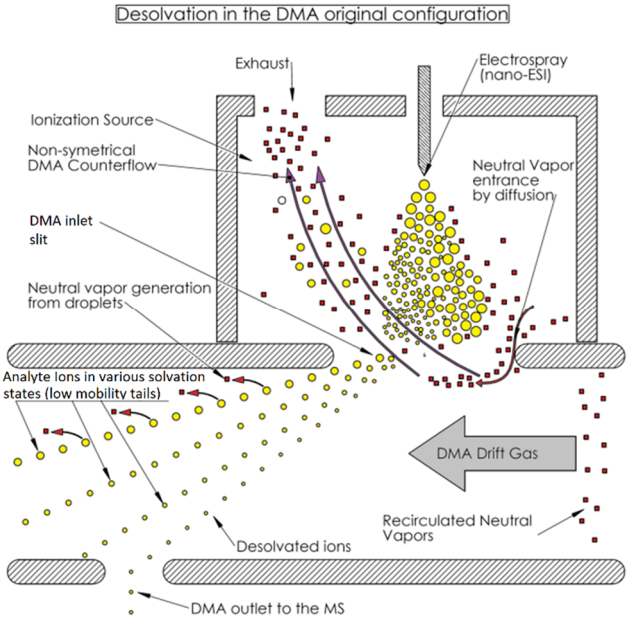

Figure 4. The high leftward gas velocity within the DMA creates a horizontal component in the drying counterflow jet exiting the slit upward, facilitating partial vapor penetration from the spray region into the analyzer.

Therefore, the first objective of this work was to optimize the analytical performance of the planar differential mobility analyzer (DMA) and the secondary electrospray ionization source (SESI), so as to bring their performance closer to the ideal level. Chapter 1 covers the improvements in the DMA and the ionization source that enabled to obtain tail-free Gaussian peaks matching the theoretical shape imposed by the Brownian ion diffusion and, at the same time, further improving the vapor ionization efficiency of the previous LFSESI ion source.[32] As described in Chapter 1, to completely eliminate the tailing phenomenon in the mobility peaks, it was not enough just to eliminate neutral vapors coming from the ionization source, it was also necessary to eliminate vapors coming from the internal circuit of the DMA and from the gas supply source. Sources of vapors in the DMA circuit were the plastics at high temperature (outgassing) and the DMA blower, which when run at a high temperature (70 ºC) released vapors into the DMA's drift gas, most likely from the lubricant and the plastic shaft seal. The solutions adopted to minimize drift gas contamination from the internal sources are reported in Chapter 1. Furthermore, an assessment of the influence of the gas purity on the mobility peak tailing was carried out, defining the minimum gas purity compatible with tail-free mobility peaks. A sensitive diagnostic tool was developed to assess the effectiveness of the different actions performed during the research period on the level of gas-phase contamination in the closed DMA sheath gas circuit.

In addition to the improvements of the DMA and the SESI ion source described in Chapter 1, and to fully comply with the first objective of this thesis, Chapter 2 covers the improvements in the DMA that promoted an important resolving power improvement. The resolving power attained virtually matches the theoretical limit imposed by both the Brownian diffusion and the sheath to sample flow rate ratio in the DMA. The enhanced DMA was coupled to a triple quad mass spectrometer to perform a mobility/mass analysis of a complex sample, illustrating the additional information provided by a high resolution DMA to a mass spectrometry analysis.

The improvements in the ionization efficiency and the DMA tailing suppression (Chapter 1), in combination with the improvement of DMA resolution (Chapter 2), significantly enhanced the analytical performance of the planar DMA. This enabled the fulfillment of the second objective of this thesis which was the development of an explosive vapor detector, based on DMA-MS/MS technology, capable of detecting explosives at sub-ppq concentrations. The sensitivity delivered by the state-of-the-art technology (SEADM´s explosive vapor detector ACES E1) is reported in Table 2.

The new explosive vapor detector capable of detecting explosive vapors of TNT and RDX at sub-ppq concentrations was named ACES E2.1 and, like its predecessor, was developed for the air cargo security application. Unlike other competing technologies, explosive vapor screening allows to scan a full truck without the need to unload its cargo (see Figure 5), resulting in significant savings in terms of time and cost. It is the evolution of the pre-existing ACES E1 explosive vapor detector, and besides incorporating the abovementioned improvements in the ionization source and the DMA, it also equips a new variable temperature desorber, which allows it to liberate the vapors collected in the adsorption filter according to their pressure vapor. The variable temperature desorption enables to remove those atmospheric interferences with vapor pressure different from the analyte of interest. From the analytical perspective, the variable temperature desorber can be viewed as a low-resolution gas chromatography system.

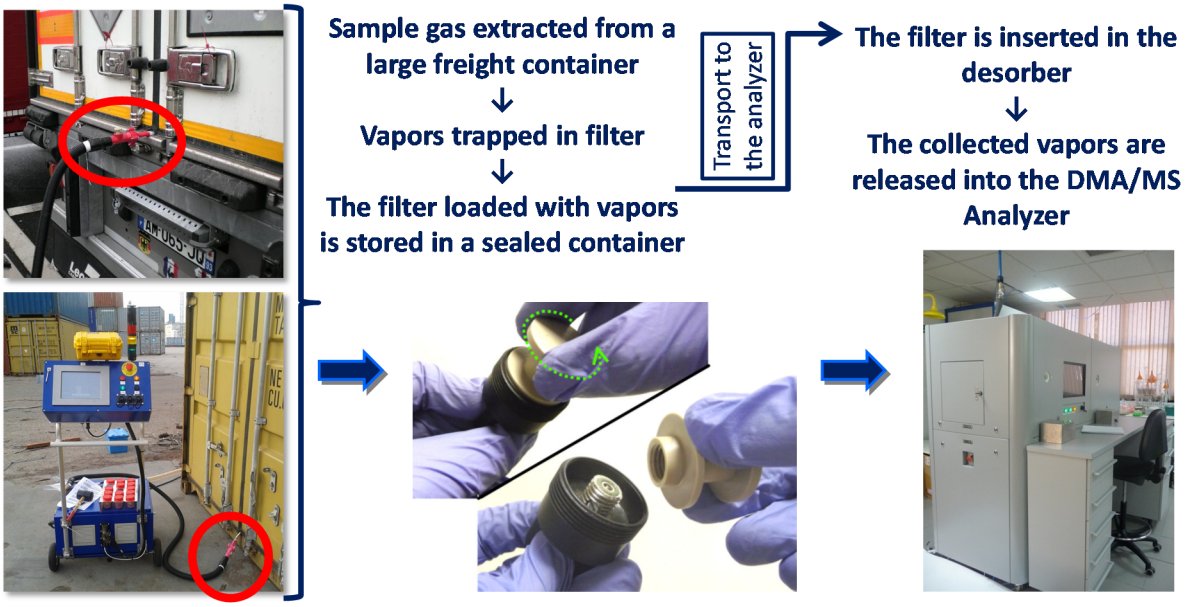

Figure 5. Concept of operation of the explosive vapor detector (EVD) based on DMA-MS/MS.

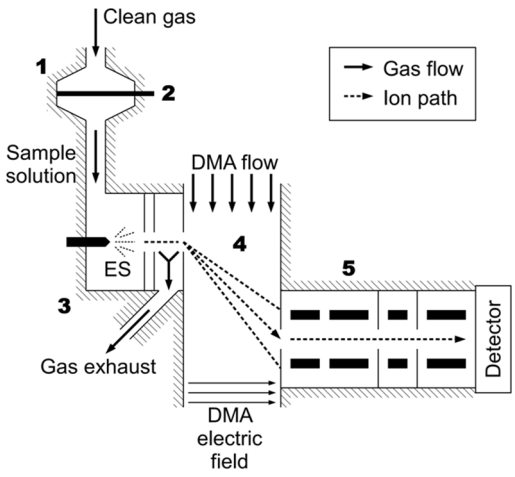

Figure 6. Schematic of the components of the DMA-MS/MS analyzer. 1.- Desorption system. 2.- Adsorption filter containing the vapors collected by the sampling system, which are liberated during the desorption and conveyed by a small flow of gas into the ionizer. 3.- Secondary electrospray ionizer (SESI). 4.- Differential mobility analyzer (DMA). 5.- Triple quadrupole (MS/MS) mass spectrometer.

The operation mode of the DMA-MS/MS explosive vapor detector is shown in Figure 5, whereas the analysis sequence is exposed in Figure 6.

The DMA-MS/MS operation principle, the validation tests conducted as well as the results obtained are thoroughly explained in Chapter 3. Chapter 4 is devoted to explaining the vapor detection method, which was patented. The detection limits achieved by this technology are world records at the time of this writing.

In spite of the outstanding performance of the DMA-MS/MS explosive vapor detector, one of the world's leading security agencies, and potential customer of SEADM´s explosive vapor detectors, advised SEADM to design a new detector not relying on mass spectrometry due to its high cost and volume. This customer´s requirement gave rise to the third and last objective of this work, consisting

in the development of an explosive vapor detector based on analyzers and detectors far simpler and more economical than mass spectrometry, yet still capable of detecting explosive vapors at concentrations of a few ppq.

Ion mobility spectrometry (IMS) allows for the rapid, inexpensive and portable classification of ions at atmospheric pressure, though with a modest resolving power compared to that achieved by mass spectrometry. One approach to overcome this limited selectivity is to combine IMS with other devices (such as chromatography or mass spectrometry), often at the cost of analysis speed, simplicity or affordability. Another approach, preserving the positive characteristics of IMS, is to benefit from the chemical orthogonality provided by selective ion transformations in a tandem IMS configuration: mobility-selected ions from a first IMS analysis region are modified in an intermediate reaction region, and the products are analyzed again in a second IMS analysis region. Tandem analysis with intermediate ion fragmentation has been exploited for many years in the triple quadrupole mass spectrometry Q^3-MS. A key to the success of this analyzer is the singular ability of the quadrupole to extract, for as long as desired, a single mass-to-charge ratio out of a complex ion mix before and after ion manipulation. As commented above, several IMS systems, including the DMA, also function as narrow-band ion-mobility filters separating ions in space, delivering a continuous stream of selected mobility ions. Besides, the DMA has demonstrated having the highest resolving power among the mobility filters (Chapter 2), in combination with a short ion residence time within the analyzer and a desolvation system which prevents mobility peak tailing (Chapter 1). For all these valuable features, the DMA is proposed as the apparently most suitable IMS for tandem configuration.

Controlled fragmentation of the selected parent ion by broadly applicable methods, however, is a key requirement where atmospheric pressure surrogates of the triple quadrupole have lagged behind their vacuum kin. This lag has greatly diminished thanks to extensive pioneering studies by Eiceman and colleagues on ion fragmentation at ambient pressure. Ion fragmentation at atmospheric pressure has been studied in single drift-time IMS with thermal activation at temperatures below 224 °C, leading to the observation of fragmentation of species such as butyl acetate[34] and proton bound dimers. [35] Thermal and electric field energy has been combined to study the ion fragmentation in a single DMS.[36,37] Tandem drift-time IMS studies have demonstrated the feasibility of fragmentation of explosive chloride adducts within the second IMS analysis region.[38,39,40] Tandem DMS (FAIMS-DMS) has been used to study the different responses of the two instruments, either without altering the precursor ion[41] or dissociating it through the intense electric fields present in the first mobility analysis region (FAIMS) while analyzing the products in the second one (DMS). [42]

In the cited studies,[35-42] ion fragmentation takes place within the mobility analysis region, such that some product ions are dispersed in a mobility tail distributed between the natural precursor and product ion mobility peaks. However, when the reaction region is located between the two mobility analysis regions, the product ion intensity is ideally concentrated in a single Gaussian peak with no tailing. The first tandem IMS study with intermediate ion reactant region took place in the mid 1980s.[43,44] Similar configurations have been used in later years under reduced pressure (below 12 Torr of helium gas), under which electrically activated fragmentation is simpler to achieve.[45,46] The feasibility of an atmospheric pressure tandem IMS with fragmentation is accordingly proven. What remains is selecting the most appropriate of the various IMSs, as well as increasing the available activation energy to successfully fragment the most resilient species.

The first DMA-F-DMA prototype, described in Chapter 5, demonstrates the feasibility of explosive fragmentation at ambient pressure using exclusively thermal energy. The analyzed samples were electrosprayed from liquid solutions and showed clean product ion mobility spectra proving the absence of ion decomposition within the mobility analysis regions (DMA_1 and DMA_2) demonstrating

the suitability of DMAs for the tandem DMA configuration. Previous studies with drift time IMS showed wide mobility tails between the precursor ion and its fragments.[34,35]

A purely thermal fragmenter was used to provide ions with the necessary activation energy to achieve explosive ion decomposition at ambient pressure. This is in contrast to prior studies by Eiceman and colleagues[36,37,42] in which ion decomposition was achieved by a combination of intense oscillating electric fields and moderate heating up to about 200 ºC. The reason for this simplification is explained below.

As previously observed,[38,39,40] the fragmentation of some explosives such as EGDN, NG and DNT, follows a first-order rate law expressed by the equation (1):

$$Rate = e^{-kt}, \qquad (1)$$

where k is the rate constant and t is the time. The Arrhenius equation relates the rate constant k with the temperature of the system T, the activation energy E, the gas constant R and the pre-exponential factor A:

$$k = Ae^{-E/RT} \qquad (2)$$

Since in (2) the decomposition rate k increases exponentially with T, given a fragmenter capable of reaching high temperatures, the approach of relying exclusively on heating to achieve the necessary activation energy for decompositions seems simple. This assumption was confirmed through the fragmentation results reported in Chapter 5. However, the fact of achieving jointly high temperatures and an efficient ion transmission along the fragmentation chamber (hereafter fragmenter) is not a trivial matter. Achieving high temperatures means placing the heating metallic elements very close to the ion path, shielding the electric field created between the fragmenter inlet and outlet electrodes, seriously hampering ion transmission.

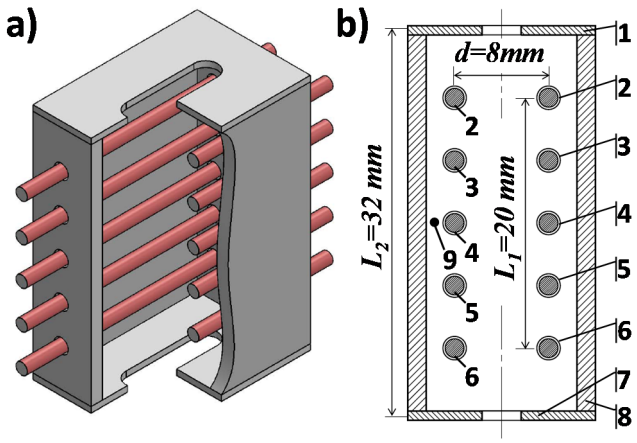

Figure 7. Isometric view (a) and transversal section (b) of the fragmenter (sketch). (1) Fragmenter inlet electrode at voltage V_1. (2), (3), (4), (5) and (6) are the different heating coil levels at voltage V_n and through each coil passing an electrical current I_n. (7) Fragmenter outlet electrode at voltage V_7. (8) Mirror polished walls. (9) Thermocouple position. *d* represents the transversal coil distance (orthogonal to the ion flow direction).

This weakness was overcome with the development of a completely new thermal fragmenter, shown in Figure 7 and thoroughly described in Chapter 6. This thermal fragmenter, placed between the

DMAs, allows independent control of the thermal and electric fields inside the fragmenter, which enables the improvement of both thermal fragmentation and ion transmission.

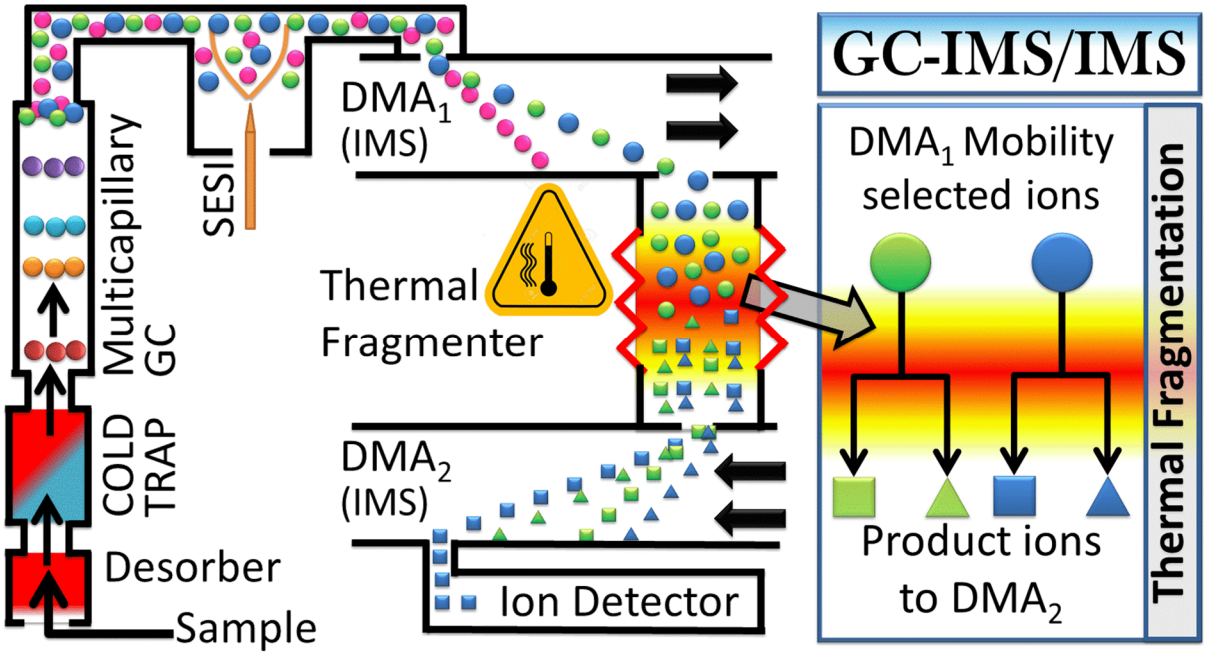

Figure 8. Schematics of the GC-DMA-F-DMA. Ambient vapors collected in a filter are liberated in the thermal desorber, separated in time in the GC and ionized in the ion source. Ions are then selected in the DMA_1, thermally decomposed in the fragmenter, while the generated product ions are mobility selected in the DMA_2 and, finally, quantified in the ion detector.

Chapter 6 covers the design, tests and results of the second prototype version named GC-DMA-F-DMA (Figure 8), and demonstrates its capacity to detect explosives in air at ppq concentrations.

In addition to the new thermal fragmenter (Figure 7), this new prototype includes a thermal desorber connected to a multicapillary GC. The thermal desorber allows for the desorption of atmospheric samples (500 Litres) collected on Tenax GR adsorbent filters. The liberated vapors are led to a cold trap, in order to focus the vapor injection into the multicapillary GC. The multicapillary GC separates the different desorbed compounds in time, delivering them for ionization to the SESI charger which is coupled to the DMA-F-DMA instrument. Both the multicapillary GC and the ion fragmentation provide orthogonal separation to the mobility analysis, maintaining the analysis time within 3 minutes. The atmospheric chemical background is evaluated through the analysis of real blank atmospheric samples of 500 L of air. Samples taken from cargo pallets loaded with commercial explosives (EGDN, NG, TNT, PETN and RDX) are analyzed, assessing the ability of detection under this scenario for the different explosives.

AIM OF THE THESIS AND OBJECTIVES

This doctoral thesis is aimed at the development of new analytical instrumentation for the detection of trace elements in the atmosphere at concentrations of parts per quadrillion (ppq = $1x10^{-15}$ atmospheres of partial pressure) and below.

As outlined in the introduction section, this thesis has three overall objectives:

1. To optimize the analytical performance of the planar differential mobility analyzer (DMA) and the secondary electrospray ionization source (SESI), so as to bring their performance closer to the ideal level.
2. To develop an explosive vapor detector, based on DMA-triple quadrupole mass spectrometry technology (DMA-MS/MS), capable of detecting explosive vapors at sub-ppq concentrations.
3. To develop an explosive vapor detector, based on analyzers and detectors far simpler and more economical than mass spectrometry, yet still capable of detecting explosive concentrations of a few ppq.

Specific objectives for the new SESI ionization source (Chapter 1).

- To develop a new SESI ionization source by integrating a desolvation stage to efficiently prevent droplets and neutral vapor from entering the DMA.
- To maintain or, if possible, improve the ionization efficiency obtained by its predecessor.[32]
- To develop an electrospray solvent cooling system to enable the use of low boiling point electrospray solvents while maintaining the ion source temperature at 170 ºC.

Specific objectives for the enhanced planar DMA to achieve ideal Gaussian mobility peaks (Chapter 1).

- To minimize the internal outgassing in the DMA components in order to maintain, as low as possible, the presence of vapors in the DMA sheath gas.
- To minimize the lubricant emissions of the DMA sheath gas blower.
- To develop a sheath gas heating system capable of operating the DMA at a high temperature.
- To assess the influence of the gas purity on the mobility peak tailing, defining the minimum gas purity compatible with tail-free mobility peaks.
- To develop a sensitive diagnostic tool to evaluate the level of gas-phase contamination of the closed DMA sheath gas circuit.

Specific objectives of the enhanced planar DMA to bring its resolution closer to the theoretical limit (Chapter 2).

- To study the influence of the sheath gas pre-laminarization as a way to minimize turbulence in the mobility analysis region.
- To minimize the steps or gaps between the DMA laminarization-screen exits and the wetted surfaces following immediately after them.
- To reduce the residence time in the DMA as much as possible in order to minimize ion-beam spreading by Brownian diffusion.

Specific objectives of the explosive vapor detector based on DMA-MS/MS technology (Chapters 3 and 4).

- To efficiently integrate the enhanced ionization source and DMA with the desorber and the mass spectrometer.
- To develop a variable temperature desorber that releases vapors of decreasing volatility at increasing times, according to a temperature history.
- To study the cutoff size and material for a prefilter to remove the aerosol particles present in the atmosphere in order to reduce the statistical noise which forces having to raise the threshold for positive detection, artificially reducing the sensitivity of the instrument
- To develop an explosive vapor sampler and a filterholder to host the vapor collector (adsorption filter) and the prefilter.
- To research and develop strategies to prevent explosive contamination in the sampler, the filterholder, the analyzer and the sampling and analyzers' surroundings.
- To study in detail the atmospheric background in each of the explosive DMA-MS/MS channels (TNT, RDX, NG and PETN) in order to assess the probability of detection (PoD) and the false alarm rate (FAR) of the instrument. For that purpose, hundreds of atmospheric blank and loaded samples must be analyzed.

Specific objectives of the first version of the explosive vapor detector not based on mass spectrometry: DMA-F-DMA (Chapter 5).

- To develop a reaction region (fragmenter) capable of fragmenting explosive ions at atmospheric pressure by thermal means, transmitting the generated products along the reaction region.
- Testing the developed fragmenter with EGDN, NG, PETN, TNT and RDX explosive ions and assessing the ability to fragment some or all of them.
- To develop an ion transmission system in charge of transmitting the precursor ions from the first DMA, introducing them into the fragmenter, extracting the product ions from the fragmenter and finally introducing them into the second DMA. The ion transmission must be fundamentally assured by electrical fields in order to avoid the effects of the uncontrolled gas currents in the ion transmission system between the DMAs. Particular attention must be paid to the design of the DMA_1's electrical ion outlet since the sample of the DMA had previously always been dragged by a gas stream.

Specific objectives of the second version of the explosive vapor detector not based on mass spectrometry: GC-DMA-F-DMA (Chapter 6).

- The new fragmenter must achieve independent control of the thermal (fragmentation) and electric fields (ion residence time) inside the fragmenter.
- The temperature in the fragmenter ion path must exceed 700 ºC enabling the fragmentation of the five explosives studied (TNT, RDX, PETN, NG and EGDN).
- To obtain the product ions reported in the literature.
- To increase the selectivity of the DMA-F-DMA by connecting a multicapillary GC between the desorber and the SESI ionization source.
- To maintain the analysis time within 3 minutes.
- To optimize the fragmentation temperature for each target explosive.
- To assess the atmospheric background for TNT, RDX, PETN, NG and EGDN.
- To assess the sensitivity gain provided by the F-DMA by comparing the GC-DMA-F-DMA and the GC-DMA configurations.
- To test the analyzer with commercial explosives hidden in cargo pallets and evaluating the capacity of detection under such conditions.

THESIS STRUCTURE

This thesis is presented under the modality of compendium of publications (BOCYL 117/2016). The following five research articles cover the lines of research defined through the thesis objectives:

- Mario Amo-Gonzalez, Juan Fernández de la Mora. Mobility Peak Tailing Reduction in a Differential Mobility Analyzer (DMA) Coupled with a Mass Spectrometer and Several Ionization Sources. **Journal of The American Society for Mass Spectrometry 2017**, 28, 1506-1517. Presented in Chapter 1.

- Mario Amo-González, Sergio Pérez. Planar Differential Mobility Analyzer with a Resolving Power of 110. **Analytical Chemistry 2018**, 90 (11), 6735-6741. Presented in Chapter 2.

- D. Zamora, M. Amo-Gonzalez, M. Lanza, G. Fernández de la Mora, J. Fernández de la Mora. Reaching a Vapor Sensitivity of 0.01 Parts Per Quadrillion in the Screening of Large Volume Freight. **Analytical Chemistry 2018**, 90 (4), 2468-2474. Presented in Chapter 3.

- Mario Amo-González, Irene Carnicero, Sergio Pérez, Rafael Delgado, Gary A. Eiceman, Gonzalo Fernández de la Mora, Juan Fernández de la Mora. Ion Mobility Spectrometer-Fragmenter-Ion Mobility Spectrometer Analogue of a Triple Quadrupole for High-Resolution Ion Analysis at Atmospheric Pressure. **Analytical Chemistry 2018**, 90 (11), 6885-6892. Presented in Chapter 5.

- Mario Amo-González, Sergio Perez, Rafael Delgado, Gonzalo Arranz and Irene Carnicero. Tandem Ion Mobility Spectrometry for the Detection of Traces of Explosives in Cargo at Concentrations of Parts Per Quadrillion. **Analytical Chemistry 2019**, 91 (21), 14009-14018. Presented in Chapter 6.

The “Journal of The American Society for Mass Spectrometry” got an impact factor of 3.2 in 2018 (InCites Journal Citation Reports), being in the first quartile in the disciplines of Analytical Chemistry (75.6 %) and Spectroscopy (86.6 %). The journal “Analytical Chemistry” got an impact factor of 6.4 in 2018, appearing at the head of the first quartile Q1 in the discipline of Analytical Chemistry (92.3%).

Each article is presented as a chapter of this thesis (chapters 1-3, 5-6).

Besides, the patent covering the explosive vapor detection method is also presented as material for this thesis. The patent identification is as follows:

- Title: Method for Detecting Atmospheric Vapors at Parts Per Quadrillion (PPQ) Concentrations. Patent No. **US 9.297,785 B2**. **Mar. 29, 2016**. Inventors: Mario Amo, Daoiz Zamora, Alejandro Casado, Gonzalo Fernandez de la Mora, Guillermo Vidal-de-Miguel, Juan Fernandez de la Mora.

RESEARCH FUNDING SOURCES

The resources necessary to carry out this thesis are listed below:

- The developments in the DMA to avoid peak tailing, including the development of the DMA ionization sources, were funded internally by SEADM.

- The developments in the DMA to increase the resolving power were co-funded under the project **RESOLVE** (Proyectos en I+D en PYMES, file number 04/16/VA/0031) by the Castile and Lion Regional Government ADE Agency and the FEDER (ERDF) Program under the responsibility of the European Commission.

- The last stage of development of the Air Cargo Explosive Screener (ACES E2.1) based on DMA-MS/MS technology was co-funded under the **ACES** project by the EU within its H2020 SME Phase 2 Programme (grant agreement number: 672001).

- The development of the explosive vapor detector not based on mass spectrometry (GC-DMA-F-DMA) was funded by the Future Aviation Security Solutions Programme, a joint UK programme run by the Department for Transport and the Home Office under contract numbers 1000112322 (**EffeX project phase I**) and 1000121217 (**EffeX project phase II**).

At the moment of completing this thesis, two more projects have been granted to continue with the development of the GC-DMA-F-DMA detector, albeit the results and developments achieved with this funding are beyond the scope of this thesis. The projects are as follows:

- The **COSMIC** project has received funding from the European Research Council (ERC) under the European Union's Horizon 2020 Research and Innovation Programme (grant agreement n° 786945).

- Project **HITEX** has been funded by the Future Aviation Security Solutions Programme, a joint UK programme run by the Department for Transport and the Home Office under contract number DSTLX1000139141.

CHAPTER 1. MOBILITY PEAK TAILING REDUCTION IN A DIFFERENTIAL MOBILITY SPECTROMETER COUPLED WITH A MASS SPECTROMETER AND SEVERAL IONIZATION SOURCES

J. Am. Soc. Mass Spectrom. (2017) 28:1506–1517
DOI: 10.1007/s13361-017-1630-2

RESEARCH ARTICLE

Mobility Peak Tailing Reduction in a Differential Mobility Analyzer (DMA) Coupled with a Mass Spectrometer and Several Ionization Sources

Mario Amo-Gonzalez,[1] Juan Fernandez de la Mora[2]

[1]SEADM, Parque Tecnológico de Boecillo 205, Valladolid, Spain
[2]Mechanical Engineering Department, Yale University, New Haven, CT 06520-8286, USA

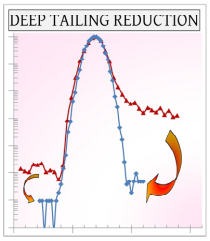

Abstract. The differential mobility analyzer (DMA) is a narrow-band linear ion mobility filter operating at atmospheric pressure. It combines in series with a quadrupole mass spectrometer (Q-MS) for mobility/mass analysis, greatly reducing chemical noise in selected ion monitoring. However, the large flow rate of drift gas (~1000 L/min) required by DMAs complicates the achievement of high gas purity. Additionally, the *symmetry* of the drying counterflow gas at the interface of many commercial MS instruments, is degraded by the lateral motion of the drift gas at the DMA entrance slit. As a result, DMA mobility peaks often exhibit tails due to the attachment of impurity vapors, either (1) to the reagent ion within the separation cell, or (2) to the analyte of interest in the ionization region. In order to greatly increase the noise-suppression capacity of the DMA, we describe various vapor-removal schemes and measure the resulting increase in the tailing ratio, (*TR* = signal at the peak maximum over signal two half-widths away from this maximum). Here we develop a low-outgassing DMA circuit connected to a mass spectrometer, and test it with three ionization sources (APCI, Desolvating-nano ESI, and Desolvating low flow SESI). While prior *TR* values were in the range 100–1000, the three new sources achieve *TR* ~ 10^5. The SESI source has been optimized for maximum sensitivity, delivering an unprecedented gain for TNT of 190 counts/fg, equivalent to an ionization efficiency of one out of 140 neutral molecules.

Keywords: Background suppression, Differential mobility analyzer, IMS-MS, Ion mobility spectrometry, Desolvation, Curtain gas

Received: 3 November 2016/Revised: 8 February 2017/Accepted: 14 February 2017/Published Online: 30 May 2017

Introduction

In spite of the much larger resolving power of other mass analyzers, the quadrupole mass spectrometer (Q-MS) remains one of the most widely used types, thanks to its ability to operate as a narrow-band mass filter. Indeed, extracting a single ion mass out of a complex mix for subsequent study or manipulation is key in many scientific and analytical situations. An ion mobility spectrometer (IMS) capable of continuously drawing a narrow range of ion mobilities out of a complex mixture is equally useful, with the added advantage of performing its function in a gas that may be at atmospheric pressure. This filter type permits, for instance, studying the kinetics of ion [1] or neutral [2] evaporation, carrying out spectroscopy in mobility-selected species, etc. The combination in series of such a mobility filter with a Q-MS for single ion monitoring (SIM) offers transmission efficiencies and analysis times similar to those required for Q-MS analysis, but with greatly increased resolving power [3].

Several narrow-band ion mobility filters operating in a steady or quasi-steady form are known. Field asymmetric IMS (FAIMS), also referred to as differential mobility spectrometry (DMS), combines a strong AC and a weak DC field [4]. Its original poor resolution has been considerably alleviated by the choice of a drift gas including either polar vapors, such as 2-propanol [5], or light components, such as He and H_2 [6]. FAIMS separation depends on nonlinearities of the drift velocity on the electric field, which are difficult to interpret in terms of cross-section. Transversal modulation IMS (TMIMS) combines a DC axial field with an orthogonal AC field of comparable magnitude, to continuously focus on an exit slit only those ions whose (mobility-dependent) axial time of flight

Correspondence to: Juan Fernandez de la Mora;
e-mail: juan.delamora@yale.edu

(TOF) resonates with the imposed period of transverse oscillation [7]. TMIMS operates in the linear mobility regime, hence providing cross-section information. In addition to the main resonance, TMIMS also passes higher harmonics, and leaks a small amount of other mobilities in the form of pulses at the imposed transverse frequency. These problems can, however, be overcome, for instance with two TMIMS filters in series [8]. Other promising proposals are the periodic focusing differential mobility analyzer (PFDMA) [9], where ions of a selected mobility are purified by selective passage over numerous slits in the presence of electric and flow fields, and overtone mobility spectrometry [10] that allows a linear drift tube to be operated as a continuous ion mobility filter.

Here, we focus on the differential mobility analyzer (DMA) [11], a member of a class of narrow-band ion mobility filters combining a DC electric field and a steady flow field of drift gas [12], and providing linear mobility separation. The DMA operates at ambient pressure, and can be easily added or removed from the ion source region of atmospheric pressure ionization (API) MS systems [13], a combination (DMA-MS) having demonstrated excellent performance in a variety of analytical and basic applications [14–17]. From the analytical perspective, the DMA can be viewed as a chromatography of sorts, removing 98%–99% of the ion mobilities in a complex mix [18], while being able to shift from one mobility to another in a few milliseconds. This noise-suppression ability has been demonstrated in monitoring for explosives in the exceedingly complex mixture of vapors characteristic of the atmosphere at concentrations as low as 0.01 parts per quadrillion (1 ppq = 10^{-15} atmospheres of partial pressure) [19]. At this sensitivity, a limiting feature as important as resolution [defined as the mean ion mobility divided by the full mobility width at half maximum (FWHM)] is the presence of small tails (often associated with incomplete desolvation of abundant contaminant species), which may completely obscure the presence of traces of analytes of interest. This tailing is illustrated in the mobility spectrum of Figure 1c, where the DMA voltage, shown as horizontal variable, is inversely proportional to ion mobility. One sees substantial background in the voltage range 2200 > V_{DMA} (Volt) > 1070, where any small peaks present would be undetectable. In order to quantify these tails, we define the tailing ratio *TR* as the signal at the peak maximum divided by the signal two half-widths away from this maximum (*TR*; Figure 1a). For a Gaussian peak (characteristic of diffusion broadening) $TR = 2^{16} \sim 0.655 \times 10^5$, yet *TR* values found in Figure 1c and in prior DMA-MS studies are rather in the range 10^2–10^3.

No systematic study is available on such tailing phenomena in DMAs, but two characteristic features of this instrument suggest that it would be more prone to peak tailing than other IMS systems: First, DMAs of high resolving power use large flows of drift gas (~1000 L/min), complicating the achievement of gas dryness levels common in drift-time IMS. Additionally, conventional curtain [21, 22] or counterflow [23] heated drying gas schemes used in API-MS to avoid vapor ingestion owe much of their success to the coincidence of the symmetry axes of the drying gas flow and the inlet orifice to the MS. This symmetry and the corresponding high drying efficiency, however, is broken at the sample inlet slit of the DMA, due to the motion of the DMA drift gas orthogonally to this axis (Figure 2). Accordingly, our main goal here is to develop more effective vapor-suppression schemes for DMAs, so as to minimize peak tailing, to reach *TR* values close to those for an ideal Gaussian peak (0.655×10^5).

Several typical tailing phenomena arising in DMAs are illustrated in Figure 1c, which is a mass-selected mobility spectrum for nitroglycerin (NG), where the DMA is followed by a triple quadrupole transmitting the 262/46 ion, with parent at 262 *m/z* ($NG + Cl^-$) and its NO_2^- fragment at 46 *m/z*. The DMA voltage variable shown in the mobility spectrum is inversely proportional to ion mobility (hence high and low mobility tails are, respectively, to the left and to the right of the peak). The ions were formed by electrospraying a solution of dimethyl sulfoxide:octanol 75:25 in volume, HCl 0.1% + nitroglycerin (NG) 5 ppmv. This high boiling point solvent maintains a stable electrospray at 200 °C, but complicates an effective desolvation of the ES cloud. For this reason, it has been replaced by methanol/water (9/1) in all the electrospray ionization sources subsequently used in this study.

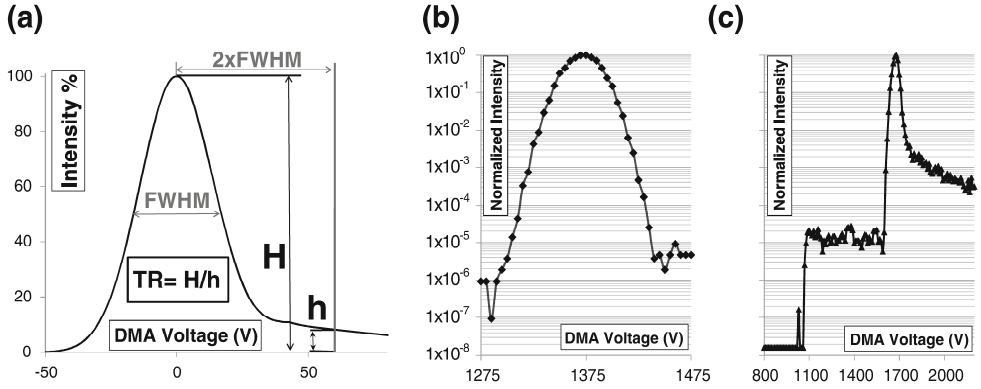

Figure 1. Illustration of the Tailing Ratio *TR* in several settings: (**a**) Definition of *TR*. (**b**) Normalized nitroglycerin peak in a high *TR* DMA configuration (*TR* ~ 10^5) using Desolvating-nanoESI as ionization source. (**c**) Normalized nitroglycerin peak in a DMA configuration with a low *TR* of 3.2×10^2, using LFSESI [20] as ionization source

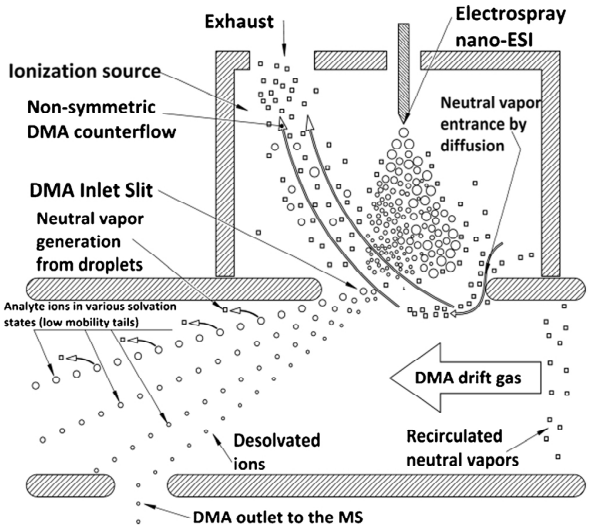

Figure 2. The high leftward gas velocity within the DMA creates a horizontal component in the drying counterflow jet exiting the slit upward, facilitating partial vapor penetration from the spray region into the analyzer

The peak of the dominant ionizing species Cl^- (not shown in the figure), appears at V_{DMA} = 1070 V, coinciding with the beginning of the high mobility tail of the NG-Cl^- peak. This creates a uniform background intensity ~10^{-5} invading the space between the voltages corresponding to the peaks of pure Cl^- (V_{Cl} = 1070 V) and pure NG-Cl^- (V_{NG} ~ 1700 V). This continuous signal between V_{Cl} and V_{NG} is due to attachment within the DMA of a neutral NG molecule to the Cl^-. This results in a mobility spanning all intermediate values between the mobilities of Cl^- and NG-Cl^-. The presence of a neutral analyte vapor inside the DMA is explained by the imperfect DMA counterflow drying (Figure 2), which allows small quantities of neutral vapors to reach the DMA. This long left-tail structure is not unique to NG and Cl^-, but arises similarly with many other analyte mobility peaks and ionizing species.

The low mobility tail of the NG-Cl^- peak shown in Figure 1c extends from V_{DMA} 1750 V to 2200 V (the end of the registered data), with signal intensity considerably higher than the high mobility tail. Low mobility tails are most likely due to various states of solvation of NG-Cl^- ions formed prior to their entrance into the DMA and, to a lesser extent, due to the attachment within the DMA of some contaminant vapors to a specific ion formed upstream of the DMA.

Both high and low mobility tails are evidently undesirable. Both result from the presence of neutral vapors, and both would be removed with a thorough elimination of condensable species from the whole DMA circuit. These vapors have several possible origins. As in conventional IMS, they may be due (1) to an insufficiently purified source gas, (2) inadequate desolvation at the interface between the DMA and the ES source, and (3) internal outgassing within the instrument. The last source is harder to control in DMAs than in drift-time IMS because of the need for a blower to recirculate gas flow rates of the order of 1000 L/min. Particularly critical is the possibility of leakage of vapors from lubrication fluids penetrating into the recirculating DMA gas flow through the shaft powering the compressor blades.

Here we describe three new ionization chambers that significantly reduce solvent vapors at the interface with the DMA, as well as a low outgassing closed DMA circuit, the conduits of which are kept at high temperature except at the blower. The blower is preceded by an intercooler that maintains it near room temperature, limiting its vapor emissions.

Experimental

MS

Either AB Sciex's QTRAP 5500 or AB Sciex's TripleQuad 5500 were both operated as triple quadrupoles.

DMA

We used SEADM's DMA P5-f, with critical dimensions collected in Table 1, which includes improvements over a similar instrument previously described [13]. An important practical innovation is that the flow-limiting orifice is no longer at the outlet slit of the DMA, but in the MS. The DMA can then be quickly removed or installed without breaking the MS vacuum. The DMA combines a horizontal laminar flow of gas with a vertical electric field between two parallel plates, such that ions of different mobilities penetrating through a slit in the upper plate open up in a fan as they drift towards the other plate, whereby only a small range of mobilities is sampled through a second slit in the lower plate (Figure 2) and transmitted to the MS. The materials used in the DMA are stainless steel (SS) AISI316 for the inlet/outlet electrodes and the drift gas recirculation circuit, aluminum for the DMA entrance and outlet diffuser parts, PEEK for the DMA insulator box, and Teflon encapsulated o-rings for the sealing between the different parts. The DMA-MS interface is made of SS AISI316, PEEK, and Teflon encapsulated O-rings. The DMA was operated at 120 C, thanks to a heater (aluminum) located between the DMA blower and the DMA.

Pump

The sealed DMA blower (Domel d.o.o., 791 series brushless blower) is made of aluminum and SS, with the exception of the shaft seal (unknown plastic). Ideally, this shaft should avoid the entrance of vapors emitted by the lubricated bearing located right beside it. However, as demonstrated later, when the blower runs at a high temperature (70 °C), vapors are released into the DMA's drift gas, most likely from the lubricant and the plastic shaft seal. To further minimize these vapor emissions, an air intercooler (aluminum) placed between the blower inlet and the DMA outlet could cool the blower below 35 °C.

Table 1. Critical Dimensions (mm) of SEADM's P5 DMA

	W_{DMA}[a]	H_{DMA}[b]	W_{slit}[c]	H_{slit}[d]	D[e]
Inlet	17	10	7	0.6	
Outlet	14.9	10	4.5	0.17	0.8

[a]Channel width.
[b]Channel height.
[c]Slit width.
[d]Slit length.
[e]Orifice diameter

Analyte Vapor Ion Generation

Controlled amounts of sample vapor were introduced in the ionizer by heating a solid sample in a desorber consisting of an SS AISI 316 Swagelok T embedded within an aluminium heating block, whose temperature could be accurately set by a PID control. The solid samples to be desorbed are introduced into a SS AISI316 mesh that is inserted into the T. In order to minimize outgassing, use of plastic materials has been avoided also in the desorber and the transfer line. The solid source of vapor was a pill containing NG, commonly used for heart disease (Parke-David S.L., Vernies 0.4 mg Nitroglycerin). In order to have an adequate signal to noise ratio, we selected a desorber temperature yielding 10^6 cps of NG at the maximum of the mobility peak.

For some experiments involving an electrospray, 500 ppb of NG (Isostandards M-8330-ADD-1) is added to the electrospray solvent, which produces NG ions directly from the liquid phase. This approach injected into the system a minute NG flux of 3.6 pg/s. These vapor concentrations are large enough for the peak height to exceed 10^5 times the minimum detectable signal, a necessary condition to be able to measure *TR* ~10^5.

DMA-MS

Using the APCI source (Figure 3a) described in a later section, two-dimensional DMA-MS scans (Figure 4) were generated by sweeping the DMA voltage between 0 and –2500 V at 10 V steps. At each voltage step, a *m/z* Q1 sweep of 15–800 Da in negative mode at 1000 Da/s was carried out, with the experiment lasting 3.3 min in total. The aim of these experiments was not to infer *TR*, but to diagnose the content of vapors in the DMA circuit (see the Results section).

TR Measurement

Ion mobility peaks are obtained by scanning the voltage difference applied between the two DMA plates, with the triple quadrupole mass spectrometer operating in multiple reaction monitoring mode, selecting the nitroglycerin precursor ion in the first quadrupole, and the product ion in the third quadrupole. Table 2 details the precursor and product ions depending on the ionization source used.

Measuring *TR* ~10^5 is not straightforward because the MS needs to have a dynamic range exceeding this high value. When no analyte is introduced, the NG MS/MS channel is practically free of background, while the MS detector saturates at ~5×10^6 counts/s. We therefore used a dwell time of 1 s and could quantify a minimum MS signal of one count per second (cps) and signals of about 10^6 cps. The dynamic range of the MS under those conditions was accordingly ~10^6, not limiting the measurement of *TR*.

APCI Source

A leading cause of solvation in the DMA is the penetration of ES solvent from the ionization region into the DMA. This *external* vapor source was eliminated to evaluate the influence on the *TR* of background from either the N_2 gas used, or outgassing from either the DMA, the recirculation circuit or the blower. A discharge ionization source (APCI) entirely free from ES vapors was accordingly developed (Figure 3a). This chamber, due to its plastic-free construction, has a low level of outgassing. Its body is made of AISI316 stainless steel (SS). The gas inlet and outlet, like the 1/16″ tungsten electrode discharge inlet, is achieved through three Swagelok fittings welded to the chamber. The electric insulation between the tungsten discharge electrode and the chamber body (equipotential with the DMA inlet electrode) is achieved by using a ceramic insulator (Macor, Corning Inc., New York, USA) (Figure 3a- item 2). Aluminum flat gaskets are used to seal the various parts of the chamber, including unions between metallic and ceramic parts (Figure 3a- item 3). The metallic parts have sharp edges (Figure 3a- item 4) that create plastic deformation in the aluminium gaskets and a perfect seal between the parts. It is not possible to put sharp edges in the ceramic insulator because the high compressive stress created would break them, but because of the good surface finish of the ceramic insulator and the aluminum gaskets, the pressure created in the seat plane seals also the contact between the ceramic and the metallic gasket. No bubbles were observed when the assembly was pressurized at 1 bar with N_2 and immersed in methanol. The gas used in the DMA drift gas circuit and the sample flow through the desorber was 99.9992% pure bottled nitrogen. The sample and counterflow flow-rates were 0.3 and 0.4 l/min, respectively. In order to compensate for the MS consumption of 2.5 L/min through its sampling orifice, 2.9 L/min of nitrogen were introduced into the recirculating DMA drift gas (2.5 L/min for the MS and 0.4 L/min for the counterflow). The N_2 supply lines were of Teflon and stainless steel. The fittings (Swagelok) were made of SS. The valves were made of SS with PFA (Teflon) or PEEK seats, and the flowmeters used were SMC PFM710, wherein the parts in contact with the fluid were made of liquid crystal polymer (LCP), polybutylene terephthalate (PBT), brass (electroless nickel plated), nitrile butadiene rubber + fluoro coated, viton + fluoro coated, Au, stainless steel 304.

A cartridge heater connected to a PID control system allows the temperature of the ion source to be selected in the range of 40–350 °C. The ionization chamber is connected to the desorber by means of heated fused silica-lined stainless steel tubing.

Desolvating-NanoESI Ionization Source

The study with the APCI ionization source revealed that high DMA *TR*s were possible in the low outgassing DMA

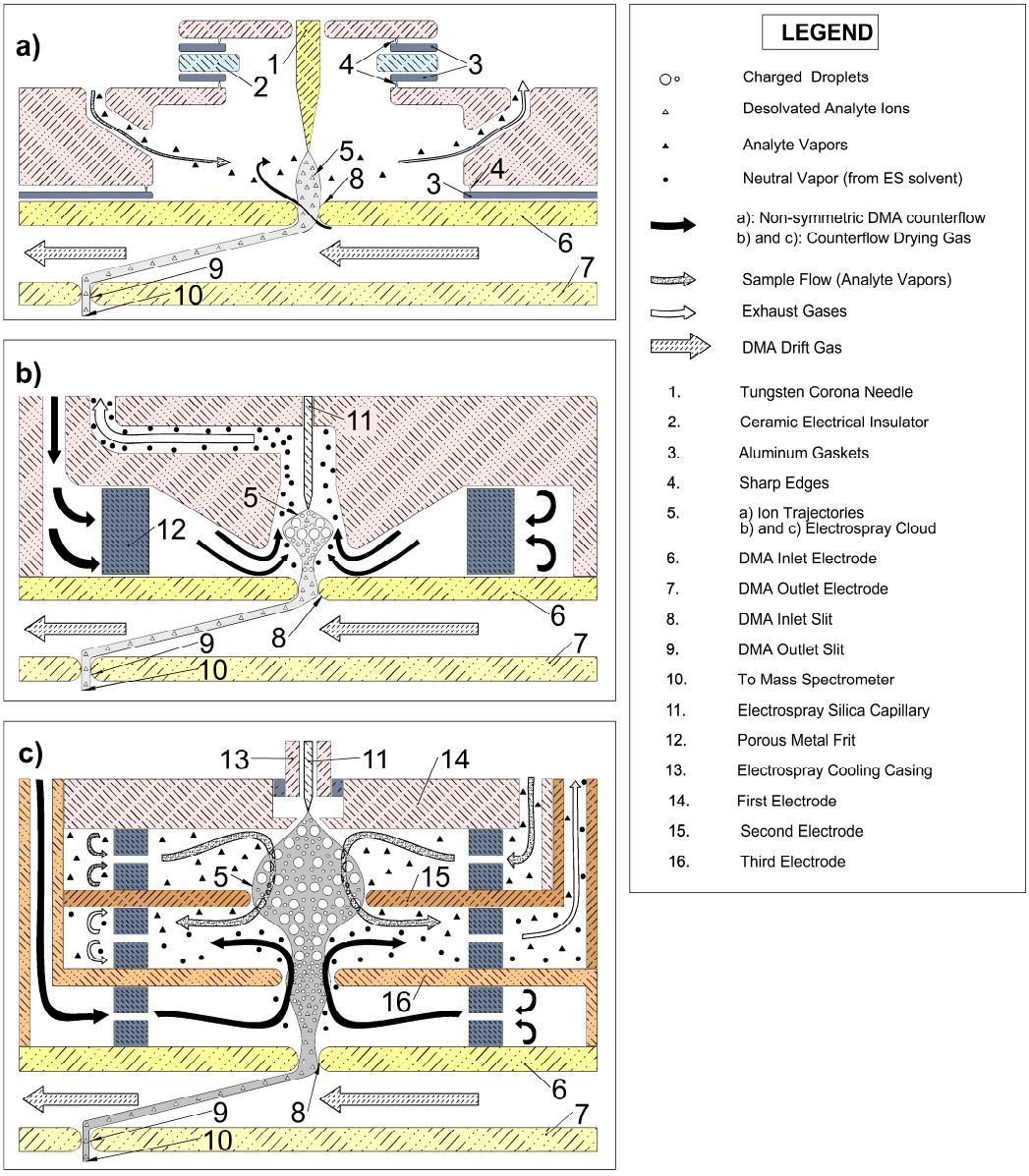

Figure 3. (**a**) APCI source + DMA. (**b**) Desolvating-nanoESI + DMA: the laminar flow of heated drying gas enters laterally through a metal frit and is symmetrically directed upwards, efficiently desolvating the ES drops, and preventing neutral vapors from entering the DMA. (**c**) Desolvating-LFSESI + DMA, where hot dry gas rises vertically through electrode 16 to meet frontally the electrospray cloud

configuration, as long as no ES solvent was introduced. The next challenge was to achieve comparable *TR*s with an electrospray source. A custom nano-ESI source was designed specifically to achieve complete removal of vapors. It provides a heated drying gas flow upstream of the DMA inlet slit, symmetrically directed towards the electrospray cloud (Figure 3b). In this case the analyte ions were electrosprayed from the electrospray solvent (MeOH-H_2O 9:1/HCl 0.1%) containing 500 ppb of NG.

In prior DMA-ES source interfaces, the drying gas originates from inside the DMA (Figure 2), where it moves towards the left at speeds of many tens of m/s. Therefore, the drying gas jet emerging outwards through the slit impacts the ES cloud at a substantial angle, being unable to fully avoid diffusion of vapors from the spray into the DMA. In the present design, 1.5–3 L/min of drying gas are symmetrically injected through a metallic frit (Figure 3b- item 12) into the spray region, opposing the spray cloud head on (Figure 3b- item 5). In order to further reduce penetration through the slit of DMA gas carrying a leftward velocity, it is possible to inject a small amount of drying gas into the DMA. In practice, the drying performance is

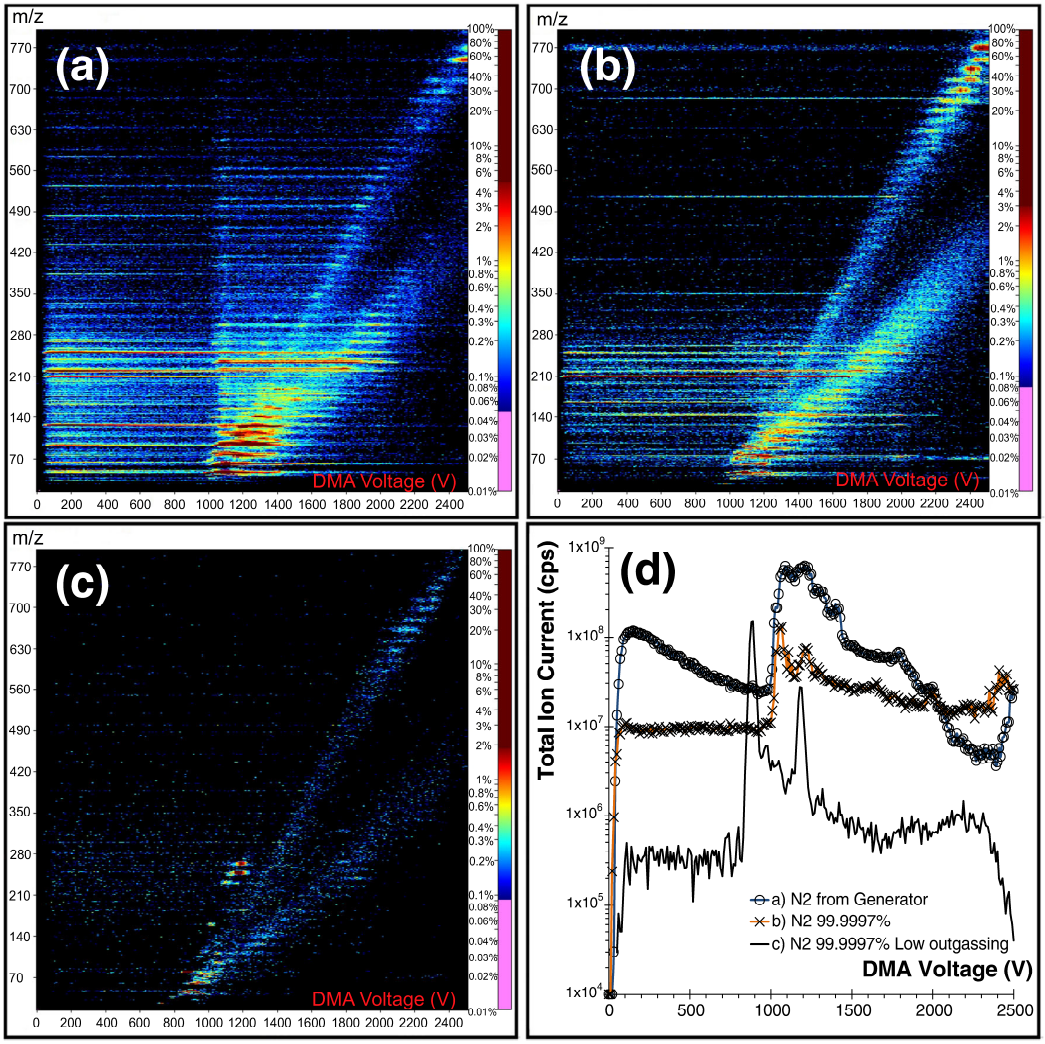

Figure 4. Mobility-MS spectra for vapor background in the APCI source. (**a**) N_2 from a generator (99.5% purity) with DMA/ion source temperature of 40 °C. (**b**) After running the system for 90 min with bottled N_2 (99.9992% purity), with DMA and ion source temperature of 40 °C. (**c**) bottled N_2 (99.9992% purity), with DMA at 120 °C (DMA heater present), DMA blower actively cooled to 35 °C, ion source at 230 °C. (**d**) DMA mobility spectra summing over all masses for experiments a, b, and c

not found to be impaired even if this flow through the slit is slightly reversed (–0.2 L/min). The temperature of the drying gas is adjustable between 70 °C and 220 °C via heaters acting upstream from the metallic frit and in the frit itself.

The internal source geometry through which the drying gas desolvates the sample ions includes an initially lateral entry through the frit, followed by a 90° upward turn, with a slightly converging region 13 mm long, which accelerates the gas to avoid turbulent transition. The fluid velocities in the electrospray region were 3 and 6 m/s for flow rates of 1.5 and 3 l/min, with corresponding Reynolds numbers Re = 180 and 360 (based on a lateral characteristic length of 1.6 mm and a kinematic viscosity $\nu = 2.5\ 10^{-5}$ m^2/s for nitrogen at 120 °C). These moderate Re values suffice to preclude diffusion of neutral vapors and incompletely dried drops from the ionization chamber into the DMA slit.

In order to compensate for the MS consumption of 2.5 L/min through its sampling orifice, the same flow of nitrogen was introduced into the recirculating DMA drift gas. The electrospray silica capillary used was a New Objective (Woburn, Massachusetts, USA) TaperTip: 360 µm o.d., 50 µm i.d., 50 cm in length, noncoated (ref. TT360-50-50-N-5).

Table 2. Precursor and Product Ions Analyzed Depending on the Ionization Source Used for the Calculation of *TR*

Source	Precursor ion		Product ion	
	Identity	Mass (Da)	Identity	Mass (Da)
APCI	NG-NO_3^-	289	NO_3^-	62
ES	NG-Cl^-	262	NO_2^-	46

The gas used in the DMA drift gas circuit and in the heated drying gas was produced by a nitrogen generator (NitroFlow basic from Parker Hannifin (Cleveland, USA) 99.95% purity). This nitrogen is subsequently purified using oxygen and hydrocarbon traps (SGT Oxigen TrapCO1002 and Hydrocarbon Trap CO1003). With this nitrogen configuration, the same DMA *TR* is found as when using 99.9992% purity bottled nitrogen, indicating that extremely high nitrogen purity is not essential to achieve good DMA *TR*.

The nozzle guiding the drying gas is metallic and floats 1.8 kV above the DMA inlet electrode, yielding a local electric field of ~1 kV/mm. The electrospray tip floats above the metallic nozzle at a voltage of 1.2 kV. With this electric configuration, the residence time of an ion with mobility of 1 cm^2/V/s, from the electrospray to the DMA (separated 3 mm), is approximately 37.5 μs, resulting in negligible dilution effects by space charge and diffusion.

The DMA, the drift gas recirculation circuit, and the DMA blower were the same ones used with the APCI source. The intercooler and DMA heater were used at all times. Only Teflon tubing was used in the N_2 supply lines.

Desolvating-LFSESI Ionization Source

After successful development of the Desolvating-nanoESI ionization source, a secondary ESI (SESI) source was designed for vapor ionization. This SESI source differs from the prior ESI source in that the drying gas cannot be allowed to flow through the ES region. Otherwise it would dilute the incoming sample vapor, whose flow rate needs to be very small in order for the sample to be efficienly ionized [20]. An intermediate "impact" chamber (Figure 3c- region between electrodes 15 and 16) must therefore be introduced, where the small sample flow collides frontally against the drying gas, both streams being rejected laterally, while the ionized species are driven downstream by the field [20]. Evaluation of *TR* for the SESI setup relied as before on NG ions introduced by electrospraying a 500 ppb NG solution. This convenient ion source was suitable to test the system's ability to remove vapors, but could not measure the SESI ionization efficiency. For evaluation of the ionization efficiency the NG was withdrawn from the ES solvent, and small quantities (pg) of a solution containing various explosives was deposited in a filter. This material was subsequently vaporized in a thermal desorber into the sample gas fed to the ionizer. A relatively volatile electrospray solution MeOH-H_2O 9:1, HCl 0.05% was used, which tends to boil at the high temperature (170 °C) required to prevent internal contamination in the ionization source (analyte memory effects). The lack of an electrospray cooling casing had limited the viable range of liquid flow rates and temperatures in the prior ESI source (Figure 3b), so this feature (Figure 3c- item 13) was added here to protect the liquid meniscus from the heated first electrode facing it (Figure 3c- item 14).

An electric field between the electrospray liquid and a first electrode (Figure 3c- item 14) (1.5 kV/mm) drives the ions and droplets generated by the electrospray towards the vapor ionization region, defined by the first and second electrodes (Figure 3c- items 14 and 15, respectively). A 0.2 lpm sample flow carries the explosive vapors from the desorber to the vapor ionization region through eight holes that create an approximately symmetric flow (Figure 3c- sample flow lines). In the ionization region, analyte vapor molecules interact with the electrospray ions and droplets, generating analyte ions that drift towards the next region through an electric field (0.3–0.08 kV/mm) between the first and second electrodes. The magnitude of this electric field modifies the trajectories of the field lines in the ionization region. The corresponding change in ion residence time has a strong influence on the efficiency of vapor ionization, which should ideally be optimized for each analyte. High electric fields improve the gain (counts/femtogram) for chemically labile analytes, while low electric fields improve the gain for stable and temperature-resistant analytes.

The *impact region* defined between the second and third electrodes (Figure 3c- items 15 and 16, respectively) prevents the drying gas counterflow (Figure 3c- black filled lines) from diluting the sample vapors, avoiding associated reductions in the efficiency of ionization [20]. Large droplets and neutral vapors from non-ionized sample and from the electrospray solvent are eliminated through this *impact region*. The electric field between the second and third electrodes (0.4 kV/mm), pushes the ions towards the next *desolvation region*, delimited by the third electrode and the DMA inlet electrode (Figure 3c- items 16 and 6, respectively). Small charged droplets are completely desolvated in this region via a symmetric heated drying gas counterflow N_2 current (Figure 3c- black filled lines). This stream (1–3 L/min) desolvates small droplets, dragging upwards the neutral vapors produced by the evaporation process to the impact region and later to the exhaust outlet. An electric field (0.5 kV/mm) between the third electrode and the DMA inlet electrode drives the ions downwards against the drying counterflow current, injecting them into the DMA. The drying gas reaches the temperature of the third electrode while transiting through a labyrinthine path milled in this part. The temperature in each electrode is independently adjustable, though the temperature used in this study was 170 °C in all three electrodes. Small flows (~0.25 lpm) through the DMA entrance slit in both directions do not affect the desolvation efficiency.

The DMA outlet electrode (Figure 3c- item 7) is at the same potential as the MS orifice (approximately grounded), whereas the inlet electrode (Figure 3c- item 6) floats above it; the high voltage power supply (HVPS) used to ramp the DMA inlet electrode voltage was an applied kilovolts HP-005ZIP025. The HVPSs used in the three electrodes of the Desolvating-LFSESI and in the electrospray (Figure 3c- items 16, 15, 14, and 11) were EMCO E-series. In the Desolvating-nanoESI two EMCO E-series were used for the nozzle electrode and for the electrospray, and in the APCI only one EMCO E-series was used for the corona discharge.

At a DMA blower speed of 12000 revs/min, all the explosives left the DMA at voltages lower than −1700 V. Table 3 shows the voltages used in the different electrodes and electrospray in the test reported in this work, as well as in the optimization tests.

The EMCO HVPS, especially the electrospray HVPS, which is at the highest voltage (it floats above the other voltages), withstood the voltages reported with no failure.

The electrospray silica capillary used was a New Objective TaperTip: 360 µm o.d., 50 µm i.d., 15 µm tip i.d., 80 cm in length, noncoated (ref. FS360-50-15-N-5-C80). The desorber is made of aluminum with Viton gaskets, and the transfer line that joins the desorber with the ionization chamber consists of heated fused silica-lined stainless steel tubing. The N_2 used, the DMA, the drift gas recirculation circuit, the DMA blower, and the N_2 supply lines were as in the Desolvating-nanoESI source. The DMA blower intercooler and the DMA heater were used at all times.

For the gain calculations presented in Table 4, 2 µL of explosive dissolved in MeOH are deposited into a stainless steel mesh filter + Tenax GR + glass fiber. The concentration of the explosive in the solvent is 50 ppb for EGDN, 12.5 ppb for NG, and 2.5 ppb for RDX, PETN, and TNT. After the solvent evaporates, the filter is inserted into the desorber, where the solid sample vaporizes at a temperature of 200 °C, the same temperature as the transfer line that carries the sample vapors to the ionization chamber. The DMA is synchronized with the MS (TripleQuad 5500), and selects an explosive every 100 ms, which the MS measures in multiple reaction monitoring mode. The DMA voltage is calibrated periodically by an internal calibrant present in the ES solvent. Extrapolation allows the voltage V_{DMA} for each explosive's peak to be determined, as this value varies with changes in atmospheric pressure. The extrapolation coefficients were calculated prior to the experiment.

The gain factor is obtained by integrating, for 45 s, the counts per second registered in the desorption spectrum, omitting the background present before inserting the filter into the desorber.

Results

APCI Source

As previously noted, the lack of ES solvent in this ionization source permits studying the effect of N_2 purity and DMA blower temperature, on the internal background and on the *TR* of the DMA.

Figure 4 includes several two-dimensional (2D) DMA-MS spectra with *m/z* for the first quadrupole Q1 (no fragmentation in Q2, with Q3 transmitting all ions) in the vertical axis, the DMA voltage V_{DMA} (inversely proportional to ion mobility) in the horizontal axis, and ion signal represented in a logarithmic color scale. Figure 4a (relatively impure gas from the N_2 generator) shows numerous long horizontal lines, bound to the left at ~50 V (Z_{max} > 40 $cm^2/V/s$), and to the right by a broad inclined band. Z_{max} is far too large to correspond to ions drifting in N_2, so these long lines must originate from electrons entering into the DMA. These electrons attach to neutral vapors within the analyzer region, resulting in mobilities intermediate between their own (left bound of the line) and that of the ionized vapor (right bound of the line). Many electrons generated by the negative discharge evidently survive in the N_2 environment of the ionizer, and then attach to electronegative species present dominantly in the closed DMA circuit. Electron attachment to vapor species within the DMA accordingly provides a sensitive diagnostic tool to evaluate the level of gas-phase contamination of the closed DMA circuit.

Figure 4a shows additional horizontal bands beginning at ~1050 V. This voltage corresponds to NO_2^- and NO_3^- ions (*m/z* 46 and 62), abundantly produced by the negative discharge. Like the electrons, these ions penetrate the DMA and ionize vapor impurities in the drift gas. Interestingly, the mass interval separating the most intense high-mobility tails is 50 Da, both for vapor ionization with electrons and ions; *m/z* = 50 corresponds to CF_2, the repeat unit of Teflon [24, 25], probably from the compressor pistons of the N_2 generator used. The striking observation that neutral $(CF_2)_n$ fragments with masses going well beyond 700 *m/z* are volatile enough to produce such a considerable signal may be explained in part by the high electron ionization efficiency of electronegative species.

Comparing Figure 4a and b, one notices a significant (5-fold) reduction in internal background, achieved by substituting N_2 from a generator (99.5% purity) with N_2 from a bottle (99.9992% purity) (Figure 4d, circles and crosses). The marked reduction in the high mobility tails with 50 Da separation confirms that most of the $(CF_2)_n$ impurities originate from the N_2 generator. Indeed, when using the vapor traps on the line coming from the N_2 generator, the high mobility tails decay substantially, but remain more intense than when using 99.9992% purity bottled N_2.

In view of the high purity of the N_2 used in Figure 4b, much of the remaining background must originate from the DMA. We substantially reduced vapor release from the DMA blower

Table 3. Voltages Used in the DMA and in the Different Electrodes of the Desolvating-LFSESI During the Optimization and in the Final Configuration (Explosive Gain Test)

		DMA inlet electrode	DMA outlet electrode	Electrode 3	Electrode 2	Electrode 1	ES
Voltages used in tests reported	Relative voltage (V)	-1700	-950	-1512	-293	-1822	
	Absolute voltage (V)	0	-1700	-2650	-4162	-4455	-6277
Maximum voltages tested in optimization	Relative voltage (V)	-1700	-950	-1512	-1480	-1822	
	Absolute voltage (V)	0	-1700	-2650	-4162	-5642	-7464

Table 4. Gain (Counts per Femtogram) for Different Explosives with the LFSESI Ionizer and the New SEADM's Desolvating-LFSESI Ionizer

Explosive	LFSESI	Desolvating-LFSESI	Gain factor
EGDN	0.43	1.30	3.1
RDX	76	130	1.7
PENT	21	78	3.6
NG	15	42	2.8
TNT	40	190	4.8
Average improvement factor			3.2

by refrigerating it down to 35 °C via an intercooler. The DMA and the rest of the drift gas recirculation circuit are maintained at 120 °C by a DMA heater, with the aim of minimizing surface adsorption of contaminants. We also heat up the ionization chamber, in this case up to 230 °C, leading to the "*Low Outgassing DMA*" spectrum shown in Figure 4c. Comparing scenarios (c) and (a), the counts received in the MS detector are reduced by a factor of 30 (Figure 4d, continuous line versus circles). The high mobility tail levels (between 0 and 600 V) quantifying vapor contamination within the DMA are reduced by a factor >200, but traces of them remain, perhaps from the Teflon-coated o-rings used in the DMA.

Figure 5 shows mass-resolved mobility spectra for nitroglycerin, with and without pump cooling. Both the heater and the intercooler were included in the DMA circuit. However, in the first experiment (line with triangles in Figure 5 left) the intercooler fan was not working, resulting in a DMA pump temperature of 83 °C with both high and low mobility tails in the spectrum that yielded $TR = 1.5 \times 10^4$. Since we were working with a solvent-free source, acceptable *TR* were obtained even with a hot DMA blower. Forty min after the intercooler fan started working and the blower temperature reached 28 °C, both high and low mobility tails were strongly reduced, yielding $TR \sim 10^5$ (line with squares in Figure 5 left).

We have analyzed the *TR* of NG peaks in the *Low Outgassing* scenario of Figure 4c. In a sample of five mobility sweeps, we obtain an average TR of 1.7×10^5. The fact that it exceeds the ideal value for a Gaussian (0.655×10^5) suggests that the tails of our mobility peaks do not have a perfect Gaussian shape. Figure 5 right shows the shape of a NG peak obtained with the APCI source. Intensity points higher than 1×10^{-1} fit a Gaussian well, but the deeper tail of the peak decays faster, explaining the larger *TR* obtained.

Desolvating-NanoESI Ionization Source

At fixed electrospray conditions and electric fields, the two factors affecting desolvation most are the drying gas flow rate and its temperature. The heated drying gas effectively desolvates the ES droplets, limiting low mobility tails. The drying gas avoids vapor ingestion and DMA drift gas contamination responsible for low and high mobility tails. Figure 6a and b show the dependence of *TR* on drying gas flowrate and temperature (a), or on signal intensity (b). Higher drying gas counterflows achieve better desolvation for the same drying gas temperature, but the signal is far higher at the smaller gas counterflow. Working with a 160 °C drying gas temperature, the *TR* achieved is approximately the same in both drying flow rate scenarios, about $TR = 1.3 \times 10^5$. Figure 6b shows a moderate loss of signal working with 1.5 L/min drying gas counterflow, due to thermal degradation of nitroglycerin when the temperature increases. This loss is not noticeable at 3 L/min drying gas counterflow.

The optimal operational conditions depend on the analyte, but it is generally preferable to operate with low drying gas flow rates (1.5 L/min) and as high as possible drying gas temperatures (160 °C), in order to reduce the residence time of the ions in the ionization chamber, in turn minimizing the loss of transmission associated to Brownian diffusion and space charge.

Desolvating-LFSESI Ionization Source

In view of the excellent performance of the Desolvating-nanoESI ionization source (with NG ions originating from the liquid phase), we proceeded to test the Desolvating-LFSESI

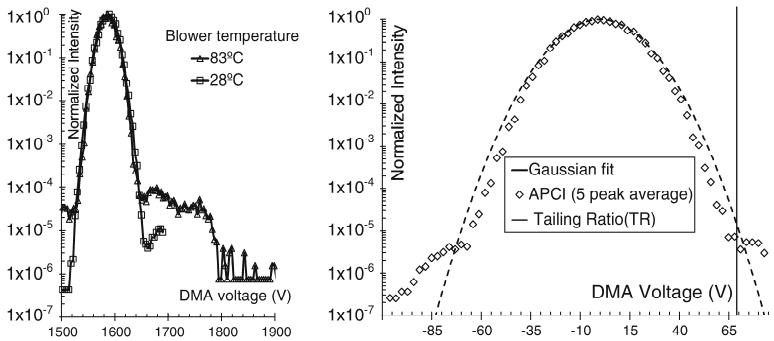

Figure 5. Left: mass-resolved mobility spectrum for NG, comparing the performance with and without blower cooling. Right: NG peak shape (average of 5 peaks) compared to a Gausian

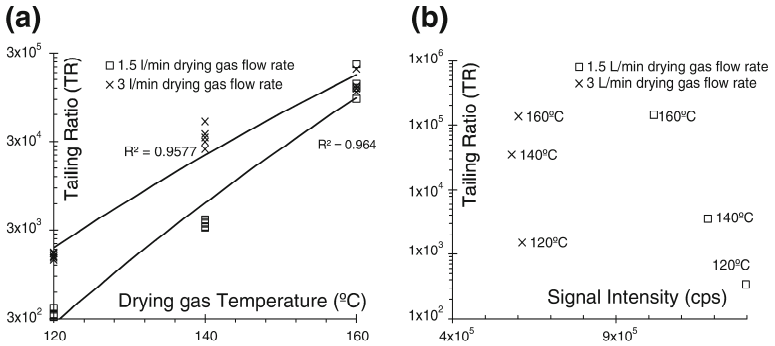

Figure 6. *TR* dependence on (**a**) drying gas counterflow temperature and flow rate; (**b**) signal intensity for the two drying gas flow rates tested at the indicated drying gas temperatures

designed to ionize neutral vapors in the gas phase. The parameters defining the operating point are drying gas flow, residence time (that depends on the sample flow rate from the desorber and on the electric fields in the ionization source), the temperature of each of the three ionization source electrodes, the pressure in the capillary of the electrospray, and its tip diameter. Figure 7 presents *TR* results obtained after optimizing these parameters, also comparing them with those of SEADM's prior LFSESI, having no intercooler for the DMA blower and no DMA heater. The average enhancement factor of *TR* for SESI is 143. Table 4 compares the gain obtained with these two ionizers for various explosives, with MS/MS settings summarized in Table 5. These tests introduced the explosives in vapor form with the sample gas. The operational conditions for the comparison are summarized in Table 6. The mass spectrometers were the same. The DMAs changed slightly due to a modification in the depth of the entrance slit, which was reduced from 0.15 mm (P5-e DMA) to 0.093 mm (P5-f DMA).

The optimization of electric fields and other design parameters have increased the sensitivity by a factor of 3. These improvements include a smaller capillary tip (15 µm versus 50 µm, with a smaller tendency to arc in negative mode), and the shift to a methanol/water electrospray that dries much faster yielding ions closer to the tip. The depth reduction in the DMA entrance slit also contributed to the improvement of gain registered. Notice that a TNT ion is detected for each 1.4 10^4 neutral TNT molecules desorbed. Assuming that the MS transmission efficiency of ions from the atmospheric inlet to the detector is 10^{-2} in MS/MS mode, and taking the DMA to transmit 100% of the ions, one out of every 140 neutral TNT molecules would be ionized! This ionization probability may appear as small given that electrospray ionization is in some instances able to convert 100% of specific solution species into ions. Notice, however, that SESI (secondary ESI) ionizes gas-phase vapors rather than solutes, and does so far less efficiently by charge transfer from solution ions (Cl^- in our case) into neutral vapors. Given enough time of exposure of the vapors to the spray, an equilibrium condition is reached where the rate of ion production is balanced by the rate of dilution by space charge. In this limit the estimated equilibrium ratio between ionized and neutral vapors for a unipolar charger is of the order of $n_i/n_v \sim 10^{-4}$ [26]. The vapor ionization probability achieved of 1/140 is accordingly remarkably high. Much of the improvement observed

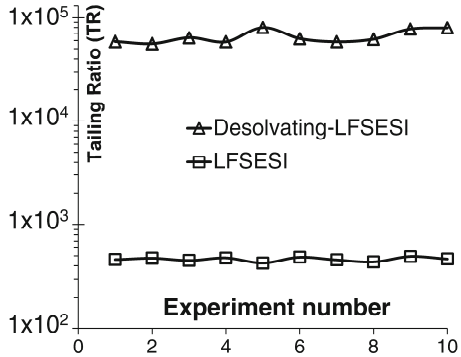

Figure 7. Comparison of *TR* for the Desolvating-LFSESI (6.6 10^4 mean) and its predecessor the LFSESI (4.6 10^2 mean)

Table 5. Ionization Mechanism and Precursor and Product Ions Selected in the MS Using Negative Multireaction Monitoring Mode (MRM)

Explosive	Precursor ion		Product ion	
	Mass (Da)	Composition	Mass (Da)	Composition
EGDN[a]	187	EGDN-Cl^-	62	NO_3^-
RDX[b]	257	RDX-Cl^-	46	NO_2^-
PENT[c]	351	PETN-Cl^-	62	NO_3^-
NG[d]	262	NG-Cl^-	46	NO_2^-
TNT[e]	226	$(TNT\text{-}H^+)^-$	46	NO_2^-

[a]Ethylene glycol dinitrate.
[b]1,3,5-Trinitroperhydro-1,3,5-triazine.
[c]Pentaerythritol tetranitrate.
[d]Nitroglycerin.
[e]Trinitrotoluene.

Table 6. Operation Conditions of Configurations Compared in Table 4

	LFSESI	Desolvating-LFSESI
ES Solvent	DMSO:Octanol 75:25 HCl 0.1%	MeOH:H_2O 9:1 HCl 0.05%
Ion source temperature (°C)	170	170
Electrospray liquid pressure (mbar)	570	249
Sample flow (l pm)	0.2	0.2
Electrospray voltage (V)	–2600	–1822
Electric field between ES and El1 (V/mm)	–433	–911
El1 voltage (V)	–1600	–293
Electric field between El1 and El2 (V/mm)	–744	–117.2
El2 voltage (V)	–600	–1512
Electric field between El2/DMA (LFSESI) and El2/El3 (D-LFSESI) (V/mm)	–400	–385
El3 voltage (V)	–	–950
Electric field between El3 and DMA (V/mm)	–	–452
DMA used	DMA P5-e	DMA P5-f
Mass spectrometer	TripleQuad5500	TripleQuad5500

is due to the previously described low flow SESI approach [20], based on which a gain of 30 counts/fg had been demonstrated previously. The ionization probability of LFSESI manages to exceed greatly the equilibrium n_i/n_v value because the ions are quickly extracted by the fields as they are produced, while the vapor is discarded very slowly by the prevalent low sample flow rate. Our measurements here with that earlier SESI source achieve a slightly higher 40 counts/fg, while the new Desolvating LFSESI source reaches 190 counts/fg, almost five times larger.

Conclusions

Three new ionization sources specially designed to be coupled to a DMA have achieved complete elimination of vapors and associated ion clustering. Combined with an essentially vapor-free DMA gas recirculation circuit (including a cooled commercial blower), this improvement yields ideal tail-free mobility peaks with a *TR* much larger than previously observed, reaching the theoretical limit ~10^5. This improvement has led to a greatly enhanced capacity of the DMA-MS combination to analyze complex mixtures, including explosives in the atmosphere at concentrations below 10^{-2} ppq [19]. The Desolvating-LFSESI source has been optimized for maximum sensitivity, delivering an unprecedented gain for TNT of 190 counts/fg, equivalent to an ionization efficiency of one out of 140 neutral molecules. Electron, Cl, NO_2 and NO_3 ionization within the DMA was used as a sensitive diagnostic tool to evaluate the level of gas-phase contamination of the closed DMA circuit. Extremely high nitrogen purity is not essential to achieve good DMA *TR* in a background free MS/MS channel, as comparable *TR* values are obtained with 99.9992% and 99.95% purity nitrogens.

Acknowledgements

The authors thank Dr. Anatoly Verenchikov for stressing the interest of improving the *TR* in DMA-MS coupling.

Compliance with Ethical Standards

Conflict of Interest Following Yale rules, Juan Fernandez de la Mora declares a financial interest in the company SEADM.

References

1. Hogan, C.J., Fernandez de la Mora, J.: Ion-pair evaporation from ionic liquid clusters. J. Am. Soc. Mass Spectrom. **21**, 1382–1386 (2010)
2. Hogan, C.J., Fernandez de la Mora, J.: Tandem ion mobility-mass spectrometry (IMS-MS) study of ion evaporation from ionic liquid-acetonitrile nanodrops. Phys. Chem. Chem. Phys. **11**, 8079–8090 (2009)
3. Fernández de la Mora, J., Casado, A., Fernández de la Mora, G.: Method to accurately discriminate gas phase ions with several filtering devices in tandem. US patents 7,855,360 (December 21, 2010), 278,622 (2/October/2012)
4. Purves, R.W., Guevremont, R., Day, S., Pipich, C.W., Matyjaszczyk, M.S.: Mass spectrometric characterization of a high-field asymmetric waveform ion mobility spectrometer. Rev. Sci. Instrum. **69**, 4094–4104 (1998)
5. Schneider, B.B., Covey, T.R., Coy, S.L., Krylov, E.V., Nazarov, E.G.: Chemical effects in the separation process of a differential mobility/mass spectrometer system. Anal. Chem. **82**(5), 1867–1880 (2010)
6. Shvartsburg, A.A.: Differential Ion Mobility Spectrometry: Nonlinear Ion Transport and Fundamentals of FAIMS. CRC Press, Boca Raton (2008)
7. Vidal-de-Miguel, G., Macía, M., Cuevas, J.: Transversal modulation ion mobility spectrometry (TM-IMS), a new mobility filter overcoming turbulence-related limitations. Anal. Chem. **84**, 7831–7837 (2012)
8. Vidal-de-Miguel, G., Macía, M., Barrios, C., Cuevas, J.: Transversal modulation ion mobility spectrometry (IMS) coupled with mass spectrometry (MS): exploring the IMS-IMS-MS possibilities of the instrument. Anal. Chem. **87**(3), 1925–1932 (2015)
9. Gillig, K.J., Chen, C.H.: Increasing the performance of portable ion mobility analyzers: development of the periodic focusing differential mobility analyzer (PFDMA), Mass Spectrom (Mass Spectrometry Society of Japan, Tokyo, Japan), **3**, Special Issue S0032 (2014). See also Gillig K.J. and Chen, C.H.: Periodic field differential mobility analyzer. US Patent Application Publication US 2013/0187042 A1, Jul. 25 (2013)
10. Kurulugama, R.T., Nachtigall, F.M., Lee, S., Valentine, S.J., Clemmer, D.E.: Overtone mobility spectrometry: part 1. Experimental observations. J. Am. Soc. Mass Spectrom. **20**(5), 729–737 (2009)
11. Knutson, E., Whitby, K.: Aerosol classification by electric mobility: apparatus, theory, and applications. J. Aerosol Sci. **6**, 443–451 (1975)
12. Labowsky, M., Fernandez de la Mora, J.: Novel ion mobility analyzers and filters. J. Aerosol Sci. **37**(3), 340–362 (2006)
13. Rus, J., Moro, D., Sillero, J.A., Royuela, J., Casado, A., Fernández de la Mora, J.: IMS-MS studies based on coupling a differential mobility

analyzer (DMA) to commercial API-MS systems. Int. J. Mass Spectrom. **298**, 30–40 (2010)
14. Hogan, C.J., Ruotolo, B., Robinson, C., Fernandez de la Mora, J.: Tandem differential mobility analysis-mass spectrometry reveals partial gas-phase collapse of the GroEL complex. J. Phys. Chem. B **115**(13), 3614–3621 (2011)
15. Larriba-Andaluz, C., Fernandez de la Mora, J.: Gas-phase structure of Coulombically stretched polyethylene glycol ions. J. Phys. Chem. B **116**, 593–598 (2012)
16. Criado, E., Fernández-García, J., Fernández de la Mora, J.: Mass and charge distribution analysis of large polyethylene glycol chains by negative electrospray ion mobility mass spectrometry (NES-IMS-MS). Anal. Chem. **85**(5), 2710–2716 (2013)
17. Fernández-García, J., Fernández de la Mora, J.: Measuring the effect of ion-induced drift-gas polarization on the electrical mobilities of multiply-charged ionic liquid nanodrops in air. J. Am. Soc. Mass Spectrom. **24**, 1872–1889 (2013)
18. Javaheri, H., Le Blanc, Y., Thomson, B.A., Fernandez de la Mora, J., Rus, J., Sillero-Sepúlveda, JA.: Analytical characteristic of a differential mobility analyzer coupled to a triple quadrupole system (DMA-MSMS), poster 061, in: proceedings of the Annual ASMS Conference. Denver, 1–6 June (2008) Available at: http://www.seadm.com/descargas/ASMS_2008_DMA_Poster_Bruce_V3.pdf)
19. Zamora, D., Amo-Gonzalez, M., Lanza M., Fernández de la Mora, G., Fernández de la Mora, J.: Reaching a vapor sensitivity of 0.01 parts per quadrillion in the screening of large volume freight. [submied to Anal. Chem., March/3/2017] Also, Amo, M., Zamora, D., Casado, A., Fernandez de la Mora, G., Vidal-de-Miguel, G., Fernandez de la Mora, J.: Method for detecting atmospheric vapors at parts per quadrillion (ppq) concentrations, US Patent 9,297,785, 29 March (2016)
20. Vidal-de-Miguel, G., Macia, M., Pinacho, P., Blanco, J.: Low-sample flow secondary electrospray ionization: improving vapor ionization efficiency. Anal. Chem. **84**(20), 8475–8479 (2012)
21. French, J.B., Reid, N.M., Buckley, J.A.: Method and apparatus for analyzing trace components using a gas curtain. US Patent 4,137,750 (1979)
22. Thomson, B.A., Iribarne, J.V.: Field-induced ion evaporation from liquid surfaces at atmospheric pressure. J. Chem. Phys. **71**(11), 4451–4463 (1979)
23. Yamashita, M., Fenn, J.B.: Electrospray ion source, another variation of the free jet theme. J. Phys. Chem. **88**(20), 4459–4465 (1984)
24. Amo, M., Fernández-de la Mora, J.: Limits to the chemical background and the mobility-selected current transmitted in a differential mobility analyser (DMA). Proceedings of the 62nd ASMS Conference on Mass Spectrometry and Allied Topics; Baltimore, Jun (2014)
25. Maißer, A., Thomas, J.M., Larriba-Andaluz, C., He, S., Hogan Jr., C.J.: The mass-mobility distributions of ions produced by a Po-210 source in air. J. Aerosol Sci. **90**, 36–50 (2015)
26. Fernandez de la Mora, J.: Ionization of vapor molecules by an electrospray cloud. Int. J. Mass Spectrom. **300**, 182–193 (2011)

CHAPTER 2. PLANAR DIFFERENTIAL MOBILITY ANALYZER WITH A RESOLVING POWER OF 110

analytical chemistry

Article

Cite This: *Anal. Chem.* 2018, 90, 6735−6741

pubs.acs.org/ac

Planar Differential Mobility Analyzer with a Resolving Power of 110

Mario Amo-González* and Sergio Pérez

SEADM, Parque Tecnológico de Boecillo 205, Valladolid 47151, Spain

ABSTRACT: Planar differential mobility analyzers (DMAs) have previously achieved resolving powers of 60−80 in air or N_2 at the mobility of the tetraheptylammonium ion (THA^+, ~0.97 $cm^2/V/s$). For unclear reasons, this performance is considerably below the theoretical limit. In this work, a performance close to this ideal limit is attained in SEADM's P5 DMA via improved flow laminarization, under otherwise the same flow conditions as in prior work. The new laminarizer remains effective at unusually large gas velocities (reached with two blowers in series), yielding a resolving power of 110. The selectivity of the improved DMA combined with a mass spectrometer was assessed by the analysis of a real sample of extra virgin olive oil.

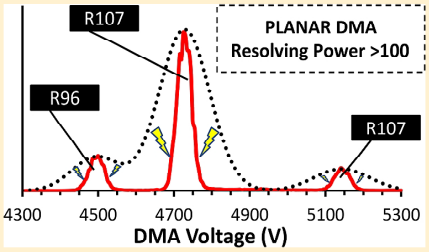

In spite of the much larger resolving power of other mass spectrometers (MS), the quadrupole MS (Q-MS) remains one of the most widely used MS types, thanks to its ability to operate as a narrow-band mass filter, which extracts a single ion mass-to-charge ratio out of a complex mix for subsequent study or manipulation. Various narrow-band ion-mobility filters achieving a similar function at atmospheric pressure are known. Examples include field asymmetric ion-mobility spectrometry (FAIMS, also referred to as differential-mobility spectrometry, DMS),[1−4] transversal-modulation IMS (TMIMS),[5,6] the periodic-focusing differential-mobility analyzer (PFDMA),[7] overtone mobility spectrometry (OMS),[8] and others. With singly charged ions, the current resolving power of narrow-band ion-mobility filters is below that of other mobility devices, such as drift-tube IMS (DT-IMS),[9−11] high-resolution ion-cyclotron-mobility spectrometry (HR-ICMS),[12] and trapped-ion-mobility spectrometry (TIMS,[13] see the resolution comparison in Table 1).

Here we focus on the differential mobility analyzer (DMA),[14] which combines a DC electric field and a steady-flow field of drift gas[15] to select a narrow range of linear mobilities at ambient pressure. The DMA can be easily included in the ion-source region of atmospheric-pressure-ionization (API) MS systems,[16−20] thereby removing 98−99% of the ion mobilities in a complex mix,[21] while being able to shift from one mobility to another in a few milliseconds. Its combination in series with a Q-MS for single-ion monitoring (SIM) offers transmission efficiencies and analysis times similar to those required for Q-MS analysis but with greatly increased resolving power.[22,23] Planar-DMA transmission was studied by Rus and co-workers,[24] reporting transmissions of ~50%. The DMA's noise-suppression ability has been demonstrated in monitoring for explosives in the exceedingly complex mixture of vapors characteristic of the atmosphere at concentrations as low as 0.01 parts per quadrillion (1ppq = 10^{-15} atmospheres of partial pressure).[25,26] At this sensitivity, there are two main limiting features: the DMA resolving power (defined as the mean ion mobility divided by the full mobility width at half-maximum, fwhm) and the tailing ratio (TR, defined as the signal at the peak maximum divided by the signal two half-widths away from this maximum). TR is primarily limited by incomplete desolvation of abundant contaminant vapors, which obscure the presence of traces of analytes of interest. The tailing ratio of the DMA has recently been raised to the theoretical limit (~10^5) by improving gas purity.[27] Increasing the resolving power, R, of DMAs, however, has been challenging.

Assuming that variances are additive,[28] the full width at half-maximum for a planar DMA is given by the following formula:

$$\left(\frac{\Delta L_{0.5}}{L}\right)^2 = \left(\frac{W}{L_{slit}}\frac{q_a + q_s}{Q_c + Q_m}\right)^2 + \left(\frac{2\sigma\sqrt{2\ln 2}}{L}\frac{\sqrt{L^2 + h^2}}{h}\right)^2 \quad (1)$$

where W is the width of the DMA channel at the outlet slit (14.9 mm), L_{slit} is the monodisperse-sampling-slit length (6.5 mm), q_s is the monodisperse-sampling flow rate, q_a is the polydisperse-aerosol flow rate, Q_c is the flow rate at the DMA sheath-gas inlet, Q_m is the flow rate at the DMA sheath-gas outlet, $2\sigma(2\ln 2)^{1/2}$ is the width at half-maximum of a Gaussian distribution, L is the separation-channel length, h is the normal distance between electrodes, and $((L^2 + h^2)^{1/2})/h$ is the projection of the Gaussian-distribution width into the outlet electrode. In short, the first term of eq 1 is the Knutson−Whitby[14] relative half-width of the mobility band for a planar DMA in which the monodisperse-aerosol-slit length is shorter than the DMA-channel width, whereas the second term takes into account the effect of Brownian diffusion studied by Tammet[29] and Stolzenburg.[30] In this planar DMA, the

Received: February 3, 2018
Accepted: May 7, 2018
Published: May 7, 2018

   DOI: 10.1021/acs.analchem.8b00579
Anal. Chem. 2018, 90, 6735−6741

Table 1. Comparison among Different Ion-Mobility-Spectrometry Technologies in Terms of Resolving Power for Singly Charged Particles

	mobility filter	resolving power	ion	analyte	m/z
FAIMS/DMS	yes	69	$[M + H]^+$	reserpine	609.3
OMS	yes	70	$[M + Na]^+$	raffinose	527.4
PFDMA	yes	40	$[M - Br]^+$	THABr	410.8
TMIMS	yes	70	$[M - Br]^+$	THABr	410.8
DMA	yes	110	$[M - Br]^+$	THABr	410.8
DT-IMS	no	100−150	$[M + H]^+$	peptides	—
DT-IMS	no	162	$[M + H]^+$	arginine	175.2
DT-IMS	no	172	C_{60}^+	fullerene	720.6
HR-ICMS	no	215	$[M + Na]^+$	raffinose	527.4
TIMS	no	355	$[M - H]^-$	3-OH-BDE-47	500.7

polydisperse sample is electrically pushed through the inlet slit; indeed, a small counterflow q_a (0.5 L/min in this work) is exhausted through the inlet slit in order to prevent droplets from entering the DMA. Then, for the relative half-width calculation, q_a is considered as 0. The flow balance in the DMA is $Q_c = Q_m + q_s + q_a$. Because q_a and q_s are much lower than Q_c and Q_m, the following simplification may be assumed with little error: $Q_c \sim Q_m \rightarrow Q_c = Q_m = Q$, where Q is the sheath-gas flow rate through the separation channel. Hereafter, only Q will be considered.

The variance of a Gaussian distribution, $\sigma^2 = 2Dt$, is controlled by the ion's time of residence in the DMA, t, and the diffusion coefficient of the ions in the sheath gas, D. The Einstein relation ($D = ZkT/N_e$), relates D with the electrical mobility, Z; the Boltzmann's constant, k; the gas absolute temperature, T; and the net charge on the particle, N_e. The time of residence, t, in the planar DMA can be expressed as follows:

$$t = \frac{L}{U} = \left(\frac{h}{ZEL}\right)L = \frac{h^2}{ZV_{DMA}} \tag{2}$$

where E is the electric field between the DMA electrodes, and V_{DMA} is the voltage between the electrodes. Therefore, σ^2 can be expressed as

$$\sigma^2 = 2Dt = 2\frac{ZkT}{N_e}t = 2\frac{ZkT}{N_e}\frac{h^2}{ZV_{DMA}} = \frac{2kTh^2}{V_{DMA}N_e} \tag{3}$$

Q can be expressed as a function of the Reynolds number:

$$\mathrm{Re} = \frac{Uh}{\nu} = \frac{Q}{W\nu} \tag{4}$$

where U is the sheath-gas velocity in the DMA channel, and ν is the kinematic viscosity of the gas. Then, eq 1 can be rewritten as

$$R^{-1} = \frac{\Delta L_{0.5}}{L} = \frac{q_a}{L_{slit}2\mathrm{Re}\nu} + \sqrt{\frac{16\ln 2kT}{V_{DMA}N_e}\left[1 + \left(\frac{h}{L}\right)^2\right]} \tag{5}$$

Convective-diffusion problems at large Reynolds numbers are well-known to be governed by the Peclet number, Pe,[31] defined as

$$\mathrm{Pe} = \mathrm{Re}\frac{\nu}{D} = \frac{Uh}{D} = \frac{ZV_{DMA}L}{hD} = \frac{V_{DMA}LN_e}{hkT} \tag{6}$$

Therefore, eq 5 can be expressed as a function of Pe:

$$R^{-1} = \frac{\Delta L_{0.5}}{L} = \frac{q_a}{L_{slit}2\mathrm{Re}\nu} + \sqrt{\frac{16\ln 2}{\mathrm{Pe}}\left(\frac{L}{h} + \frac{h}{L}\right)} \tag{7}$$

For a fixed DMA geometry and a fixed ion-gas pair (i.e., ν and D are constant), the resolving power increases essentially with $\sqrt{\mathrm{Re}}$, and because the sheath-gas velocity, U, and the DMA voltage are linearly connected, ultimately the resolution in the DMA increases with $\sqrt{V_{DMA}}$, which is limited by electrical-breakdown considerations. For a fixed Reynolds number, the resolution will increase when the Schmidt number (ν/D) increases; that is to say it will be better for the less diffusive ions, increasing approximately with $\sqrt{\mathrm{Pe}}$ or $1/\sqrt{D}$. Achieving a resolving power of 110 then requires a very large Pe, $\sim 8.7 \times 10^5$. However, Pe is proportional to the fluid velocity, and given that small ions have D/ν ratios of order unity, it follows that Re must also be on the order of 1.4×10^5, a condition under which most flows tend to become turbulent. There are two types of challenges. First, to achieve such high Re in a device of small dimensions, the flow velocity needs to be of hundreds of meters per second (U_{max} = 214 m/s in this work). Second, the natural instability of high-Re flows must be counteracted by an inlet free from perturbations that would otherwise quickly result in turbulence.[32] In this work, we will optimize the laminarization stage of the P5 DMA and increase the Reynolds number in the separation region.

METHODS

DMA. SEADM's DMA P5-G was used with the critical dimensions collected in Table 2.

Table 2. Critical Dimensions (mm) of SEADM's P5-G DMA

	W^a	h^b	L^c	$W_{slit}{}^d$	$L_{slit}{}^e$	D^f
inlet	17	10	40	0.6	7	
outlet	14.9	10		0.17	6.5	1.0

[a]Channel width. [b]Channel height. [c]Channel length. [d]Slit width. [e]Slit length. [f]Orifice diameter, if the slit-to-orifice-adaptor part is placed at the outlet. Otherwise, the outlet geometry remains as a slit. (This part was used in the DMA-MS tests.)

This DMA operates laminarly at very high Reynolds numbers, allowing the classification of charged nanoparticles and ions with sizes between 0 and 4 nm. It includes improvements over a similar instrument previously described.[16] An important practical innovation is that when it is coupled to a mass spectrometer (MS), the flow-limiting orifice is no longer at the outlet slit of the DMA but in the MS. The DMA can then

DOI: 10.1021/acs.analchem.8b00579

be quickly removed or installed without breaking the MS vacuum. The DMA combines a horizontal laminar flow of gas with a vertical electric field between two parallel plates, such that ions of different mobilities penetrating through a first (inlet) slit in the upper plate open up in a fan as they drift toward the other plate (Figure 1b); therefore, only a small range of mobilities are sampled through a second (sampling) slit in the lower plate and transmitted to the electrometer or MS.

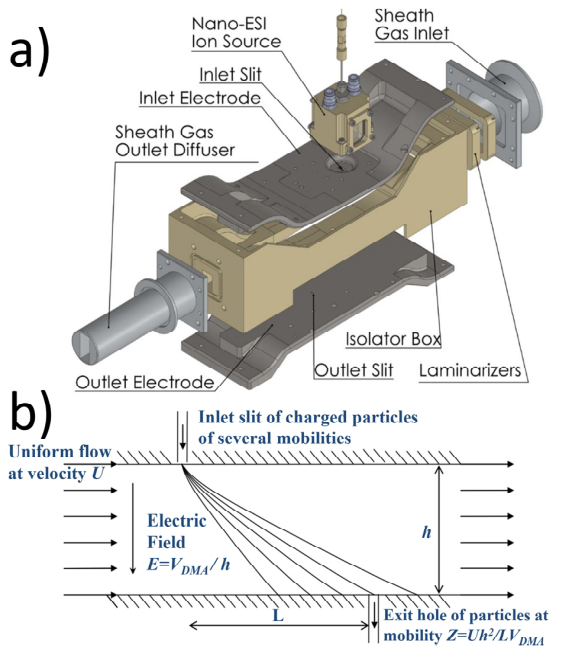

Figure 1. (a) DMA P5-G architecture and (b) DMA principle of operation (after Rus et al.).[16]

P5 DMA comprises eight parts: an inlet electrode, an outlet electrode, an insulator box (PEEK) to electrically separate the two stainless-steel electrodes without allowing gas leakage, an NW50 drift-gas inlet port, an NW40 diffuser extension, and three laminarization screens located at the entrance of the DMA. The DMA internal geometry is complex, including regions with material discontinuities (insulator−metal), where the presence of small steps or gaps in the walls in contact with the flow tend to generate small vortices, which negatively affect the level of flow steadiness required to achieve high DMA resolving power. In the present study, careful attention was paid to avoid such gaps, especially immediately downstream of the junction between the insulating-screen holders and the metallic inlet and outlet electrodes.

Ionization Source. The ionization source is SEADM's nano-ESI ionization source. It is made of Peek in order to eliminate electric-shock risks. It has a 1/8 in. inlet port for the stainless-steel capillary guide, which enables suitable silica-capillary alignment, and two fittings for 6 mm tubes. One of the 6 mm fittings can be used to introduce vapors into the ionization chamber (SESI ionization), whereas the other is used to exhaust the DMA inlet-slit counterflow gas and the sample vapors introduced through the other 6 mm fitting. In this work, only ESI ionization is tested, so one of the 6 mm tube ports is blocked with a blanking plug. The other port is used to exhaust the inlet-slit counterflow gas (0.5 L/min). Two glass windows allow orthogonal vision of the capillary tip, facilitating the electrospray optimization. The position of the capillary tip is easily and safely adjusted using a micrometric capillary positioning system. The electrospray silica capillary used was a New Objective TaperTip (Scientific Instrument Services Inc., Ringoes, NJ) with the following characteristics: 360 μm o.d., 50 μm i.d., 15 μm tip i.d., 50 cm length, noncoated, ref FS360-50-15-N-5-C50.

Electrospray Solutions. The tetraheptylammonium ion (THA^+) used to determine the resolving power was produced by electrospraying, in positive mode, its bromide salt (THABr, 1 mM in 9:1 methanol/water). Its mobility in air is 0.97 cm^2V/s.[33] In the DMA-MS tests, extra virgin olive oil (Olimora, Mora de Toledo, Spain) was 1000-fold diluted in a mixture of 60% dichloromethane and 40% 10 mM ammonium acetate in methanol. This solution was used in negative mode to ionize the fatty acids present in the oil.

DMA Blower. One or two sealed brushless blowers (model 792.3.265-852, Domel d.o.o., Železniki, Slovenija) were used. The rotational speed was controlled by means of a 0−10 Vdc analogue signal. The blower provides a 0−5 Vdc TTL (digital) signal, whose frequency is equal to 6 times the blower frequency (6 pulses per revolution). To precisely control the blower rotational speed, a PID-based control system developed by SEADM was used. The rotational set point is transmitted from a computer to the microcontroller using a COM port. The blower rotational speed is adjustable in the 4000−18 500 rpm range, providing flow rates of 465 and 1640 L/min, respectively, when it is connected to the circuit shown in Figure 2a. After each of the DMA blowers, an aluminum heat exchanger connected to a fan (see Figure 2a item 5) cools down the DMA drift gas to near ambient temperature.

DMA Recirculation Circuit and Prelaminarizers. NW50 corrugated stainless-steel tubes were used for the drift-gas recirculation circuit. A 90° elbow preceded the DMA sheath-gas inlet (Figure 2a, item 4) with a pair of prelaminarizer screens (Figure 2a, item 3) placed before and after this elbow to filter the turbulence created by the pump and the corrugated tubes. These prelaminarizer screens had a significant effect on the achievement of high resolving powers. The effects of working with two prelaminarizers, one prelaminarizer, or none is analyzed in the Results section. The prelaminarizer screens are composed of a commercial NW50 #72-mesh-screen centering ring (LDS Vacuum, Longwood, FL) to which another finer screen (#165 mesh, stainless-steel wire, 50 μm diameter, 104 μm aperture, open area 46%; The Mesh Company, Cheshire, U.K.) is attached as indicated in Figure 2c. The fluid first crosses the fine screen and then the coarse screen. The fine screen is cut in a circular shape and then placed in the same ring groove as the coarse screen.

Electrometer. SEADM's Lynx E12 electrometer was used for the DMA-electrometer tests. Its amplification is 10^{11} V/A, with an unusually fast half-height rise time of 29 ms,[34] which makes it well suited to be coupled to a DMA with an ion residence time of ~200 μs.

DMA-Electrometer Software. SEADM's DMA One software allows the user to introduce the DMA voltage-sweep parameters: the initial and final V_{DMA}'s, the voltage step, and the dwell time for each V_{DMA}. Then, the software sends a vector with the DMA voltage-sweep parameters to the data-acquisition card (DAQ; model USB-6002, National Instruments, Austin, TX). A bipolar high-voltage power supply (model HP010ZIP025, Applied Kilovolts, Worthing, U.K.) amplifies

DOI: 10.1021/acs.analchem.8b00579

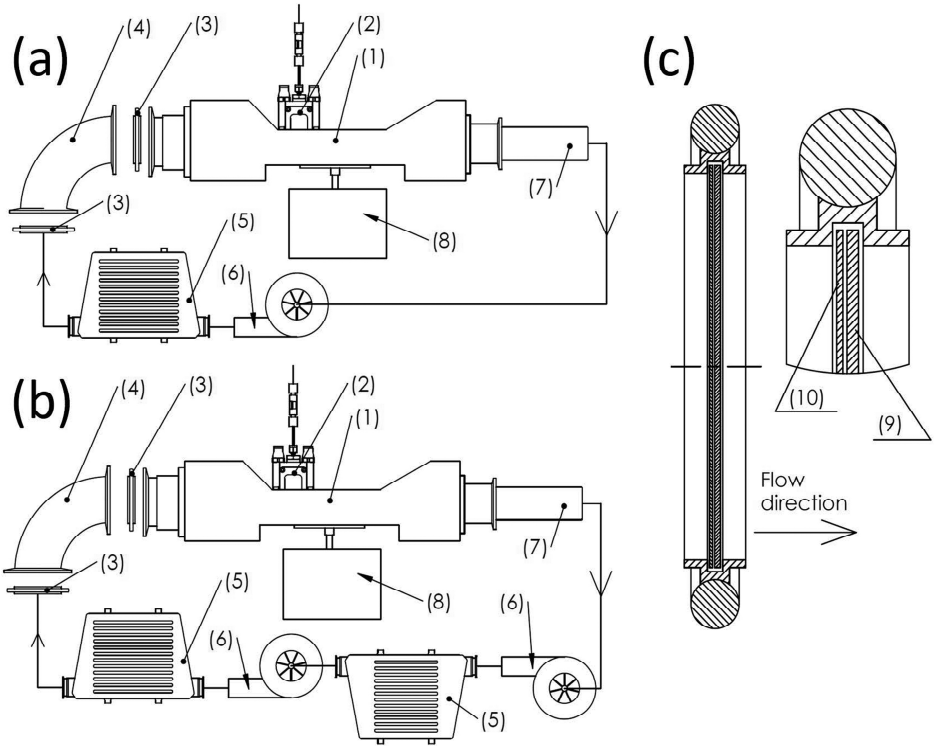

Figure 2. (a) DMA standard configuration with one DMA blower, (b) high-Re operation with two DMA blowers in series, and (c) detail of the prelaminarizers: (1) DMA P5-G, (2) nano-ESI ion source, (3) prelaminarizers, (4) 90° NW50 elbow, (5) cooler, (6) DMA blower, (7) DMA external diffuser, (8) ion detector (electrometer or MS), (9) original #72 mesh of the NW50 centering ring, and (10) #165 mesh screen added to the centering ring to create the prelaminarizer.

the DAQ analogue output by a factor of 1000, allowing V_{DMA}'s from −10 to 10 kV. Once the experiment is running, the DAQ reads the electrometer output voltage at a frequency of 50 kHz, averaging it during the dwell time to produce a single value every V_{DMA}. The software plots a mobility spectrum, where the horizontal axis is the V_{DMA} (inversely proportional to ion mobility), and the vertical axis is the electrometer voltage. In this work, the dwell time used was 1 s.

Mass Spectrometer. The DMA-MS tests relied on Sciex's QTRAP 5500 operated as a single quadrupole. Negative multiple-ion Q1 mode was used to acquire the mobility spectra (signal intensity on the vertical axis and V_{DMA} on the horizontal axis). Negative Q1 mode was used to acquire the DMA-MS contour-plot spectra (m/z, V_{DMA}, and signal intensity). The V_{DMA} was directly provided by the MS internal ion-spray (IS) source, so the MS software allowed the simultaneously programming of the DMA and MS-scan parameters as well as the analysis of the DMA-MS spectra.

Gaussian Fitting. The mean value and fwhm of the peak were determined by least-squares fitting of the logarithm to a parabola.

RESULTS

Resolving Power versus V_{DMA}. Figure 3 shows the measured resolving power compared with the theoretical values (eq 5). The circles correspond to the THA^+ ion (positive electrospray ionization, ion mobility = 0.97 $cm^2/V/s$), under different DMA sheath-gas flow rates. The first five groups of circles, from left to right, in Figure 3 correspond to one DMA blower configuration (Figure 2a) working at 6000 rpm (36 $V^{1/2}$), 9000 rpm (46 $V^{1/2}$), 12 000 rpm (54 $V^{1/2}$), 15 000 rpm (61 $V^{1/2}$), and 18 000 rpm (69 $V^{1/2}$). The last group of circles (74 $V^{1/2}$), correspond to two DMA blowers working in series at full power (Figure 2b). The horizontal segments correspond to several peaks of oleic acid in m/z channel 281.3 with the negative-electrospray-ionization and two-blowers-in-series configuration. Because the ion mobility is higher for oleic acid than for THA^+, the corresponding V_{DMA} is lower for oleic acid at the same sheath-gas conditions. For unknown reasons, the resolving power of the experiments in which the DMA is

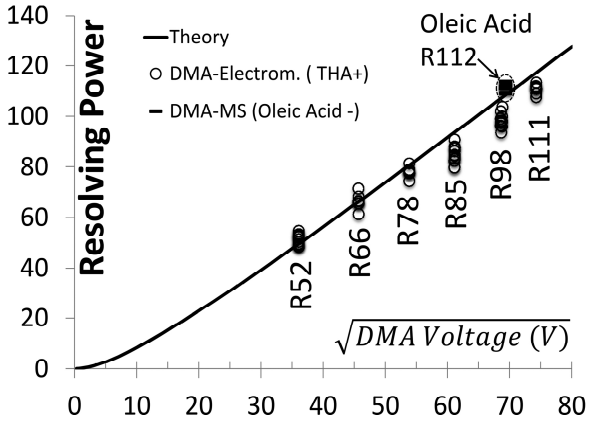

Figure 3. Resolving power as a function of the square root of the DMA voltage. The circles and horizontal segments represent the experimental data. The continuous line represents the theoretical resolving power from eq 5.

DOI: 10.1021/acs.analchem.8b00579

Table 3. Peak Properties of the 11 Consecutive Peaks of Oleic Acid[a]

experiment number	peak voltage (V)	peak intensity (cps)	peak width (V)	coefficient of determination of the Gaussian fitting	resolving power	averaged resolving power	resolving-power standard deviation
1	4807	3.1×10^{05}	44.1	99.5%	108.9	111.7	1.6
2	4809	2.7×10^{05}	42.6	99.5%	112.9		
3	4808	2.8×10^{05}	43.3	99.5%	111.0		
4	4808	3.0×10^{05}	42.3	99.6%	113.6		
5	4811	2.9×10^{05}	42.4	98.7%	113.4		
6	4810	2.9×10^{05}	42.3	98.4%	113.7		
7	4809	2.9×10^{05}	44.0	99.1%	109.3		
8	4808	3.1×10^{05}	42.9	99.4%	112.0		
9	4809	2.8×10^{05}	43.3	99.1%	111.0		
10	4811	3.1×10^{05}	43.1	99.0%	111.5		
11	4812	3.1×10^{05}	43.1	99.4%	111.8		

[a]The peak analyzed is the one with higher intensity in the spectra of Figure 8a. The Gaussian fitting is performed with the points above 5% of the peak intensity.

connected to the mass spectrometer (horizontal segments) is slightly better than that of the experiments in which the DMA is coupled to the electrometer (circles) and is slightly above the calculated theoretical limit (eq 5). To verify the validity of this result, a calibration line of the ion-spray (IS) internal source of the MS was calculated from −1000 to −8000 V, with steps of −1000 V, using a high-voltage probe (TESTEC HVP40) and a multimeter (Proinsa 3511927). The regression-line equation was $y = 0.972x + 67$; the error in the resolution calculation caused by the offset of +67 V is approximately 1.4% (oleic acid $V_{DMA} \sim 4800$ V), allowing us to conclude that the DMA-MS results are reasonably accurate. The peak properties of the oleic acid obtained with the DMA-MS configuration are collected in Table 3. Note the low dispersion in the 11 consecutive peak series and the excellent coefficient of determination of the Gaussian fitting.

Effect of the Prelaminarization Screens. Figure 4 shows the crucial effect of the prelaminarizer screens on the resolving

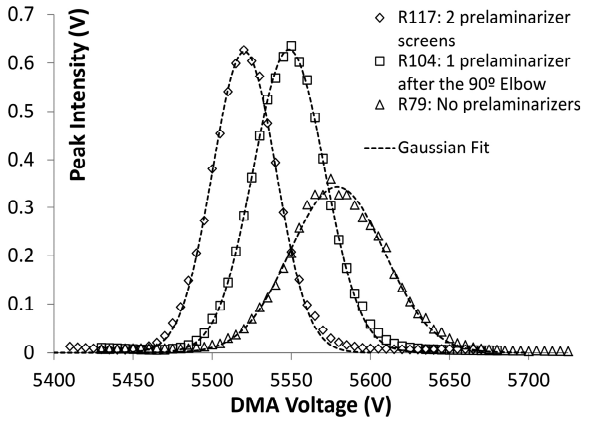

Figure 4. Effect of the prelaminarizer screens on the THA^+-peak resolving power.

power R. $R = 79$ was found without prelaminarizers, $R = 104$ was found with one prelaminarizer screen after the 90° elbow (Figure 2), and $R = 117$ was found with prelaminarizers before and after the 90° elbow. The coefficient of determination of the Gaussian fitting also improved with the better prelaminarization, reflecting the improved flow uniformity.

Effect of the Electric Field Upstream of the DMA Entrance Slit. Ions enter the planar DMA by being pushed by the electric field that penetrates through the DMA entrance slit. If the electric field in the DMA, hereafter called E_{DMA}, is stronger than the electric field upstream of the entrance slit, hereafter called E_{ES}, the electric-field lines will come together (focusing effect), making the inlet ion beam narrower than the inlet-slit width ($W_{slit} = 0.6$ mm). Figure 5 shows the effect of

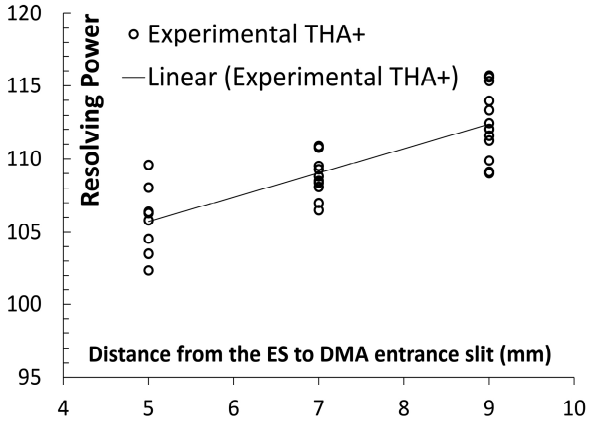

Figure 5. Resolving power vs the distance from the electrospray tip to the DMA entrance slit (d), working with two blowers in series (Figure 2b). The electric field in the DMA was maintained constant.

modifying E_{ES} while maintaining a fixed E_{DMA} on the resolution. E_{ES} is modified through the distance, d, from the electrospray tip to the DMA entrance slit. The potential difference between the electrospray liquid and the DMA inlet electrode was maintained fixed at 2200 V for all the experiments described in this work. Figure 5 shows a clear improvement in the resolution when E_{ES} decreases. Unless otherwise stated, $d = 9$ mm was set for the rest of the experiments.

Effect of the Monodisperse-Sample Flow Rate, q_s. The calculated theoretical resolution (eq 5) is limited by the ratio $q_s/2Q$.

Figure 6 shows the theoretical and experimental effects of changing the monodisperse-sample flow rate, q_s, while maintaining the sheath-gas flow rate, Q, as constant. The experimental data was acquired with two blowers in series (Figure 2b). The electrospray tip was moved away from the DMA entrance slit as q_s was increased to avoid saturating the electrometer. Table 4 shows the distance, d, used for the different q_s tested. For unknown reasons, the performance at

DOI: 10.1021/acs.analchem.8b00579

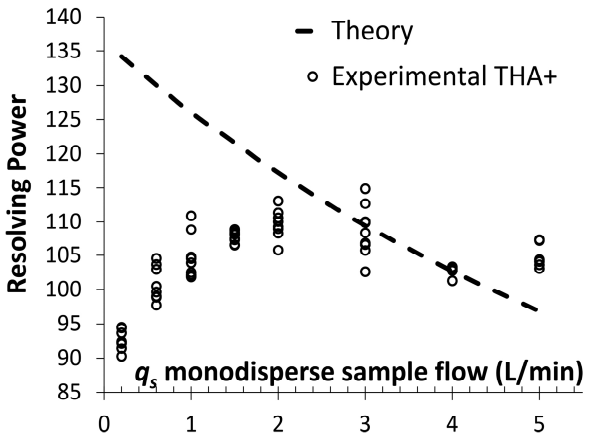

Figure 6. Resolving power as a function of the monodisperse-sample flow rate, q_s, working with two blowers in series (Figure 2b).

Table 4. Distance (d) from the Electrospray Tip to the DMA Entrance Slit Used for the Different Monodisperse-Sample Flow Rates (q_s) Tested in Figure 6

q_s (L/min)	0.2	0.6	1	1.5	2	3	4	5
d (mm)	5	5	5	6	8	8.5	9	9.5

low q_s values is worse than those at middle to high q_s values. Figure 5 shows that working with d = 5 mm implies a loss in resolution of only 6% with respect to working at d = 9 mm; therefore, apart from d, there are additional unknown effects limiting the experimental resolution at low q_s values. At q_s = 5 L/min, the experimental resolving power was slightly larger than the theoretical one (eq 5), meaning that other effects not considered, such as the electric field in the slits, were affecting the maximum resolving power attainable. The optimum q_s was 2 L/min, which was the q_s used in all the experiments with THA^+ ions unless otherwise stated. For the DMA-MS experiments with oleic acid, q_s was equal to 2.4 L/min, which was the critical flow rate sucked by the MS in the DMA-MS configuration.

Analysis of an Extra Virgin Olive Oil Sample by DMA-MS. Figure 7 shows the DMA-MS contour plot of the electrosprayed olive oil solution. This two-dimensional spectrum shows many ions with the same m/z perfectly separated in mobility, illustrating that high-resolution ion-mobility separation is an excellent tool for increasing the selectivity of a mass spectrometer.

Figure 8 shows the mobility spectra for the selected mass-to-charge ratios, m/z 281.3 and 279, corresponding to the masses of oleic and linoleic acids, respectively. The mobility spectrum for the m/z corresponding to oleic acid shows three peaks completely resolved. This graph also shows the hypothetical spectrum in for a DMA with a resolving power of 30, in which the first and the second peaks partially overlap. The mobility spectrum for the m/z corresponding to linoleic acid is more complex, and thanks to the high DMA resolving power, some of the peaks are almost completely resolved.

CONCLUSIONS

The narrow-band planar differential mobility analyzer (DMA P5) has demonstrated a high transmission and a resolving power exceeding 100 for ion mobilities slightly lower than Z = 1 $cm^2/V/s$. The keys to the low ion-beam spreading by

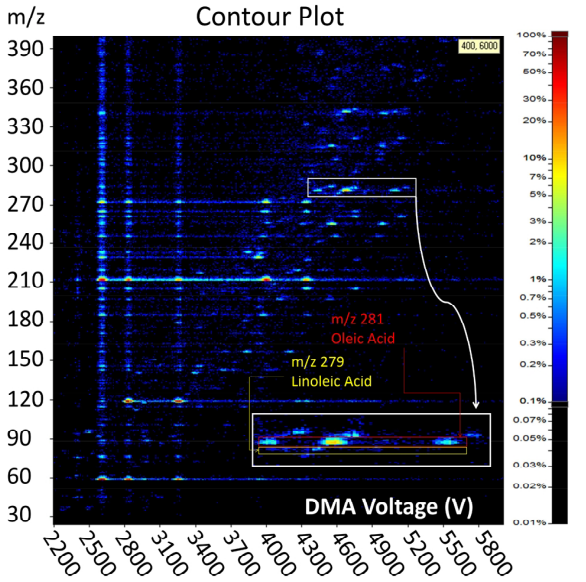

Figure 7. Electrospray DMA-MS contour plot of the extra virgin olive oil solution, including a magnified version in the mass region for oleic and linoleic acids.

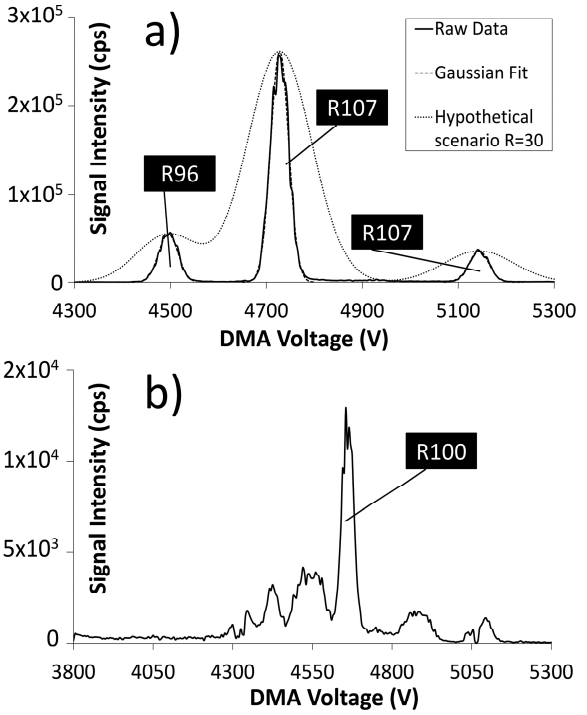

Figure 8. (a) Background-subtracted mobility spectrum at m/z 281.3 (oleic acid). The dashed line is a Gaussian fit to the three peaks. The dotted line represents the same peaks with a hypothetical resolving power of 30. (b) Mobility spectrum at m/z 279 (linoleic acid).

Brownian diffusion enabling this high performance are (i) an unusually low ion residence time in the separation channel of this instrument (200 μs for Z = 1 $cm^2/V/s$) and (ii) the effectiveness in the laminarization of the sheath gas at the inlet of the DMA. The sheath-gas laminarization was improved by (i) the use of two prelaminarizer screens before and after the

DOI: 10.1021/acs.analchem.8b00579

90° elbow placed at the DMA sheath-gas inlet and (ii) the introduction of laminarization-screen holders with minimal steps or gaps between their laminarization-screen exits and wetted surfaces following immediately after them. After these two actions, the DMA performed at the ideal resolving power, delivering reproducible mobility peaks with excellent Gaussian-fitting R^2 values. Its excellent resolving power working with highly diffusive small ions, its high transmission, and its ability to perform voltage changes in a few milliseconds make it an excellent option for IMS-MS analysis.

AUTHOR INFORMATION

Corresponding Author

*E-mail: mario.amo@seadm.com.

ORCID

Mario Amo-González: 0000-0001-6227-1365

Notes

The authors declare no competing financial interest.

ACKNOWLEDGMENTS

The authors gratefully thank the FEDER (ERDF) Program under the responsibility of the European Commission for cofunding the project RESOLVE (Proyectos en I+D en PYMES, file number 04/16/VA/0031) and Professor Juan Fernandez de la Mora for his advice in the optimization of the prelaminarization and laminarization stages of the DMA.

REFERENCES

(1) Purves, R. W.; Guevremont, R.; Day, S.; Pipich, C. W.; Matyjaszczyk, M. S. *Rev. Sci. Instrum.* **1998**, *69*, 4094−4104.

(2) Schneider, B. B.; Covey, T. R.; Coy, S. L.; Krylov, E. V.; Nazarov, E. G. *Anal. Chem.* **2010**, *82* (5), 1867−1880.

(3) Shvartsburg, A. A. *Differential Ion Mobility Spectrometry: Nonlinear Ion Transport and Fundamentals of FAIMS*; CRC Press: Boca Raton, FL, 2008.

(4) Shvartsburg, A. A.; Seim, T. A.; Danielson, W. F.; Norheim, R.; Moore, R. J.; Anderson, G. A.; Smith, R. D. *J. Am. Soc. Mass Spectrom.* **2013**, *24*, 109.

(5) Vidal-de-Miguel, G.; Macía, M.; Cuevas, J. *Anal. Chem.* **2012**, *84*, 7831−7837.

(6) Vidal-de-Miguel, G.; Macía, M.; Barrios, C.; Cuevas, J. *Anal. Chem.* **2015**, *87* (3), 1925−1932.

(7) Gillig, K. J.; Chen, C. H. *Mass Spectrom.* **2014**, *3*, S0032.

(8) Kurulugama, R. T.; Nachtigall, F. M.; Lee, S.; Valentine, S. J.; Clemmer, D. E. *J. Am. Soc. Mass Spectrom.* **2009**, *20* (5), 729−737.

(9) Srebalus, C. A.; Li, J.; Marshall, W. S.; Clemmer, D. E. *Anal. Chem.* **1999**, *71*, 3918−3927.

(10) Asbury, G. R.; Hill, H. H. *J. Microcolumn Sep.* **2000**, *12*, 172.

(11) Dugourd, Ph.; Hudgins, R. R.; Clemmer, D. E.; Jarrold, M. F. *Rev. Sci. Instrum.* **1997**, *68*, 1122−1129.

(12) Merenbloom, S. I.; Glaskin, R. S.; Henson, Z. B.; Clemmer, D. E. *Anal. Chem.* **2009**, *81* (4), 1482−1487.

(13) Adams, K. J.; Montero, D.; Aga, D.; Fernandez-Lima, F. *Int. J. Ion Mobility Spectrom.* **2016**, *19*, 69−76.

(14) Knutson, E. O.; Whitby, K. T. *J. Aerosol Sci.* **1975**, *6*, 443−451.

(15) Labowsky, M.; Fernandez de la Mora, J. *J. Aerosol Sci.* **2006**, *37* (3), 340−362.

(16) Rus, J.; Moro, D.; Sillero, J. A.; Royuela, J.; Casado, A.; Estevez-Molinero, F.; Fernández de la Mora, J. *Int. J. Mass Spectrom.* **2010**, *298*, 30−40.

(17) Hogan, C. J.; Ruotolo, B.; Robinson, C.; Fernandez de la Mora, J. *J. Phys. Chem. B* **2011**, *115* (13), 3614−3621.

(18) Larriba, C.; Fernandez de la Mora, J. *J. Phys. Chem. B* **2012**, *116*, 593−598.

(19) Criado-Hidalgo, E.; Fernández-García, J.; Fernández de la Mora, J. *Anal. Chem.* **2013**, *85* (5), 2710−2716.

(20) Fernández-García, J.; Fernández de la Mora, J. *J. Am. Soc. Mass Spectrom.* **2013**, *24*, 1872−1889.

(21) Javaheri, H.; Le Blanc, Y.; Thomson, B. A.; Fernandez de la Mora, J.; Rus, J.; Sillero-Sepúlveda, J. A. Presented at the 56th ASMS Conference, Denver, CO, June 1−5, 2008; Poster 061.

(22) Fernández de la Mora, J.; Casado, A.; Fernández de la Mora, G. Method to accurately discriminate gas phase ions with several filtering devices in tandem. U.S. Patent 7,855,360, Dec 21, 2010.

(23) Fernández de la Mora, J.; Casado, A.; Fernández de la Mora, G. Method and apparatus to accurately discriminate gas phase ions with several filtering devices in tandem. U.S. Patent 8,278,622, Oct 2, 2012.

(24) Rus, J.; Moro, D.; Sillero, J. A.; Freixa, J.; Fernández de la Mora, J. A high flow rate DMA with high transmission and resolution designed for new API instruments. Presented at the 56th ASMS Conference, Denver, CO, June 1−5, 2008; Poster 042. Available at http://www.seadm.com/wp-content/uploads/2016/03/ASMS_2008_DMA_MS_Poster_num042.pdf.

(25) Zamora, D.; Amo-Gonzalez, M.; Lanza, M.; Fernandez; de La Mora, G.; Fernandez de la Mora, J. *Anal. Chem.* **2018**, *90*, 2468−2474.

(26) Amo, M.; Zamora, D.; Casado, A.; Fernandez de la Mora, G.; Vidal-de-Miguel, G.; Fernandez de la Mora, J. Method for Detecting Atmospheric Vapors at Parts per Quadrillion (ppq) Concentrations. U.S. patent 9,297,785, March 29, 2016.

(27) Amo-Gonzalez, M.; Fernandez de la Mora, J. *J. Am. Soc. Mass Spectrom.* **2017**, *28* (8), 1506−1517.

(28) Rosell-Llompart, J.; Loscertales, I. G.; Bingham, D.; Fernández de la Mora, J. *J. Aerosol Sci.* **1996**, *27* (5), 695−719.

(29) Tammet, H. F. *The Aspiration Method for the Determination of Atmospheric-Ion Spectra Atmospheric-Ion Spectra* (original work in Russian from 1967); Israel Program for Scientific Translations: Jerusalem, Israel, 1970.

(30) Stolzenburg, M. Ph.D. Thesis, University of Minnesota, 1988.

(31) Rosner, D. E. *Transport Processes in Chemically Reacting Flow Systems*; Butterworths: Boston, 1986.

(32) Peixinho, J.; Mullin, T. *Phys. Rev. Lett.* **2006**, *96* (9), 094501.

(33) Ude, S.; Fernández de la Mora, J. *J. Aerosol Sci.* **2005**, *36* (10), 1224−1237.

(34) Fernandez de la Mora, J.; Perez-Lorenzo, L. J.; Arranz, G.; Amo-Gonzalez, M.; Burtscher, H. *Aerosol Sci. Technol.* **2017**, *51* (6), 724−734.

DOI: 10.1021/acs.analchem.8b00579

CHAPTER 3. REACHING A VAPOR SENSITIVITY OF 0.01 PARTS PER QUADRILLION IN THE SCREENING OF LARGE VOLUME FREIGHT

analytical chemistry

Article

Cite This: *Anal. Chem.* 2018, 90, 2468−2474

pubs.acs.org/ac

Reaching a Vapor Sensitivity of 0.01 Parts Per Quadrillion in the Screening of Large Volume Freight

D. Zamora,[†] M. Amo-Gonzalez,[†] M. Lanza,[†] G. Fernández de la Mora,[†] and J. Fernández de la Mora*[,‡]

[†]SEADM, Parque Tecnológico de Boecillo, 205; 47151 Boecillo, Valladolid Spain

[‡]Yale University, Mechanical Engineering Department, PO Box 208286 New Haven, Connecticut 06520, United States

Supporting Information

ABSTRACT: The feasibility of detecting explosives in the atmosphere at concentrations as low as 0.01 ppq hinges on the poorly known question of what interfering species exist at these or higher concentrations. To clarify the issue, hundreds of samples of ambient air, either clean or *loaded* with explosives (from lightly contaminated environments) have been collected in fiberglass/stainless steel filters coated with Tenax-GR, thermally desorbed at variable temperature, and ionized with Cl^- via secondary electrospray (SESI). They are analyzed with a narrow-band mobility filter (SEADM's P5 DMA) and a triple quadrupole mass spectrometer (Sciex's 5500), configured in series to transmit precursor and fragment ions of the explosives Nitroglycerin, PETN, RDX, and TNT. Blanks were sampled outdoors at a rural site (Boecillo, Valladolid, Spain), and *loads* were sampled at diverse locations. For RDX and TNT, atmospheric background inhibits detection below 1 part/trillion (ppt) without mobility filtering. This interference was drastically reduced by the DMA, allowing detection up to 1 part/quadrillion (ppq). Further sensitivity increase was achieved by scanning over a mobility region several percent around that of the target explosive, to separate various isobaric compounds by Gaussian deconvolution. (i) All four MS/MS channels analyzed exhibit several background peaks within the narrow mobility intervals investigated. At least one of these interferents is much stronger than the instrument background at the explosive's mobility, making DMA separation most helpful. (ii) For Nitroglycerin and PETN the combined filtering techniques have not lowered ambient chemical noise down to 0.01 ppq. (iii) Interferents are greatly reduced for TNT and RDX, resulting in minimal chemical noise: 322 blank tests for RDX yielded *mean* signal of 0.0012 ppq and standard deviation σ = 0.0035 ppq (*mean* + 3σ detection limit of 0.01 ppq).

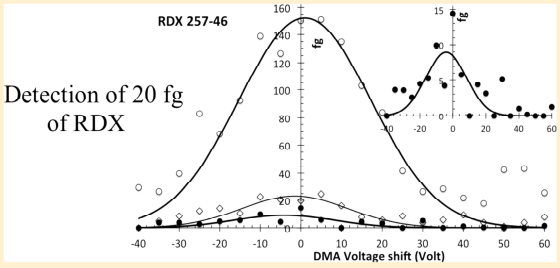

The chemical complexity of multicomponent media, such as the atmosphere, may be defined as the number N of species it contains. N is fractal-like, as it depends on the sensitivity of the detector probing the medium. For instance, analyzing the atmosphere with a detector sensitive to a partial pressure p = 0.8 atm, N = 1; at p = 0.01 atm, N = 5 (N_2, O_2, Ar, CO_2, H_2O), etc. For an analytical instrument to distinguish these N components from each other at decreasing p, one needs to increase the sensitivity, as well as the resolution R or the selectivity.[1] The functional dependence $N(p)$ is accordingly highly relevant to someone attempting to probe the composition of a complex medium at increasing sensitivities. We are embarked in an effort to detect explosives through the vapors they release to the ambient. Given that the room temperature vapor pressure of RDX is ~10^{-12} atm and that a dilution factor of 10^{-3}−10^{-5} may be expected when a charge of explosive is carefully packed, a sensitivity down to 10^{-17} atmospheres (0.01 ppq) is desirable. This is a theoretically possible task, since a cubic meter of ambient air (easily sampled in a few minutes) contains 2.7 × 10^8 molecules of a species present in the ambient at 0.01 ppq. This vast number of molecules suggests the need to reconsider the common view that it is impossible to sniff plastic explosives in the ambient, a point already directly demonstrated in real time and without sample preparation.[1−3] Even allowing for limitations of current triple quadrupole mass spectrometer (MS) performance (~10^{-4} vapor ionization efficiency, as estimated from eq 13 in ref 4 and by measurements,[5] 1% ion transmission and detection efficiency,[6] and 10% vapor capture efficiency in a vapor collector filter (see below), 270 ion counts are still available for detection of a species present in the ambient at 0.01 ppq. Modern mass spectrometers therefore do have the sensitivity required to probe the atmosphere, not just at 0.01 ppq, but even at 0.001 ppq. What is completely unknown and is the subject of this study is if they have the resolving power to distinguish one species from the competing other 10^{17} species accompanying it.

Atmospheric scientists have long monitored open air for the presence of stunning numbers of species present at concentrations sometimes as low as ppt.[7] From this body of

Received: March 3, 2017
Accepted: November 9, 2017
Published: November 9, 2017

   DOI: 10.1021/acs.analchem.7b00795
Anal. Chem. 2018, 90, 2468−2474

work one could perhaps derive some general conclusions on how much resolving power R it takes to monitor ambient vapors at 1 ppq. More generally, one would like to know how fast R must increase at decreasing vapor partial pressure, given in the form of a curve $R(p)$. The present study considers this question at subppq concentrations, where no prior publications are available. Although the issue is too complex to be amenable to a general answer, it may be formulated in relatively simple practical terms for a given instrument and a specific vapor being monitored. Take for instance a triple quadrupole MS in multiple reaction monitoring (MRM), selecting ions of given initial mass m_1, fragmenting them, and selecting one specific fragment of mass m_2. If the ion monitored is ordinarily not present in the atmosphere, its lowest detection limit (LDL) will be set by the highest concentration of interfering vapors ordinarily present in the atmosphere. This will evidently depend on the mode of vapor collection, release, and ionization, as well as on the time and position dependence of the interfering vapor. We present such a study for the vapors of the explosives nitroglycerin, PETN, RDX, and TNT, ionized through chloride produced by secondary electrospray ionization (SESI), with MS filtering conditions m_1 and m_2 compiled in Table 1. In our experience and that of others,[3] none of these

Table 1. Settings for Triple Quadrupole Analysis of the Explosives Monitored

Explosive	NG[a]	PETN[b]	RDX[c]	TNT[d]
m_1 (Da)	262	351	257	226
m_2 (Da)	46[e] or 62[f]	46[e] or 62[f]	46[e]	46[e] or 196[g]
Precursor	$NG+Cl^-$	$PETN+Cl^-$	$RDX+Cl^-$	$[TNT-H^+]^-$
Structure	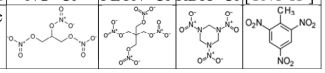			

[a]Nitroglycerin. [b]Pentaerythritol tetranitrate. [c]1,3,5-Trinitroperhydro-1,3,5-triazine. [d]Trinitrotoluene. [e]NO_2^-. [f]NO_3^-. [g]$C_6H_2N_2O_5CH_2^-$.

vapors can be unambiguously detected in ambient air at 0.01 ppq with just a triple quadrupole. We have accordingly increased the resolving power with a variable temperature desorber and a differential mobility analyzer (DMA) acting as a narrow-band mobility filter in unison with the triple quadrupole.[8] Scanning over a finite mobility region several percent above and below that of the target explosive and using a Gaussian deconvolution to separate various mass isomers, brings the LDL for TNT and RDX to the 0.01 ppq level sought.

EXPERIMENTAL SECTION

Vapor Sampling and Collection. In view of the potentially high dilution of explosive samples hidden in cargo loads, our analysis involved an accumulation process, where between 300 and 1000 Liters of air (from either a box, a pallet, or a cargo container) were sampled at ∼160 L/min through a disposable line forcing passage of the air through a collector filter of fiberglass/stainless steel coated with Tenax-GR[9] (provided by TeknoScan Systems, Ontario, Canada). This sampling system is highly mobile, and was used throughout the year from Mediterranean to Northern European locations. The fraction p_{trap} (typically <20%) of the explosive vapor in the sampled gas trapped by the filter was determined by atomizing continuously a known flow rate of an explosive solution of given concentration into 1 L/min of N_2 gas flow. This produced a known concentration of gas phase explosive, which was mixed with ambient air and sampled into the collection filter for a period of time. The filter was then desorbed and the resulting explosive signal determined in the MS, allowing the calculation of p_{trap} (fg detected/fg sampled). Note that p_{trap} is the product of the filter capture efficiency η times a transmission factor t associated with vapor losses in the prefilter and the sampling lines. An improved tandem filter method to measure η is given in the Supporting Information. Although a lack of an accurate method to measure t precludes obtaining a better value of the relevant group $p_{trap} = t\eta$, this study has revealed that some filters have over twice the capture efficiency of others. Since most measurements were carried out without distinguishing between filters, this 2-fold ambiguity affects all our measurements.

Open-air samples are collected at a height of 1.5 m above ground, with the sampling probe pointing downwind (to avoid inertial impaction of atmospheric particles inside the probe line). Cargo samples are collected by introducing inside the cargo volume a Teflon tube held at the sampling probe end. The tube enters through the gap between the two doors, on the lower end. The *loaded* data to be presented correspond to various lightly contaminated environments with no active introduction of condensed phase explosive. The only tests made with purposefully introduced explosives are the calibration measurements described in the **instrument gain** subsection.

Particle Prefiltration. The sensitivity of most analyzers used for trace detection precludes direct vapor detection, so that their response is primarily based on collecting particles. Conventional analyzers often protect themselves from contamination by relatively large organic objects (insects or their fragments) via a prefilter. The potential advantage of sampling explosive particles larger than 50−100 μm rarely compensates for the associated contamination risks, since they tend to settle along the sampling lines or impact on their curved sections. Consequently, a typical prefilter will retain particles larger than 100 μm, and pass smaller particles for their potential content of the target substances to be captured on the main filter. We have experimented with conventional prefilters (80−120 μm low-size cutoff). This led to a high variability in the background, forcing a high threshold for positive detection, and artificially reducing the sensitivity of the instrument. This large statistical background variation was eliminated by removing essentially all the particles with a 10 μm prefilter, and basing the detection entirely on vapors. This approach is inappropriate in the common situation when the detector does not have enough sensitivity to detect vapors, since the only information available is an occasional explosive particle. However, once a continuous signal associated with vapors is detectable, this approximately steady information is far more statistically significant by itself than when combined with rare particle events.

Desorption. Following sampling, the collecting filters were stored in clean containers, transported to the analyzer and inserted in a desorber. The desorber released collected vapors into a stream of clean nitrogen according to a temperature history spanning the range $90 < T\ (°C) < 180$ over 3 min. This desorption time is divided into periods, each with an almost fixed temperature optimally chosen to desorb most of one or more explosives. Only a few chosen explosives are monitored during each temperature step, resulting in a *multistage correction factor* η_d. η_d is initially measured as the fraction of the ion signal from the full desorption collected over the appropriate temperature step (Figure SI-4). This approach increases the duty factor of the MRM measurement, decreasing the noise.

DOI: 10.1021/acs.analchem.7b00795

The clean gas carrying vapors of decreasing volatility at increasing times was directed to the ionizer and the DMA-MS analyzer. All components in the gas path from the desorber (90−180 °C) to the ionizer (170 °C) were kept at a temperature near 200 °C.

Vapor Ionizer and Mass Spectrometer. An earlier version of our evolving instrument, based on Sciex's API 5000 triple quadrupole mass spectrometer (MS) combined with secondary electrospray ionization (SESI),[10] reported the ability to detect in real time several explosive vapors at concentrations between 6 and 20 ppq in a background of clean air,[2] similarly as recently reported.[3] The ionization probability was estimated at 10^{-4}, in agreement with the space charge equilibrium limit for the ratio between the concentrations of ions and neutrals for a trace vapor.[4] The current system is commercially available (ACES 2.1 Model). It relies on Sciex's 5500 triple quadrupole mass spectrometer. It has an improved Desolvating-Low Flow SESI (D-LFSESI) increasing the ionization probability by over an order of magnitude. This surprising ability to overcome what appeared as an upper equilibrium limit follows from the fact that the ions are not drawn from the ionization region into the analyzer by a gas flow. Rather, the flow of sample gas (0.2 L/min) is considerably smaller than the flow rate of gas ingested by the MS (~2.6 L/min), whence the vapors have long residence times in the ionization chamber, and are primarily extracted by the electric field as they become ionized.[11] An additional key improvement of the present SESI source is a new counterflow drying system that completely eliminates vapors from ES solvents,[12] decreasing tailing in mobility peaks by a factor of 100−1000 (as quantified by a ratio of 10^5 for the ion signals at the peak and two half-widths away from it). This performance required also suppressing vapor release from the DMA blower by cooling it to near room temperature. The solvent negatively electrosprayed by the SESI ionizer was water/methanol/HCl 1/9/0.0005 (v), producing predominantly Cl^-. TNT is deprotonated, while all the other explosive vapors studied ionize by Chloride attachment (Table 1).

Ion Mobility Filter. A first approach used to increase the already substantial resolving power of the triple quadrupole filter was to put it in series with a differential mobility analyzer (DMA), a narrow-band mobility filter operating near atmospheric pressure immediately downstream the ionizer. Like the quadrupole, the DMA separates ions in space, not in time. The use of these three narrow band ion filters in series (DMA-MS-MS) produces a drastic reduction in chemical noise, without significant penalty in terms of analysis time and ion transmission,[13] with respect to an analysis based on a single or a triple quadrupole MS alone. The DMA used here was SEADM's P5 model, with a resolving power of about 60 for the tetraheptylammonium ion (THA^+ m/z = 410 Da). It achieves in real time a chemical noise reduction comparable to that of liquid chromatography.[14] Except for the DMA blower and its cooler, all the DMA circuit was heated at 140 °C.

The response of a DMA is such that the peak voltage of an ion is inversely proportional to its mobility. Accordingly, day-to-day pressure (and temperature) variations were exactly (and approximately) canceled by normalizing all the DMA voltages at which explosives appear with the peak voltage of an impurity prominently present in the ion background created by our SESI ionizer. Small differences in the temperature dependence of the mobilities of the various ions with respect to this standard are insignificant because the DMA temperature is regulated.

Numerous prior studies combining in series a DMA with a time-of-flight (TOF) mass spectrometer have illustrated the power of this combination for discovery studies spanning a wide range of mobilities and masses.[15−18] The DMA-quadrupole combination is inefficient in discovery mode because of the need to scan over two dimensions; but it is particularly advantageous for monitoring the moderate number of ions of interest here. In the simplest Hybrid-MRM (HMRM) approach, the voltages of the quadrupoles and mobility filter are set sequentially at the values required to pass a desired ion for a desired time period, one ion at a time.

Mobility Spectrum. The pure HMRM extension of the MS's (MRM) mode typically transmits several interferents with slightly different mobilities having partially overlapping tails. This is shown in the mobility spectrum of Figure 1 for the NG

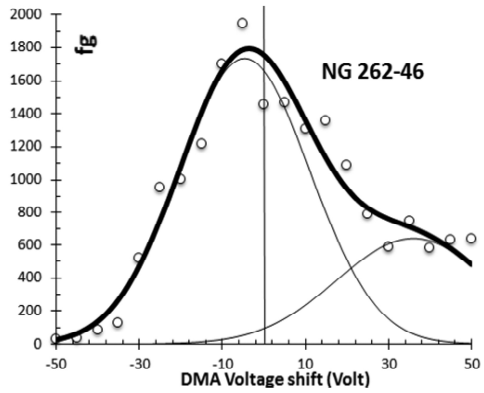

Figure 1. Mass-selected mobility spectrum for a NG *load*, including Gaussian fittings for the NG peak, an interferent to its right, and their superposition (Thick line). The originally measured signal (ions/s) is first turned into total ion counts by integrating over time during the full desorption history, and then converted to fg applying the instrument gain (counts/fg).

262/46 channel, where we fix the precursor and product masses (262 and 46 m/z) while scanning the DMA voltage to span mobilities ~3% above and below that of NG. The voltage scale (inversely proportional to ion mobility) is translated 1574 V such that the NG peak appears at zero voltage. The approach requires taking 21 data instead of 1, therefore reducing signal/noise (S/N) relative to the value achievable without voltage scanning (by a factor considerably smaller than $21^{1/2}$, since the algorithm uses all 21 data). Within each of the desorber's temperature steps, the various mobility scans for the few ions monitored in this time window are launched sequentially, each scan taking 1.05 s (50 × 21 ms). Mobility spectra such as those shown in Figure 1 are obtained by integrating in time each of the 21 mobility points.

Quantification. For blank (and *loaded* sample) quantification we use the following definitions to distinguish between signal relevant to sample concentration and lowest detection level.

Counts. Time integral of the MS signal (counts/s) as if it were fixed 100% of the time at a particular MS^2 channel during the active desorption temperature period (*Counts* are hence uncorrected by the factor η_d). This MS signal (counts/s) is reported by the instrument as the number of ions detected (*events*) divided by the actual dwell time (s). The total number of counts during the desorption period is related through a

DOI: 10.1021/acs.analchem.7b00795

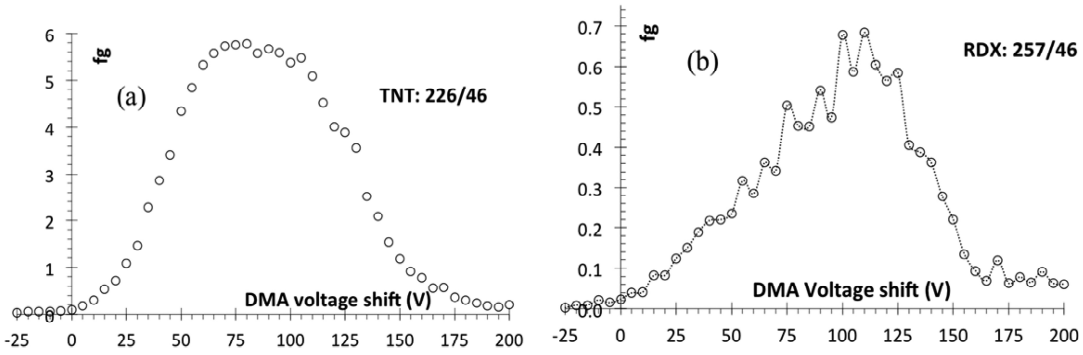

Figure 2. Blank mobility spectra recorded on the mass channels for TNT and RDX, both extending to 200 V and showing a complex contamination peak. 0 V correspond to the mobility of the explosive ions.

calibration process to the total dose of a particular species collected in the filter. This quantity is hence key for quantitation.

Events. Time integral of the MS signal for a given MS^2 channel during the fraction of the time when the MS monitors this channel and the DMA sits at the peak voltage for that ion. The number of *events* is considerably smaller than the number of *counts* because of an MS duty factor associated with the monitoring of other ions, and the 1/21 duty factor associated with the scanning of the DMA peak voltage. When the sensitivity is determined by the sample (no unfiltered contaminants), it is determined by *events* rather than *counts*.

Instrument Gain. To relate the measured counts to an explosive dose we periodically (typically daily) measure the gain of the instrument (counts/fg) as follows. A volume of solvent with a known mass of one or several dissolved explosives (500 fg for RDX) is pipetted into a filter, then desorbed and analyzed. The desorption is monitored in HMRM mode for approximately 45 s, sufficient to complete the relatively fast vapor release of pipetted samples. The sensitivity thus obtained is unaltered by multistage inefficiency effects. It is therefore multiplied by the η_d factor to correctly convert *Counts* into fg in routine sample desorption measurements, as done in Figure 1.

Five such pipette measurements are made, the first pair to verify the stabilization of the measurement procedure, the last three to provide an average gain (38.5 counts/fg in this case). To confirm the linearity of the response with sample mass, fuller calibration curves were similarly generated (once) with samples of 20, 100, 200, and 500 fg deposited on the pipette. The corresponding curves, shown in Figure SI-5 for TNT and RDX, display an approximately linear response. Table SI-4 collect instrument gain for the various explosives.

The sensitivity of 38.5 counts/fg just quoted for RDX corresponds to 4.99×10^7 molecules for a 10 fg dose, with an associated counting efficiency of 2.76×10^{-5} ions per RDX molecule. Notwithstanding the outstanding sensitivity demonstrated, this counting efficiency may seem small. It is however substantially larger than might have been expected, given that just the equilibrium ionization probability is $\sim 10^{-4}$,[4] and the ion transmission efficiency from the atmospheric source to the detector in our triple quadrupole filter is $\sim 10^{-2}$. Key to this performance are the singular ionization efficiency of our desolvating low-flow SESI[12] and the high DMA transmission.

Combining the gain information just reported with the measured filter retention efficiency p_{trap} enables the conversion of an MS signal (i.e., from the desorption of a filter) into the corresponding ambient vapor concentration of sampled air. This concentration is finally compared to the predetermined LDL of each vapor being monitored in order to establish whether or not to launch an alarm.

Elimination of External Peaks. The initial step of the algorithm is to identify Gaussian curves whose peaks lie outside the mobility interval investigated. This process is based on an iterative algorithm that evaluates all the different combination of Gaussian curves in the spectrum. Because the main interferents lie outside the ±50 V mobility scan, it is vital in this initial step to avoid bad peak identification that would provide unreal residues that could generate false alarms or lack of detections. Once identified, these external Gaussian peaks are subtracted from the mobility spectrum, providing clear plots based only on the target compound. Hundreds of samples have been mathematically treated to optimize the configuration parameters.

White Noise. As a second step to minimize False Alarms, the mobility spectrum is analyzed through an autocorrelation process in order to distinguish between a real signal and white noise. Gaussian deconvolution proceeds only when the spectrum is classified as nonwhite noise.

Gaussian Deconvolution. The mobility spectrum (data circles in Figure 1) is first noise-filtered with a Fast Fourier transform algorithm. Individual peaks are then sequentially identified in this filtered spectrum through a Gaussian fitting process (thick black lines). Once a peak is identified, it is subtracted from the filtered spectrum, and the process is repeated until no more peaks above a certain threshold remain.

DMA Fitting. Each identified peak is further analyzed to determine if it qualifies as DMA-generated according to two criteria: (i) The R^2 in its fitting with a Gaussian curve and (ii) the peak width, since the DMA generates peaks with a known width.

Mobility. For peaks classified as DMA-generated, we determine if their position differs by $<\pm 10$ V from that of the target explosive. If so, the height is compared with the threshold to launch the Alarm.

RESULTS

Presence of Interferents. Only a small number of interferents appear in the MS/MS channels of each explosive, apparently due to contaminants commonly present in the local atmosphere. This trend is illustrated in the mobility spectra of Figure 2 for the MS^2 settings of TNT46 and RDX46. The relatively broad peaks seen at positive voltages are due to several rather than a single interferent vapor.

DOI: 10.1021/acs.analchem.7b00795

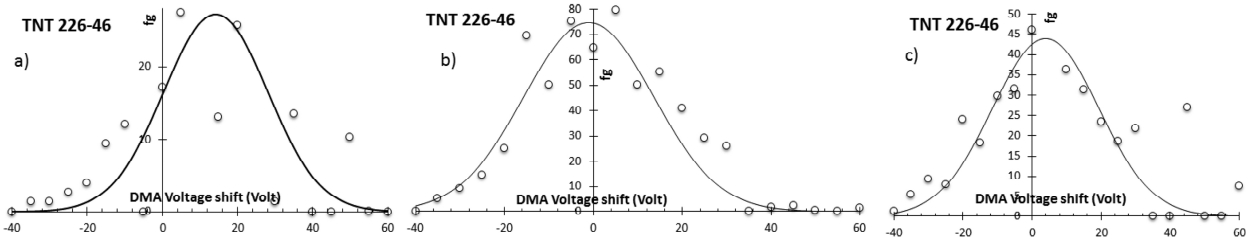

Figure 3. Mobility plots for the three TNT 226/46 Blank tests giving False Alarms. The interferent peak has been removed via Gaussian deconvolution.

False Alarm Rate. Among the 322 blank tests carried out on RDX, two delivered False Alarms indicative of the presence of RDX above 20 fg. Their mobility plots (Figure SI-1) reveal the presence of RDX at 22−24 fg levels, perhaps resulting from incidental RDX contamination. If we conservatively took these two events to be true False Alarms, an upper limit of 0.6% would result for RDX's False Alarm Rate (FAR; i.e., alarms generated by chemical noise or atmospheric interferents). Only three among the 295 blank tests carried out on the TNT 226/46 channel delivered a False Alarm above 20 fg. Their mobility plots are shown in Figure 3. If we interpret all of them as False Alarms, then FAR = 1%. The explosive mass in events b and c (44 and 74 fg), and the fact that there are no interferents in these channels, suggests that these are true detections due to accidental explosive contamination.

PETN Detection. Figure 4, inferred from a large number of ambient and *loaded* samples, is a fragment ratio (FR) plot

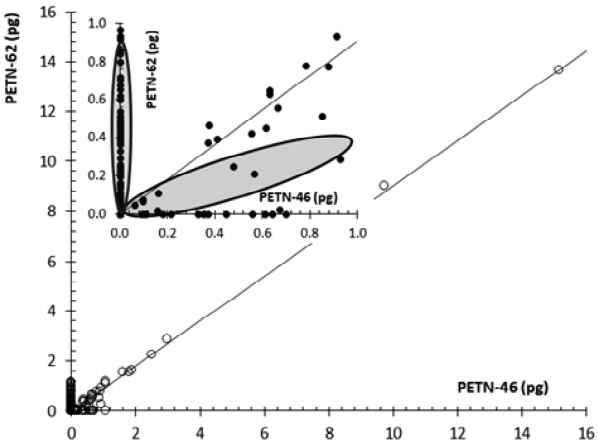

Figure 4. Abundance of PETN351/62 versus PETN351/46 for PETN *loaded* tests. The continuous line corresponds to the fragmentation ratio of PETN. The inset zooming on the lowest concentration region reveals the presence of several contaminant species falling away from the continuous line.

representing the intensity of the PETN351/62 fragment versus that for the PETN351/46 fragment.[19] The slope of the continuous line is the abundance ratio for both fragments under the prevailing fragmentation conditions. While the main image shows the well-defined FR expected for PETN (data points near the continuous line), the inset zooming on the smallest concentrations shows highlighted clouds of points with quite different PETN62/PETN46 ratios. Several interferents can be clearly separated: One appearing prominently only in the PETN62 channel, and possibly another weakly present only in the NG46 channel can be readily distinguished from PETN at sub ppq concentrations. Another interferent with a fragment ratio about 70% that of PETN is also clearly present, but cannot be separated from PETN at sub ppq concentrations. PETN detection is evidently limited by chemical noise.

Nitroglycerin Detection. A similar study carried out for NG (Figure SI-2) shows that the detection threshold in the NG channel is also limited by chemical noise.

Probability of RDX Detection. Table 2 shows results for 314 *loaded* tests. The Probability of Detection (PoD) is shown

Table 2. Probability of Detection (PoD) for RDX

signal level (fg)	number of tests	detections	PoD (%)
0−10	41	0	0.0
10−20	67	20	29.9
20−30	52	49	94.2
30−40	30	30	100.0
>40	124	124	100.0
total	314	223	71.0

as a function of the femtograms measured on the filter. As illustrated in the mobility spectra of Figures 5 and SI-3, the small signal/noise ratio below 10 fg yields null detection probability. The probability increases to nearly 30% for

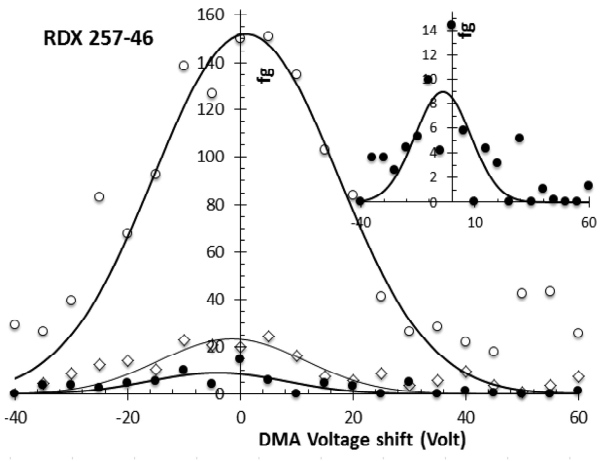

Figure 5. Mobility spectra for three selected RDX 257/46 analyses from ambient samples taken in areas contaminated with explosives. The lowest signal (10 fg, shown also in the inset) approaches the noise level. 94% of *loaded* tests are detected for the middle signal (slightly above 20 fg). The noise does not interfere with detection for the largest signal (150 fg), for which the contaminant peak was not present and is not corrected.

DOI: 10.1021/acs.analchem.7b00795

intensities between 10 and 20 fg, reaching 100% for signals above 30 fg.

To detect 0.01 ppq of RDX with a PoD above 90%, 20 fg are needed in the filter, equivalent to a sampling volume of 1075 L. Collecting this sample at 160 L/min takes 6.7 min.

TNT Detection in the Channel 226/46. The detection of TNT is harder than that of RDX because of an intense interferent appearing around +80 V (Figure 2a). Quantification of TNT hence requires first a Gaussian fitting to subtract the background peak, and a second fitting to extract the TNT peak from the residue of the first deconvolution. This situation amplifies the noise, significantly reducing the Probability of Detection for this TNT channel at low signals. Figure 6 shows

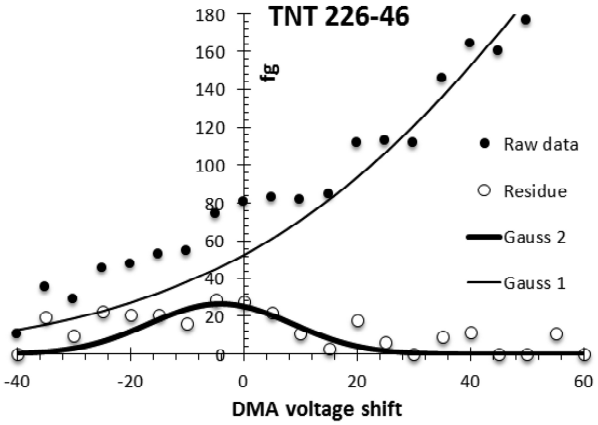

Figure 6. Mobility plot for a TNT 226/46 sample taken in an explosive-contaminated area, illustrating the removal of a large right tail to produce a residue associated with TNT. This positive detection involves 23.4 fg.

the analysis of a TNT 226/46 test. The resulting PoD in the 308 tests carried out for TNT (77.6%) was slightly higher than for RDX (71%), even though the mean vapor pressure in the complete set of TNT tests was 8 times higher than for the RDX tests. The threshold for detection was fixed as 10 fg.

FUTURE DEVELOPMENTS

Since the RDX and TNT channels do not present chemical noise, it is possible to increase the sensitivity in these channels by increasing the signal, without the need for resolution improvements. Developments in DMA resolution currently underway have improved our ability to analyze explosives for which sensitivity is limited by chemical noise (PETN and NG). The Gaussian deconvolution process is also simplified by improved DMA resolution, confirming the correctness of prior conclusions based on deconvolution. For instance, the new DMA cleanly separates the TNT contaminant shown in Figure 6 from the TNT peak, without any deconvolution.

CONCLUSIONS

We have investigated with unprecedented sensitivity and resolution the false alarm rate (FAR) and the probability of detection (PoD) of explosives with vapor pressure between 0.01 ppq and 0.10 ppq, combining mobility filtration and triple quadrupole MS. We conclude the following:

(i) The atmosphere contains interfering vapors at concentrations above 0.01 ppq with the same MS/MS signature as all explosives investigated.
(ii) Within the narrow mobility interval analyzed for all four channels, the atmosphere contains several mobility-resolvable species, one of which at least is typically much more abundant than the 0.01 ppq sensitivity target.
(iii) Mobility separation, through a combination of a DMA and a peak discrimination algorithm, is accordingly vital to exclude these interfering vapors and bring the LDL down to 0.01 ppq.
(iv) RDX can be detected at partial pressure of 0.01 ppq with a PoD higher than 90% and a FAR below 1%.
(v) Interferents and chemical noise in the RDX and TNT channels have been reduced below the equipment sensitivity. Their detection threshold is accordingly limited only by the equipment.
(vi) Detection in the NG and PETN channels is limited by atmospheric compounds which the system cannot distinguish from targets.

ASSOCIATED CONTENT

Supporting Information

The Supporting Information is available free of charge on the ACS Publications website at DOI: 10.1021/acs.analchem.7b00795.

(i) Mobility spectra associated with apparent false alarms for RDX; (ii) fragment ratio plots showing the presence of atmospheric interferents of NG; (iii) magnified versions of the mobility spectra of Figure 5; (iv) temporal desorption profiles and multistage desorption efficiency; (v) calibration; (vi) conversion of ion counts to explosive dose (fg); (vii) characterizing filter sampling efficiency by placing two filters in series; (viii) minimization of contamination sources (PDF)

AUTHOR INFORMATION

Corresponding Author

*E-mail: juan.delamora@yale.edu.

ORCID

J. Fernández de la Mora: 0000-0002-9077-2877

Notes

The authors declare the following competing financial interest(s): J.F.d.l.M. declares a substantial interest in the company, SEADM, manufacturing the detector used in this study.

ACKNOWLEDGMENTS

We acknowledge funding from the UE H2020 SME Phase 2 program through the ACES project, the Spanish Ministry of Industry, Energy and Tourism through the SETRAMAR Project, the Spanish Ministry of Economy and Competitivity through the CARGO Project, and the Regional Government of Castilla & Leon. We thank the Spanish Guardia Civil and the Port of Vigo for their vital role in the maritime container measurements. The long-term support of Professor Jose Ramón Perán (CARTIF) and Dr. Bruce Thomson (Sciex) is gratefully acknowledged, as are numerous contributions from SEADM's Alejandro Casado, Guillermo Vidal and Arturo Alvaro.

DOI: 10.1021/acs.analchem.7b00795

REFERENCES

(1) Ewing, R. G.; Atkinson, D. A.; Clowers, B. H. *Anal. Chem.* **2013**, *85*, 389−397.

(2) Mesonero, E.; Sillero, J. A.; Hernandez, M.; Fernandez de la Mora, J. Secondary electrospray ionization (SESI) detection of explosive vapors below 0.02 ppt on a Triple quadrupole with an atmospheric pressure source, Poster Presented at the ASMS Annual Conference, May 31−June 4, 2009, Philadelphia, PA. http://www.seadm.com/descargas/Poster_Api%205000_09_EMS%203.pdf.

(3) Ong, T. H.; Mendum, T.; Geurtsen, G.; Kelley, J.; Ostrinskaya, A.; Kunz, R. *Anal. Chem.* **2017**, *89*, 6482−6490.

(4) Fernandez de la Mora, J. *Int. J. Mass Spectrom.* **2011**, *300*, 182−193.

(5) Martinez-Lozano Sinues, P.; Criado, E.; Vidal, G. *Int. J. Mass Spectrom.* **2012**, *313*, 21−29.

(6) Javaheri, H.; Thomson, B. A. *Proceedings of the 57th ASMS Conference on Mass Spectrometry and Allied Topics*, Indianapolis, IN, June, 2009; American Society for Mass Spectrometry, 2009.

(7) Goldstein, A. H.; Galbally, I. E. *Environ. Sci. Technol.* **2007**, *41*, 1514−1521.

(8) Rus, J.; Moro, D.; Sillero, J. A.; Royuela, J.; Casado, A.; Fernández de la Mora, J.; et al. *Int. J. Mass Spectrom.* **2010**, *298*, 30−40.

(9) Cao, X. L.; Hewitt, C. N. *Atmos. Environ., Part A* **1993**, *27* (12), 1865−1872.

(10) Wu, C.; Siems, W. F.; Hill, H. H., Jr. *Anal. Chem.* **2000**, *72*, 396−403.

(11) Vidal-de-Miguel, G.; Macia, M.; Pinacho, P.; Blanco, J. *Anal. Chem.* **2012**, *84* (20), 8475−8479.

(12) Amo-Gonzalez, M.; Fernandez de la Mora, J. *J. Am. Soc. Mass Spectrom.* **2017**, *28*, 1506.

(13) Fernández de la Mora, J.; Casado, A.; Fernández de la Mora, G. U.S. Patent 8,278,622, October 2, 2012.

(14) Javaheri, H.; Le Blanc, Y.; Thomson, B. A.; Fernandez de la Mora, J.; Rus, J.; Sillero-Sepúlveda, J. A. Analytical characteristic of a differential mobility analyzer coupled to a triple quadrupole system (DMA-MSMS), poster 061. Presented at the Annual ASMS Conference, 1−6 June, 2008, Denver, Colorado. http://www.seadm.com/descargas/ASMS_2008_DMA_Poster_Bruce_V3.pdf.

(15) Hogan, C. J.; Ruotolo, B.; Robinson, C.; Fernandez de la Mora, J. *J. Phys. Chem. B* **2011**, *115* (13), 3614−3621.

(16) Larriba, C.; Fernández de la Mora, J. *J. Phys. Chem. B* **2012**, *116*, 593−598.

(17) Criado-Hidalgo, E.; Fernández-García, J.; Fernández de la Mora, J. *Anal. Chem.* **2013**, *85* (5), 2710−2716.

(18) Fernández-García, J.; Fernández de la Mora, J. *J. Am. Soc. Mass Spectrom.* **2013**, *24*, 1872−1889.

(19) Schlittenbauer, L.; Seiwert, B.; Reemtsma, T. *Rapid Commun. Mass Spectrom.* **2016**, *30* (13), 1560−1566.

DOI: 10.1021/acs.analchem.7b00795

CHAPTER 4. METHOD FOR DETECTING ATMOSPHERIC VAPORS AT PARTS PER QUADRILLION (PPQ) CONCENTRATIONS


US009297785B2

(12) **United States Patent**
Amo et al.

(10) **Patent No.: US 9,297,785 B2**
(45) **Date of Patent: Mar. 29, 2016**

(54) **METHOD FOR DETECTING ATMOSPHERIC VAPORS AT PARTS PER QUADRILLION (PPQ) CONCENTRATIONS**

(75) Inventors: **Mario Amo**, Boecillo (ES); **Daoiz Zamora**, Boecillo (ES); **Alejandro Casado**, Boecillo (ES); **Gonzalo Fernandez de la Mora**, Madrid (ES); **Guillermo Vidal-de-Miguel**, Madrid (ES); **Juan Fernandez de la Mora**, New Haven, CT (US)

(73) Assignee: **Sociedad Europea de Analisis Diferencial de Movilidad**, Madrid (ES)

(*) Notice: Subject to any disclaimer, the term of this patent is extended or adjusted under 35 U.S.C. 154(b) by 587 days.

(21) Appl. No.: **13/532,146**

(22) Filed: **Jun. 25, 2012**

(65) **Prior Publication Data**

US 2012/0325024 A1 Dec. 27, 2012

Related U.S. Application Data

(60) Provisional application No. 61/500,931, filed on Jun. 24, 2011.

(51) **Int. Cl.**

G01N 1/20	(2006.01)
G01N 27/62	(2006.01)
H01J 49/16	(2006.01)
G01N 33/00	(2006.01)

(52) **U.S. Cl.**

CPC ***G01N 27/622*** (2013.01); ***H01J 49/165*** (2013.01); *G01N 33/0057* (2013.01)

(58) **Field of Classification Search**

CPC ... B01D 29/01; G01N 1/4077; G01N 1/2035; G01N 1/2258

USPC 73/863.24

See application file for complete search history.

(56) **References Cited**

U.S. PATENT DOCUMENTS

5,345,809 A * 9/1994 Corrigan et al. 73/23.2
2006/0192097 A1 8/2006 Anttalainen

(Continued)

OTHER PUBLICATIONS

Pal Tamas Szabo et al: "Electrospray mass spectrometry of hydrophobic compounds using dimethyl sulfoxide and dimethylformamide as solvents" Rapid Communications in Mass Spectrometry, vol. 15, Nov. 20, 2001, pp. 2415-2419, XP55042578 DOI: 10.1002/rcm.526.

Primary Examiner — Hezron E Williams
Assistant Examiner — Rodney T Frank
(74) *Attorney, Agent, or Firm* — Hoffmann & Baron, LLP

(57) **ABSTRACT**

Improvements are provided in the detection of atmospheric vapors by ionizing them near ambient pressure, and analyzing them as ions. Lowest detection limits of parts per quadrillion (ppq) concentrations are enabled by a combination of improvements, including the use of a filter to remove occasional intense signal from explosive particles. Several sources of chemical background are identified and solutions for their reduction or elimination are presented. Gains in response time may be achieved by operating at elevated temperature. When the ionizer is an electrospray source, the use of high boiling point solvents is indicated. An increased selectivity is achieved by operating a differential mobility analyzer (DMA) in series with a mass spectrometer. However, ppq sensitivities require various improvements in the DMA system including a special coupling to the ionizer, controlling the temperature in the DMA pump circuit, avoidance of induction on the DMA electrodes from heating devices, etc.

11 Claims, 7 Drawing Sheets

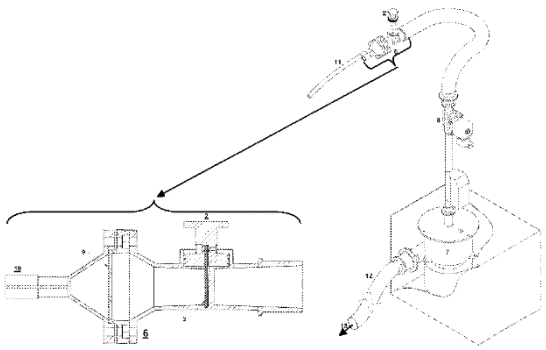

(56) **References Cited**

U.S. PATENT DOCUMENTS

2007/0029477 A1 2/2007 Miller et al.
2008/0101995 A1 5/2008 Gabowitcz et al.
2009/0248319 A1* 10/2009 Call et al. 702/22
2010/0176290 A1 7/2010 Vidal-De-Miguel
2011/0186436 A1* 8/2011 Novosselov et al. 204/600

* cited by examiner

U.S. Patent Mar. 29, 2016 Sheet 1 of 7 US 9,297,785 B2

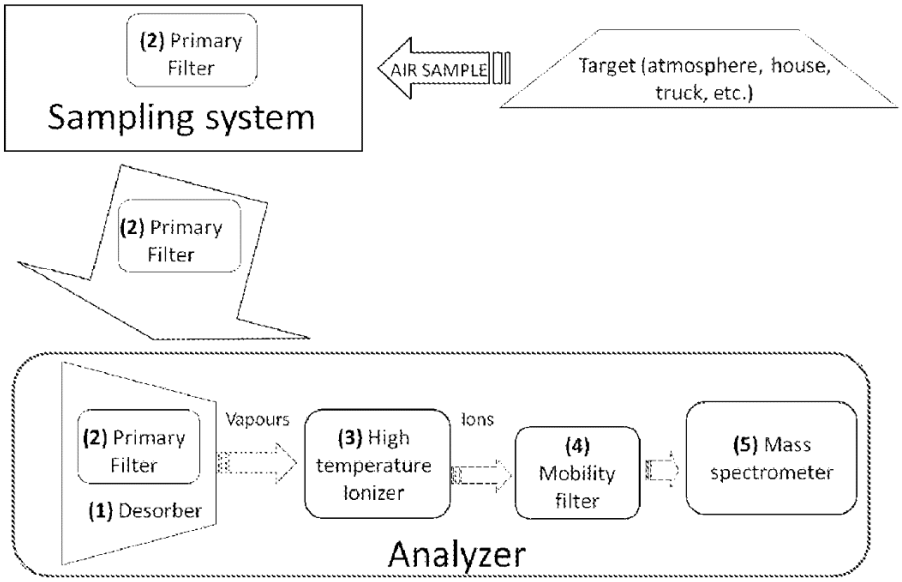

FIG 1

U.S. Patent Mar. 29, 2016 Sheet 2 of 7 US 9,297,785 B2

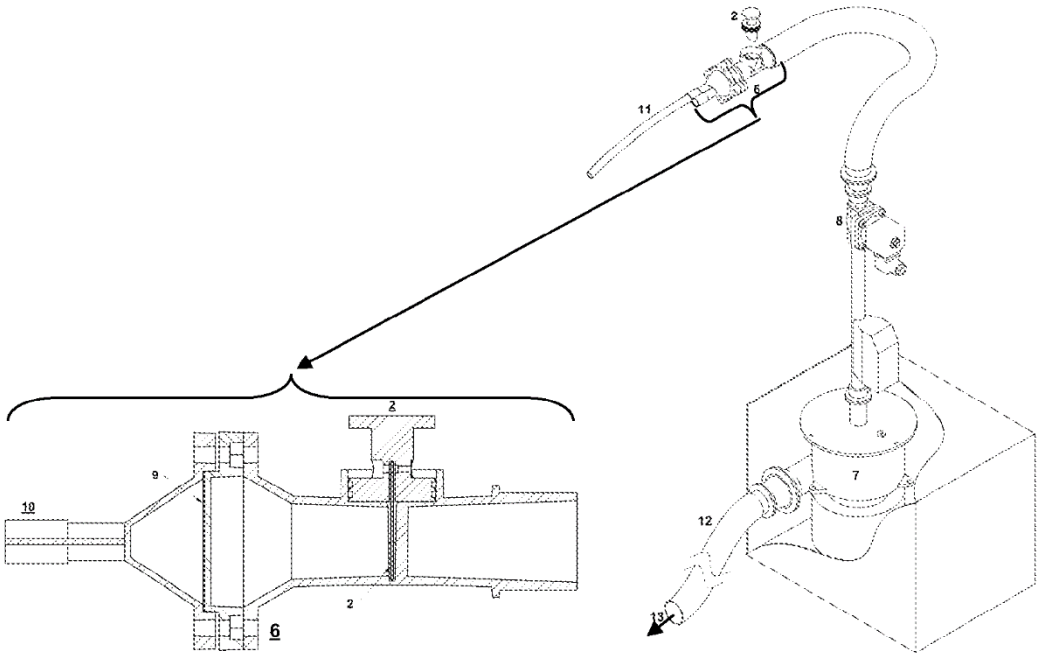

FIG 2

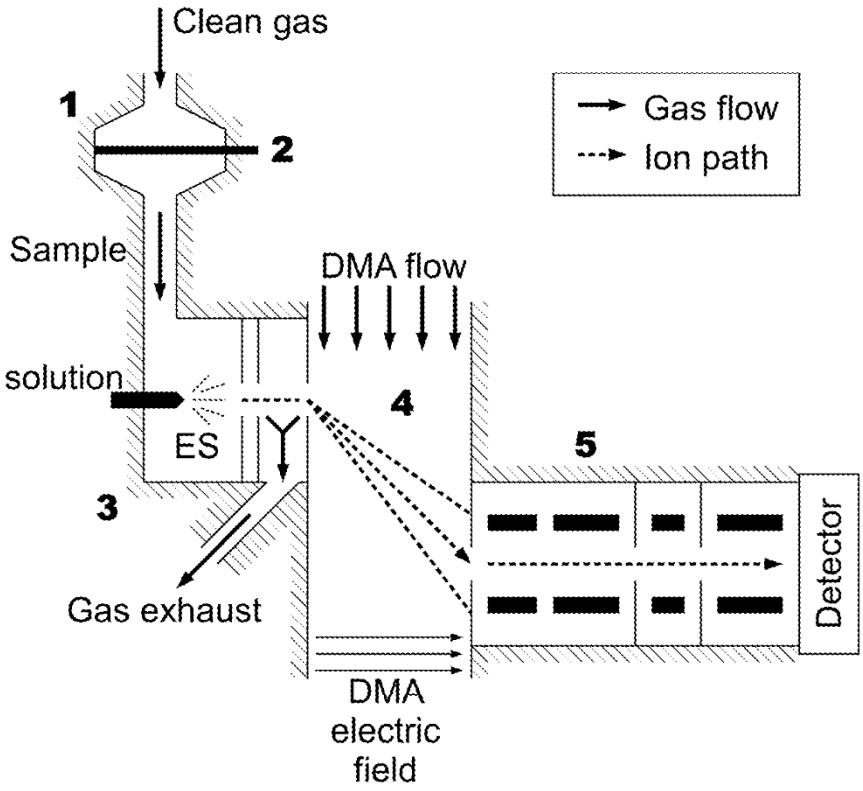
Clean gas
1
2
Gas flow
Ion path
Sample
DMA flow
solution
4
ES
5
3
Detector
Gas exhaust
DMA
electric
field

FIG 3

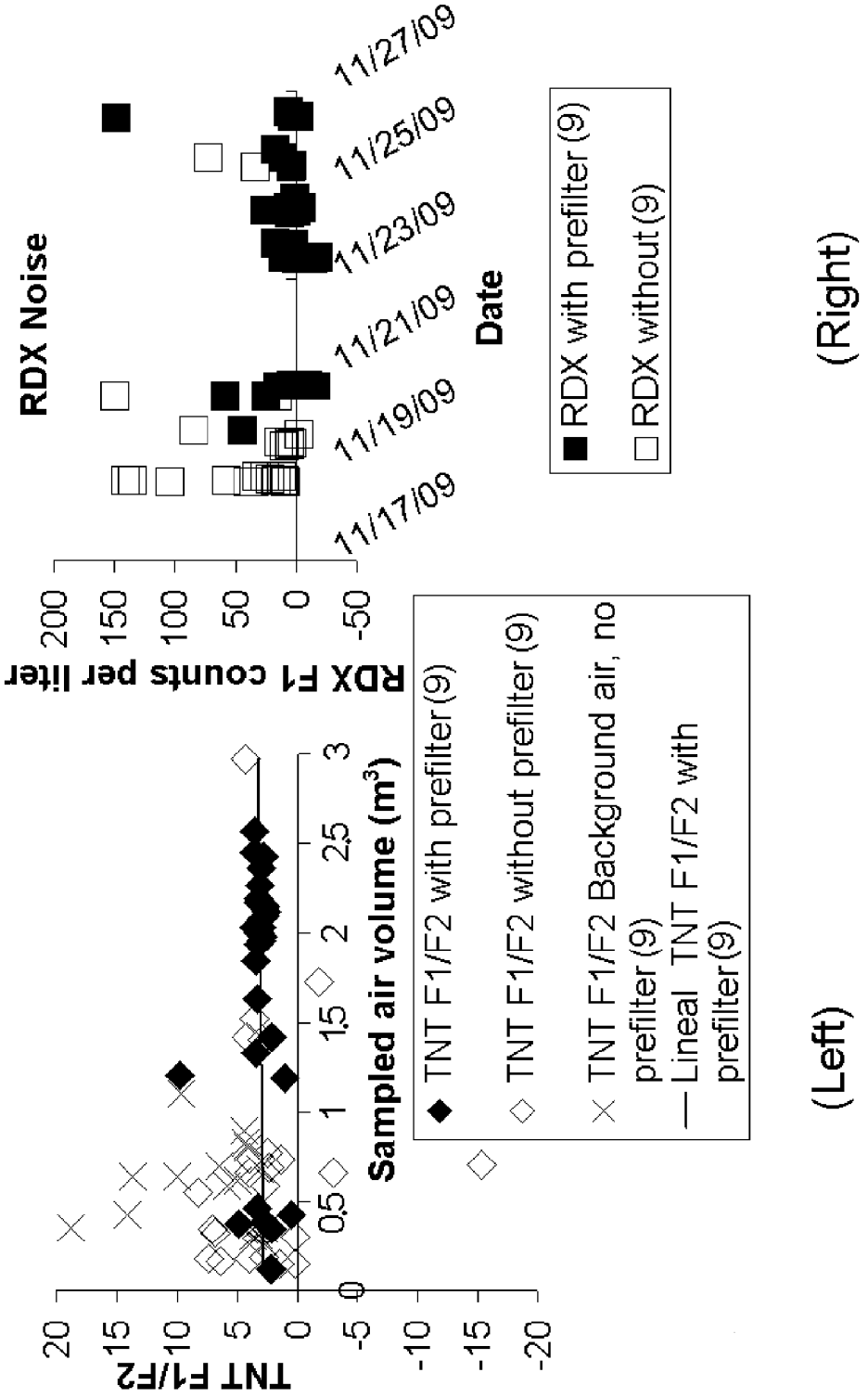
RDX Noise
Date
11/27/09
11/25/09
11/23/09
11/21/09
11/19/09
11/17/09
RDX with prefilter (9)
RDX without (9)
RDX F1 counts per liter
200
150
100
50
0
-50
(Right)
Sampled air volume (m³)
0
0,5
1
1,5
2
2,5
3
TNT F1/F2
20
15
10
5
0
-5
-10
-15
-20
TNT F1/F2 with prefilter (9)
TNT F1/F2 without prefilter (9)
TNT F1/F2 Background air, no prefilter (9)
Lineal TNT F1/F2 with prefilter (9)
(Left)

FIG 4

U.S. Patent Mar. 29, 2016 Sheet 5 of 7 US 9,297,785 B2

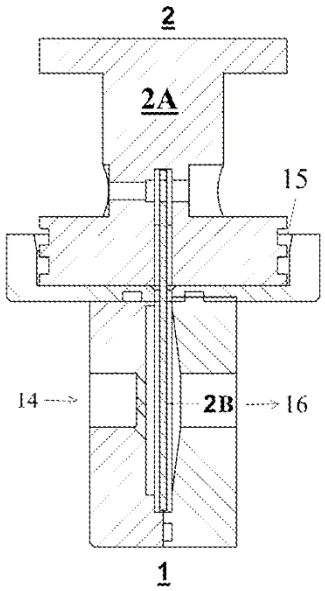

FIG 5

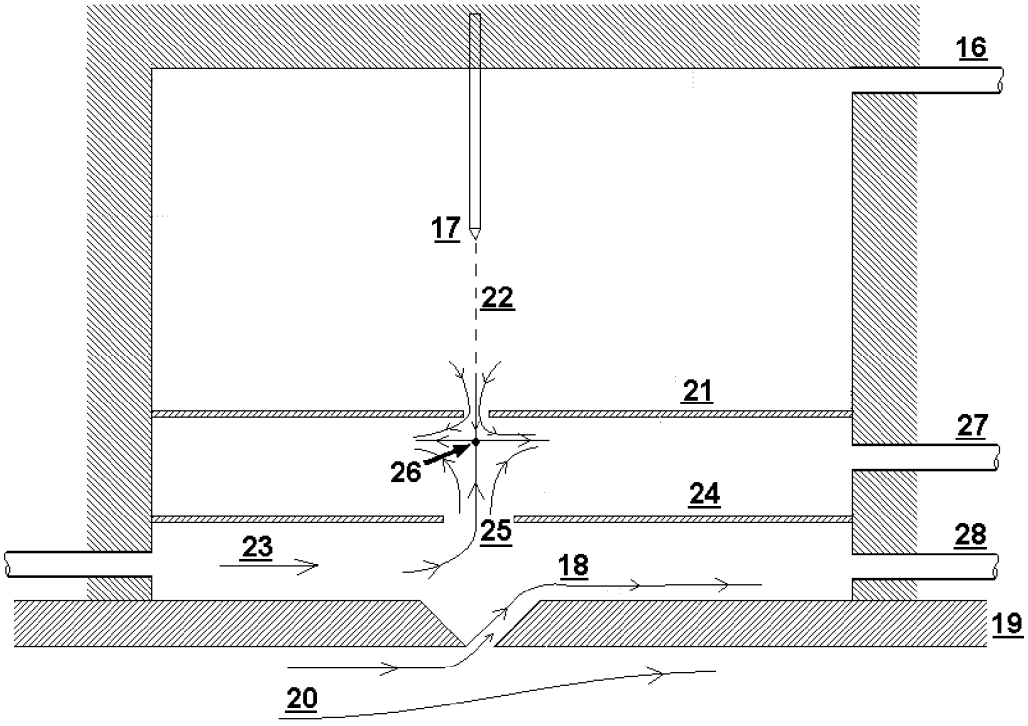
16
17
22
21
27
26
24
25
28
23
18
19
20

FIG 6

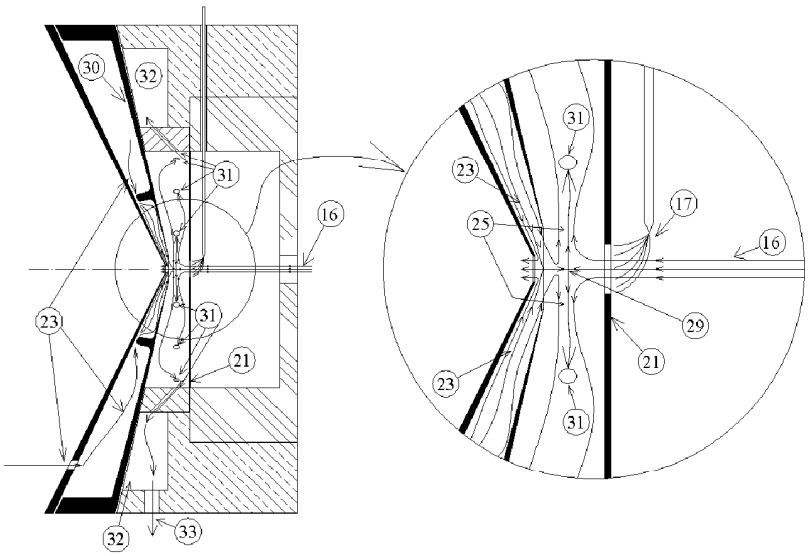
30
32
31
16
23
31
21
32
33
31
23
25
17
16
29
21
23
31

FIG 7

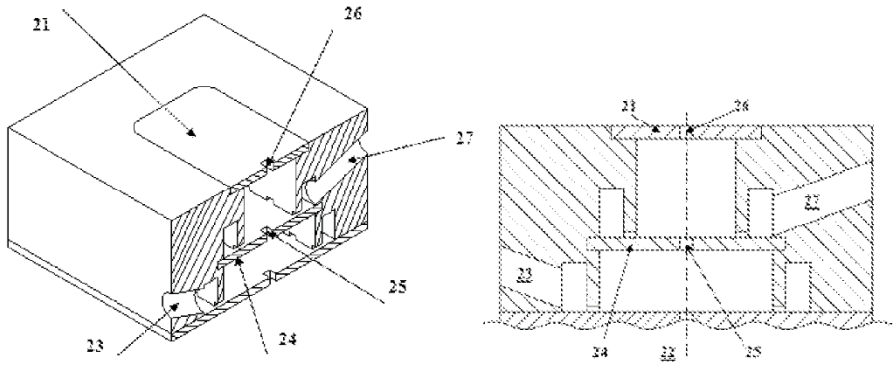

FIG 8

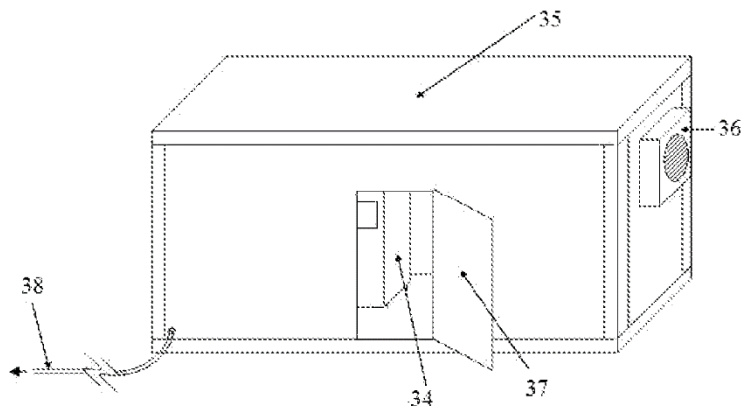

FIG 9

METHOD FOR DETECTING ATMOSPHERIC VAPORS AT PARTS PER QUADRILLION (PPQ) CONCENTRATIONS

CROSS-REFERENCE TO RELATED APPLICATION

This application claims priority to U.S. Provisional Patent Application No. 61/500,931, filed Jun. 24, 2011, the entire contents of which is incorporated herein by reference.

US PATENTS AND PATENT APPLICATIONS CITED

U.S. Pat. No. 7,855,360, J. Fernández de la Mora, A. Casado, G. Fernández de la Mora, Method to accurately discriminate gas phase ions with several filtering devices in tandem, issued Dec. 21, 2010.

US Patent Application 20100264304, P. Martinez-Lozano and J. Fernandez de la Mora, Method for detecting volatile species of high molecular weight.

U.S. patent application Ser. No. 12/686,669, G. Vidal-de-Miguel 2010, Ionizer for vapor analysis decoupling the ionization region from the analyzer. Publication No: US-2010-0176290-A1 Jul. 15, 2010.

U.S. patent application Ser. No. 11/786,688, J. Rus, J. Fernandez de la Mora, Resolution improvement in the coupling of planar differential mobility analyzers with mass spectrometers or other analyzers and detectors. 11 Apr. 7. Publication 20080251714, October 2008. Allowed, January 2011.

U.S. Pat. No. 7,928,373, J. Rus, J. Fernandez de la Mora, Resolution improvement in the coupling of planar differential mobility analyzers with mass spectrometers or other analyzers and detectors. Issued Apr. 19, 2011.

OTHER PUBLICATIONS CITED

E. Mesonero, J. A. Sillero, M. Hernandez, J. Fernandez de la Mora, Secondary electrospray ionization (SESI) detection of explosive vapors below 0.02 ppt on a Triple quadrupole with an atmospheric pressure source, in: Poster Presented at the ASMS Annual Conference, May 31-Jun. 4, 2009, Philadelphia, Pa., 2009.

Wittmer, D.; Chen, Y.-H.; Luckenbill, B. K.; Hill, H. H., Jr. *Anal. Chem.* 1994, 66, 2348.

C. Wu, W. F. Siems, H. H. Hill Jr., Secondary electrospray ionization ion mobility spectrometry/mass spectrometry of illicit drugs, Anal. Chem. 72 (2000) 396-403.

Juan Fernandez de la Mora, Ionization of vapor molecules by an electrospray cloud, Int. J. Mass Spectrom., 300 182-193 (2011).

J. A. Riddick, W. B. Bunger, T Sakano 1986, Organic solvents: Physical Properties and Method of Purification, 3rd edn. Wiley-Interscience.

J. Fernández de la Mora, and I. G. Loscertales, The current emitted by highly conducting Taylor cones, J. Fluid Mechanics, 260, 155-184, 1994.

J. B. Fenn, M. Mann, C. K. Meng, S. K. Wong, C. Whitehouse (1989) Electrospray ionization for mass spectrometry of large biomolecules, *Science* 246, 64-71.

B. K. Ku, J. Fernandez de la Mora, D. A. Saucy and J. N. Alexander, IV, Mass distribution measurement of water-insoluble polymers by charge-reduced electrospray mobility analysis, Analytical Chemistry, 76, 814-822, 2004.

S. Ude, J. Fernandez de la Mora, J, N. Alexander IV, D, A. Saucy, Aerosol size standards in the nanometer size range: II, Narrow size distributions of polystyrene 3-11 nm in diameter, J. Colloid and Interface Sci., 293, 384-393 (2006).

J. Fernandez de la Mora, Fluid dynamics of electrosprays, Annual Review of Fluid Mechanics, 39, 217-243 (2007).

J. B. Fenn, M. Mann, C. C. Meng, C. F. Wong and C. M. Whitehouse, electrospray ionization for mass spectrometry of large biomolecules, Science, 246 (4926), 64-71, 1989.

P. Martinez-Lozano, J. Rus, G. Fernández de la Mora, M. Hernández, J. Fernández de la Mora, Secondary Electrospray Ionization (SESI) of Ambient Vapors for Explosive Detection at Concentrations Below Parts Per Trillion. J. Am. Soc. Mass Spectr. 2009, 20, 287-294

FIELD OF THE INVENTION

This invention relates to the detection of chemical species present in vapor form in the atmosphere.

BACKGROUND OF THE INVENTION

The detection of vapor species present in the atmosphere is of great interest in numerous applications. It is the basis of olfaction in the biological world. Man's sense of smell is relatively weak, so the most demanding aspects of this function must be taken up by various artificial detectors. Examples of the actual or potential usefulness of vapor detectors are clear in various fields, such as food and aromas; medical diagnosis; security applications (explosive detection, person recognition, identification of pathogens, etc.); monitoring of atmospheric pollutants, etc.

The detection of vapors becomes increasingly difficult when they are present at decreasing concentrations in a gas (i.e. the atmosphere) for two reasons. First, one needs an increasingly more sensitive detector. Second, the number of competing vapors present in the atmosphere (or other complex gaseous mixtures) at concentrations comparable to those of the target vapor increases rapidly as the concentration of the target vapor decreases. Consequently, the discriminating power or resolution of the detector must increase along with its sensitivity. Few detectors have been available capable of sensing vapors at concentrations below parts per billion (1 ppb=10^{-9} atmospheres of partial pressure). This is a concentration range at which animals such as dogs are believed to often be still sensitive, and at which many useful vapor detection tasks can be performed. Many other applications require detecting still smaller concentrations down to parts per trillion (1 ppt=10^{-12} atmospheres of partial pressure) or parts per quadrillion (1 ppq=10^{-15} atmospheres of partial pressure). This is necessary, for instance, to detect low vapor pressure substances such as plastic explosives. The most advanced state-of-the-art artificial detectors of substances in the atmosphere are used for security screening of explosives in the civil aviation field, and are called Explosive Trace Detectors, or ETDs. ETDs are based on ion mobility spectrometers (IMS), and though they claim sometimes the ability to detect low volatility materials, generally do not do so directly in the gas phase through olfaction. Rather, detection is achieved by swiping a target surface with a cloth in the hope of collecting some condensed sample of the target substance (typically one or several microscopic particles). The cloth is then introduced into a heated region where any particle present is volatilized, ionized and detected.

The most advanced state-of-the-art detectors for low volatility substances are the explosive detectors used for airport explosive screening, since they target, among others, plastic explosives, whose vapor pressure is extremely low. All airport ETD detectors currently deployed rely on high speed gas jets

or on swabbing for sampling from surfaces, with the obvious goal of dislodging small particles from the person or object probed. A device relying on vapor analysis would simply sample the gas from the vicinity of the suspected point, without the help of auxiliary jets which necessarily greatly dilute the sample vapor.

The particle collection occurrence is highly randomized in real environment. The amount of target substances (or contaminants) that present detectors measure depends on the size and number of particles collected, which is highly variable between tests. As a result, the signals produced by particle based detectors are highly scattered, and the operator needs to increase the detection thresholds accordingly. As a result, the Probability of Detection (PoD) and the False Alarm Ratio (FAR) of these detectors become very poor.

As reported in June 2010 by Mr. Steve Lord, Director Homeland Security and Justice Issues, before the House of Representatives [Subcommittee on Transportation Security and Infrastructure Protection, Committee on Homeland Security, GAO-10-880T; see web page http://www.gao.gov/new.items/d10880t.pdf)], there is currently no technology approved or qualified by TSA to screen cargo once it is loaded onto a ULD pallet or container. Pallets and containers are common means of transporting air cargo on wide-body passenger aircraft. Prior to May 1, 2010, canine screening was the only screening method, other than physical search, approved by TSA to screen such cargo. However, TSA officials still have some concerns about the effectiveness of the canine teams, and effective May 1, 2010, the agency no longer allows canine teams to be used for primary screening of ULD pallets and containers. The Transport Security Administration (TSA), (see web page http://www.tsa.gov/assets/pdf/non_ssi_acstl.pdf) has produced a document entitled "TSA Air Cargo Screening Technology List (ACSTL)", which defines the technologies accepted for air cargo screening. In the first page of this document, the TSA declares the following: "Despite what some manufacturers advertise, TSA has not approved any equipment for any ULD screening. The maximum size cargo configuration that may be screened is a 48"×48"×65" skid." A ULD is a well known acronym in the air cargo community; it stands for "Unit Load Device", and is a pallet or container used to load luggage, freight, and mail on wide-body aircraft. It can be understood as a precise definition of specific containers used for aircrafts. One can therefore conclude that no detection method presently exists for explosive screening of containers for air cargo, neither canine, nor technology-based.

We have for some time expressed our view that vapors can be detected at ppt concentrations, but have met wide skepticism from the experts. No instrument comparable in sensitivity with the one described in this invention has been available to others to discover what it takes to go from the barely credible ppb detection level down to the ppt level, not to speak of the ppq sensitivities aimed at in this invention.

In contrast, the focus of the present invention is on the detection of species present in the gas phase as vapors, rather than of species present on a surface in solid or liquid form. Vapors diffuse smoothly and produce much more repeatable signals that allow the operator to reduce detection thresholds. This pure gas phase approach had for a long time been considered as hopeless for detection of low volatility substances. However, we have recently demonstrated its suitability in certain situations to detect volatiles at concentrations below 1 ppt (Mesonero et al. 2009). Initially we used a sensitive mass spectrometer having an atmospheric pressure source (API-MS) preceded by an ionizer. In a preferred embodiment, vapor ionization was achieved by putting the gas to be analyzed in contact with a cloud of charged particles produced by electrospray (ES) ionization (Fenn et al. 1989). Although a sensitivity to sub ppt concentrations was unprecedented, we found that detection at these concentrations still made use of a very large number of individual molecules, on the order of 10^8. A lowest detection level in the ppt range therefore implies a sensing efficiency of 10^{-8}. The room and the need for substantial improvements are therefore clear. We reported two kinds of barriers to achieving improved sensing efficiencies. One was a low vapor ionization probability of the order of 10^{-4} (i.e., only one in 10^4 vapor molecules contained in the sample volume passed through the ionizer and become an ion sucked into the mass spectrometer). This difficulty has been alleviated by an improved Secondary Electrospray Ionization (SESI) scheme, taught in U.S. patent application Ser. No. 12/686,669 by Vidal. The other obstacle was the impossibility to distinguish the signal of a target molecule from that of other species having a similar chemical signature (chemical noise). The use of Differential Mobility Analyzer (DMA) in tandem with MS-MS also alleviated this problem. As described in U.S. Pat. No. 7,855,360, the use of these three narrow band ion filters in series (DMA-MS-MS) produces a drastic reduction in chemical noise, without significant penalty (with respect to an analysis based on a single or a triple quadrupole MS alone) in terms of analysis time and ion transmission.

The first experimental system incorporating a Sampler preconcentrator, a desorber, and a SESI-DMA-MS-MS ionizer and analyzer used for our preliminary explorations, and which is incorporated in the present invention, was unique in the world in its ability to sense vapors at concentrations below 1 ppt. However, systematic work with this apparatus and its subsequent improvements have provided for the first time a clear picture of a number of previously unsuspected difficulties:

i) Sampler contamination. Consider for concreteness an attempt to detect the presence of the plastic explosive RDX as a vapor in the atmosphere. Its equilibrium vapor pressure at ambient temperature is quoted to be in the range of a few ppt (This value, however, must be taken as provisional, as no reliable method to measure such a low vapor pressure has been available prior to the development of our detector). There are many thousands of other vapors present in the ambient at higher partial pressures that could produce background signals. However, we were able to determine confidently after DMA-MS-MS analysis that at least part of the background signal remaining in the detector after removal of the source of RDX vapor was due to contamination of the analyzer with RDX itself. This forced us to review with exquisite care all possible sources of RDX contamination resulting from previous tests with RDX samples. We had of course followed conventional practices to avoid contamination from samples. In particular, all gas lines were heated to remove any RDX deposited and absorbed on the walls of the system during a measurement with RDX vapor. However, at the unusual sensitivity levels of our instrument, these common practices were clearly insufficient. Eventually we discovered several sources of contamination in the sampling system. Most important was the fact that, upon removing the filter from the sampler, some RDX collected on the filter was transmitted to the surface of the filter holder and remained there as a contaminant. Then, on introducing a new clean filter to collect a new sample of ambient air, part of the RDX contaminant left on the sampler was transferred to the new filter. Sometimes vapors or particles of RDX were collected on the walls of the sampler. In this case there was no direct or indirect contamination of the filter via condensed phase contact. But the finite vapor pressure of the adsorbed RDX mol-

ecules and particles led still to a sufficient release of RDX vapors from the contaminated sampler surfaces into the sampled gas and from this gas into the collecting filter. These forms of contamination were always indirect, and therefore weak and hard to detect. But they were certainly sufficient to preclude detection levels in the ppq range, and could be unambiguously identified with our sensitive instrument, particularly after careful cleaning and decontamination. Another subtler form of indirect contamination was subsequently discovered. Upon completing a sampling experiment on a particular filter, the pump sampling the air at the exit of the sampling system was stopped. Occasionally, however, ambient gas entered backwards into the system, moving upstream from the pump into the sampler. This backward flow resulted in contamination of the sampler very much as when RDX contamination came from upstream.

ii) Ambient contamination. Many other conventional practices need to be refined for vapor detection at ppq levels. Military installation rooms presumed to be clean, where explosives had been manipulated in the past, were found to be heavily polluted. We therefore have often installed the analyzer in its own external cabin, whose cleanness we could more easily control. Even so, we found that this cabin tended to become contaminated after several days of analysis of samples. As a consequence, background levels measured rise and so does the detection threshold. Similar problems may be encountered in various operational scenarios. For instance, when sampling large volumes from a truck or other large containers, the effluents from the sampling pump, if improperly handled, may artificially contaminate a neighboring truck or cargo container.

An important aspect in the development of ppq level detectors is their test with standards. This invention is therefore concerned not only with the improvement of unusually sensitive vapor detectors, but also with the development of methods to rigorously test such detectors. Careful avoidance of contamination is as relevant in such testing grounds as in the analyzer cabin just discussed. Contamination can arise from the most unsuspected sources. For instance, we find that dogs trained to detect RDX and believed to be capable of actually detecting it, are in fact detecting trace quantities of other far more volatile explosives such as TNT or EGDN, accidentally present in the training sample of RDX. Careful examination of the sample handling procedure confirms the likelihood of slight cross contamination between the low volatility and the high volatility test samples. The sample may be polluted even without physical contact, for instance when a volatile and an involatile sample are placed in a common container, since the volatile sample can diffuse through the gas and adsorb on the surfaces of the container or the other solid samples held within it. One can hence easily envision situations where certain seemingly effective detectors could in fact have been for long periods entirely ineffective with uncontaminated low volatility samples. Standards for such tests need therefore to be handled with unusual care. For biological or other non-chemically specific (i.e. non-MS) detectors, testing samples must be analyzed periodically with chemically specific detectors in order to confirm the lack of such cross contamination. Many other subtle contamination schemes have been found during our studies. For instance, testing for explosives is frequently carried out in specialized facilities, often in closed buildings with unusually large volumes and little ventilation. Boxes of various shapes and volumes containing substantial quantities of explosive sample are then introduced into such buildings, and the interior volumes of such boxes are sampled in various forms. If the gas leaving the pump of the sampler pre-concentrator exits directly into the testing building, it contributes to its background, since the collector collects typically less than half of the vapor sample.

iii) Particulate associated chemical noise. Most samplers used for trace detection are primarily based on collecting and detecting particles. The reason is that their modest sensitivity precludes direct vapor detection, whence, their only hope to detect low vapor pressure substances is to collect them in the form of particles, typically carrying far more mass than the vapor molecules in the gas. Conventional samplers often use a pre-filter. Since particles are the main source of detected low vapor substances, the aim of this filter is evidently not to remove small particles potentially carrying the target substance. Its purpose is rather to remove relatively large organic objects, such as insects or their fragments, whose capture in the filter would overwhelm and often seriously contaminate the analytical system. The size of the particles typically intercepted by the pre-filter in such samplers varies from one to the other. Generally, explosive-bearing particles are believed to have sizes from a few microns to hundreds of microns. Explosive vapors are generally sticky, so they tend to attach to particulate matter, and by aerodynamically removing such particles from a surface one hopes to collect a measurable amount of explosive. It is therefore desirable to collect as much as possible of the suspended particles to maximize the amount of explosive collected on their surface. This desire must of course be moderated somehow to minimize the risk of capturing large chunks of organic matter, which upon heating would release inordinate doses of volatile contaminating materials. A reasonable cutoff size for the pre-filter is therefore certainly to remove debris in the mm size range. More conservatively, samplers tend to remove even smaller particles, typically down to 100 μm. One rational for this lower size range is that larger particles settle rapidly into the floor, are harder to bring into the gas phase, and after being aerosolized tend to settle along the sampling lines or impact on their curved sections. The potential advantage of sampling particles larger than 100 μm therefore rarely compensates for the associated contamination risks. Consequently, a typical pre-filter will retain particles larger than 100 μm, and pass most of the smaller particles for their potential content of the target substances to be captured on the main filter. In other words, sampling systems for low vapor pressure substances typically rely on particle collection in the size range below 50-100 μm. In many detection applications, one must set a threshold concentration to launch an alarm. In order to avoid false alarms, this threshold must be higher than the background. But if the background rises (even rarely) every time a big particle of chemical interfering species is captured, the threshold needs to be raised above this value. And under such circumstances the lower detection level of the system is not set by the real sensitivity of the detector, but by the high threshold required to reduce the FAR.

iv) Electrospray limited temperature. Following detection of a low vapor pressure substance, the detector often tends to give a positive leftover signal for that substance. This leftover or memory effect decreases steadily over time, but does not fall to zero for extended periods due to adsorption into and slow release of the vapor from the walls of the analyzer. In order to accelerate the complete decay to zero of this leftover signal, IMS systems and other analytical devices often operate at elevated temperatures, at which adsorbed vapors are rapidly released into the gas. It is accordingly important to heat all system components where such adsorption could take place.

One of the most effective vapor ionization sources available, often referred to as a Secondary Electro-Spray Ionizer (SESI), simply mixes the sample vapors with a cloud of

charged droplets of a relatively clean volatile solvent (Fernandez de la Mora 2011). Other more common ionizers rely on an electrical discharge or a radioactive source, often based on a foil of ^{63}Ni. These two later ionizers are readily heated, but not the first. Indeed, an electrospray source requires that the electrosprayed solvent be in liquid form, which forces an operational temperature below its boiling point. It is important that all parts of the ionizer in contact with the sample gas be hot, ideally at a temperature in the range of 150° C., preferably higher. This is well above the boiling point of most common solvents, certainly those previously used for SESI applications. Wittmer et al. (1994) have developed a water cooled electrospray source, which has been used by Wu et al. (2000) for vapor ionization. Still, the sample gas cannot flow over the water-cooled regions (including the tip of the Taylor cone where the ionizing spray drops are produced), as cold surfaces would trap the gas and lead to the undesirable memory effect one seeks to avoid via heating. Mixing between the sample gas and these charged drops (or the ions they release after drop evaporation), must therefore occur downstream from the ion source, in an uncooled region. However, as shown by Fernandez de la Mora (2011), ionization is considerably more effective when the vapor to be ionized is present at the very tip of the Taylor cone. Achieving this more efficient condition hence requires an approach free from cooled surfaces.

v) Contamination from the electrospray solvent and nitrate-based explosives. SESI-based ionization of vapors offers certain advantages over corona ionization. First, because of the absence in SESI of energetic and potentially reactive phenomena taking place in the corona region, where impurity species may be created from preexisting vapor species in the sample. Another advantage of SESI is that certain additives introduced in the electrosprayed liquid readily produce desired reagent ions in the gas phase. For instance, a good option for ionizing many explosives is to produce halogen ions (i.e. Cl^-) by seeding them into the electrospray solvent in salt or acid form (i.e., NaCl or HCl). The acid form is generally preferable because acids are far more volatile than salts so the spray of drops produces fewer solid residues. However, we find that commercial aqueous HCl is typically supplied with considerable proportions of impurities of sulfates, nitrates and other inorganic anions. This is true even for specialty reagents used for metal analysis, which have indeed very small levels of metal cation contaminants, but still contain substantial quantities of anions such as nitrate. The NO_3^- ion is therefore abundantly formed upon electrospraying such solutions. This impurity ion interferes with the detection of nitrate explosives, typically represented in the gas phase by its volatile decomposition products NO_3H and NH_3. Indeed, NO_3H vapor ionizes into NO_3^- in negative ionization, so solution and gas phase nitrate are indistinguishable, posing a difficult obstacle to the successful sniffing of ammonium nitrate. A first step to the solution of this serious interference is to identify nitrate-free halides, which can indeed be obtained. This is however insufficient to safely sniff ammonium nitrate explosives because other abundant sources of nitric acid exist in the atmosphere. It is in fact well known that ammonium nitrate itself forms naturally in the atmosphere over polluted sites where ammonia and nitric acid preexist at sufficient concentration.

The problem of detecting vapors in the ppq level is currently not solved. It is commonly believed by those skilled in the art that detection of vapors at the ppq level in real environments is impossible. Moreover, substances with low vapor pressures such as plastic explosives are believed to be non-volatile, and their detection is based on particle collection and detection, however, particle detection occurrence is highly randomized, and particle based explosives detection is not functional in the real field.

Consequently, one purpose of this invention is to teach how to detect atmospheric vapors by means of a system built from a Sampling system which acts as pre-concentrator, a primary filter which retains vapors and vehicles information from the sampling system to the Analyzer, and an Analyzer incorporating a thermal desorber, a SESI ionizer, and a DMA-MS-MS analyzer. Other purposes of the present invention are to teach:

(i) how to prevent sampler contamination,
(ii) how to prevent contamination of the analyzer through the atmospheric background during operation,
(iii) how to prevent chemical noise produced by aerosol particles present in the air to be analyzed,
(iv) how to prevent contamination produced by the electrospray used in some embodiments of the invention, and
(v) how to operate a SESI at high temperature,

so as to detect low volatility species directly in the gas phase and at concentrations down to the ppq level.

SUMMARY OF THE INVENTION

A first aspect of the invention constitutes a detector for vapors, sensitive below parts per trillion (ppt) concentrations, and which can reach sensitivities below parts per quadrillion (ppq) for certain volatiles. The aim of this detector is to determine the concentration of volatiles of interest within a gas, which typically is air. This detector is built from three basic units illustrated in FIG. **1**: (i) A sampling system, (ii) A primary filter, and (iii) An Analyzer. The sampling system and the Analyzer are physically independent units, while the primary filter vehicles the information from the sampling system to the Analyzer. The sampling system extracts gas from the target to be analyzed, which can be the atmosphere, or any partially confined or closed environment such as a house, a truck, a container, etc., and deposits vapors within this gas in the primary filter. At the end of the sampling process, the primary filter is extracted from the sampling system, and inserted into the Analyzer, which can be physically separated from the sampling system. Once the primary filter is inserted into the Analyzer, this unit determines the concentration of the volatiles of interest up to concentrations of 1 ppq.

The sampling system extracts selected vapors from the sampled gas, preferably after passing this sampled gas through a prefiltering stage, which may be in the form of a prefilter, aimed at removing particles larger than a certain threshold size. The sample gas then goes through a primary filter intended to trap vapors. The prefilter could alternatively be substituted by an impactor in the prefiltering stage. A preferred size cutoff for the prefiltering stage is 25 μm, preferably 10 μm. One preferred embodiment of the sampling system uses a disposable holder for all components upstream of the primary filter and a diversity of approaches to reduce various subtle sources of contamination. The second unit of the detector is the primary filter, which traps the molecules of low volatility vapors because they are naturally bound to it. The filter can be made of TENAX, stainless steel, fiber glass, or other materials selected by those skilled in the art to trap the desired vapors.

The third unit is the Analyzer, which is self-contained, and incorporates the following components: (i) A thermal desorber, (ii) A high temperature ionizer, and (iii) An atmospheric pressure ionization mass spectrometer, preferably preceded by a mobility filter. The function of the thermal

desorber is to liberate the vapors collected on the primary filter into a stream of clean gas, and to transport these vapors to the high temperature ionizer. The high temperature ionizer is an ionization source, whose function is to turn some of the vapor molecules into ions. A preferred ionizer relies on a cloud of charged drops formed from electrospraying a solvent with boiling point of 150° C. or more, but other options are also included. A third component of the Analyzer is an atmospheric pressure ionization mass spectrometer, preferably preceded by a mobility filter.

A second aspect of the invention makes use of the know-how associated to the sensitive detector just described to develop a method to evaluate other detector systems with lower detection levels below 1 part per trillion, even to detect levels in parts per quadrillion.

BRIEF DESCRIPTION OF THE DRAWINGS

FIG. **1** is a schematic of the complete detector, showing the sampling system, the primary filter and the Analyzer, along with the main elements within the Analyzer: Desorber, Ionizer, and the Mass Spectrometer with a mobility filter. FIG. **1** also shows the transport of the primary filter from the sampling system to the Analyzer.

FIG. **2** shows, on the right, a schematic of an embodiment of the sampling system apparatus used in this invention, where a relatively large volume of the gas to be analyzed is passed through the primary filter, where selected vapor species are captured. The figure on the left presents the disposable part of the sampling system. Note the particle pre-filtering stage located upstream the primary filter, included in a preferred embodiment.

FIG. **3** is a schematic of the components of the Analyzer, showing a desorption system where the vapors collected in a filter by the sampling system are heated, released and conveyed by a small flow of gas into the ionizer, and then to the DMA-MS-MS system.

FIG. **4**: Illustrates the effect of the prefilter in reducing the noise level.

FIG. **5**. Shows various components of the desorber.

FIG. **6** shows details of the coupling between the ionization region and the analyzer.

FIG. **7** Shows details on how to maintain the symmetry of the impinging flows below plate (**21**) when the analyzer inlet is cylindrically symmetrical.

FIG. **8** Shows details on how to maintain the symmetry of the impinging flows below plate (**21**) when the analyzer is a DMA with a rectangular slit.

FIG. **9** shows the environment surrounding the components of the detector of FIG. **3**, designed to minimize contamination of its components.

DETAILED DESCRIPTION OF THE INVENTION

A sketch of the Analyzer used for vapor detection is given in FIG. **3**, showing a desorption system (**1**) where the vapors collected in a filter (**2**) by the sampling system are heated, released and conveyed by a small flow of gas into the ionizer (**3**), the DMA (**4**) and the MS system (**5**), where several target species are detected sequentially during the desorption period. The effectiveness of the analyzer used in the present invention is increased by incorporating a sampling system departing in several ways from conventional samplers.

Low cut-off pre-filter: One solution adopted to remove the large statistical noise produced by aerosol particles according to the present invention is to remove essentially all the particles with a pre-filter having the lowest practical size cut. This is equivalent to base the detection mostly on vapor molecules rather than on both particles and molecules. A less extreme alternative is to remove only the largest particles, whose low frequency of appearance causes the largest statistical noise. In general, however, we find that for systems like ours, sensitive well below 1 ppt of vapor pressure, the lower the cut of the pre-filter the better the results. There are of course practical considerations familiar to those skilled in the art of filtration. Filtering particles in the range from 0.1 μm up to 1-5 μm is relatively difficult, often harder than removing vapors. The reason is that the diffusivity of vapors is much larger than that of particles. Accordingly, particles small enough not to be trappable by phenomena other than diffusion (inertia, interception, etc.) require filters in which vapors are more efficiently caught than the particles themselves. These considerations therefore call for the adoption of practical limits to the smallest particle size to be removed by the pre-filter. A variety of solutions to remove the particles and pass efficiently the vapors are available to those familiar with the art. One is to use filter materials which are inert towards the vapor. In this case, vapor molecules do occasionally collide with the filter, but they re-evaporate and are not captured. This approach is effective with reasonably inert vapors, but is harder with other reactive or sticky vapors. An alternative approach is to use a pre-filter with a cutoff size from a few tens of μm down to one or a few μm, preferably 10 μm. This size range leads to acceptable pressure drops and tolerable vapor losses in the pre-filter. With such pre-filters we have greatly decreased the lowest detection levels for vapors compatible with a minimal level of false alarms. A pre-filter with an uncommonly small cutoff size is therefore an important component of the present invention. An aerosol impactor with a comparable size cut would also serve as a prefilter, with the advantage that its impact surface could be relatively small, and vapor losses by diffusion would be substantially lower than in a filter. Another advantage of impactors is that the particle size cut-off can be easily defined and be well below 1 micron, with a manageable corresponding pressure drop. Both in the case of impactors and prefilters, the material collected in the filter or the impaction plate could, if desired, also be used for separate analysis.

We note an important additional advantage of detection systems primarily based on vapor sensing, over systems relying on the capture of particles. In a situation of positive detection of a large improvised explosive device, the particle sampling components of the detector in contact with a person or luggage cannot be hot. Yet, some of these components may collect large doses of particles, becoming highly contaminated and inoperable for an extended cleanup period. This situation is almost inevitable in a passenger portal where a substantial quantity of explosive is introduced by the passenger. The usual particle removal system involves various high speed jets that will dislodge the particles from the subject. Some of these particles will be ingested into the heated components of the analyzer, but many others will inevitably acquire relatively high speeds from the jet, and be thrown into the walls of the portal. There they will remain as long term contaminants until a special cleanup is implemented. In contrast, all critical non-disposable components of our particle-free system are fully heated, and recover very fast (~1 min) from high concentration events without the need for an ad hoc cleanup.

Contamination upstream the primary filter was reduced or eliminated by various schemes. One method that offered improvements was heating the sampler to elevated temperature while passing gas through it in order to remove all contamination from prior measurements. This approach was

most effective with moderately volatile explosives such as EGDN and TNT. In general, and particularly for the least volatile explosives such as RDX and PETN, the best solution found to eliminate upstream contamination was the use of a new disposable filter holder for every new sample taken. Downstream contamination by the same procedure would require a disposable pump. A more practical solution is the installation of a unidirectional valve (**8**), or any alternative system precluding backflow from the pump into the sampler. Once these precautions were implemented according to this invention, we were able to maintain a relatively consistent level of background signal before and after sampling vapors of RDX (or other substance of interest) into the detector.

FIG. **2** shows a preferred embodiment of a disposable sampler designed to collect the sample vapor. The sampler includes an inlet (**10**) that can be connected to various implements in order to sample air from various spaces. These implements include among others a polytetrafluoroethylene (PTFE) tube (**11**) that can be inserted into a pallet, a truck, etc., from which gas is to be sampled. Following the inlet (**10**) is a prefiltering stage (**9**), which preferably is in the form of a prefilter, introduced to remove particles and avoid their collection in primary filter (**2**). For illustrative purposes, the prefiltering stage (**9**) shall be discussed as being a prefilter. Other means to remove or separate from the sample stream particles larger than a certain size are also included in this invention, such as with an impactor. A preferred alternative embodiment is an impactor, but other well known devices such as inertial separators (virtual impactors, cyclones), etc. are also included. Both the prefilter (**9**) and the primary filter (**2**) are backed downstream by a plastic mesh (Acrylonitrile butadiene styrene, ABS) to keep them in place against deformations due to the large flows of sample gas passed. Unlike conventional prefilters having typically a particle size cutoff in the range of 100 μm, this prefilter has a size cutoff typically smaller than 25 μm, and preferably of 10 μm, so as to remove most particles containing sample and therefore base the detection process primarily on species in the vapor phase. Prior to sampling, the primary filter (**2**) is introduced in its holder (**6**), where it fits tightly so as to avoid ingesting clean background air instead of air coming through the inlet (**10**) carrying the desired sample. The primary filter (**2**) is removably secured to the holder (**6**) to allow for later removal thereof. Various modes of securement may be utilized including a threaded, bayonet or snap-fit engagement. The sampling system elements upstream of the filter are preferably disposable, so as to avoid contamination of the primary filter (**2**) by material collected during a previous sampling operation on the filter holder (**6**) or on other parts of the sampler. The flow of sample is drawn through the primary filter (**2**) for a desired period by pump (**7**), whose outlet flow is driven through a tube (**12**) into a region sufficiently distant to avoid contamination of the environment surrounding the analyzer by the rejected sample gas (**13**). A no-return valve (**8**) is preferably interposed between the primary filter (**2**) and the pump (**7**) in order to avoid retrograde entry of ambient gas through the generally highly contaminated pump (**7**) into the vicinity of the primary filter (**2**). Such a situation could otherwise easily present itself when the pump (**7**) is turned off, either before the beginning or after the end of the sampling period, while the primary filter (**2**) is either installed or removed. A lesser level of upstream contamination may still occur via vapor diffusion. For this reason it is preferable to turn the pump (**7**) on immediately after connecting a new disposable filter holder (**6**) with its new primary filter (**2**) to the line leading to the pump (**7**) through valve (**8**).

Several quantitative measures of the improvement produced by the new sampling system are shown in FIG. **4**. The left plot shows the ratio of two fragments of the TNT peak measured in the triple quadrupole mass spectrometer upon desorbing a plurality of primary filters having collected ambient air, some with the prefiltering stage and others without it. The ratio should be close to 3 for TNT, and a departure from this value is indicative of chemical noise from a contaminant different from TNT. The horizontal scale is the volume of gas sampled. It is immediately clear that the noise disappears by using a 5 μm prefilter and sampling more than about 1000 liters, and is otherwise fairly large. The right plot shows the background signal of the detector at the mass channel corresponding to RDX, showing similarly a substantial reduction in the noise as a result of using a 5 μm prefilter. The one case shown of high RDX noise (−149 counts/lit) was due to accidental contamination.

Ambient contamination is produced by the effluents of the sampling system and the Analyzer. It is therefore important to drive these contaminated gases outside the enclosed space(s) in which the sample and the Analyzer are located, including possibly driving the contaminated gases outside the relevant building. For the same reason, the disposable filter holder (**6**) component of the sampler should not be carelessly discarded within any enclosed working space.

This problem was solved by systematically releasing the effluents from the Analyzer and the sampler not within the enclosed working space(s), but outside it. The need for this practice follows from the fact that the ionization efficiency of vapors is relatively small, so most of the vapor sampled is not consumed, but returned to the environment. Even better results were obtained by releasing these effluents at some distance from the enclosed working spaces, for instance, at the end of a chimney outside the relevant building. Use of relatively leak-tight windows and air conditioning tubes is also most desirable to avoid return into the Analyzer of some of these released contaminants.

Once the primary filter (**2**) is removed from the sampling system, it is preferably introduced into a clean container (preferably an air tight container) to avoid contamination during the period between sampling and desorption. The primary filter (**2**) includes a handle portion (**2**A) for handling, with a filter (**2**B) (vapor collector) fixed thereto. The desorber is shown in more detail in FIG. **5**. Several special characteristics distinguish it from other desorbers in other sampling systems. One taught in U.S. Ser. No. 12/686,669 is the use of unusually small sample flow rates (0.1-0.5 lit/min), substantially less than the sampling flow into a typical modern API-MS. This feature avoids diluting with carrier gas the limited sample captured by the primary filter, as well as increases the ionization probability as explained in Ser. No. 12/686,669. U.S. Ser. No. 12/686,669 is incorporated by reference herein. Another important feature is that the clean carrier gas (**14**) entering the desorber is preheated to the desired desorber temperature. This feature may seem trivial, but it is in fact not. Our early desorbers were commercial, and did not have this feature. It took some effort to realize that the desorption process did not take place uniformly over the diameter of the filter, leading to a non-ideal desorption history and poor use of the sample. The desorber has a leak tight housing (**15**) where the primary filter (**2**) is introduced. The same feature is present in the sampling system. The primary filter (**2**) may be secured using any of the various modes of securement discussed above with respect to the filter holder (**6**). The heating process is controlled by the same software launching the measurement process of the DMA and the MS. Once most of the sample has evaporated from the filter (as determined by

the detector response), the desorber temperature is increased substantially for another set period in order to achieve a thorough decontamination prior to the analysis of another primary filter. Primary filters are typically loaded in the sampling system for periods from one or a few minutes up to 10 minutes, while the desorption process and the final cleanup take about one minute. Sixty samples/hour may therefore be typically analyzed with this detector.

The desorber (**1**) is followed by a variant of the ionizer (**3**), some of whose details have been described by Vidal in Ser. No. 12/686,669. The gas (**16**) leaving the desorber and entering the ionizer is contained within a conduit whose temperature is carefully controlled to avoid condensation of the vapors released from the filter at the desorber.

High boiling point electrospray: when SESI ionization is employed it is important to use electrospray solvents with boiling points higher than the gas temperature to permit proper spraying while the hot gas is in direct contact with the cloud of drops produced by the electrospraying tip (**17**). Pure solvents generally produce large drops, while better ionization is provided by smaller drops. To favor their production it is important to add the proper ionic additive to the solvent. When promoting negative ionization of explosives, a concentration typically larger than 0.01% by volume of chloride or other halogen ions in acid or salt form is desirable. Other ionizers such as those based on a corona discharge, a radioactive source or other sources of ionizing radiation are also included in this invention. We have implemented a high temperature SESI electrospray as part of this invention based on high boiling point solvents. Many high boiling point solvents are available. For instance, Riddick et al. (1986) order their vast compilation of solvent properties according to boiling point, from which numerous solvents with boiling temperatures T_b>150° C. can be identified. However, more than a high boiling point is required for a successful SESI device. The solvent needs also to be available in high purity (to avoid creating too many undesirable or uncontrolled impurity ions). It must be relatively polar in order to become sufficiently conducting to produce very small drops (Fernandez de la Mora and Loscertales, 1994). It must further have a moderately low surface tension in order for a Taylor cone to be stable against electrical discharges, particularly for negative ionization (Fernandez de la Mora, 2007). All these properties except the high boiling point are met by combinations of water with relatively polar organic solvents. Of these, the most widely used is 50/50 water/methanol, first introduced in Fenn's pioneering work on electrospray ionization (Fenn et al., 1989). A few polar solvents of relatively high boiling points are listed in Table 1, with a note on those that are presently commercially available in high purity for high performance liquid chromatography (HPLC) or liquid chromatography mass spectrometry (LC-MS) grade. Comparably polar and high boiling liquids are familiar to those skilled in the art and can be generally selected from the group consisting of amides, alcohols, glycols, esters, ketones, organic carbonates, organic phosphates, and their mixtures.

TABLE 1

Properties of several solvents: T_b = boiling temperature; γ = surface tension; ϵ = dielectric constant. μ = viscosity coefficient.

Solvent	T_b (C.)	γ (dyn/cm)	ϵ	μ (g/s/cm)	HPLC
Dimethylformamide (DMF)	153				Yes
N-Methyl 2-Pyrrolidone (NMP)	202	40.7	32.2	0.0166	Yes
Dimethyl sulfoxide (DMSO)	189	43	46.4	0.02	Yes
1-Octanol	195	27	10.34	0.074	Yes
2-heptanol	159		9.21	0.065	
Formamide (FM)	210.5 (dec)	53.8	111	0.0376	No
Propylene carbonate (PC)	241.7	41.93	64.9	0.028(20 C)	No
Tributyl phosphate (TBP)	289	28	8.91	0.034(25 C)	No
Sulfolane	287		43.2	0.103(30 C)	No

Commercial availability of HPLC grade solvent is a convenient feature, even though its lack can be compensated by in-house purification. The most polar solvents listed in Table 1 and available in HPLC grade are DMF, NMP and DMSO. NMP can be electrosprayed by adding to it some special salts or acids (Ku et al. 2004; Ude et al. 2006), but its properties are borderline, which limits its effectiveness as an ionizer. DMSO is an excellent choice for ionization in positive mode. In negative mode its relatively high surface tension makes it difficult to spray, though this problem can be alleviated by mixing it with a low surface tension solvent. An excellent additive for surface tension reduction is 1-octanol, or another high boiling alcohol. 1-Octanol should not be added in excessive proportions, as its modest dielectric constant would then lead to poor electrospraying. For instance, a mixture of DMSO/1-Octanol 75/25 vol. produces excellent negative mode electrosprays. Note that it is much easier to stabilize such negative sprays at elevated temperature (T~150° C.) than at room temperature due to the reduction of the surface tension at increasing temperature. Those skilled in the art of electrospraying can similarly find alternative mixtures achieving high boiling point, good electrosprayability and moderate surface tension by combinations of polar solvents such as DMF, formamide, propylene carbonate, sulfolane, etc., mixed with less polar solvents of lower surface tension. For instance, if a boiling point higher than 200° C. is desired, a mixture of sulfolane and tributylphosphate is an excellent option. Note however that the two solvents must be purified. Also, sulfolane freezes above room temperature, so, depending on the proportion of TBP added, the whole electrospray solvent line may need to be heated.

The notion of using high boiling point solvents for SESI of heated vapors may appear at first sight as evident to those familiar with the fields of vapor analysis and SESI. The literature on SESI and related methods is in fact substantial (see the recent review by Fernandez de la Mora, 2011). Much of this literature is concerned with gas chromatography, where heating the gas sample to temperatures in the range of 150° and above is common. Yet, none of these studies has relied on electrospraying high boiling point liquids. As already discussed, the most advanced SESI configuration used at elevated gas temperature has involved the use of water-cooled electrosprays of conventional (low boiling point) solvents. The conventional-wisdom barrier against the use of high boiling point solvents provides a first reason not to follow this

path. Low volatility solvents are evidently a source of hazard in conjunction with expensive equipment such as mass spectrometers, whose vacuum system is generally unheated. If unevaporated solvent drops are ingested in the system, they will survive in its interior for long periods. We have in the past used room temperature electrosprays of the solvent formamide for basic research involving borrowed mass spectrometers, never without serious objections on the part of the instrument owner. If such brief uses raised eyebrows, the notion of a long term use of comparably volatile solvents would be immediately rejected by most. Particularly when a seemingly far simpler and much less potentially damaging solution is available in the form of a water cooled electrospray source. Furthermore, water/methanol has been the workhorse of electrospraying for so long, that the very notion of using an unusual and apparently dangerous solvent for the same purpose is highly unappealing. Finally, there has been no awareness of any advantage of high boiling point solvents over the cooled water/methanol electrospray. Our proposal therefore does not appear to the trained eye as an obvious cure for any clearly perceived problem in existing SESI sources. The problem we aim at curing is real, but it has been previously unperceived. Our aim is to increase the efficiency of the ionization process. This calls for physical contact between the vapors and the high density region of the spray of charged drop, which is within microns from the tip of the electrospraying meniscus. The spray of high boiling point liquids permits this close contact, while the cooled spray of water methanol does not.

SESI Electrospray contamination is another problem solved in the present invention, which affects specially the detection of Ammonium Nitrate. Under equilibrium conditions, when condensed ammonium nitrate coexists as an aerosol with ammonia and nitric acid vapors, the product of the concentrations of ammonia and nitric acid vapors is a constant. Even under conditions below this saturation equilibrium, in the absence of ammonium nitrate aerosol, both ammonia and nitric acid are often abundantly present in the atmosphere from natural and industrial sources. How could one then infer the presence of ammonium nitrate from its volatile components if its two volatile makers are so pervasive in the atmosphere? One answer to this question included in this invention is that indeed, independent and abundant sources of ammonia and nitric acid exist in the atmosphere, but the ratio NH_3/NO_3H differs from one source to the other. This ratio can vary from almost zero to almost infinity depending on source conditions, but should be close to unity in the vicinity of a substantial sample of condensed ammonium nitrate. It may sound paradoxical, but one could in principle detect a package of ammonium nitrate even in an atmosphere having reached saturation conditions leading to the formation of ammonium nitrate aerosol. The reason is that this aerosol is typically formed in the atmosphere from separate gas phase sources of NH_3 and NO_3H (rather than from condensed ammonium nitrate) when the product of their concentrations reaches a critical value, yet the NH_3/NO_3H ratio may take any value. In contrast, when ammonia and nitric acid are released from condensed NO_3NH_4 by the opposite reaction, the NH_3/NO_3H ratio will immediately shift from its initial ambient value to a value closer to unity. Therefore, by monitoring both vapors periodically one can follow closely their background concentration. Any occasional drastic departure from this background can be taken as a probable sign of the presence of either ammonium or nitrate salts (including nitrate explosives), or concentrated ammonia or nitric acid. Other readily measurable signals would ordinarily serve to strengthen or weaken the suspicion of the presence of nitrate-based explosives. For instance, ammonium nitrate is oxygen rich, so its effectiveness as an explosive is generally increased by mixing it with hydrocarbon fuels. These in turn are generally far more volatile than even the most volatile explosives, and are therefore easily detected by many forms of olfaction. The bouquet of nitrate-based explosives is consequently identifiable by a number of simple strategies resting on the general considerations just discussed. Many variations of this method of detection can be devised by a skilled chemist. For instance, the inconvenience of a double analysis in positive and negative mode is not strictly essential. If one probes periodically the background concentration of only nitric acid, its sudden shift would be almost as sure a sign of the presence of condensed nitrate as would the shift in the NH_3/NO_3H had both vapors been probed.

Reagents can also be introduced in the gas phase for corona ionization, but only as neutral vapors that then need to be converted into ions. This discussion highlights one potential disadvantage of SESI with respect to corona ionization, where no solvent is required. Corona ionization in air or nitrogen, however, produces abundant nitrate ions via gas phase reactions. On the other hand, it is possible in SESI to greatly reduce ionizer contamination by choosing very pure electrospray solvents and reagents.

In our preferred embodiment the Analyzer includes first a DMA, though sampling the ions directly into the mass spectrometer is sometimes also of interest. The DMA is a very useful element in increasing the resolving power of the Analyzer, and hence distinguishing the desired vapors from others having very close masses and fragmentation patterns not unambiguously distinguishable by mass spectrometry alone. However, successful coupling of a DMA to an ionizer to achieve sub-ppt sensitivities requires numerous unprecedented precautions now discussed.

The coupling described by Vidal in Ser. No. 12/686,669 between the ionizer and the analyzer is shown schematically in the upper part of FIG. **6** for the special case when the analyzer is a DMA. Vidal's coupling relies on drawing the ionized vapor from the ionization region into the entry slit of the DMA (or orifice to the MS) by means of electric fields. When using a DMA it is important to preclude the ingestion of un-evaporated drops or low mobility clusters from the ionizer into the DMA. This is particularly important when using low volatility liquids, especially when the temperature of the DMA is lower than that in the desorber and the ionizer. Otherwise such drops would penetrate in the DMA providing a source of vapors that could condense on the analyte ions. This is often undesirable, as the electrical mobility of these ions would be affected by vapor attachment. Given sufficient vapor in the DMA, various solvation states of each ion may be simultaneously present, while only one can be efficiently passed by the DMA into the MS. These eventualities may be avoided by use of a counterflow of gas from the interior of the DMA into the ionization region. Note that the electric velocities of the ions are unusually high in Vidal's Ser. No. 12/686,669 ionizer, whereby a proportional increase of the velocity of the counterflow gas is necessary to preclude access of low mobility ions and drops into the DMA interior. One approach to exclude such contaminants from entering into the DMA has been described in U.S. Pat. No. 7,928,373 by Rus et al., which is incorporated by reference herein. They operate the DMA in closed flow circuit, and continuously inject a certain flow Q of clean gas into that circuit. Part of this flow exits the DMA as sample to the MS. The remaining portion exits the inlet slit of the DMA towards the ionization region in the form of a jet of counterflow gas (**18**). This exiting jet then opposes the entry of neutral gases and low mobility ions towards the

interior of the DMA. Not taught in U.S. Pat. No. 7,928,373 but relevant to the present invention is the fact that this counterflow jet (**18**) does not exit normally to the direction of the DMA flow, but proceeds instead in a direction as close as possible to the direction of the main DMA flow. It is therefore attached to the downstream exterior lip to the inlet slit formed on the upper DMA electrode (**19**), and moves initially close to parallel to the DMA flow. The effectiveness of this counterflow jet is therefore limited by its direction as well as by its rather large velocity, comparable to the velocity in the main DMA flow (**20**). An additional complication in the coupling of Vidal's Ser. No. 12/686,669 ionizer to this DMA results from the fact that the counterflow gas heading towards the impact plate (**21**) of the ionizer is presumed to move along the axis of the orifice or the symmetry plane (**22**) of the slit leading to the analyzer, while we have just seen that this is not the case for the DMA counterflow. The present invention therefore has introduced the alternative counterflow configuration shown schematically at the bottom of FIG. **6**. Instead of coinciding with the jet (**18**) coming from the DMA, the counterflow gas (**23**) is here provided separately, and is passed through a new intermediate plate (**24**). As a result, this gas (**23**) exits the hole (**25**) drilled in plate (**24**) to form a new jet with the symmetry appropriate to meet frontally the sample flow jet. This frontal collision forms the stagnation point (**25**), similarly as in Vidal's ionizer. The gas brought by these two jets into the impact region is similarly removed through exit line (**27**), and an electric field is maintained between plates (**21**) and (**24**), exactly as in Vidal. A comparable field must also be maintained between plate (**24**) and the upper DMA electrode (**19**), such that ions are quickly driven from the ionization region through the openings in plates (**21**) and (**24**) into the analyzing region of the DMA. Once the new chamber described is added to Vidal's Ser. No. 12/686,669 ionizer, there is no need for the jet (**18**) exiting the DMA. This flow can be allowed if desired, but then it must exit through line (**28**) to avoid interfering with he counterflow gas (**23**), which one wishes to be as unperturbed as possible.

This invention includes an alternative embodiment of the coupling of the DMA to the ionizer useful in cases when the approaches discussed to avoid ingestion of vapors in the DMA circuit are considered too complex. In one preferred mode of operation of the ionizer, a mixture of DMSO/Octanol (75/25 volume percent) seeded with a source of halide ions is used for electrospray ionization. The temperature in the ionizer is about 200° C., close to the boiling point of the solvent, so that a substantial quantity of solvent vapor is present in the ionizer. If even a modest fraction of this vapor is able to penetrate into the DMA circuit, the detector sensitivity will decay considerably over time. This is in part due to spreading of the ions among various solvation states, and also because the mean electrical mobility of the various analyte ions drifts as the quantity of solvent in the circuit increases, and with it the level of ion solvation. An effective approach to eliminate ion solvation by solvent vapors is to increase the temperature of the circulating gas in the DMA circuit. Note however that this circulating flow must be maintained by a pump moving of the order of one thousand liters per minute. This may be achieved at moderate pump weight and power by special pumps similar to those used in vacuum cleaners. These pumps, however, are generally not designed to run at temperatures of 150-200° C. because the life of the pump is reduced. Also, lubricant vapors may be injected from the pump into the circulating gas, making the situation worse rather than better. A temperature in the range from 70 to 100° C., preferably 80° C. offers a good compromise, as it is high enough to greatly reduce solvation problems, and low enough to preclude pump problems.

As already indicated, heating of the surfaces in contact with the sample gas is meant to avoid memory effects from adsorption of sample vapors on cold surfaces. Because the plate is at high voltage, Joule heating with an alternating current is a convenient solution. However, the desired close proximity of plate (**21**) to the upper DMA electrode (**19**) may then induce an oscillation in the DMA voltage, drastically decreasing DMA resolution. One solution is provided by the use of plate (**24**), which is bathed by clean gas (**23**) on the analyzer side, and does not strictly require heating. This plate may then be held at a fixed potential and designed so as to shield the DMA electrode to greatly reduce the ripple induced on (**19**) by voltage variations in (**21**). Another solution is provided by the use of heating elements in (**21**) relying on small resistances, with higher currents and considerably smaller voltage drops. In another scheme, direct current would be used for heating the plates. Those familiar with the fields of heating and induction could provide solutions to this difficulty once being made aware of it. However, because the identification of the existence of this problem has been difficult, its solution is included within this invention.

Returning now to the DMA circuit, typical operating conditions in recirculating flow produce by themselves significant heating in the pump. If unchecked, this heating not only eventually damages the pump. In addition it could release vapors from pump components which may be incorporated into the DMA circuit and attach to the ions analyzed modifying their mobility. This problem may be partly alleviated by operating the DMA circuit at a pressure slightly higher than atmospheric pressure, so that vapors produced in the pump outside of the compression circuit leak through the axis of the rotor from the closed DMA circuit into the atmosphere rather than vice-versa. In one embodiment, the DMA circuit is maintained at a slight superatmospheric pressure by communicating it with the atmosphere through a flowmeter and verifying that gas flows from the closed circuit to the atmosphere. Another important measure to reduce or eliminate pump damage and contamination of the circuit is to cool either the pump motor or the circulating gas. Such pumps are conventionally cooled by a fan blowing surrounding atmospheric air, and this effect can be augmented by use of more powerful external fans or other cooling methods employed by those familiar with the art. In addition, our preferred embodiment includes an air cooler in the closed circuit, similarly as in racing car, truck or tractor radiators. The gas in the closed circuit circulates through the fins of the radiator (designed to allow the high circulation flows of the DMA without substantial pressure drop). These fins are in turn actively cooled from outside with a fan blowing room air. The circuit temperature needs to be stabilized in order to fix the electrical mobility of the ions analyzed. A variation of this temperature could lead to incorrect assignment of the DMA voltage and reduced transmission of the desired ions to the MS. The present invention includes an active temperature control of the gas temperature in the DMA circuit. The control system keeps the temperature at a preset constant value via active control by sensing the temperature in the DMA gas flow following the analyzing region, and providing heating or cooling instructions to either the cooler just described or to a heating bundle surrounding a part of the recirculation circuit. In one preferred embodiment, the gas flowing through the DMA is kept in the vicinity of 80° C. This suffices to mitigate undesirable clustering effects of vapors having for some reason penetrated into the circuit, but is still low enough for proper

operation of the pump. It is equally important to actively stabilize the pump to maintain the gas velocity constant within 1% or better. This is typically not possible by simply connecting the pump to a wall socket, as the provided voltage is not sufficiently steady and depends on the power drawn by other elements such as air conditioning. Our preferred embodiment measures the speed of pump rotation and adjusts accordingly the power supplied to its motor so as to keep this angular speed constant.

Returning now to the ionizer and its coupling to the analyzer, it is important to introduce further refinements in the symmetry of the various flows involved, particularly when a stagnation point (**26**) is formed upon frontal impact of the sample flow and the clean gas flow (**23**) downstream from the opening in the first plate (**21**). The greater the symmetry achieved in the impact region, the smaller the likelihood of penetration of clean gas into the ionization region. A preferred approach to achieve this goal is first illustrated in FIG. **7** for the simpler case (enjoying approximate cylindrical symmetry) resulting when the ionizer is coupled to a mass spectrometer. The coupling illustrated corresponds to the particular case when the inlet to the MS is an axi-symmetrical orifice. In this case the coupling is greatly simplified not only by the prevailing circular symmetry, but also because the counterflow gas leaving the analyzer through opening (**29**) in the conical curtain gas plate (**30**) can be heated, and also because its flow rate is substantially higher than that of the (also heated) sample gas flow (**16**). Unlike in the DMA, which tends to operate colder than the ionizer, whereby the clean gas (**23**) is relatively cold when reaching the impact region (**26**), here, plate (**21**) is maintained passively hot by these surrounding gases and suitable insulation on its supports. Symmetry in the jet of sample gas exiting the opening in (**21**) is naturally assured by its small flow rate and associated rather small flow velocity in the ionization region. Given the larger magnitude of the corresponding flow rate of counterflow gas (**23**) entering the impact zone through opening (**29**) its symmetry is not automatically satisfied, but must be forced by the geometry of the region through which it flows upstream from (**29**). Similarly the flow of the gas downstream from the stagnation point (**25**) must be drawn with cylindrical symmetry. This is achieved in the design of FIG. **6** by pulling it out of the impact region through numerous symmetrically placed perforations (**31**). These many holes connect the impact region to an exhaust chamber (**32**), from which the flow is drawn (asymmetrically) out of the instrument via a single conduit (**33**). In both cases the symmetry of the flow in an incompletely symmetric geometry is guaranteed by the right balance of pressure drops in the various key components. For instance, the pressure drop for the flow to move from one end to the other within the exhaust chamber (**32**) is very small compared to the pressure drop required for the gas to flow through each of the perforations (**31**). Consequently, since these various holes are geometrically identical, each passes essentially the same flow into the exhaust chamber. And because the spacing between the various holes is uniform, the gas is pulled out of the ionization chamber almost axisymmetrically.

Similar considerations apply when coupling the ionizer to a DMA. In this case, we have already noted that the clean gas (**23**) may be relatively cold, so plate (**21**) needs to be actively heated. Also, the openings in the various plates and in the inlet to the DMA are no longer circular holes, but linear slits. The right symmetry in the various flows can nonetheless be achieved similarly as before. For instance, the sample gas will naturally form a rectangular jet because here again the gas velocity is small in the ionization region. However, the exhaust gas (**27**) will not naturally flow symmetrically. The proper flow restrictions with rectangular symmetry must therefore be installed. FIG. **8** illustrates one embodiment of this principle.

Even though our description of the ionizer has referred specifically to plates, elements (**21**) and (**24**) need not be flat plates. They may be cones in axisymmetric situations, such as electrode (**30**) in FIG. **7**. When the analyzer coupled to the ionizer has planar symmetry (as in the case of a DMA with a rectilinear inlet slit), these plates may be substituted by "bent plates" (the two-dimensional analogs of cones). One clear advantage of this alternative geometry (illustrated by elements (**21**) and (**30**) in FIG. **7**) is that these cones or "bent plates" may be placed closer to each other, with considerable advantage in reducing space charge dilution and increasing ion transmission. The term plate in this specification should therefore be interpreted in this broader sense. We shall also refer generally to such non-planar plates as perforated electrodes. Indeed, their purpose is to partially isolate certain regions from each other, providing limited communication between adjacent regions, and permitting establishing electric fields meant to rapidly guide the ions from one chamber to the next.

Coupling of the DMA to the MS has been also described in U.S. patent application Ser. No. 11/786/688, incorporated by reference herein. A particularly efficient way of coupling the DMA to a quadrupole MS that does not increase the time for DMA-MS analysis with respect to that required for pure MS analysis has been described in U.S. Pat. No. 7,855,360, incorporated by reference herein. These various approaches are incorporated in the present invention.

An important aspect of the Analyzer is the procedure to minimize contamination of all key components of the system. A preferred embodiment of the environment of the Analyzer facilitating this goal is shown in FIG. **9**. The Analyzer (**34**) is enclosed in a room or a cabin (**35**) (subsequently referred to as the cabin), preferably with an air conditioning system (**36**) to maintain the DMA and the mass spectrometer at a temperature close to that of their specifications to keep accurate mass and mobility calibrations. The fitting of the air conditioning system (**36**) to the cabin (**35**) should preferably have no imperfections enabling entry of unfiltered air. The doors (**37**) and windows to the cabin are preferably leak tight for two reasons. First to avoid entry of vapors and particles from the often contaminated surrounding (for instance in a cargo environment). Second and even more importantly, to preclude entry into the cabin of air contaminated by the explosives analyzed by the detector. For the same reason, the effluent gases from the Analyzer is preferably vented via exhaust tube (**38**) not only outside the cabin, but also at a considerable distance from it so as to minimize the probability of their return into the cabin through the air conditioning system. When safe disposal of effluent gases at a distance of tens of meters from the cabin is not possible, an equally safe alternative is using two air conditioning entries on opposite sides of the cabin. This should be complemented with an automatic system switching on the upwind and off the downwind entry depending on meteorological conditions. Optionally, portions of the system may be made disposable such as to be replaceable to avoid contamination of future uses. For example, a portion of the system after the prefilter may be made disposable and replaceable. Likewise, the desorber and/or the primary filter as a unit may be replaceable.

A second aspect of the present invention includes an evaluation system for other sensitive vapor detectors trained to recognize certain target odors, but lacking the chemical specificity of a mass spectrometer. One such system would rely, for instance, on canine olfaction. Another would mimic animal

olfaction with a multitude of different solid state gas detectors, each responding to a limited family of vapors, with the full set being capable of recognizing many vapors after suitable training. Such detectors may perhaps recognize a familiar scent presented to them, but cannot ascertain the nature or purity of the substance releasing it. It is therefore evident that the vapor standard must be very pure to train a detector of this kind. This is particularly necessary in the case of low volatility target substances, as any trace of a more volatile impurity would tend to produce a far more potent olfactive signature. If the detector is trained with this contaminated target, it will almost surely be incapable of recognizing the uncontaminated substance. Even if it is initially correctly trained, any subsequent contamination of the training sample will rapidly corrupt what was initially properly learned. The evident difficulty of controlling the reliability of such detectors is compounded by many other factors. The training of biological detectors needs to be continuous, pure standards are expensive, and contamination is in the long term unavoidable in repeatedly manipulated samples. This being so with each target substance taken separately, imagine the problem of avoiding cross contamination among the dozen different target substances each trainer needs to manipulate and each dog needs to recognize separately. The TSA's reservations towards such biological detectors are hence readily understood as a simple consequence of the lack of a safe method to train non-chemically specific vapor detectors. The remedy for this problem, however, becomes simple in light of our invention. It involves periodically testing the purity of the standards used to train such detectors, by analyzing them with a chemically specific detector sensitive to ppt concentrations, such as the one described in this invention. More specifically one would (a) provide an uncontaminated environment where to carry out the required testing and training; (b) Provide a highly purified standard for each vapor for which training is required; (c) Generate ppt or sub-ppt concentrations of each individual vapor (i.e., as described by Martinez Lozano et al. in J. Am. Soc. Mass Spectr. 2009, 20, 287-294) to be used for training or testing; (c) provide a protocol to handle each individual standard within said set of standards, so as to minimize cross contamination; (d) provide a protocol to handle said environment so as to avoid its contamination by said standards during training or testing; (e) Occasionally using a chemically specific detector of vapors having sub-ppt sensitivity to test for possible contamination in either said standards, or said doses of individual training vapors.

Much of the discussion has involved the combination of a sampling and a desorbtion system with an analyzer. However, many of the improvements discussed relating to the analyzer, the ionizer and the coupling between both are equally useful for analysis of ambient volatiles directly, without their prior accumulation in a collection device. These separate improvements are also considered part of this invention.

We claim:

1. A method to detect the presence of substances based primarily on the vapors they release to a surrounding gas, involving:

a) sampling said gas to which said vapors have been released and passing it through a prefiltering stage including means configured for removing particles larger than 25 μm carried by said gas,

b) passing said prefiltered gas into a vapor capture stage including a collection chamber containing a vapor collector, such that a fraction of said vapors are captured into said vapor collector, said vapors not captured into said vapor collector being residual vapors,

c) where said vapor capture stage includes at least one contamination prevention means, such that said residual vapors having circulated through said collection chamber during one vapor capture event are not released to the vapor collector during a subsequent vapor capture event into said gas, and therefore are not captured by the vapor collector during said subsequent vapor capture event, and

d) a desorption-ionization and analysis stage where said vapors captured into said vapor collector are thermally released into a flow of clean gas and passed through an ionization chamber where a fraction of said thermally released vapors are turned into ions, and said ions are finally analyzed and detected in an analytical instrument.

2. The method of claim **1** where said at least one contamination prevention means includes:

a) said collection chamber is disposed of after use;

b) said gas is sampled into said collection chamber via a source of negative pressure, said source of negative pressure drawing said residual vapors from said collection chamber, and a no-return valve is introduced between said source of negative pressure and said collection chamber, so as to avoid backflow of said residual vapors into said collection chamber; and

c) a sample gas outlet flow of said source of negative pressure is released to the atmosphere at a place remote from the location where said sampling of said gas takes place, so as to moderate contamination of the surroundings of said collection chamber.

3. The method of claim **1** where said vapors thermally released onto said flow of clean gas are cleanly disposed of following said ionization and said analysis, such as to avoid contamination of either said analytical instrument or a room or cabin housing it.

4. The method of claim **1** where said analytical instrument includes a mass spectrometer.

5. The method of claim **4** including a differential mobility analyzer.

6. The method of claim **1** wherein the means for removing particles larger than 25 μm carried by said gas includes a prefilter.

7. The method of claim **1** wherein the means for removing particles larger than 25 μm carried by said gas includes an impactor.

8. A method to detect the presence of substances based primarily on the vapors they release to a surrounding gas, involving:

a) sampling said gas to which said vapors have been released and passing it through a prefiltering stage including means configured for removing particles larger than 25 μm carried by said gas,

b) passing said prefiltered gas into a vapor capture stage including a collection chamber containing a vapor collector, such that a fraction of said vapors are captured into said vapor collector,

c) where said vapor capture stage includes at least one contamination prevention means, such that residual vapors having circulated through said collection chamber during one vapor capture event are not released to the vapor collector during a subsequent vapor capture event into said gas, and therefore are not captured by the vapor collector during said subsequent vapor capture event, and

d) a desorption-ionization and analysis stage where said vapors captured into said vapor collector are thermally released into a flow of clean gas and passed through an

ionization chamber where a fraction of said vapors are turned into ions, and said ions are finally analyzed and detected in an analytical instrument,

where said vapors are ionized by bringing said vapors into close contact with an electrospray cloud, and where an electrified liquid meniscus producing said cloud is kept at a temperature greater than 100° C., such that said gas can be simultaneously maintained at a temperature greater than 100° C. and kept in direct contact with said meniscus.

9. The method of claim **8** where said liquid meniscus includes liquids with dielectric constants in excess of 10 and ambient pressure boiling points higher than 110° C.

10. The method of claim **9** where said liquids include one of the following:

N-Methyl 2-Pyrrolidone, dimethylformamide, Dimethyl sulfoxide, alcohols containing more than four carbon atoms, Formamide, Propylene carbonate, Tributyl phosphate, Sulfolane, or are more generally selected from the group consisting of amides, alcohols, glycols, esters, ketones, organic carbonates, organic phosphates, and mixtures of one or more of the foregoing.

11. The method of claim **9** where said analytical instrument includes a DMA whose recirculating gas is kept at a temperature higher than 70° C.

* * * * *

CHAPTER 5. ION MOBILITY SPECTROMETER-FRAGMENTER-ION MOBILITY SPECTROMETER ANALOGUE OF A TRIPLE QUADRUPOLE FOR HIGH-RESOLUTION ION ANALYSIS AT ATMOSPHERIC PRESSURE

analytical chemistry

Article

Cite This: *Anal. Chem.* 2018, 90, 6885–6892

pubs.acs.org/ac

Ion Mobility Spectrometer-Fragmenter-Ion Mobility Spectrometer Analogue of a Triple Quadrupole for High-Resolution Ion Analysis at Atmospheric Pressure

Mario Amo-González,*[,†] Irene Carnicero,[†] Sergio Pérez,[†] Rafael Delgado,[†] Gary A. Eiceman,[‡,§] Gonzalo Fernández de la Mora,[†] and Juan Fernández de la Mora[∥]

[†]SEADM, Parque Tecnológico de Boecillo 205, Valladolid, Spain 47151

[‡]Department of Chemistry and Biochemistry, New Mexico State University, Las Cruces, New Mexico 88003, United States

[§]Chemistry Department, Loughborough University, Loughborough, U.K. LE11 3TU

[∥]Mechanical Engineering Department, Yale University, New Haven, Connecticut 06520-8286, United States

Supporting Information

ABSTRACT: Two differential mobility analyzers (DMAs) acting as narrow band mobility filters are coupled in series, with a thermal fragmentation cell placed in between, such that parent ions selected in DMA_1 are fragmented in the cell at atmospheric pressure, and their product ions are analyzed on DMA_2. Additional mass spectrometer analysis is performed for ion identification purposes. A key feature of the tandem DMA is the short residence time (~0.2 ms) of ions in the analyzer, compared to tens of milliseconds in drift tube ion mobility spectrometers (IMS). Ion fragmentation within the analyzer and associated mobility tails are therefore negligible for a DMA but not necessarily so in conventional IMS. This advantage of the DMA is demonstrated here by sharply defined product ion mobility peaks. Ambient pressure ion fragmentation has been previously demonstrated by both purely thermal means as well as rapidly oscillating intense electric fields. Our purely thermal fragmentation cell here achieves temperatures up to 700 °C measured inside the heating coil of a cylindrical ceramic heater, through whose somewhat colder axis we direct a beam of mobility-selected ions. We investigate tandem separation of chloride adducts from the explosives EGDN, nitroglycerine (NG), PETN, and RDX and from deprotonated TNT. Atmospheric pressure fragmentation of the first three ions yields one or several previously reported fragments, providing highly distinctive tandem DMA channels for explosive identification at 1 atm. RDX ions had not been previously fragmented at ambient pressure, yet $[RDX + Cl]^-$ converts up to 7% (at 300 °C) into a 166 m/z product. The known high thermal resilience of TNT is confirmed here by its rather modest conversion, even when the ceramic is heated to 700 °C. At this temperature some previously reported fragments are found, but their mobilities are fairly close to each other and to the one of the far more abundant parent ion, making their identification by mobility alone problematic. We anticipate that moderately higher fragmenter temperatures will produce smaller fragments with mobilities readily separated from that of $[TNT - H]^-$.

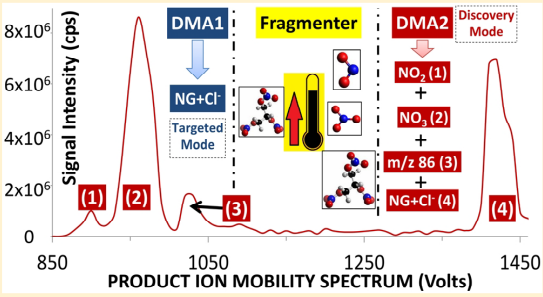

The triple quadrupole mass spectrometer Q^3-MS has remained one of the most successful mass spectrometer types, in spite of the development of other instruments with the vastly larger resolving power of the time of flight (TOF) MS or the Orbitrap. This ability to withstand such sophisticated competitors is evidently due to the unique Q^3 features of filtering (for as long as desired) a narrow range of masses before and after fragmentation, yielding unmatched transmission and resolution for targeted analysis. For this reason, a variety of efforts have been aimed at developing much lighter and economic analogues of the Q^3-MS. A promising line of research has relied on ion mobility filters operating near atmospheric pressure. Most ion mobility spectrometers (IMS) separate ions in time[1] and are the high-pressure analogues of TOF rather than quadrupole MS. Two of them can certainly be pulsed in series, but it is an entirely different principle. There are nonetheless several narrow band mobility filters that, like the quadrupole MS, separate ions in space rather than time and may be similarly ordered in tandem: field asymmetric IMS (FAIMS), also referred to as differential mobility spectrometry (DMS),[2−4] the differential mobility analyzer (DMA),[5] and its many variants,[6,7] and the periodic focusing differential mobility analyzer (PFDMA).[8] There are also creative schemes such as

Received: March 10, 2018
Accepted: April 25, 2018
Published: April 25, 2018

   DOI: 10.1021/acs.analchem.8b01086

overtone mobility spectrometry[9] and transversal modulation IMS (TMIMS)[10] that form effective steady beams of mobility-selected ions based on time periodic electric fields akin to those used in the conventional linear drift tube IMS. The use of pairs of these narrow band filters in tandem has been previously demonstrated in a variety of applications,[11−14] some via conversion of the parent ion into a different product by a spontaneous physical mechanism such as evaporation of neutrals[11,14] or ions,[13,14] others using the different responses of the two tandem instruments without altering the parent ion.[15] Controlled fragmentation of the selected parent ion by broadly applicable methods, however, is a key requirement where atmospheric pressure surrogates of the triple quadrupole have lagged behind their vacuum kin. This lag has greatly diminished thanks to extensive pioneering studies on ion fragmentation at ambient pressure. Single or tandem drift-time IMS with thermal activation at temperatures typically below 200 °C has led to the observation of fragmentation of species such as butyl acetate,[16] proton bound dimers,[17,18] and chloride adducts of various explosives.[19−21] Substantial thermal fragmentation taking place at the ∼10 ms time scale of the drift tubes was reported, resulting in pronounced tails in the mobility spectra. Following earlier studies,[22] electrically activated ion fragmentation has been also investigated, taking place naturally in DMS (FAIMS) instruments operating at high frequency with peak electric fields as high as 30 and even 60 kV/cm (ultra-FAIMS). FAIMS may accordingly be used in three stages, one to select the parent ion, another to fragment it, even at room temperature, and a final stage to analyze the fragments.[23] The feasibility of an atmospheric pressure tandem narrow band mobility filter with fragmentation is accordingly proven. What remains is selecting the most appropriate among the various known narrow band mobility filters as well as increasing the available activation energy to successfully fragment the most resilient species.

The present study explores two aspects of the problem. First, we select the differential mobility analyzer (DMA) as the apparently most suitable narrow-band mobility filter for tandem mobility analysis in single (or multiple) ion monitoring mode. The current resolving power ∼100 of DMAs[24] is below that of other mobility devices working with singly charged ions.[25,26] However, to our knowledge, this resolution is unmatched by any narrow band mobility filter operating with atmospheric pressure air or N_2. Another important feature of the DMA is its analysis time of ∼0.2 ms, several orders of magnitude below typical atmospheric pressure fragmentation times and IMS drift times. This circumstance precludes ion fragmentation within the analyzer, resulting in tail-free mobility peaks for the parent and its fragments, as narrow as in the absence of fragmentation. Note that the drying system used in our ion source eliminates completely any tails beyond the natural Gaussian shapes associated with diffusion.[27] Second, we use a purely thermal fragmenter oven operating up to ∼700 °C, achieving for the first time atmospheric pressure fragmentation of resilient species such as RDX and TNT. This oven design has the potential to reach considerably higher temperatures, to emulate under ambient conditions the fragmentation flexibility of the middle stage of a triple quadrupole. Note in this respect that a key difficulty in the pioneering studies of Yost and Enke[28] was achieving high efficiency in both fragmentation of the parent ions and transmission of the products. Products are not scattered out of the ion beam under atmospheric pressure, so no containment tool equivalent to the middle quadrupole is needed. The main difficulty is fragmenting thermally stable ions under atmospheric pressure.

METHODS

Figure 1 shows the schematic of the DMA-F-DMA instrument.

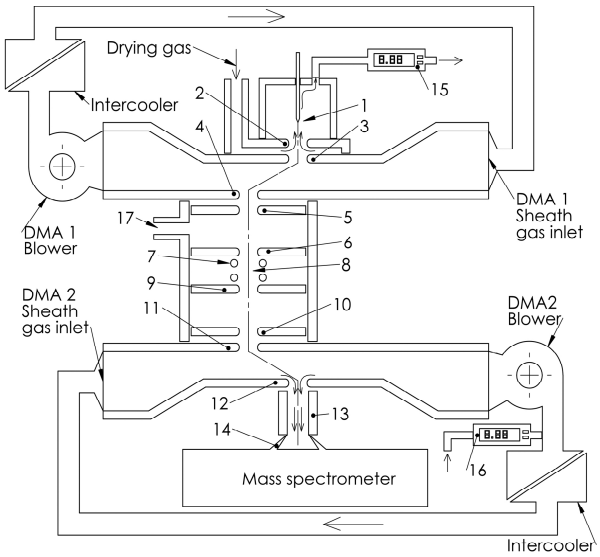

Figure 1. Schematics of the DMA-Fragmenter-DMA (DMA-F-DMA) coupled to a triple quadrupole mass spectrometer: (1) electrospray ionization source (ESI), (2) desolvating heated electrode, (3) DMA_1 inlet slit, (4) DMA_1 outlet slit, (5) DMA_1 extracting electrode, (6) fragmenter inlet electrode, (7) nichrome heating coils, (8) fragmenter region, (9) fragmenter outlet electrode, (10) DMA_2 focusing electrode, (11) DMA_2 inlet electrode, (12) DMA_2 outlet electrode, (13) resistive glass capillary, (14) mass spectrometer inlet orifice, (15) auxiliary exhaust flow meter, (16) auxiliary compensation flow meter, and (17) auxiliary gas inlet to the fragmenter region.

DMAs. We used SEADM's DMAs P5-G and P5-E for DMA_1 and DMA_2 (Figure 1), respectively, with critical dimensions collected in Table 1, which includes improvements over a similar instrument previously described.[29] An important practical innovation is that the flow-limiting orifice is no longer at the outlet slit of the DMA but in the MS. The DMA can then be quickly removed or installed without breaking the MS vacuum. The DMA combines a horizontal laminar flow of gas with a vertical electric field between two parallel plates, such that ions of different mobilities penetrating through a slit in the upper plate open up in a fan as they drift toward the other plate. Accordingly, only a small range of mobilities is sampled through a second slit in the outlet plate (Figure 1) and

Table 1. Critical Dimensions (mm) of SEADM's P5 DMA

		W_{DMA} [a]	H_{DMA} [b]	W_{slit} [c]	L_{slit} [d]	D [e]
both DMAs	inlet	17	10	7	0.6	
P5-E (DMA_2)	outlet	14.9	10	4.5	0.17	0.8
P5-G (DMA_1)					0.4	

[a]Channel width. [b]Channel height. [c]Slit width. [d]Slit length. [e]Orifice diameter (in P5-E the outlet geometry changes from slit to bore). For both DMAs the distance between the inlet and outlet slits is 40 mm (channel length).

DOI: 10.1021/acs.analchem.8b01086

Table 2. Voltage and Material for the Different DMA-F-DMA Electrodes, and Distance and Electric Field between Them

	voltage (V)	material	distance (mm)	electric field (kV/cm)	slit (width × length) or orifice (diameter) dimensions (mm)
electrospray	−8800				
desolvating electrode	−7300	SS 316	3	5.0	0.75 × 7
DMA_1 inlet electrode	−6300	SS 316	2.1	4.8	0.6 × 7
DMA_1 outlet electrode	−4300	SS 316	10	2.0	0.4 × 4.5
DMA_1 extracting electrode	−2300	SS 316	4	5.0	2 × 5
fragmenter inlet electrode	−300	SS 316	32	0.6	5 × 20
fragmenter outlet electrode	+300	SS 316	10	0.6	5 × 20
DMA_2 focusing electrode	+2300	SS 316	32	0.6	2 × 5
DMA_2 inlet electrode	+4300	SS 316	32	0.6	0.6 × 7
DMA_2 outlet electrode	+6300	SS 316	10	2.0	0.17 × 4.5 to diameter 0.8
mass spectrometer orifice	0 (grounded)		105	−0.6	diameter 0.6

transmitted to DMA_2 or to the MS, depending on which of the two DMAs we are considering.

Pump, Intercooler, and Sheath Gas Circuit. We used a sealed blower (792 series brushless blower, Domel d.o.o., Slovenia). To moderate vapor emissions into the closed gas circuit, an air intercooler (aluminum) placed between the blower outlet and the DMA inlet maintains the DMA and the blower temperature below 35 °C. The sheath gas circuit is formed by stainless steel corrugated NW50 tubes.

Analyte Ionization and ES Desolvation. Between 10 and 50 ppmv of explosive (AccuStandard Inc., New Haven, CT) were added to the electrospray liquid ($MeOH/H_2O$ 9:1, HCl 0.05%), which produced explosive ions directly from the liquid phase. This approach injected into the system an explosive flux of 6.8 pg/s/ppm. The explosives analyzed were ethylene glycol dinitrate (EGDN), nitroglycerin (NG), pentaerythritol tetranitrate (PETN), 1,3,5-trinitroperhydro-1,3,5-triazine (RDX), and trinitrotoluene (TNT). The negative ions generated were all chloride adducts of the explosive vapor, except for TNT, which ionized into the deprotonated vapor. The silica capillary (TaperTip: 360 μm o.d., 50 μm i.d., 50 cm in length, noncoated, ref TT360-50-50-N-5, New Objective, Woburn, MA) was placed in front of a desolvating electrode[26] through which a heated drying N_2 current desolvates the electrospray cloud.

Fragmenter. Prior FAIMS studies[22,30−33] have demonstrated the fragmentation power of strong radiofrequency (rf) electric fields. Indeed, a small ion with a (hypothetical) mobility in N_2 of 2 $cm^2/V/s$ in a near breakdown electric field of 35 kV/cm would move at a mean speed of 700 m/s. According to eq 1, a comparable thermal speed in N_2 may be achieved by raising the gas temperature to 825 K.

$$v_p = \sqrt{(2kT/m)} \quad (1)$$

where v_p is the most probable speed, k is Boltzmann's constant, T the absolute gas temperature, and m is the particle mass. In fact, using the tails of the Bolzmann velocity distribution, which always dominate reactive collisions, the same impact speeds may be achieved at substantially lower temperatures. Furthermore, higher molecular weight ions would have mobilities closer to 1 than to 2 $cm^2/V/s$, reducing 4-fold their center of mass collision energy. Atmospheric pressure fragmentation has also been demonstrated by purely thermal activation at gas temperatures as high as 200 °C.[21,20] Also by combinations of thermal and electrical activation. For instance, 30 kV/cm and gas temperatures from 30 to 110 °C gave effective temperatures exceeding the gas temperature by 260° at 30 °C and 100° at 110 °C.[34] In view of the fact that resistive heating of metallic wires to temperatures in excess of 900 K is commonly achieved in simple devices, and because of the greater simplicity and lesser power consumption of a heater versus a high voltage high frequency power supply (particularly at high temperature), we have opted for the purely thermal fragmenter depicted in Figure 1 (see also Figure S1 in the Supporting Information).

The fragmenter (Figure 1) includes an inlet electrode, a Macor insulator, and an outlet electrode. The Macor insulator supports two Nichrome coils that may reach temperatures of 700 °C, measured by a thermocouple placed inside the coil. However, the temperature in the plane of symmetry (ion beam path) between the heating coils was lower than the temperature measured inside the coil. Temperatures in the plane of symmetry were measured during the integration (not in operation) and are detailed in the Supporting Information (Table S1). In combination with an electrometer as ion detector, a second version of the same fragmenter was tested (referred to as v2 in the results), in which the Nichrome heating coil separation from the plane of symmetry (ion beam) was reduced from 4 (v1) to 2 mm (v2), in order to reach higher temperatures in the ion beam with the same heating coil temperature. In what follows, the terms *fragmenter temperature* or *oven temperature* will refer to the temperature read in the thermocouple inside the coils.

Because the rest of the system, including PEEK and Viton components, is incompatible with temperatures above 200 °C, the high temperature region must be confined. This requirement is achieved by housing the coiled Nichrome heating coils in a ceramic oven, covered by metal electrodes above and below. In preliminary work we observed that outgassing in the heater had drastic effects in obscuring the observation of the fragments, generally small ions (NO_2^-, NO_3^-) having a high tendency to solvate with vapors in the environment. Fragmenter materials were accordingly selected as metals and ceramics (Macor). Heater wires were supplied with an adjustable voltage power supply between 0 and 50 Vdc. When the coil temperature measured was 600 °C, the power consumption was 47 W and the voltage 33.6 Vdc. Since the voltage of the fragmenter inlet and outlet electrodes (Figure 1, items 6 and 9, respectively) is moderate (−300 V and +300 V, respectively), electric isolation was not a problem.

Electric Field Configuration. Table 2 details the voltages and materials of the DMA-F-DMA electrodes as well as the distance and the electric field between them. An electric field between the electrospray liquid and the desolvating electrode

DOI: 10.1021/acs.analchem.8b01086

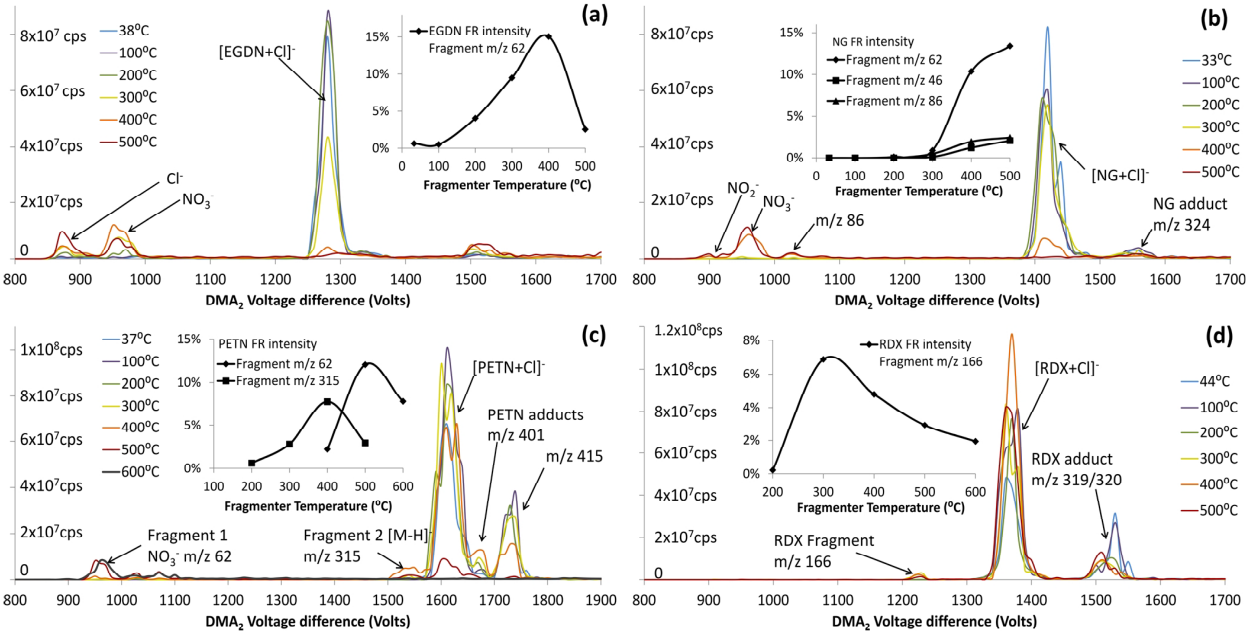

Figure 2. Oven temperature dependence of fragment ion mobility spectra in DMA_2, with DMA_1 transmitting the chloride adduct of the parent explosives EGDN, NG, PETN, and RDX. The insets show the ratios of the main fragment intensity at one fragmenter temperature divided by the precursor ion intensity at room temperature (33−44 °C). The explosives are introduced from electrospray solutions with 50 ppm of EGDN (a) or 10 ppm of NG, PETN, or RDX (b−d, respectively).

(Figure 1, item 2) drives the ions and droplets generated by the electrospray against the drying conterflow current (1 L/min at 160 °C), which desolvates small droplets, dragging upward (to the exhaust port of the ionization chamber) the neutral vapors produced by the evaporation process. The electric field between the desolvating electrode and the DMA_1 inlet electrode (Figure 1, item 3) drives the ions into DMA_1 where only one narrow mobility band is able to reach the outlet slit. In P5-G DMA (DMA_1), ions do not leave the DMA dragged by a sample flow (as in the P5-E; DMA_2), but they are extracted by the electric field between the outlet slit of DMA_1 (Figure 1, item 4) and the extracting electrode (Figure 1, item 5). The electric field between this extracting electrode and the inlet electrode (Figure 1, item 6) preceding the fragmenter drives the ions into the fragmenter (Figure 1, item 8). The voltages supplied to the two ends of the Nichrome heating coils (Figure 1, item 7) are 30 Vdc and zero, keeping it everywhere near ground. The separation of the Nichrome heating coils from the axis of the ion beam allows penetration of the electric field created by the fragmenter inlet and outlet electrodes (Figure 1, items 6 and 9, respectively). Another electric field between the fragmenter outlet electrode and the focusing electrode of DMA_2 (Figure 1, item 10) drives ions along this long region. The intense electric field between the focusing electrode of DMA_2 and the inlet electrode of DMA_2 (Figure 1, item 11) focuses ions into DMA_2, minimizing their losses in the inlet slit. DMA_2 classifies ions coming from the fragmenter according to their mobility. Downstream from the outlet slit of DMA_2 (Figure 1, item 12) there is a resistive glass capillary (Figure 1, item 13) (RGP T 6.15-0.94/100 model, Photonis, Mérignac, France) with an inner diameter of 0.94 mm, which allows ions to be dragged by the gas flow into the MS (Figure 1, item 14) against the adverse electric field along the capillary required to bring them from a high voltage to the inlet potential of the MS.

Fluid Configuration. In order to compensate for gas consumption into the sampling orifice of the MS (~2 L/min in the current configuration), 2 L/min of nitrogen were introduced into the drift gas of DMA_2. This flow rate is adjusted with the help of an auxiliary flowmeter placed downstream the ionization chamber exhaust port (Figure 1, item 15); the flow rate introduced to DMA_2 (Figure 1, item 16) is initially >2 L/min and is progressively decreased until this auxiliary flow meter reads no output flow, assuring that there is no counterflow through the DMA_2 inlet slit. Once the input flow to DMA_2 is adjusted, 1 L/min of nitrogen is heated and introduced through the desolvating electrode, leaving the ionization source through its exhaust port. In this situation the exhaust flow meter reads 1 L/min. Under this fluid configuration, ideally there is no flow in the fragmenter region (from the DMA_1 outlet slit to the DMA_2 entrance slit), so the ion velocity between both DMAs is controlled by the electric fields between the different electrodes of the system. This feature is critical to control the ion residence time in the fragmenter.

TNT did not fragment in pure nitrogen. Accordingly, in the TNT studies, 0.2 L/min of the more efficient infrared photon absorber CO_2[35] were introduced through the auxiliary gas inlet of the fragmenter v1 (Figure 1, item 17) to achieve higher temperatures in the ion beam path. Since there is no N_2 current coming from DMA_1, the atmosphere in the fragmenter was primarily CO_2. In this case, only 1.8 L/min of nitrogen were introduced into the drift gas of DMA_2, so that the 0.2 L/min input of CO_2 circulated through the ion path on its way to DMA_2 and the MS. The introduction of CO_2 led indeed to TNT fragmentation.

DMA-F-DMA-MS Software. The developed software allows the user to define the mobility range of both DMAs, jointly with the definition of the m/z range measured by the

DOI: 10.1021/acs.analchem.8b01086

MS in negative Q1 method, generating a batch of experiments in the MS experiment queue. The software assures the synchronization of the DMAs and the MS by means of a synch signal emitted by the MS at the beginning of every Q1 mass scan. Once the batch has been acquired, the software opens the MS files and generates either 2D DMA_2-MS contour plots or DMA_2 mobility plots.

DMA-F-DMA Mobility Calibration. As the voltage in DMA_1 (V_{DMA1}) selecting the precursor ion varies with changes in the atmospheric pressure, the value V_{DMA1} corresponding to the explosive of interest is determined periodically as follows: (1) a rough tandem DMA spectrum is acquired in order to determine approximately V_{DMA1} and V_{DMA2} for the precursor ion (fragmenter turned off). (2) V_{DMA2} is fixed at the approximate value obtained in step 1 and a detailed mobility spectrum is acquired sweeping the voltage in DMA_1 ±50 V away from the approximate V_{DMA1} value obtained in step 1. (3) The DMA_1 mobility spectrum obtained in step 2 is fitted to a Gaussian curve and the user is informed about the corresponding mean voltage V_{DMA1}. This routine takes 1.5 min, and it was usually performed first thing in the morning and when the studied explosive changed.

DMA-F-DMA-MS Measurement. V_{DMA1} is fixed at the mobility of the precursor ion of interest, while DMA_2 sweeps its voltage generating a mobility spectrum of all the ions leaving the fragmenter. At each V_{DMA2}, the mass spectrometer takes 1.22 s to scan in Q1 mode the range 30−1250 m/z. This enables the generation of 2D DMA_2-MS contour plots (Figure 3a) to identify fragment ions, or (in the case of TNT) to resolve fragments not properly distinguished in the mobility spectrum. In order to show a fragment mobility spectrum comparable to that produced by an electrometer detector, the vertical axis of the DMA_2 spectra shown in Figure 2 and Figure 3b represents the Total Ion Current Q1 (TIC), summing all ion intensities reaching the MS detector, regardless of m/z. In Figure 4 the fragment mobility spectra acquired with the MS have been postprocessed in order to show only the parent and fragment ions m/z, removing the signal associated to other m/z. Since DMA_1 only passes small ions (with mobilities comparable to those of the explosives studied), we do not expect that ions with m/z higher than the upper MS limit (1250 m/z), that are not sensed by the MS, would ever be detected in an electrometer.

DMA-F-DMA-Electrometer Measurement. The DMA-F-DMA instrument was disconnected from the MS and connected to SEADM's LYNX E12 faraday cup electrometer,[36] which is a low noise fast electrometer (response time of 25 ms). The experiments were programmed and postprocessed using SEADM's tandem DMA software. This software allows the user to either select V_{DMA1} and scan over DMA_2 or vice versa. The software reads the signal of the electrometer by means of a data acquisition card (DAQ) (USB-6002 model, National Instruments, TX) and plots the tandem DMA contour plots or the DMA_2 mobility spectra if V_{DMA1} is fixed. The dwell time at each V_{DMA2} was 250 ms, during which the DAQ read the electrometer output voltage at a frequency of 50 kHz, averaging it to produce a single value for every V_{DMA2}.

RESULTS

DMA-F-DMA Studies in Series with a Mass Spectrometer. Figure 2a−d shows fragment mobility spectra obtained in DMA_2 for EGDN, nitroglycerin (NG), PETN, and RDX, when DMA_1 is set to transmit the chloride adduct of

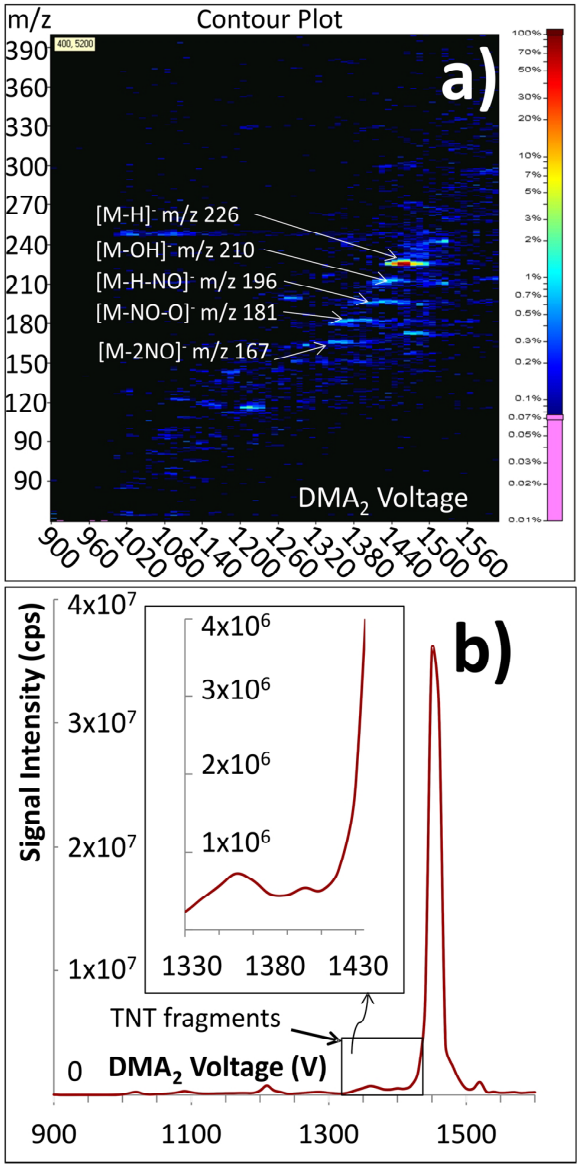

Figure 3. (a) DMA_2-MS ion product spectrum contour plot of electrospray solution containing 50 ppm TNT, with the fragmenter at 700 °C. The first DMA is fixed at the mobility of $[TNT - H]^-$ and (b) mobility spectrum (no m/z separation) for the same experiment.

the respective neutral vapors. Note the well-defined fragment mobility peaks, free from any tail that might have resulted from reactions in DMA_2. The most abundant fragments of $[EGDN + Cl]^-$ (a) are Cl^- and NO_3^-. However, since Cl^- is the charger ion in the electrospray solution, very many ions will produce Cl^- in their fragmentation spectra, delivering, in principle, less selectivity than the NO_3^- fragment. The inset in Figure 2a shows a maximal 15% conversion of EGDN into nitrate at 400 °C. This value is calculated as the fragment intensity at one fragmenter temperature divided by the precursor ion intensity at room temperature, due to the fact that at high fragmenter temperatures the precursor ion intensity for EGDN, NG, and PETN drops to background levels. NG (Figure 2b) yields three main fragments, two of which are identified in the MS as NO_2^- and NO_3^-. The larger fragment appearing at 86 m/z was also

DOI: 10.1021/acs.analchem.8b01086

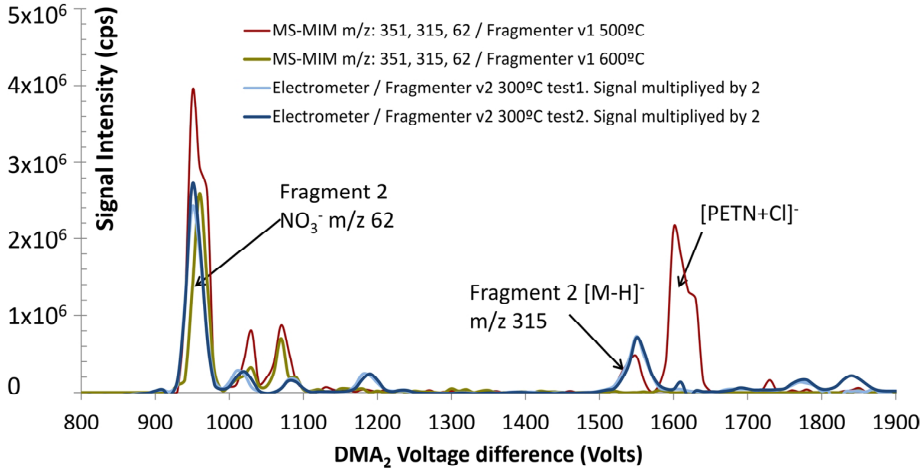

Figure 4. Fragment mobility spectra in DMA_2 with DMA_1 transmitting $[PETN + Cl]^-$, when electrospraying a solution with 10 ppm of PETN. Red and gold spectra were acquired using the MS as ion detector, working in multiple ion monitoring (MIM) selecting only the m/z corresponding to the parent ion (351 m/z) and the fragments (315, 62 m/z). The electrometer signal has been multiplied by a factor of 2 in order to approximately match the fragment intensities to facilitate comparison. The MS and electrometer tests have been carried out with the v1 and v2 versions of the fragmenter, respectively.

found in a previous NG fragmentation study performed with the triple quadrupole mass spectrometer. The main fragments found for $[PETN + Cl]^-$ (Figure 2c) are NO_3^- and $[M - H]^-$ (315 m/z). Both are common fragmentation products of PETN in vacuo.[37,38]

RDX is particularly stable and has, to our knowledge, not been previously thermally or electrically fragmented at atmospheric pressure. Exceptionally, RDX fragments provisionally identified as NO_3^- and NO_2^- have been reported in drift tubes heated from 120 to 200 °C,[39] though only in the presence of abundant electrons (produced by a negative discharge in N_2). The electrons were undoubtedly the cause of these reactions, which, since the mobility peaks exhibited no tails, must have taken place upstream of the analyzer. Discharge electrons would be effective fragmentation agents, though at the cost of a high discharge nitrate background in DMA_2, which would be fatal to the specific analysis of explosive fragments. As seen in Figure 2d, we observe only one RDX fragment, at 166 m/z. Although we have found no vacuum precedent for this product ion, it does arise repeatedly at atmospheric pressure and does not appear in blank experiments without RDX infusion.

TNT is expected to be even more thermally stable than RDX and has not been previously thermally or electrically fragmented at atmospheric pressure (though it can also be fragmented by thermal electrons). It is accordingly an excellent candidate to test the fragmenting capacity of our oven. Figure 3a is a DMA_2-MS contour plot for the product ions of the thermal fragmentation of $[TNT - H]^-$, obtained at the maximal oven temperature of 700 °C we can presently attain. The DMA-MS spectrum shows clearly the presence of a series of common $[TNT - H]^-$ fragments previously reported in fragmentation studies in vacuo.[34,40] These observations suggest for the first time that thermal activation at atmospheric pressure is likely to be effective with most ions, especially in future improved versions of the current oven. Notice however that the series of contiguous fragments dominating the picture at 700 °C are fairly close in mass to each other and cannot be individually resolved by mobility alone. This point is better seen in the fragment mobility spectrum of Figure 3b, where the low intensity mobility peaks created by the fragments (see inset) are overlapped among themselves and with the left tail of the dominating precursor ion. It is apparent that our oven has reached the required threshold to begin fragmenting TNT, but the temperature needs to be further increased to produce more distinctive and more abundant fragment ions.

DMA-F-DMA Studies with an Electrical Detector. The main practical advantage of the tandem DMA arrangement over a triple quadrupole is evidently in its portability and cost, which precludes using a MS as its detector. Once favorable parent/product channels for explosive identification have been found with the help of the MS, we proceed to test the quality of these channels when the detector is a simple electrometer. The red and gold spectra of Figure 4 reproduce the experiments of Figure 2c for PETN fragments, acquired at fragmenter v1 oven temperatures of 500 and 600 °C and using the MS as ion detector. In this case, the data have been postprocessed to show only the signal corresponding to the parent and the fragments ions (351, 315, 62 m/z, respectively). The dark and pale blue spectra were acquired in the new fragmenter v2 at an oven temperature of 300 °C, using an electrometer as the ion detector. As indicated in the legend, the electrometer signals were multiplied by a factor of 2 to match the MS signals and facilitate the comparison. Although the precursor ion $[PETN + Cl]^-$ decomposes fully in v2 at 300 °C, it requires 600 °C in v1, confirming the anticipated advantages of the new oven geometry in terms of higher temperatures in the ion beam path. However, the shorter distance between the coils in the v2 fragmenter weakens the electric field created between its inlet and outlet electrodes, limiting transmission. The sensitivity of the electrometer (the Johnson noise of about 600 cps) is some 3 orders of magnitude below that of single ion MS detectors. This disadvantage (not evident in Figure 4 because of the relatively high signal/noise) may be partially compensated by a higher ion transmission efficiency under atmospheric pressure than under vacuum. We expect that this potential compensation will result in the future in about an order of magnitude higher electrometer signal. It is, however, not yet realized in our

DOI: 10.1021/acs.analchem.8b01086

Table 3. Signals Registered at the Mobility of NO_3^- at Different Concentrations of PETN (Parent Ion) In the Electrospray Liquid[a]

		PETN concentration (ppb)				
		0 (blank)	100	500	1000	10000
signal intensity at NO_3^- DMA voltage (955 V)	S1	2.0×10^3	6.2×10^4	2.0×10^5	4.2×10^5	5.7×10^6
	S2	0.0	2.6×10^4	9.0×10^5	9.3×10^5	4.8×10^6
	S3	2.0×10^3	2.4×10^4	1.4×10^5	4.6×10^5	5.0×10^6
	S4	2.0×10^3	1.0×10^4	1.6×10^5		
	S5	2.0×10^3	2.2×10^4			
average (cps)		1.6×10^3	2.9×10^4	1.5×10^5	6.0×10^5	5.2×10^6
standard deviation (cps)		8.9×10^2	2.0×10^4	4.6×10^4	2.8×10^5	4.7×10^5

[a]The column with 0 ppm concentration is a blank containing only electrospray solution, to calculate the limit of detection of the instrument. S1, S2, S3, S4, and S5 = samples 1, 2, 3, 4, and 5.

system due to the greater losses in the v2 oven used for the electrometer measurements.

Limit of Detection. In our extensive experience with a DMA in tandem with a triple quadrupole, the background of explosives is dominated by atmospheric impurities.[41] However, at the lower resolution of the tandem DMA and the present early state of development of the ES source, the background appears to be dominated by electrosprayed impurities. Accordingly, as a rather preliminary measure of the system's sensitivity, we have investigated the background generated by the electrospray liquid in the DMA-F-DMA channel $[PETN - Cl]^- \rightarrow NO_3^-$ (DMA_2 voltage of 955 V) to infer the average signal received at that channel and its standard deviation. Quintuplicate measurements at varying PETN liquid concentrations are collected in Table 3 together with their mean value and standard deviation.

The limit of detection is calculated as $LOD = X + 3S$, where X is the background average (cps) of the 5 blank samples at the fragment mobility, and S is the standard deviation. Taking $X = 1.6 \times 10^3$ cps and $S = 8.9 \times 10^2$ cps yields LOD = 4 283 cps.

The analyte concentration to reach the LOD (y = 4283 cps) can be calculated as $LOD_{concentration}$ = 33.9 ppb by using the calibration line provided in the Supporting Information (Figure S2) ($y = 518.47x - 13280$).

The explosive, contained in the electrospray liquid solution, is sprayed continuously in the ionization source. The volumetric flow rate of electrospray solution can be calculated through Poiseuille's law (eq 2), where Δp is the pressure difference between both ends of the capillary, D is the inner diameter of the capillary, L is its length, η is the dynamic viscosity, and Q is the liquid flow rate,

$$Q = \frac{\Delta p \pi D^4}{128 L \eta} \quad (2)$$

Taking $\Delta p = 0.15 \times 10^5$ Pa, $D = 50 \times 10^{-6}$ m, $L = 0.5$ m, and $\eta = 5.4 \times 10^{-4}$ Pa, we find $Q = 8.6 \times 10^{-12}$ m^3/s. Multiplying by the electrospray solution density we obtain the mass flow rate of electrospray solution:

$$8.6 \times 10^{-12}\ m^3/s \times 792\ kg/m^3 = 6.8 \times 10^{-9}\ kg/s$$

Once the electrospray mass flow rate and the analyte concentration required to reach the LOD (34 ppb) are known, the analyte mass flow rate necessary to reach the limit of detection can be obtained:

$$LOD_{Analyte} = 34 \times 10^{-9} \times 6.8 \times 10^{-9}\ kg/s$$
$$= 2.3 \times 10^{-16}\ kg/s = 0.2\ pg/s$$

CONCLUSIONS

We confirm that the short ion transit time in DMAs facilitates a complete absence of ion fragmentation within the analyzer, sidestepping poor fragment resolving power previously observed in IMS^2 studies. Both parent and fragment ions can accordingly be cleanly resolved via DMA-F-DMA. This offers a simple analogue to the triple quadrupole, with improved resolution over previously demonstrated $FAIMS^3$, and a drastic increase in the resolving power of conventional IMS.

Effective fragmentation of EGDN, NG, PETN, RDX, and TNT was achieved. The first four explosives have produced clean tandem IMS spectra enabling high-resolution explosive identification by IMS alone. New fragmentation channels have been discovered here for the far more thermally stable $[RDX - Cl]^-$ and $[TNT - H]^-$ ions, which had not been previously fragmented at atmospheric pressure. Fragmentation of TNT is particularly demanding due to its singular thermal stability. Here we confirm and extend this previously known fact by showing that the beam of $[TNT - H]^-$ survives at atmospheric pressure in close proximity to a surface heated up to 700 °C. Our high-temperature fragmenter yields product ions (m/z 210, 197, 182, and 167) of TNT. HOwever, the proximity between fragment mobility peaks and their low abundance in comparison with the parent ion do compromise the clear recognition of these fragment peaks by IMS alone. Accordingly, TNT detection will benefit from the development of a fragmenter oven achieving temperatures above 700 °C.

ASSOCIATED CONTENT

Supporting Information

The Supporting Information is available free of charge on the ACS Publications website at DOI: 10.1021/acs.analchem.8b01086.

Photograph of the thermal fragmenter v1, experimental temperatures measured in the thermal fragmenter v1, and calibration curve for the determination of PETN limit of detection (PDF)

AUTHOR INFORMATION

Corresponding Author

*E-mail: mario.amo@seadm.com.

DOI: 10.1021/acs.analchem.8b01086

ORCID
Mario Amo-González: 0000-0001-6227-1365
Juan Fernández de la Mora: 0000-0002-9077-2877

Notes

The authors declare the following competing financial interest(s): Following Yale rules, Juan Fernandez de la Mora declares a financial interest in the company SEADM.

■ ACKNOWLEDGMENTS

This work has been funded by DSTL Contract 1000112322.

■ REFERENCES

(1) Eiceman, G. A.; Karpas, Z.; Hill, H. H. *Ion Mobility Spectrometry*, 3rd ed.; CRC Press: Boca Raton, FL, 2016.
(2) Purves, R. W.; Guevremont, R.; Day, S.; Pipich, C. W.; Matyjaszczyk, M. S. *Rev. Sci. Instrum.* **1998**, *69*, 4094−4104.
(3) Schneider, B. B.; Covey, T. R.; Coy, S. L.; Krylov, E. V.; Nazarov, E. G. *Anal. Chem.* **2010**, *82* (5), 1867−1880.
(4) Shvartsburg, A. A. *Differential Ion Mobility Spectrometry: Nonlinear Ion Transport and Fundamentals of FAIMS*; CRC Press: Boca Raton, FL, 2008.
(5) Knutson, E.; Whitby, K. J. *J. Aerosol Sci.* **1975**, *6*, 443−451.
(6) Tammet, H. F. *The Aspiration Method for the Determination of Atmospheric-Ion Spectra* [Original work in Russian from 1967]; Israel Program for Scientific Translations: Jerusalem, Israel, 1970.
(7) Labowsky, M.; Fernandez de la Mora, J. *J. Aerosol Sci.* **2006**, *37* (3), 340−362.
(8) Gillig, K. J.; Chen, C. H. *Mass Spectrom. (Tokyo)* **2014**, *3*, S0032. See alsoGillig, K. J.; Chen, C. H. *Periodic field differential mobility analyzer*. U.S. Patent Application Publication 20130187042 A1, July 25, 2013.
(9) Kurulugama, R. T.; Nachtigall, F. M.; Lee, S.; Valentine, S. J.; Clemmer, D.E. J. *J. Am. Soc. Mass Spectrom.* **2009**, *20* (5), 729−737.
(10) Vidal-de-Miguel, G.; Macía, M.; Cuevas, J. *Anal. Chem.* **2012**, *84*, 7831−7837.
(11) Rader, D. J.; McMurry, P. H. J. *J. Aerosol Sci.* **1986**, *17* (5), 771−787.
(12) Vidal-de-Miguel, G.; Macía, M.; Barrios, C.; Cuevas, J. *Anal. Chem.* **2015**, *87* (3), 1925−1932.
(13) Attoui, M.; Fernandez-García, J.; Cuevas, J.; Vidal, G.; Fernandez de la Mora, J. *J. Aerosol Sci.* **2013**, *55*, 149−156.
(14) Attoui, M.; Paragano, M.; Cuevas, J.; Fernandez de la Mora, J. *Aerosol Sci. Technol.* **2013**, *47* (5), 499−511.
(15) Menlyadiev, M. R.; Eiceman, G. A. *Anal. Chem.* **2014**, *86* (5), 2395−2402.
(16) Eiceman, G. A.; Shoff, D. B.; Harden, C. S.; Snyder, A. P. *Int. J. Mass Spectrom. Ion Processes* **1988**, *85* (3), 265−275.
(17) Ewing, R. G.; Eiceman, G. A.; Harden, C. S.; Stone, J. A. *Int. J. Mass Spectrom.* **2006**, *255*−*256*, 76−85.
(18) Rajapakse, M. Y.; Stone, J. A.; Eiceman, G. A. *J. Phys. Chem. A* **2014**, *118* (15), 2683−2692.
(19) Rajapakse, M. Y.; Stone, J. A.; Eiceman, G. A. *Int. J. Mass Spectrom.* **2014**, *371*, 28−35.
(20) Rajapakse, M. Y.; Stone, J. A.; Eiceman, G. A. *J. Phys. Chem. A* **2014**, *118* (15), 2683−2692.
(21) Rajapakse, M. Y.; Fowler, P. E.; Eiceman, G. A.; Stone, J. A. *J. Phys. Chem. A* **2016**, *120* (5), 690−698.
(22) Atkinson, J.; Clark, A.; Grant, B. *Ion Modification*. U.S. Patent Application 20160203967 A1, July 14, 2016 (Application No. 14/913,946; PCT No. PCT/GB14/52540).
(23) Menlyadiev, M. R.; Tarassov, A.; Kielnecker, A. M.; Eiceman, G. A. *Analyst* **2015**, *140* (9), 2995−3002.
(24) Amo-González, M.; Pérez, S. Planar Differential Mobility Analyzer (DMA) with Resolving Power of 110. *Anal. Chem.*. **2018**, DOI: 10.1021/acs.analchem.8b00579, Just Accepted Manuscript.
(25) Merenbloom, S. I.; Glaskin, R. S.; Henson, Z. B.; Clemmer, D. E. *Anal. Chem.* **2009**, *81* (4), 1482−1487.
(26) Adams, K. J.; Montero, D.; Aga, D.; Fernandez-Lima, F. *Int. J. Ion Mobility Spectrom.* **2016**, *19*, 69−76.
(27) Amo-Gonzalez, M.; Fernandez de la Mora, J. *J. Am. Soc. Mass Spectrom.* **2017**, *28* (8), 1506−1517.
(28) Yost, R. A.; Enke, C. G.; Mcgilvery, D. C.; Smith, D.; Morrison, J. D. *Int. J. Mass Spectrom. Ion Phys.* **1979**, *30* (2), 127−136.
(29) Rus, J.; Moro, D.; Sillero, J. A.; Royuela, J.; Casado, A.; Fernández de la Mora, J. *Int. J. Mass Spectrom.* **2010**, *298*, 30−40.
(30) An, X.; Eiceman, G. A.; Räsänen, R. M.; Rodriguez, J. E.; Stone, J. A. *J. Phys. Chem. A* **2013**, *117*, 6389−6401.
(31) Kendler, S.; Coy, S. L.; Nazarov, E. G. *Int. J. Mass Spectrom.* **2007**, *263*, 137−147.
(32) An, X.; Eiceman, G. A.; Rodriguez, J. E.; Stone, J. A. *Int. J. Mass Spectrom.* **2011**, *303* (2), 181−190.
(33) Ruszkiewicz, D. M.; Thomas, C. L. P.; Eiceman, G. A. *Analyst* **2016**, *141*, 4587−4598.
(34) An, X.; Eiceman, G. A.; Raesaenen, R. M.; Rodriguez, J. E.; Stone, J. A. *J. Phys. Chem. A* **2013**, *117* (30), 6389−6401.
(35) Burch, D. E.; Gryvnak, D. A.; Williams, D. *Appl. Opt.* **1962**, *1*, 759−765.
(36) Fernandez de la Mora, J.; Perez-Lorenzo, L. J.; Arranz, G.; Amo-Gonzalez, M.; Burtscher, H. *Aerosol Sci. Technol.* **2017**, *51* (6), 724−734.
(37) Radauscher, E. J.; Keil, A. D.; Wells, M.; Amsden, J. J.; Piascik, J. R.; Parker, C. B.; Stoner, B. R. *J. Am. Soc. Mass Spectrom.* **2015**, *26*, 1903−1910.
(38) Yinon, J.; McClellan, J. E.; Yost, R. A. *Rapid Commun. Mass Spectrom.* **1997**, *11*, 1961−1970.
(39) Khayamian, T.; Tabrizchi, M.; Jafari, M. T. *Talanta* **2003**, *59*, 327−333.
(40) Fu, X.; Zhang, Y.; Shi, S.; Gao, F.; Wen, D.; Li, W.; Liao, Y.; Liu, H. *Rapid Commun. Mass Spectrom.* **2006**, *20*, 2906−2914.
(41) Zamora, D.; Amo-Gonzalez, M.; Lanza, M.; Fernandez De La Mora, G.; Fernandez de la Mora, J. *Anal. Chem.* **2018**, *90*, 2468.

DOI: 10.1021/acs.analchem.8b01086

CHAPTER 6. TANDEM ION MOBILITY SPECTROMETRY FOR THE DETECTION OF EXPLOSIVES IN CARGO AT CONCENTRATIONS OF PARTS PER QUADRILLION

analytical chemistry

Article

Cite This: *Anal. Chem.* 2019, 91, 14009−14018

pubs.acs.org/ac

Tandem Ion Mobility Spectrometry for the Detection of Traces of Explosives in Cargo at Concentrations of Parts Per Quadrillion

Mario Amo-González,*[,†] Sergio Pérez,[†] Rafael Delgado,[†] Gonzalo Arranz,[†] and Irene Carnicero[†]

[†]SEADM, Parque Tecnológico de Boecillo 205, Valladolid, Spain

Supporting Information

ABSTRACT: A tandem ion mobility spectrometer (IMS^2) built from two differential mobility analyzers (DMAs) is coupled at ambient pressure with a thermal fragmenter placed in between, such that the precursor ions selected in the first DMA are thermally decomposed at ambient pressure in the fragmenter and the product ions generated are filtered in the second DMA. A thermal desorber and a multicapillary gas chromatography (GC) column are coupled to a secondary electrospray (SESI) ion source, so the adsorption sampling filters are thermally desorbed and the liberated vapors are separated in the GC column, prior to their ionization and mobility/mobility classification. The new fragmenter allows the fragmentation of the five explosives studied: RDX, PETN, NG, EGDN, and TNT. The background of the analyzer is evaluated for the five explosives using air samples of 500 L volume. An atmospheric background of only 2.5 pg (5 ppq) is found for TNT, being somewhat higher for the rest of explosives studied. The architecture GC-IMS^2 is compared with GC-IMS obtaining a 100-fold increase of sensitivity in the first configuration, confirming the high selectivity provided by the fragmentation cell and the second IMS stage for the product ion mobility analysis. The analyzer is tested also with real explosives hidden in cargo pallets achieving successful detection of four (EGDN, NG, TNT, and PETN) out of five explosives.

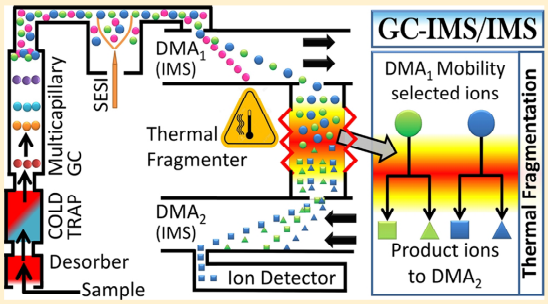

Ion mobility spectrometry (IMS) allows for the rapid, inexpensive, and portable classification of ions at atmospheric pressure, though with a modest resolving power compared to that achieved by mass spectrometry. One approach to overcome this limited selectivity is to combine IMS with other devices (such as chromatography or mass spectrometry), often at the cost of analysis speed, simplicity, or affordability. Another approach, preserving the positive characteristics of IMS, is to use the chemical orthogonality provided by selective ion transformations in a tandem IMS configuration: mobility-selected ions from a first IMS analysis region are modified in an intermediate reaction region, and the products are analyzed again in a second IMS analysis region. Among the several possibilities of ion transformation, this work will be focused on ion decomposition at atmospheric pressure.

Tandem analysis with intermediate ion fragmentation has been exploited for many years in the triple quadrupole mass spectrometry Q^3-MS. A key to the success of this analyzer is the singular ability of the quadrupole to extract, for as long as desired, a single mass-to-charge ratio out of a complex ion mix before and after ion manipulation. Several IMS systems also function as narrow-band ion-mobility filters by separating ions in space, delivering a continuous stream of selected mobility ions. This is in contrast to drift tube IMS and trapped-ion-mobility spectrometry (TIMS) which separate ions in time, therefore delivering a pulsed stream of ions. Narrow band mobility filters include field asymmetric IMS (FAIMS), also referred to as differential mobility spectrometry (DMS),[1−3] the periodic focusing differential mobility analyzer (PFDMA),[4] and the many variants[5,6] of the differential mobility analyzer (DMA).[7] The DMA, besides its quadrupole-like operation, has other interesting characteristics favoring a tandem architecture. These include a resolving power exceeding 100 for singly charged ions of mobility 1 $cm^2/V/s$,[8] and a short residence time within the analyzer in the order of 200 μs,[8] compared to tens of ms in drift time IMS. This high-speed feature precludes decomposition reactions within the analysis[9] removing the wide mobility tails observed in drift time IMS for the precursor ion and its fragments.[10,11]

Ion fragmentation at atmospheric pressure has been studied in single drift-time IMS with thermal activation at temperatures below 224 °C, leading to the observation of fragmentation of species such as butyl acetate[10] and proton bound dimers.[11] Thermal and electric field energy has been combined to study the ion fragmentation in a single DMS.[12,13]

Tandem drift-time IMS studies have demonstrated the feasibility of fragmentation of explosive chloride adducts within the second IMS analysis region.[14−16] Tandem DMS (FAIMS-DMS) has been used to study the different responses of the

Received: August 6, 2019
Accepted: September 26, 2019
Published: September 26, 2019

   DOI: 10.1021/acs.analchem.9b03589

two tandem instruments either without altering the precursor ion,[17] or dissociating it through the intense electric fields present in the first mobility analysis region (FAIMS) while analyzing the products in the second one (DMS).[18] In the cited studies, ion fragmentation takes place within the mobility analysis region, such that some product ions are dispersed in a mobility tail distributed between the natural precursor and product ion mobility peaks. However, when the reaction region is located between the two mobility analysis regions, the product ion intensity is ideally concentrated in a single Gaussian peak with no tailing. The first tandem IMS study took place in the mid 1980s.[19,20] Similar configurations have been used in later years under reduced pressure (below 12 Torr of helium gas), under which electrically activated fragmentation is simpler to achieve.[21,22] Our first DMA-F-DMA report used only a thermal fragmenter oven operating at ambient pressure to analyze several explosives electrosprayed from a liquid solution.[23] Recently, an atmospheric pressure fragmenter, combining heating with electrical activation in intense fields, was sandwiched between two drift time IMS systems to study explosives.[24]

Here we extend our prior work[23] to study explosives in air at ppq concentrations, using a thermal desorber connected to a multicapillary GC, then a SESI ionization source coupled to the DMA-F-DMA instrument. Both the multicapillary GC and the ion fragmentation provide orthogonal separation to the mobility analysis, maintaining the analysis time within 3 min. The thermal fragmenter architecture placed between the DMAs has been completely redesigned, allowing independent control of the thermal and electric fields inside the fragmenter. The GC-DMA-F-DMA has been evaluated for the detection of EGDN, NG, TNT, PETN, and RDX explosives hidden in cargo. The atmospheric chemical background has been evaluated through the analysis of real blank atmospheric samples of 500 L of air. Samples taken from cargo pallets loaded with commercial explosives have been analyzed, assessing the ability of detection under this scenario for the different explosives.

METHODS

Vapor Sampling and Collection. Vapor sampling was performed using a high flow sampler (160 L/min) which forced 500 L of air through a collector vapor filter of fiberglass/stainless steel coated with Tenax-GR[25] (provided by TeknoScan Systems, Ontario, Canada). Filter vapor collection efficiency (typically ~10%) was previously studied.[26] To reduce the background variability, explosive detection is based solely on vapors, via a 10 μm particle prefilter placed upstream of the collector vapor filter.

Blank Samples. Blank atmospheric samples of 500 L of air were collected at the end of July 2018 in Boecillo (Spain) to study the analyte interferences present in the air matrix. According to our previous experience, the presence of atmospheric compounds interfering with explosives, increases with ambient temperature, justifying the blank sampling campaign in the middle of the hottest days of summer. These blank samples were used to assess the atmospheric background of the analyzer. What we call atmospheric background is really the sum of the internal (analyzer) background and the external (atmospheric) background, the former being considerably lower than the latter.

Explosive Loaded Samples (Explosive Hidden in Cargo Pallets). A campaign with commercial explosives was performed at INTA's (Spain's National Institute of Aerospace Technology) facilities. To avoid cross-contamination, the explosives were bought specifically for these tests. The tests were conducted outdoors, in a well-ventilated area, to minimize explosive contamination issues. In order to ensure that the atmosphere in the sampling area was clean (something not trivial in an explosive test center), blank samples were analyzed in advance with the help of an explosive analyzer based on DMA-MS/MS capable of detecting subppq explosive traces.[26] Hereinafter we will refer to this singularly sensitive analyzer as ACES E2.1.

The pallets were built every morning from 27 cardboard boxes measuring 40 × 40 cm, then covered in a plastic film and placed on a wooden pallet. After taking blank samples, 50 g of explosive (see Supporting Information Table SI-1) contained in an open Tupperware container were placed in the central box of the pallet (one explosive per pallet), then the pallet was covered in plastic film again. To increase the vapor emanation, the central box containing the explosive was drilled (about 8 holes, 10 mm in diameter, were made in each face of the box apart from the top face). Four pallets were tested at the same time, keeping a distance of 10 m between pallets (see SI Figure SI-2 for a view of the test area).

The explosive was inserted in the morning (at about 10 a.m.) with ambient temperatures ranging between 10 and 13 °C. After a soaking time of 2 h, three consecutive samples of 500 L were taken from every pallet, the sampler being at a minimum distance of 20 m downwind of the pallet in order not to contaminate either the pallets or the test area. Ambient temperatures during the sampling ranged between 19 and 23 °C. Sampling was performed by cutting a small slit in the pallet film (approximately centered on the pallet top face) through which a 30 cm Teflon tube (10 mm ID) was inserted between two boxes. From the three samples taken per pallet, one sample was analyzed with the GC-DMA-F-DMA instrument, and another with ACES E2.1 to correlate the results. The third sample was stored.

System Calibration. To calibrate the gain of the instrument, controlled amounts of explosives were spiked onto the sampling filter. The explosive standards (Isostandards Material, Madrid, Spain) with an initial concentration of 100 ppm_v, were diluted in methanol to a concentration of 1 ppm_v for EGDN, NG, PETN, and RDX and 20 ppb_v for TNT. The volume of the sample spiked was 2 μL and, prior to desorption, the solvent was allowed to evaporate from the filter during a waiting period of 30 s.

Thermal Desorption and Cold Trap. The thermal desorber was operated at a fixed temperature of 200 °C, with a desorption flow rate of 0.2 L/min (N_2 99.95% purity). Preliminary experiments of the DMA-F-DMA were carried out without the GC module, then the gas from the desorber was directed to the ionization source. When the GC was introduced, the outlet of the thermal desorber was connected to a six-port valve (model VA-2C6UWE from Valco Instruments Co. Inc., Waterbury, CT), which diverted the desorber flow rate either to a custom-made cold trap or to the exhaust port (SI Scheme SI-3 details the six-port valve connection). The custom-made cold trap was built from a fused silica-lined stainless steel tube (Sigma-Aldrich, St. Louis, MO) with the dimensions: $^1/_{16}$ in. o.d., 1 mm i.d., 11.5 cm in length. Since this trap has neither a stationary phase nor adsorbents inside, during the desorption period (1 min) the cold trap was cooled by means of a coolant spray down to approximately −10 °C, to

DOI: 10.1021/acs.analchem.9b03589

efficiently trap the most volatile compounds. Once the desorption was finished, the six-port valve was manually actuated communicating the cold trap with the analysis GC column, with the carrier gas (200 mL/min) passing in the reverse direction through the trap. At the same time as the actuation of the 6-port valve, two parallel processes started: (1) the cold trap was quickly heated up to 200 °C by means of a gas heater controlled by a PID controller, liberating the retained compounds to the GC column, and (2) a limit switch was activated, starting the analysis routine coinciding with the origin of retention time (retention time R_t = 0 s).

GC Column. A 20 cm-long multicapillary gas chromatography column (MCC−GC) was used to separate in time the gas phase compounds desorbed from the cold trap. The column (model ST2−40/OV-5/0.2, Multichrom Ltd., Novosibirsk, Russia) consists of a bundle of approximately 1000 quartz parallel capillaries of 40 μm inner diameter, covered by 0.2 μm of nonpolar stationary liquid phase OV-5 (5%, diphenyl; 95%, dimethylpolysiloxane). It was operated at an isothermal temperature of 110 °C, with a N_2 (99.9992% purity) gas flow rate of 200 mL/min, matching the flow rate at which the ionization efficiency in the secondary electrospray ionization source is at the maximum. One peculiarity of the multicapillary columns is that the dependence of HETP (height equivalent to a theoretical plate) on carrier gas velocity shows a broad minimum,[27] in other words, high carrier gas flow rates are tolerated with modest losses on column efficiency.

Secondary Electrospray Ionization Source (SESI). The MCC column was connected with the ionization source by a 40 cm-long transfer line heated at 210 °C. Neutral vapors separated in the column were transported by the carrier gas, entering the desolvating-low flow SESI (D-LFSESI). The low-flow SESI (LFSESI)[28] source allows for high ionization efficiency, via a long residence time of the neutral vapors in the ionization region. An electric field draws the vapor ions as they are produced, moderating their dilution by space charge, and transmitting them efficiently into the DMA. The LF-SESI approach[28] was recently complemented by introducing a symmetric counterflow drying system (desolvating-LFSESI)[9] to efficiently desolvate the electrospray cloud, preventing neutral vapors and small droplets from entering the DMA. This improvement allowed a reduction in the mobility peak tailing by a factor of 100−1000 with respect to its predecessor, reaching the theoretical Gaussian shape.

The ion source temperature was set at 170 °C, the counterflow drying gas was set at 1 L/min and also 170 °C, the electric fields in the different regions are summarized in SI Table SI-4. The electrospray silica capillary used was a New Objective (Woburn, MA) SilicaTip: 360 μm o.d., 50 μm ID, 15 μm tip ID, 80 cm in length, noncoated (ref FS360-50-15-N-5-C80). The solvent negatively electrosprayed by the SESI ionizer was water/methanol/HCl 1/9/0.0005 (v), producing predominantly Cl^-. TNT is deprotonated, while all the other explosive vapors studied ionize by Chloride attachment.[9,26]

DMAs. We used SEADM's DMAs P5-G and P5-E for DMA_1 and DMA_2 (Figure 1) respectively. The DMAs, the blower and its circuit have been described in more detail elsewhere.[23]

Fragmenter. The function of the fragmenter cell, located between the two DMAs, is to provide ions with the necessary activation energy for decomposition. As previously observed,[14−16] the fragmentation of some explosives such as

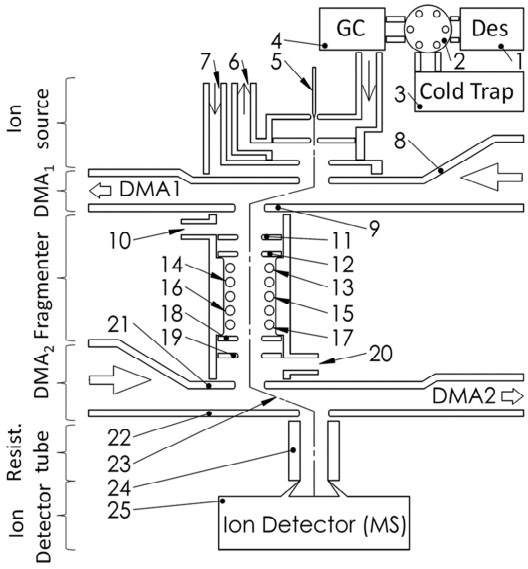

Figure 1. Schematics of the DMA-Fragmenter-DMA. (1) Thermal desorber. (2) Six-port valve. (3) Custom-made cold trap. (4) Multicapillary GC column. (5) Electrospray electrode. (6) Exhaust gas port. (7) Desolvating gas port. (8) DMA_1 inlet electrode. (9) DMA_1 outlet electrode. (10) Auxiliary gas port_1. (11) DMA_1 extractor electrode. (12) Fragmenter inlet electrode. (13), (14), (15), (16), and (17) Heating coil levels 1, 2, 3, 4, and 5 respectively. (18) Fragmenter outlet electrode. (19) DMA_2 focusing electrode. (20) Auxiliary gas port_2. (21) DMA_2 inlet electrode. (22) DMA_2 outlet electrode. (23) Ion path. (24) Resistive glass capillary. (25) Ion detector (MS).

EGDN, NG, and DNT, follows a first-order rate law expressed by the eq 1:

$$\text{rate} = e^{-kt} \quad (1)$$

Where k is the rate constant and t is the time. The Arrhenius equation relates the rate constant k with the temperature of the system T, the activation energy E, the gas constant R and the pre-exponential factor A:

$$k = Ae^{-E/RT} \quad (2)$$

Prior studies by Eiceman and colleagues[12,13,18] have achieved ion decomposition by a combination of intense oscillating electric fields and moderate heating up to about 200 °C. Since in (2) the decomposition rate k increases exponentially with T, given our new fragmenter capable of reaching high temperatures and transmitting ions efficiently, the approach of relying exclusively on heating seemed simpler. This new fragmenter design is shown in Figure 2.

It is composed of an inlet electrode, an outlet electrode and five independent pairs of heating coils, each held at a different potential, such as to create an axial electric field to transmit the ions efficiently. In other words, the heating power delivered to each pair of coils and the axial electric field created by the coils are independently controlled via the coil voltages V_n and the coil currents I_n, resulting in a desired residence time and temperature of the ions through the oven. The voltage of each electrode of the fragmenter is detailed in SI Table S-4. The averaged axial electric field inside the fragmenter is 0.9 kV/cm and the fragmenter length is 32 mm (Figure 2), so for an ion

DOI: 10.1021/acs.analchem.9b03589

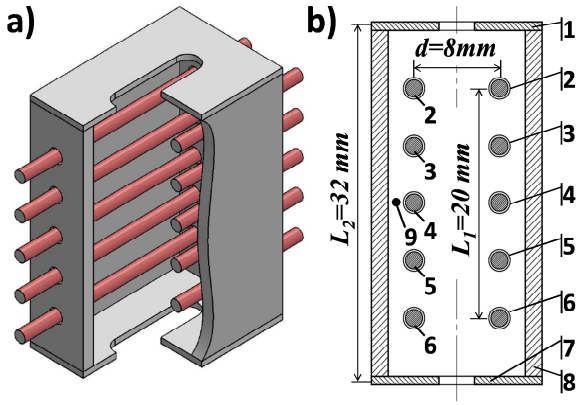

Figure 2. Isometric view (a) and transversal section (b) of the fragmenter (sketch). (1) Fragmenter inlet electrode at voltage V_1. (2), (3), (4), (5), and (6) are the different heating coil levels at voltage V_n and through each coil passing an electrical current I_n. (7) Fragmenter outlet electrode at voltage V_7. (8) Mirror polished walls. (9) Thermocouple position. d represents the transversal coil distance (orthogonal to the ion flow direction).

electrical mobility Z = 1 cm^2/V/s, the residence time within the thermal fragmenter is about 3 ms.

The temperature was measured with a type K thermocouple (mark 9 in Figure 2) placed at 2 mm of one of the intermediate heating coils. The fragmenter electronics allows independent control of I_n and V_n. The maximum electrical current available is 4 A per coil level (two coils connected in parallel). SI Figure SI-5 shows the fragmenter temperature reached for different intensity set points up to 3 A, at which a temperature of 818 °C was measured. The logarithmic fitting of the experimental points estimates a temperature of 930 °C at full power (SI Figure SI-5), however we had no need to work at such high temperatures. In fact, during the characterization of the explosive fragmentation, the maximum temperature tested was 700 °C, whereas in the GC-DMA-F-DMA final configuration, the fragmenter does not exceed 400 °C. To reduce the amount of infrared radiation absorbed by the stainless steel fragmenter walls, they are mirror polished. The fragmenter temperature set point is controlled by an Arduino microcontroller commanded by the software.

Resistive Glass Capillary Tube. Downstream from the outlet electrode of DMA_2 (Figure 1, item 22) there is a resistive glass capillary (Figure 1, item 24) (RGP T6.15−0.94/100 model, Photonis, Me′rignac, France) with an inner diameter of 0.94 mm. This allows ions to be dragged by the gas flow into the MS against the adverse electric field along the capillary required to bring the negative ions from a high positive voltage to the ground potential of the MS inlet orifice.

Mass Spectrometer. A Sciex Qtrap 5500 was used as an ion detector. To detect the TNT fragments (see Results section), the MS was used in MRM mode (MS/MS). For the rest of the results presented in this work, the MS was operated in single quad mode, performing Q3 m/z scans between 30 and 400 Da every 0.4 s. Although the m/z information is available it was not used. In order to emulate the response of an ultralow noise electrometer, we instead used the total ion current (TIC) values, corresponding to the sum of all ion intensities reaching the MS detector, regardless of m/z. Since with the exception of the TNT fragmentation results, the MS is used as an ion detector instead of as an MS, we do not include the acronym "MS" after GC-DMA-F-DMA. Our plan in the short term is to replace the MS with a low-noise electrometer.[29]

Fluid Configuration. Bottled N_2 (99.9992% purity) was used as a carrier gas in the multicapillary column, the rest of the supplied gases were nitrogen with a purity of 99.95% coming from a N_2 generator model NitroFlow basic, (Parker Hannifin, Cleveland, OH). The desorber flow rate was 0.2 L/min, the same as the carrier gas flow rate. After ionization, the carrier gas flow was exhausted together with the desolvating current[9] (1 L/min) by the ion source exhaust gas port (Figure 1 item 6). No gas flow was introduced through either the inlet or the outlet slit of DMA_1: All ions entered and left the DMA_1 driven electrically. The same applies to the inlet slit of DMA_2. An auxiliary gas of 1 L/min was introduced through the auxiliary gas port_1 and exhausted through the auxiliary gas port_2 (Figure 1 items 10 and 20, respectively). Since ion transmission is performed by electrical means from the electrospray tip until the outlet electrode of DMA_2, the auxiliary gas current is not essential. However, we found experimentally that this flow rate increased the signal by a factor of 2. Finally, ions were extracted from DMA_2 through the gas stream drawn by the mass spectrometer (∼2 L/min in the current configuration). In order to compensate for this gas consumption, the same gas flow rate was introduced into the drift gas of DMA_2.

DMA-F-DMA Mobility Calibration. As the peak voltages in DMAs vary with changes in the atmospheric pressure, an internal standard dissolved in the electrospray solution was used to calibrate both DMAs. The ratio of the mobility of the target explosives and the calibrant were determined experimentally at the beginning of the project. The calibration routine was performed automatically by the software before each experiment.

GC-DMA-F-DMA Measurement. Since the GC separates the different desorbed compounds in time, the analysis duration (2 min) was divided into five intervals (see Table 1) around the retention times (R_t) of each of the five explosives analyzed. In each interval, DMA_1 is tunned at the corresponding precursor ion mobility, the fragmenter temperature is set at the optimum explosive fragmentation temperature (see Table 1), and DMA_2 is set at the explosive product ion mobility. The MS delivers the TIC ion intensity each 0.4 s.

Although the GC-DMA-F-DMA spectra of each explosive is acquired during its full analysis interval, only the signal located at ±0.5 s away from R_t is used for explosive quantification. The signal (counts/s) is integrated over the quantification interval

Table 1. Precursor and Product Ion Selected for Each Explosive, Fragmenter Temperature, Analysis Intervals, Retention Time (R_t), and Explosive Gain

multicapillary GC-DMA-F-DMA parameters						
expl.	precursor ion	fr. temp. (°C)	product ion	analysis intervals (s)	R_t[a] (s)	gain (counts/pg)
EGDN	$[M+Cl]^-$	145	NO_3^-	0−6	3.0	105
NG	$[M+Cl]^-$	145	NO_3^-	6−15	9.3	847
TNT	$[M-II]^-$	400	$[M-II]^-$	15−60	46	12 060
PETN	$[M+Cl]^-$	189	NO_3^-	60−102	84	403
RDX	$[M+Cl]^-$	280	NO_2^-	102−120	111.5	232

[a]Retention time in the GC column.

DOI: 10.1021/acs.analchem.9b03589

(±0.5 s away from R_t) and the resulting integrated counts are converted into mass by dividing by the explosive gain (counts/pg). The explosive gain (Table 1) is calculated by spiking standards in an adsorption filter, integrating the signal over the quantification interval and dividing the resulting integrated counts between the explosive mass spiked.

RESULTS

Fragmentation of PETN, NG, and RDX in DMA-F-DMA Config. As previously explained, the MS performs Q3 m/z scans between m/z 30 and 400, however the data shown corresponds to the TIC ion intensity (m/z information is not used.) Figure 3a shows the oven temperature dependence of fragment ion mobility spectra in DMA_2, with DMA_1 transmitting the chloride adduct $[PETN+Cl]^-$. The explosive is introduced from an electrospray solution with 10 ppm of PETN. The ratio of intensities between the precursor and the NO_3^- product ion working with the current fragmenter was 39%, considerably higher than the 12% achieved by its predecessor.[23] Hereinafter, for simplicity, we will refer to this ratio by the symbol $\vartheta_{A\to B}$. The $\vartheta_{A\to B}$ ratio can be expressed as follows:

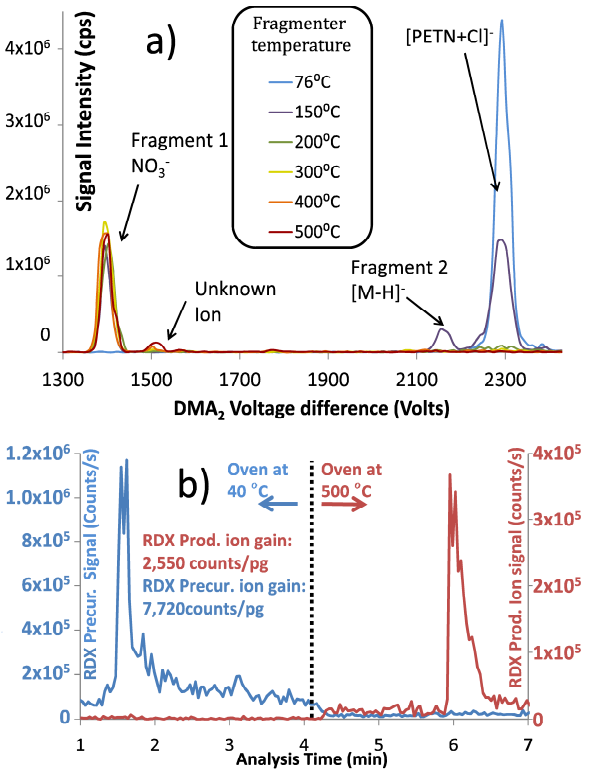

Figure 3. (a) Oven temperature dependence of fragment ion mobility spectra in DMA_2, with DMA_1 transmitting the chloride adduct $[PETN+Cl]^-$. The explosive is introduced from an electrospray solution with 10 ppm of PETN. (b) Desorption of two filters spiked with 2 ng of RDX (no GC installed) with the DMA-F-DMA working in multiple reaction monitoring mode; DMA_1 is fixed at the mobility of the precursor ion $[RDX+Cl]^-$, and DMA_2 is alternating every second between the precursor (blue spectrum) and the product (red spectrum) ion mobilities. At min. 4.2, the oven is turned on with a set point temperature of 500 °C. Note the double y-axis scale for the precursor (left) and the product (right) ions.

$$\vartheta_{A\to B} = \eta_{A\to B} \times \frac{\tau_A}{\tau_B}(Z, D) \tag{3}$$

where $\eta_{A\to B}$ is the fragmentation efficiency at the fragmenter outlet, and τ_A/τ_B is the transmission ratio between the product and the precursor ions in the resistive glass capillary tube, which depends on the ion mobility (Z) and the diffusivity (D) of the ions.[30] τ_A/τ_B is expected to be always less than unity, since the electrophoretic and diffusive ion losses in the resistive capillary are larger for the product ions (NO_2^- and NO_3^-) than for the precursors. The fragmentation efficiencies are unknown because the $\tau_A/\tau_B(Z, D)$ of the capillary tube has not been characterized. However, they are expected to be larger than the $\vartheta_{A\to B}$ reported values.

$\vartheta_{A\to B}$ was ~50% for NG, as can be seen in SI Figure SI-6. In our previous work,[23] the product ion for RDX was not the expected NO_2^- but an ion with 166 m/z, for which no vacuum precedent was found. With the new fragmenter, NO_2^- was the only fragment found (see SI Figure SI-7). Although $\vartheta_{A\to B}$ in SI Figure SI-7 seems low, subsequent experiments spiking 2 ng (2 μL of a solution containing 1 ppm_v of RDX) onto a filter and then desorbing it (Figure 3b) revealed gains of 2550 counts/pg and 7720 counts/pg for the product and the precursor ions respectively, delivering a $\vartheta_{A\to B}$ ~33%. For EGDN $\vartheta_{A\to B}$ was not explored since no fragmentation limitations were expected with this most thermolabile explosive.

Fragmentation of TNT in DMA-F-DMA-MS Config. In our previous work, minor fragmentation for TNT was observed,[23] with product ions appearing at a mobility so close to that of the precursor ion that the two could not be distinguished by mobility alone. For the first time, the new fragmenter decomposes TNT into NO_2^-. However, due to the low signal of the product ions, their quantification required running the mass spectrometer in MRM mode (MS/MS). Figure 4 shows two calibration lines for two different TNT fragments: $[TNT\text{-}CH_2NO]^-$ and $[NO_2]^-$ at fragmenter temperatures between 550 and 700 °C. The fragment $[TNT\text{-}CH_2NO]^-$ (produced in the DMA-F-DMA fragmenter) was measured in the MS in the channel Q1/Q3 183/46, confirming that, as expected, this fragment contained the NO_2^- ion in its structure when it was fragmented again in the MS/

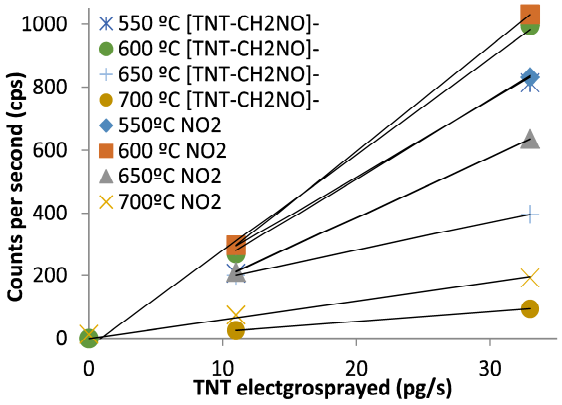

Figure 4. Calibration lines of fragmented TNT in the DMA-F-DMA at different fragmenter temperatures. The DMA_1 is fixed at the precursor ion mobility $[TNT\text{-}H]^-$ and the DMA_2 is alternating between the mobilities of the precursor ions $[TNT\text{-}CH_2NO]^-$ and $[NO_2]^-$. The MS is working in MRM as explained in the text.

DOI: 10.1021/acs.analchem.9b03589

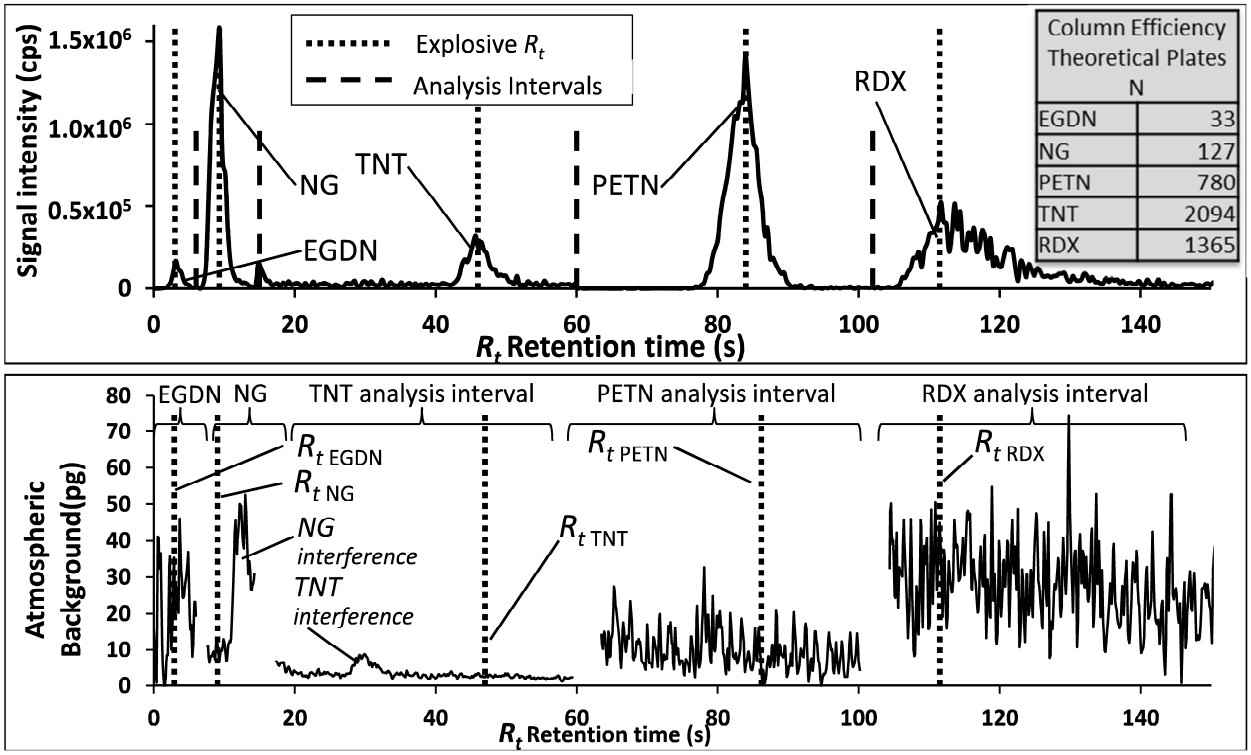

Figure 5. Analyses via GC-DMA-F-DMA. Top: Elution of the explosives spiked on a Tenax filter. The dashed lines separate the five analysis periods, whereas the dotted line indicates the R_t of the explosives. The table embedded shows the column efficiency (N) for the different elution peaks. Bottom: Analysis of four atmospheric samples of 500 L of air. The vertical axis is expressed in pg, by dividing the counts per second obtained in the analysis between the explosive gain.

MS. The NO_2^- (fragmented in the DMA-F-DMA) was detected in the MS in the Q1/Q3 46/46 channel, that is to say, it was not fragmented again in the MS/MS. The fragment signal produced in the DMA-F-DMA was linear with the TNT mass flow rate electrosprayed at its inlet (0, 11, and 33 pg/s), confirming that the product ions truly come from TNT. The delivered $\vartheta_{A\rightarrow B}$ ($[TNT\text{-}H]^- \rightarrow [NO_2]^-$) at 600 °C is in the order of 0.03%, whereas the precursor ion loss when increasing the fragmenter temperature from 500 to 600 °C is 88% (SI Table SI-8), meaning that most of the precursor ions entering the fragmenter at 600 °C are either transformed or neutralized inside. A possible hypothesis for the low abundance of TNT product ions would be that most of the disappeared TNT is decomposed into fragments (NO_2^- and others), but immediately afterward, these fragments ionize neutral contaminant vapors produced at high temperatures (>500 °C) in the fragmenter. However, SI Figure SI-9 shows how the $[RDX+Cl]^- \rightarrow [NO_2]^-$ gain decreases only by an approximate factor of 2 when the fragmenter is heated from 500 to 600 °C, discarding the hypothesis that the vast majority of fragment ions could be trapped by neutral vapors present in the fragmenter. The causes for the extremely low $\vartheta_{A\rightarrow B}$ for TNT remains unknown for the time being, however, this nonideal behavior fragmenting TNT suggests that the current fragmenter might also have limitations decomposing other stable molecules.

Even though TNT fragmentation is possible in the DMA-F-DMA, the low abundance of product ions makes this approach impractical once the MS is replaced by the far simpler and economical detector we intend to use in future versions of the instrument. As suggested by Eiceman and colleagues,[23,24] a better approach to detect TNT is to take advantage of its high thermal stability to remove in the oven most of its atmospheric interferents. In this method, of all the background transmitted by DMA_1 at the mobility of the precursor ion $[TNT\text{-}H]^-$, only TNT would be efficiently transmitted through the heated oven (400 °C) to be detected at the original mobility in DMA_2.

Fragmentation Temperature Optimization. Similarly as in MS/MS instruments, the fragmentation energy can be used to increase the selectivity of the analyzer. Depending on the relationship between the activation energies of the product and the precursor ions (E_{prec}/E_{prod}), the fragmenter temperature band at which the product ion intensity is at the maximum will be either a narrow band (E_{prec}/E_{prod} close to 1) or a wide band ($E_{prec}/E_{prod} \gg 1$). Figure 3a shows that the product ion $[PETN\text{-}H]^-$ only appears at about 150 °C, implying a well-defined optimum fragmentation temperature. However, for the NO_2^- and NO_3^- product ions (Figure 3a, and SI Figures SI-6 and SI-7) the behavior is quite different: once one reaches the effective ion temperature (T_{eff}) required to overcome the activation barrier E_{prec}, the product ion signal remains constant up to the maximum temperature tested, implying that T_{eff} must exceed 500 °C to decompose the nitrate products.

PETN is the only explosive which has delivered two fragments with good intensity. However, for the detection routine, only the NO_3^- was used since it presented a notably lower atmospheric background than the $[PETN\text{-}H]^-$ product ion. Therefore, all the product ions used to analyze the explosives have been either NO_2^- or NO_3^- (as already noted,

DOI: 10.1021/acs.analchem.9b03589

we do not fragment $[TNT-H]^-$ but rather decompose its interferents). In order to take advantage of the selectivity provided by the fragmenter temperature, the minimum temperature at which the fragmentation probability of a given explosive reaches ~100% must be determined (the ion residence time in the fragmenter is fixed by the voltage and fluid conditions). Using this optimum temperature for each explosive will reduce interferences from more thermally stable molecules, having similar precursor and product ion mobilities. The optimum explosive fragmenter temperatures found for this DMA-F-DMA instrument are shown in Table 1. For TNT, which we do not want to fragment, the optimum oven temperature was 400 °C. Higher temperatures did not further reduce the atmospheric background, but affected negatively the TNT gain (SI Table SI-8), therefore decreasing the signal-to-noise ratio. Optimizing separately the fragmenter temperature of each ion (versus fragmenting at a fixed temperature of 400 °C) allowed reductions in the atmospheric background by a factor of 4.5 for EGDN, and by factors <2 for NG, PETN, and RDX.

In the final version of the instrument, the GC separates the analysis in five different time intervals, one per explosive. Therefore, the optimum fragmentation temperature can be conveniently set in every period. The heating velocity of the fragmenter (30 to 400 °C in about 5 s) is enough to perform the temperature changes between analysis intervals in a few seconds (<3 s).

Coupling multicapillary GC with the DMA-F-DMA. To further increase the selectivity of the instrument, a cold trap and an isothermal multicapillary GC were placed between the thermal desorber and the D-LFSESI ionization source. Figure 5 (top) shows the elution of five explosives spiked (pipetted) on a filter. The inset shows the column efficiency expressed as theoretical plates (N). The column efficiency increases with R_t with the exception of RDX which is affected by tailing, created by adsorptive interactions with active surfaces in the neutral vapor circuit (this conclusion is drawn from experimental results).

Atmospheric Background in GC-DMA-F-DMA configurations. Figure 5 (bottom) shows the averaged spectra of four atmospheric blanks (500 L of air collected during the summer of 2018) analyzed in the GC-DMA-F-DMA with the parameters specified in Table 1. The atmospheric background at the R_t of each explosive is detailed in Table 2. The high gain of TNT (Table 1) also contributes to the good result obtained. The modest column efficiency (only 33 theoretical plates) at the short R_t of EGDN is potentially the cause of the relatively large atmospheric background in this explosive channel (23 pg). The column performance could be increased for the volatile explosives (EGDN, NG) using a temperature ramp instead of the isothermal mode (110 °C), however, the ramp temperature mode would mean a reduction in the analyzer throughput, so it is not contemplated for the time being. Moreover, given that EGDN is the most volatile among the explosives studied (Table 2), its detection is not expected to be problematic with the atmospheric background registered. The same conclusion applies to NG (9 pg of background) and the detection results in the pallet scenario with real explosives (see below) confirm this hypothesis.

The atmospheric background of 6 and 33 pg for PETN and RDX respectively will make its detection in cargo challenging because of their low vapor pressure. Approximately one-half of the RDX background comes from the atmosphere. The other half comes from the $[Cl]^-$ liberated in the fragmenter by ions with mobilities close to that of the RDX precursor ion, only partially removed by DMA_1. The resolving power of DMA_2 at the working conditions (Reynolds in DMA_2 channel limited) was not high enough to completely separate $[Cl]^-$ and $[NO_2]^-$ (RDX product ion), explaining the high background in the RDX channel compared to the rest of the explosives. We hope to eliminate this mobility peak overlapping in the near future by reducing the DMA_2 length. This will allow us to reduce the product ion residence time in the DMA which determines beam diffusive spreading and thus the resolution.

Atmospheric Background in GC-DMA Configuration. With the objective of performing a comparison of the background suppression capability of the GC-DMA-F-DMA and GC-DMA configurations, the stages DMA_1 + Fragmenter + resistive tube were removed. The desorber + cold trap + multicapillary GC + transfer line + D-LFSESI + DMA_2 were maintained. The D-LFSESI was dismantled from DMA_1 and assembled to DMA_2. The DMA_2 outlet was now connected directly to the MS, since the resistive tube is not necessary when working with a single DMA. SI Figure SI-10, using a double vertical axis, presents a comparison of the averaged atmospheric background in GC-DMA and GC-DMA-F-DMA configuration. Table 3 summarizes the atmospheric background of both configurations at the R_t of the different explosives. It also expresses, for each explosive, the background reduction factor achieved by the GC-DMA-F-DMA with respect the GC-DMA. Since the resistive glass capillary does not provide any selectivity, and the GC and DMA_2 systems were exactly the same, it can be concluded that the calculated background reduction factor (×99 on average) has been

Table 2. Atmospheric Background of the GC-DMA-F-DMA Obtained from the Analysis of Four Blank Samples of 500 L of Air[a]

Expl.	Vapor pressure (ppb_v)[b]	Precursor Ion	Product Ion	Atmosph. Backgr. (pg)	Atmosph. Backgr. (ppq)
EGDN	1.02×10^5	$[M+Cl]^-$	NO_3^-	23	65
NG	645	$[M+Cl]^-$	NO_3^-	9	14
TNT	9.15	$[M-H]^-$	$[M-H]^-$	2.5	5
PETN	1.07×10^{-2}	$[M+Cl]^-$	NO_3^-	6	9
RDX	4.85×10^{-3}	$[M+Cl]^-$	NO_2^-	33	60

[a]The results are expressed in pg and in ppq, considering for the latter a desorber vapor capturing efficiency of 10%.[26] [b]Vapor pressures obtained from Ewing et al. 2012.[31]

Table 3. Comparison of the Atmospheric Background (500 L Samples) of the GC Coupled with a Single or a Tandem DMA

	atmospheric background (pg)		
explosive	GC-DMA	GC-DMA-F-DMA	background reduction Factor F-DMA
EGDN	3691	23	164
NG	1838	9	195
TNT	44	3	17
PETN	679	6	107
RDX	421	33	13
average			99

DOI: 10.1021/acs.analchem.9b03589

Table 4. Analysis Results of the Explosive Loaded Pallets[a]

			explosive mass detected in the filter (pg)				
explosive	analyzer	pallet/day	EGDN	NG	TNT	PETN	RDX
blank pallet	ACES E2.1	1/1	0.00	0.00	0.02	0.00	0.03
	GC-DMA-F-DMA		29	4.5	3.0	1.7	16
Ergodyn 35	ACES E2.1	2/1	**193 000**	**2860**	0.18	0	0.02
	GC-DMA-F-DMA		**12 000**	**4020**	2.3	1.6	42
	ACES E2.1	5/2	**151 000**	**2080**	0	0	0
	GC-DMA-F-DMA		**5876**	**1176**	3.5	0	1.4
TNT	ACES E2.1	3/1	4.3	0.24	**105**	0	0.06
	GC-DMA-F-DMA		9.6	8.4	**93**	0	4.8
	ACES E2.1	3/2	0.0	0.0	**3.9**	0.0	0.0
	GC-DMA-F-DMA		51	45	**10**	9.6	16
PETN	ACES E2.1	4/1	**17**	**8.4**	**4.1**	0	0.12
	GC-DMA-F-DMA		**100**	**46**	**44**	5.7	15
	ACES E2.1	6/2	0	**1.6**	**0.31**	0	0
	GC-DMA-F-DMA		19	**30**	**6.2**	5.0	19
PG-3	ACES E2.1	7/2	5.7	1.5	0.09	0	0.03
	GC DMA F DMA		0.6	17	3.1	6.3	20

[a]Three consecutive samples of 500 L volume were taken from each pallet, one sample was analysed with the GC-DMA-F-DMA, another with the ACES E2.1 to validate the results and the last one was stored. Bold type represents positive detection.

provided by the F-DMA stage; in other words the IMS^2 (DMA-F-DMA) typically provides ×100 sensitivity increase with respect the IMS (DMA) alone.

Detection of Real Explosive Hidden in Pallets. The subppq explosive analyzer ACES E2.1 (including a desorption temperature scan, a single DMA and a triple quadrupole) was used to provide a comparison standard. ACES E2.1 analyses were performed the day after the sampling, whereas the GC-DMA-F-DMA analyses took place 70 days later, since the final configuration was not ready for the tests. Except for the shipment, the samples were stored in a fridge. The first row of Table 4 shows the results of a blank pallet, obtaining clean results with ACES E2.1. This indicates the absence of contamination in the area from prior use of explosives or by contamination from the people and/or the tools used in the pallet construction. The blank results of the GC-DMA-F-DMA were coherent with the atmospheric backgrounds reported in Table 2. The following results were obtained with real explosives: With Ergodyn 35 the two analyzers gave clear detections of thousands of pg for both EGDN and NG. The quantification by both analyzers was very similar for NG. For EGDN, the GC-DMA-F-DMA was about 1 order of magnitude lower. Since Ergodyn 35 contains both NG and EGDN (pallet 2/1 and 5/2 in Table 4), possible explanations for this anomaly are that either EGDN was preferentially degraded during the 70-day storage period, or the containers storing the filters (samples) had a leak affecting mostly EGDN due to its high volatility. In any case, the signal detected for both EGDN and NG with the GC-DMA-F-DMA was between 100 and 1000 times greater than the atmospheric background. The results expressed in concentration were 17−35 ppt for EGDN and 2−8 ppt for NG. The results were also positive for TNT, with detected TNT masses of 93 and 10 pg (184 and 20 ppq respectively) for pallet 3/1 and 3/2 respectively (Table 4). These results were similar to those obtained with ACES E2.1 (105 and 4 pg for pallet 3/1 and 3/2 respectively). The result of the detection of 10 pg of TNT via GC-DMA-F-DMA is shown in Figure 6. PETN was indirectly detected by both the

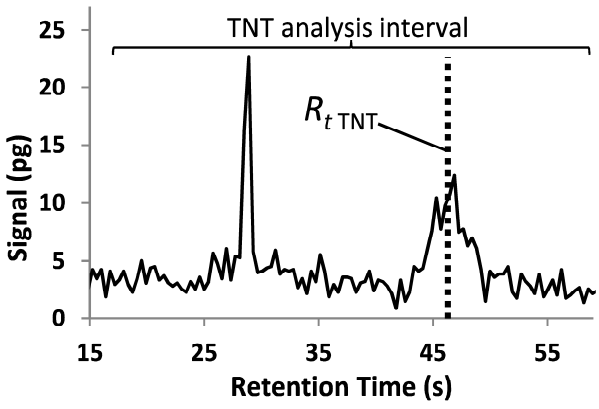

Figure 6. TNT detection of 10 pg in a pallet loaded with TNT via GC-DMA-F-DMA. The analysis parameters are detailed in Table 1. The dotted line indicates the Rt of TNT.

GC-DMA-F-DMA and ACES E2.1, through traces of TNT and NG. However, neither of the two analyzers gave a direct detection which was unexpected, at least in the case of the highly sensitive ACES E2.1 analyzer. The chromatograms for the two pallet samples containing hidden PETN cord are shown in Figure 7, displaying clear peaks at the TNT and NG channels. RDX (PG-3) was not detected with the GC-DMA-F-DMA. It was positively detected with ACES E2.1, although with a very low signal.

Detection of PETN explosive hidden in a box. Just to confirm the low emanation of the PETN explosive tested at INTA, 10 mg of PETN flakes were deposited in a 64 L cardboard box. After a soaking time of 11 min at an ambient temperature of 10 °C, an air sample of 60 L was taken from the

DOI: 10.1021/acs.analchem.9b03589

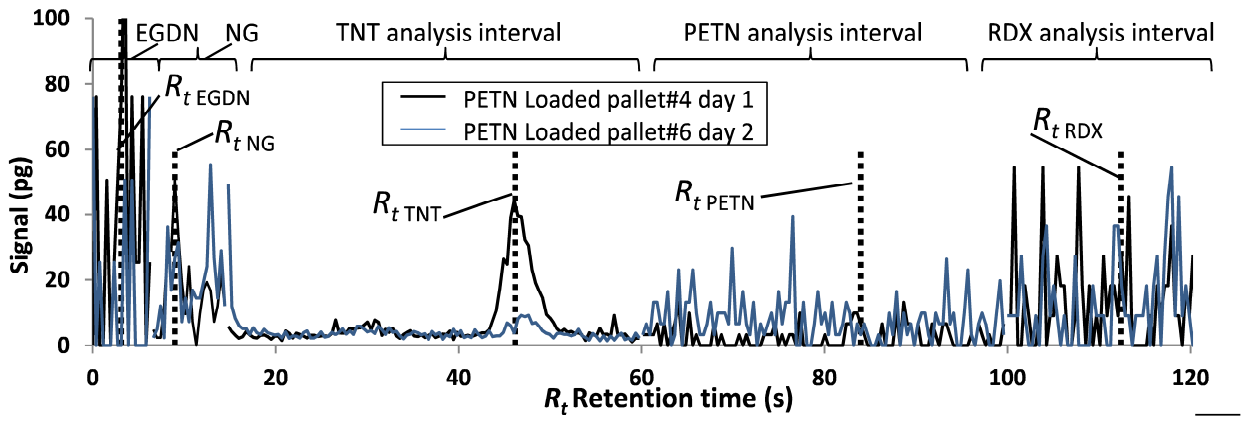

Figure 7. Analysis via GC-DMA-F-DMA of two air samples of 500 L taken from a cargo pallet containing PETN in its central box after a soaking time of 2 h. Black = pallet 4 day_1. Blue = pallet 6 day_2.

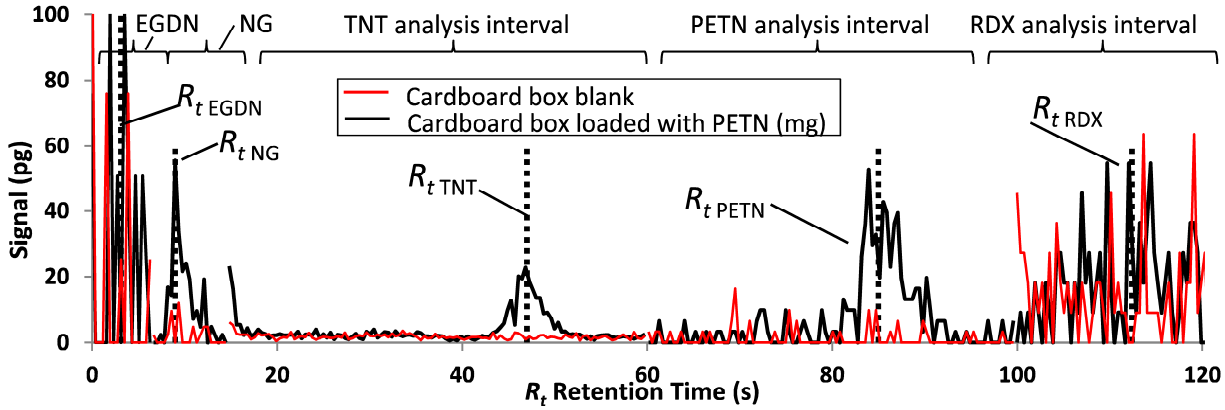

Figure 8. Analysis via GC-DMA-F-DMA of two samples of 60 L from a cardboard box. Red chromatogram: blank sample. Black chromatogram: box loaded with 10 mg of PETN flakes, soaking time before taking the sample: 11 min at 10 °C.

box, whereas a similar blank sample was taken before loading the box. As shown in Figure 8, the GC-DMA-F-DMA analysis gave a clear detection of 60 pg (709 ppq) of PETN, confirming the ability of the instrument to detect PETN and the unexpectedly low vapor emanation rate of the explosive used at INTA. Cross-contamination on the PETN explosive further allowed to clearly detect NG (55 pg/905 ppq) and TNT (20pg/329 ppq) from the same sample.

■ CONCLUSIONS

The DMA-F-DMA architecture has been successfully coupled to a multicapillary GC, allowing orthogonal separation between the GC, the IMS (DMA) and the ion fragmentation. The fragmenter has been fully redesigned allowing both high fragmentation temperatures and high transmission thanks to the decoupling of the axial electric and thermal fields. The complete analysis time was 3 min, one for sample desorption and cold trapping and 2 min for GC-DMA-F-DMA analysis. The fragmentation temperature has been optimized for each target explosive, increasing the selectivity provided by the fragmentation. TNT has been successfully fragmented into NO_2^- at oven temperatures ranging from 550 to 700 °C. However, for the time being the best TNT detection strategy is to work at temperatures of 400 °C to thermally decompose most of the interferences in the atmosphere while the high thermal stability of TNT keeps it intact. The atmospheric background of the GC-DMA-F-DMA has been evaluated for the five explosives studied through analyzing air samples of 500 L with the following results: 2.5 pg of TNT (5 ppq), 6.3 pg of PETN (9 ppq), 9.4 pg of NG (19 ppq), 23 pg of EGDN (67 ppq) and 33 pg of RDX (67 ppq). In order to assess the additional sensitivity provided by the F-DMA it was disassembled, transforming the GC-DMA-F-DMA into a GC-DMA. Similar samples of 500 L of air were analyzed, yielding atmospheric backgrounds 100 times higher on average with the GC-DMA architecture, confirming the high selectivity provided by the fragmenter and the second (tandem) DMA. The GC-DMA-F-DMA was tested with real explosives hidden in cargo pallets, successfully detecting vapors of EGDN, NG, TNT, and PETN. However, PETN was only indirectly detected through traces of NG and TNT. In those analyses the explosive detector ACES E2.1,[26] was used to correlate/validate the results of both instruments. In a later test, PETN was easily detected (direct detection) in a 64 L box after 11 min of soaking time at 10 °C. This test confirms the existence of remarkable differences in the vapor emanation rate of different forms (cord, flakes, powder, plastic) of the same explosive.

DOI: 10.1021/acs.analchem.9b03589

■ ASSOCIATED CONTENT

Supporting Information

The Supporting Information is available free of charge on the ACS Publications website at DOI: 10.1021/acs.analchem.9b03589.

SI-1. Commercial explosive samples used in cargo pallet tests. SI-2. Cargo pallet layout of the test with commercial explosives hidden in pallets carried out at INTA facilities. SI-3. Six-port valve scheme. SI-4. Voltage and material for the different DMA-F-DMA electrodes, and distance and electric field between them. SI-5. Fragmenter temperature as a function of the electric current crossing every heating coil. SI-6. Oven temperature dependence of fragment ion mobility spectra in DMA_2, with DMA_1 transmitting the chloride adduct $[NG+Cl]^-$. SI-7. Oven temperature dependence of fragment ion mobility spectra in DMA_2, with DMA_1 transmitting the chloride adduct $[RDX+Cl]^-$. SI-8. TNT gain at different fragmenter temperatures. SI-9. RDX gain analyzed in DMA-F-DMA mode at different fragmenter temperatures. SI-10. Atmospheric background comparison of GC-DMA and GC-DMA-F-DMA configurations (PDF)

■ AUTHOR INFORMATION

Corresponding Author

*E-mail: mario.amo@seadm.com.

ORCID

Mario Amo-González: 0000-0001-6227-1365

Notes

The authors declare no competing financial interest.

■ ACKNOWLEDGMENTS

This work was funded by the Future Aviation Security Solutions Programme, a joint UK programme run by the Department for Transport and the Home Office under contract number 1000121217. We also thank Daoíz Zamora for his help and advice preparing the INTA explosive loaded tests, Leticia Ruiz for providing the ACES E2.1 results, and Juan Fernandez de la Mora for his remarks on the manuscript.

■ REFERENCES

(1) Purves, R. W.; Guevremont, R.; Day, S.; Pipich, C. W.; Matyjaszczyk, M. S. *Rev. Sci. Instrum.* **1998**, *69*, 4094−4104.

(2) Schneider, B. B.; Covey, T. R.; Coy, S. L.; Krylov, E. V.; Nazarov, E. G. *Anal. Chem.* **2010**, *82* (5), 1867−1880.

(3) Shvartsburg, A. A. *Differential Ion Mobility Spectrometry: Nonlinear Ion Transport and Fundamentals of FAIMS*; CRC Press: Boca Raton, FL, 2008.

(4) Gillig, K. J.; Chen, C. H. *Mass Spectrom.* **2014**, *3* (Special Issue), S0032. See alsoGillig, K. J.; Chen, C. H. Periodic field differential mobility analyser. US Patent Application Publication US2013/0187042A1, July 25, 2013.

(5) Tammet, H. F. The Aspiration Method for the Determination of Atmospheric-Ion Spectra [Original work in Russian from 1967]. *Israel Program for Scientific Translations*, Jerusalem, 1970.

(6) Labowsky, M.; Fernandez de la Mora, J. *J. Aerosol Sci.* **2006**, *37* (3), 340−362.

(7) Knutson, E.; Whitby, K. *J. Aerosol Sci.* **1975**, *6*, 443−451.

(8) Amo-González, M.; Pérez, S. *Anal. Chem.* **2018**, *90* (11), 6735−6741.

(9) Amo-Gonzalez, M.; Fernandez de la Mora, J. *J. Am. Soc. Mass Spectrom.* **2017**, *28* (8), 1506−1517.

(10) Eiceman, G. A.; Shoff, D. B.; Harden, C. S.; Snyder, A. P. *Int. J. Mass Spectrom. Ion Processes* **1988**, *85* (3), 265−275.

(11) Ewing, R. G.; Eiceman, G. A.; Harden, C. S.; Stone, J. A. *Int. J. Mass Spectrom.* **2006**, *255*−*256*, 76−85.

(12) An, X.; Eiceman, G. A.; Rodriguez, J. E.; Stone, J. A. *Int. J. Mass Spectrom.* **2011**, *303* (2−3), 181−190.

(13) An, X.; Eiceman, G. A.; Stone, J. A. *Int. J. Ion Mobility Spectrom.* **2010**, *13* (1), 25−36.

(14) Rajapakse, M. Y.; Stone, J. A.; Eiceman, G. A. *Int. J. Mass Spectrom.* **2014**, *371*, 28−35.

(15) Rajapakse, M. Y.; Fowler, P. E.; Eiceman, G. A.; Stone, J. A. *J. Phys. Chem. A* **2016**, *120* (5), 690−698.

(16) Rajapakse, R. M. Y.; Stone, J. A.; Eiceman, G. A. *J. Phys. Chem. A* **2014**, *118* (15), 2683−2692.

(17) Menlyadiev, M. R.; Eiceman, G. A. *Anal. Chem.* **2014**, *86* (5), 2395−2402.

(18) Menlyadiev, M. R.; Tarassov, A.; Kielnecker, A. M.; Eiceman, G. A. *Analyst* **2015**, *140* (9), 2995−3002.

(19) Stimac, R. M.; Wernlund, R. F.; Cohen, M. J.; Lubman, D. M.; Harden, C. S. *Initial Studies on the Operation and Performance of the Tandem Ion Mobility Spectrometer*; Pittcon: New Orleans, LA, March 1985.

(20) Stimac, R. M.; Cohen, M. J.; Wernlund, R. F. *Tandem Ion Mobility Spectrometer for Chemical Agent Detection, Monitoring and Alarm*, Contractor Report on CRDEC Contract DAAK11 84 C 0017, PCP, Inc.: West Palm Beach, FL, May 1985, AD B093495.

(21) Koeniger, S. L.; Merenbloom, S. I.; Valentine, S. J.; Jarrold, M. F.; Udseth, H. R.; Smith, R. D.; Clemmer, D. E. *Anal. Chem.* **2006**, *78*, 4161−4174.

(22) Merenbloom, S. I.; Koeniger, S. L.; Valentine, S. J.; Plasencia, M. D.; Clemmer, D. E. *Anal. Chem.* **2006**, *78*, 2802−2809.

(23) Amo-González, M.; Carnicero, I.; Pérez, S.; Delgado, R.; Eiceman, G. A.; Fernández de la Mora, G.; Fernández de la Mora, J. *Anal. Chem.* **2018**, *90* (11), 6885−6892.

(24) Chiluwal, U.; Lee, G.; Rajapakse, M. Y.; Willy, T.; Lukow, S.; Schmidt, H.; Eiceman, G. A. *Analyst* **2019**, *144* (6), 2052−2061.

(25) Cao, X.-L.; Hewitt, C. N. *Atmos. Environ., Part A* **1993**, *27* (12), 1865−1872.

(26) Zamora, D.; Amo-Gonzalez, M.; Lanza, M.; Fernandez De La Mora, G.; Fernandez de la Mora, J. *Anal. Chem.* **2018**, *90* (4), 2468−2474.

(27) Patrushev, Y. V.; Sidelnikov, V. N. *J. Chromatogr. A* **2015**, *1426*, 183−190.

(28) Vidal-de-Miguel, G.; Macia, M.; Pinacho, P.; Blanco, J. *Anal. Chem.* **2012**, *84* (20), 8475−8479.

(29) Fernandez de la Mora, J.; Perez-Lorenzo, L. J.; Arranz, G.; Amo-Gonzalez, M.; Burtscher, H. *Aerosol Sci. Technol.* **2017**, *51* (6), 724−734.

(30) Attoui, M.; Fernandez de la Mora, J. *J. Aerosol Sci.* **2016**, *100*, 91−96.

(31) Ewing, R. G.; Waltman, M. J.; Atkinson, D. A.; Grate, J. W.; Hotchkiss, P. J. *TrAC, Trends Anal. Chem.* **2013**, *42*, 35−48.

DOI: 10.1021/acs.analchem.9b03589

CONCLUSIONS

The main conclusions of this doctoral thesis are listed below:

Thesis objective 1: To optimize the analytical performance of the planar differential mobility analyzer (DMA) and the secondary electrospray ionization source (SESI), so as to bring their performance closer to the ideal level.

Scientific article title: Mobility Peak Tailing Reduction in a Differential Mobility Analyzer (DMA) Coupled with a Mass Spectrometer and Several Ionization Sources (Chapter 1).

Three new ionization sources specially designed to be coupled to a DMA achieved complete elimination of vapors and associated ion clustering. Combined with an essentially vapor-free DMA gas recirculation circuit (including a cooled commercial blower), this improvement yielded ideal tail-free mobility peaks with a tailing ratio (*TR*) much larger than previously observed (100-1000 times better), reaching the theoretical limit ~10^5 (Gaussian peaks). This improvement led to a greatly enhanced capacity of the DMA-MS/MS combination to analyze complex mixtures, including explosives in the atmosphere at concentrations below 10^{-2} ppq. The new SESI source designed (*Desolvating-LFSESI*), enabled the complete evaporation of droplets coming from the electrospray thanks to: (i) a heated (170 ºC) drying gas flow upstream of the DMA inlet slit, symmetrically directed towards the electrospray cloud, (ii) the use of a low-boiling point electrospray solution (MeOH:H_2O 9:1 + HCl 0.05%) allowing quick droplet evaporation and (iii) an electrospray capillary cooling system integrated into the ion source design, thanks to which, the low-boiling point electrospray solution is maintained in liquid form while the rest of the ion source is at 170 ºC. In addition to the droplet evaporation function, the ion source was designed for maximum sensitivity, delivering a gain for TNT of 190 counts/fg, equivalent to an unprecedented ionization efficiency of one out of 140 neutral molecules, improving the ionization efficiency of its predecessors (1/700 of LFSESI and $1/10^4$ of SESI). Electron, Cl^-, NO_2^- and NO_3^- ionization within the DMA was used as a sensitive diagnostic tool to evaluate the level of gas-phase contamination of the closed DMA circuit. Extremely high nitrogen purity is not essential to achieve good DMA TR in a background-free MS/MS channel, as comparable TR values were obtained with 99.9992% and 99.95% purity nitrogen.

Scientific article title: Planar Differential Mobility Analyzer with a Resolving Power of 110. (Chapter 2).

The narrow-band planar differential mobility analyzer (DMA P5) demonstrated a high transmission and a resolving power exceeding 100 for ion mobilities of $Z = 1$ cm^2/V/s. The keys to enable this high performance were (i) an unusually low ion residence time t in the separation channel of this instrument (t ~ 200 μs for $Z = 1$ cm^2/V/s), which limits the ion-beam spreading by Brownian diffusion (proportional to $\sqrt{t}$), and (ii) the effectiveness in the laminarization of the sheath gas at the inlet of the DMA. The sheath-gas laminarization was improved by (a) the use of two prelaminarizer screens before and after the 90° elbow placed at the DMA sheath-gas inlet and (b) the introduction of laminarization-screen holders with minimal steps or gaps between their laminarization-screen exits and wetted surfaces following immediately after them. After these two actions, the DMA performed at the ideal resolving power, delivering reproducible mobility peaks with excellent Gaussian fitting R^2 values. Its excellent resolving power working with highly diffusive small ions, its high transmission, and its ability to perform voltage changes in a few milliseconds make it an excellent option for IMS-MS analysis. An extra virgin olive oil sample was electrosprayed and analyzed via

DMA-MS delivering a two-dimensional spectrum showing many ions with the same *m/z* perfectly separated in mobility, illustrating that high-resolution ion mobility separation is an excellent tool for increasing the selectivity of a mass spectrometer.

Thesis objective 2: Development of an Explosive Vapor Detector, based on DMA-MS/MS technology, capable of detecting explosive vapors at sub-ppq concentrations

Scientific article title: Reaching a Vapor Sensitivity of 0.01 Parts Per Quadrillion in the Screening of Large Volume Freight (Chapter 3).

The false alarm rate (FAR) and the probability of detection (PoD) of explosives with vapor pressure between 0.01 ppq and 0.10 ppq was investigated with unprecedented sensitivity and resolution, combining mobility filtration (DMA described in chapters 1 and 2) and triple quadrupole mass spectrometry (MS). The following conclusions can be drawn: (a) The atmosphere contained interfering vapors at concentrations above 0.01 ppq with the same MS/MS signature as all explosives investigated. (b) Within the narrow mobility interval analyzed for all four channels (TNT, RDX, NG and PETN), the atmosphere contained several mobility-resolvable species, one of which at least was typically much more abundant than the 0.01 ppq sensitivity target. (c) Mobility separation, through a combination of a DMA and a peak discrimination algorithm, was accordingly vital to exclude these interfering vapors and bring the lower detection limit (LDL) down to 0.01 ppq. (d) RDX was detected at partial pressure of 0.01 ppq with a PoD higher than 90% and a FAR below 1%. (e) Interferents and chemical noise in the RDX and TNT channels were reduced below the equipment sensitivity. Their detection threshold was accordingly limited only by the equipment. (f) Detection in the NG and PETN channels was limited by atmospheric compounds which the system could not distinguish from targets.

Patent: Method for Detecting Atmospheric Vapors at Parts Per Quadrillion (PPQ) Concentrations (Chapter 4).

Regarding the patented detection method, the main conclusions are as follows: A pre-filter with a cutoff size of 10 µm was proposed as a solution to remove the aerosol particles present in the atmosphere, preventing them from reaching the adsorption filter (vapor collector). When analyzed, these particles generated a large statistical noise (external background) forcing a high threshold for positive detection, and artificially reducing the sensitivity of the instrument. Consequently, the detection was based purely on vapors. A measure to minimize the analyzer's internal background was to maintain all the analyzer's vapor circuit at a high temperature (170 ºC), minimizing surface adsorption on the circuit walls. The following measures were validated to prevent contamination in the sampling process: (a) The filter holder device hosting the particle pre-filter and the sampling nozzle must be disposable. (b) The sampler (aspiration unit) must release the sampled gas to the atmosphere at a place remote from the location where the sampling takes place, so as to moderate possible contamination of the surroundings of the sampling area. (c) The sampler must include a contamination prevention means, preventing residual vapors accumulated downstream of the disposable filterholder from reaching the adsorption filter in a subsequent sampling process. (d) The exhaust of the analyzer ionization source (potentially containing non-ionized vapors) must be released at a place remote from the analyzer location to prevent these vapors from contaminating the analyzer N_2 generator and, ultimately, the analyzer.

Thesis objective 3: Development of an Explosive Vapor Detector, based on analyzers and detectors far simpler and more economical than mass spectrometry, yet still capable of detecting explosive vapors at concentrations of a few ppq.

Scientific article title: Ion Mobility Spectrometer-Fragmenter-Ion Mobility Spectrometer Analogue of a Triple Quadrupole for High-Resolution Ion Analysis at Atmospheric Pressure (Chapter 5).

A first prototype of DMA-F-DMA was built from scratch enabling ion fragmentation of explosives at ambient pressure using exclusively thermal energy and transmitting ions from the DMA_1 to the DMA_2, without the need to resort to gas streams difficult to control in complex geometries. It was confirmed that the short ion transit time in DMAs facilitates a complete absence of ion fragmentation within the analyzer, sidestepping poor fragment resolving power previously observed in tandem-IMS studies. Both parent and fragment ions can accordingly be cleanly resolved via DMA-F-DMA. This offers a simple analogue to the triple quadrupole, with a drastic increase in the resolving power of conventional IMS. Effective fragmentation of EGDN, NG, PETN, RDX, and TNT was achieved. The first four explosives produced clean tandem IMS spectra enabling high-resolution explosive identification by IMS alone. New fragmentation channels were discovered for the far more thermally stable $[RDX+Cl]^-$ and $[TNT-H]^-$ ions, which had not been previously fragmented at atmospheric pressure. Fragmentation of TNT is particularly demanding due to its singular thermal stability. This previously known fact is confirmed and extended by showing that the beam of $[TNT-H]^-$ survives at atmospheric pressure in close proximity to a surface heated up to 700 °C. The high-temperature fragmenter yields product ions (m/z 210, 197, 182, and 167) of TNT. However, the proximity between fragment mobility peaks and their low abundance in comparison with the parent ion do compromise the clear recognition of these fragment peaks by IMS alone. Accordingly, TNT detection will benefit from the development of a fragmenter oven achieving temperatures above 700 °C.

Scientific article title: Tandem Ion Mobility Spectrometry for the Detection of Traces of Explosives in Cargo at Concentrations of Parts Per Quadrillion (Chapter 6).

The DMA-F-DMA architecture was successfully coupled to a multicapillary GC, allowing a remarkable selectivity thanks to the separation by three orthogonal principles: gas chromatography, ion mobility spectrometry and selective ion dissociation. The fragmenter was fully redesigned allowing both high fragmentation temperatures and high transmission thanks to the decoupling of the axial electric and thermal fields (patent pending). The complete analysis time was 3 min, one for sample desorption and cold trapping, and 2 min for GC-DMA-F-DMA analysis. The fragmentation temperature was optimized for each target explosive, increasing the selectivity provided by the fragmentation. TNT was successfully fragmented into NO_2^- at oven temperatures ranging from 550 to 700 ºC. However, for the time being, the best TNT detection strategy is to work at temperatures of 400 ºC to thermally decompose most of the interferences in the atmosphere while the high thermal stability of TNT keeps it intact. The atmospheric background of the GC-DMA-F-DMA was evaluated for the five explosives studied through analyzing air samples of 500 L with the following results: 2.5 pg of TNT (5 ppq), 6.3 pg of PETN (9 ppq), 9.4 pg of NG (19 ppq), 23 pg of EGDN (67 ppq) and 33 pg of RDX (67 ppq). In order to assess the additional sensitivity provided by the F-DMA, it was disassembled, transforming the GC-DMA-F-DMA into a GC-DMA. Similar samples of 500 L of air were analyzed, yielding atmospheric backgrounds 100 times higher on average with the GC-DMA architecture, confirming the high selectivity provided by the fragmenter and the second (tandem) DMA. The GC-DMA-F-DMA was tested with commercial explosives hidden in cargo pallets, successfully detecting vapors of EGDN, NG, TNT and PETN. However, PETN was only indirectly

detected through traces of NG and TNT. In those analyses, the explosive detector ACES E2.1 was used to correlate/validate the results of both instruments. In a later test, PETN was easily detected (direct detection) in a 64 L box after 11 minutes of soaking time at 10 ºC. This test confirms the existence of remarkable differences in the vapor emanation rate of different forms (cord, flakes, powder, plastic) of the same explosive.

The tandem IMS technology with intermediate ion fragmentation at ambient pressure has recently been demonstrated by only one other research group worldwide (G. Eiceman research group at New Mexico State University, USA, results published in 2019), which illustrates the degree of novelty of this technology. Its potential is demonstrated by the fact that its development has been funded by the United Kingdom government by three consecutive projects (EffeX, EffeX II and HITEX) and also by the Horizon 2020 Research and Innovation Programme under the COSMIC project.

CONCLUSIONES

Las principales conclusiones de esta tesis doctoral se citan a continuación:

Objetivo 1: optimización del rendimiento analítico del analizador diferencial de movilidad plano (DMA) y de la fuente de ionización secundaria por electrospray (SESI), de manera que sus rendimientos se aproximen al ideal.

Artículo científico: Mobility Peak Tailing Reduction in a Differential Mobility Analyzer (DMA) Coupled with a Mass Spectrometer and Several Ionization Sources (Capítulo 1).

a) Se diseñaron tres nuevas cámaras de ionización para el DMA, que permiten evitar la penetración de vapores en el interior de éste último, y por tanto, su interacción perjudicial con los iones analizados (ion clustering).

b) El DMA y su circuito de recirculación se adaptaron para minimizar sus emisiones de vapores, lo que en combinación con las nuevas fuentes de ionización, permite la obtención de picos de movilidad con ratios de colas (TR) del orden de 10^5, coincidentes con el límite teórico impuesto por la difusión Browniana (picos Gaussianos).

c) Estos resultados suponen un factor de mejora comprendido entre 100 y 1.000 con respecto a la tecnología predecesora.

d) La reducción de colas incrementa significativamente la capacidad analítica de la combinación DMA-MS/MS, lo cual es esencial en el análisis de muestras complejas, como la detección de explosivos en la atmósfera en concentraciones de 10^{-2} ppq.

e) La nueva fuente de ionización diseñada, (Desolvating-LFSESI), permite la completa evaporación de las gotas provenientes del electrospray, gracias a: (1) la introducción de un flujo de gas de secado (170 ºC) aguas arriba de la ranura de entrada del DMA, simétricamente dirigido hacia la pluma del electrospray, (2) el uso de una disolución de electrospray de bajo punto de ebullición, (MeOH:H_2O 9:1 + HCl 0,05%), que facilita la rápida evaporación de las gotas, y (3) un sistema de refrigeración del capilar que conduce el líquido del electrospray, gracias al cual se evita que el calor procedente de la cámara de ionización (170 ºC), evapore la disolución de bajo punto de ebullición.

f) La fuente de ionización, además de proporcionar un excelente rendimiento en la desolvatación del electrospray (eliminación del disolvente del electrospray), fue diseñada para maximizar la sensibilidad. Se logra un valor de ganancia para el TNT de 190 cuentas/fg, equivalente a una eficiencia de ionización sin precedentes de un ión por cada 140 moléculas neutras, mejorando la eficiencia de ionización de sus predecesores (1/700 del LFSESI y $1/10^4$ del SESI).

g) La ionización en el interior del DMA por medio de electrones e iones Cl^-, NO_2^- y NO_3^-, constituye una herramienta diagnóstica de gran sensibilidad, que permite evaluar el nivel contaminación del gas que circula por el interior del DMA.

h) Se determina que, para conseguir buenos ratios de colas (TR) en el DMA, no es imprescindible el uso de un nitrógeno de muy alta pureza, ya que se consiguen ratios de colas similares con nitrógenos de pureza 99,9992% y 99,95%.

Artículo científico: Planar Differential Mobility Analyzer with a Resolving Power of 110. (Capítulo 2).

a) El analizador diferencial de movilidad plano (DMA P5), además de tener elevada transmisión de iones, demuestra en este trabajo su capacidad para funcionar con resoluciones superiores a 100, con iones altamente difusivos (movilidad Z = 1 $cm^2/V/s$). Las claves para lograr esta resolución, sin precedentes en un filtro de movilidad de banda estrecha, han sido las siguientes:

1) Un tiempo de residencia *t* en el canal de separación en movilidad extremadamente bajo (t ~ 200 μs para *Z* = 1 $cm^2/V/s$), lo que limita en ensanchamiento del haz de iones por difusión Browniana, que es proporcional a √t.

2) La eficacia en la laminarización del gas que circula por el interior del DMA, que fue optimizada a través de las siguientes dos medidas: (i) el uso de dos rejillas prelaminarizadoras ubicadas aguas arriba y aguas debajo a un codo de 90º, ubicado a la entrada del DMA y (ii) la utilización de portarejillas, que presentasen mínimos escalones o huecos entre la sección de salida del gas por la rejilla o malla laminarizadora y las superficies en contacto con el gas situadas justo a continuación de la malla.

b) Tras estas dos medidas, el DMA entregó resoluciones prácticamente coincidentes con la resolución ideal, con picos de movilidad altamente reproducibles y con un excelente coeficiente de determinación (R^2), obtenido al ajustar dicho picos a una Gaussiana.

c) La excelente resolución del DMA plano trabajando con iones altamente difusivos, su elevada transmisión y su capacidad para cambiar de un voltaje a otro en pocos milisegundos, le convierten en un excelente candidato para llevar a cabo análisis ortogonales IMS-MS, cuya capacidad analítica es notablemente superior a la ofrecida por cualquiera de las dos técnicas de separación por separado.

d) Para demostrar este punto se llevó a cabo un análisis DMA-MS sobre una muestra de aceite de oliva virgen extra, generando un espectro bidimensional (*m/z, Z*), en el que numerosos iones con relación masa carga similar, y por tanto no separables por el espectrómetro de masas, fueron perfectamente separados en movilidad por el DMA.

Objetivo 2: desarrollo de un detector de vapores de explosivo basado en la tecnología DMA-MS, capaz de detectar vapores de explosivos en concentraciones inferiores a 1 ppq.

Artículo científico: Reaching a Vapor Sensitivity of 0.01 Parts Per Quadrillion in the Screening of Large Volume Freight (Capítulo 3).

A través de la combinación del DMA, descrito en los capítulos 1 y 2, y de un espectrómetro de masas de triple cuadrupolo (MS), se investigó, con resolución y sensibilidad sin precedentes, la tasa de falsas alarmas (FAR) y la probabilidad de detección (PoD) de explosivos con presiones de vapor comprendidas entre 0,01 ppq y 0,10 ppq. A continuación se citan las conclusiones más relevantes:

a) En la atmósfera existen vapores en concentraciones superiores a 0,01 ppq para todos los canales MS/MS de los explosivos investigados.

b) Dentro del estrecho rango de movilidad analizado para los cuatro canales de explosivo (TNT, RDX, NG y PETN) existen varios iones atmosféricos resolubles en movilidad, y al menos uno de ellos, está presente en una concentración notablemente mayor que la sensibilidad objetivo de 0,01 ppq.

c) En consecuencia, la separación en movilidad a través del DMA y de un algoritmo de discriminación de picos, es esencial para separar esos vapores interferentes y bajar el límite de detección (LDL) hasta 0,01 ppq.

d) El RDX es detectado a una presión parcial de vapor de 0,01 ppq con una probabilidad de detección (PoD) mayor al 90% y una tasa de falsa alarma (FAR) por debajo del 1%.

e) El ruido químico y los interferentes atmosféricos en los canales de RDX y TNT se reducen por debajo de la sensibilidad del equipo. Por consiguiente, su límite de detección pasa a estar limitado únicamente por la sensibilidad del equipo y no por la concentración de los interferentes en la atmósfera.

f) En los canales de NG y PETN, el analizador no es capaz de separar el explosivo de los interferentes atmosféricos, quedando el límite de detección en estos canales restringido por la concentración de dichos interferentes en la atmósfera.

Patente: Method for Detecting Atmospheric Vapors at Parts Per Quadrillion (PPQ) Concentrations (Capítulo 4).

Las principales conclusiones, en relación al método de detección patentado, se citan a continuación:

a) La deposición sobre el filtro de adsorción de las partículas presentes en la atmósfera genera un gran ruido estadístico durante el análisis, que obliga a elevar considerablemente el límite de detección.

b) Como solución a este inconveniente se propone la utilización de un prefiltro con tamaño de poro de 10 µm, cuya función es la de retener las partículas evitando su deposición en el filtro.

c) A través del uso del prefiltro, la detección pasa a basarse puramente en vapores.

d) Para minimizar el ruido interno del analizador se incrementa la temperatura del circuito de vapores hasta los 170 ºC, lo que reduce drásticamente la adsorción en las paredes del circuito.

e) Además, se validan las siguientes medidas para prevenir la contaminación en el proceso de muestreo y análisis:

1) El portafiltros, que aloja el tubo de muestreo y el prefiltro de partículas, ha de ser desechable para evitar contaminación cruzada entre muestras.

2) Con el objetivo de minimizar la contaminación en el área de muestreo y sus alrededores, la manguera de salida del muestreador (unidad de aspiración) se debe conducir hasta un lugar alejado de la zona de muestreo.

3) El muestreador ha de equipar un mecanismo anti-contaminación, que evite que los vapores residuales acumulados aguas abajo del portafiltros desechable, puedan alcanzar el filtro de adsorción en un proceso de muestreo posterior.

4) El gas de salida de la fuente de ionización puede contener restos de vapores no ionizados, por lo tanto, ha de liberarse en un lugar alejado del analizador, con el propósito de que dichos vapores contaminantes no puedan retornar al analizador, a través de la toma de entrada de su generador de N_2.

Objetivo 3: desarrollo de un detector de vapores de explosivo basado en analizadores y detectores más simples y económicos que los usados en espectrometría de masas, con capacidad para detectar vapores de explosivo en concentraciones de unas pocas ppq.

Artículo científico: Ion Mobility Spectrometer-Fragmenter-Ion Mobility Spectrometer Analogue of a Triple Quadrupole for High-Resolution Ion Analysis at Atmospheric Pressure (Capítulo 5).

a) El primer prototipo de DMA-F-DMA, que se desarrolla partiendo de cero, permite demostrar la fragmentación de iones de explosivo, a través del uso de elevadas temperaturas en condiciones de presión ambiente.

b) Es de especial relevancia la transmisión por campos eléctricos de los iones desde el DMA_1 hasta el DMA_2, pues evita la necesidad de recurrir a corrientes de gas, difícilmente controlables en geometrías complejas, que no permitirían un control preciso del tiempo de residencia en el fragmentador y que generarían pérdidas de iones en las paredes.

c) Se confirma que el reducido tiempo de residencia en el interior del DMA favorece la inexistencia de fragmentación de iones dentro del analizador, a diferencia de lo que sucedía en los estudios previos de tándem-IMS, en los que la fragmentación en el interior del analizador degradaba su resolución, al aparecer colas comprendidas entre las movilidades del ión padre y de sus fragmentos.

d) De una manera análoga al triple cuadrupolo, el DMA-F-DMA permite resolver limpiamente el ión padre y sus fragmentos, lo que se traduce en un incremento drástico en la selectividad del analizador, en comparación con los IMS convencionales.

e) Se consigue una fragmentación eficiente de los iones de EGDN, NG, PETN, RDX y TNT. Los cuatro primeros explosivos generan espectros de movilidad tándem-IMS limpios, permitiendo su identificación con alta resolución, exclusivamente a través del análisis en movilidad.

f) Se descubren nuevos canales de fragmentación para los iones más estables térmicamente, $[RDX+Cl]^-$ y $[TNT-H]^-$, los cuales nunca antes habían sido fragmentados a presión atmosférica en un tándem-IMS.

g) La fragmentación del TNT es particularmente complicada, debida a la excepcional estabilidad térmica de su molécula. Este hecho previamente conocido es ahora confirmado y ampliado, demostrando que bajo condiciones de presión atmosférica la práctica mayoría de los iones $[TNT-H]^-$ son capaces de mantener su estructura molecular en las cercanías de una superficie calentada hasta una temperatura de 700 ºC. El fragmentador de alta temperatura produce los siguientes fragmentos de TNT: m/z 210, 197, 182, y 167. Sin embargo, la proximidad entre los picos de movilidad de los fragmentos, unida a su baja intensidad en comparación con la señal del ión padre, complica significativamente la identificación de estos fragmentos en el espectro de movilidad. Por consiguiente, la detección del TNT mejorará en la medida en que el fragmentador consiga temperaturas de fragmentación por encima de 700 ºC.

Artículo científico: Tandem Ion Mobility Spectrometry for the Detection of Traces of Explosives in Cargo at Concentrations of Parts Per Quadrillion (Capítulo 6).

a) El nuevo fragmentador se rediseñó por completo, incorporando una región de calentamiento notablemente más larga que la de su predecesor, lo que hace posible que la temperatura en la región central del horno sea muy cercana a la temperatura de las bobinas calefactoras. Esta notable mejora no hubiese sido posible sin el nuevo sistema de transmisión eléctrica de los iones dentro del fragmentador, que permite desacoplar los campos térmico y eléctrico, gracias al uso de las bobinas calefactoras como electrodos de enfoque de los iones (en trámites de patente).

b) La arquitectura DMA-F-DMA se combina exitosamente con una columna GC multicapilar, permitiendo una notable selectividad gracias a la separación en base a tres principios ortogonales: cromatografía de gases, espectrometría de movilidad iónica y disociación selectiva de iones.

c) El tiempo de análisis por muestra es de 3 minutos, uno se emplea en la desorción de la muestra y dos para el análisis GC-DMA-F-DMA.

d) La baja inercia térmica del fragmentador le permite cambiar rápidamente de temperatura durante el periodo de análisis de cada explosivo, de manera que la fragmentación se da en las condiciones de temperatura que maximizan la relación señal/ruido en cada canal de explosivo.

e) Gracias al nuevo fragmentador con mayor capacidad de fragmentación, se consigue, por vez primera en un tándem DMA, fragmentar el TNT en NO_2^- a temperaturas comprendidas entre 550 y 700 ºC.

f) Sin embargo, la estrategia de detección que proporciona los mejores resultados para el TNT es la de mantener el horno a una temperatura de 400 ºC, con el objetivo de descomponer la mayoría de sus interferentes atmosféricos, mientras el TNT se mantiene intacto gracias a su gran estabilidad térmica.

g) A través de análisis de muestras de aire de 500 L, el fondo atmosférico del GC-DMA-F-DMA se evalúa para los cinco explosivos estudiados, obteniendo los siguientes resultados: 2,5 pg de TNT (5 ppq), 6,3 pg de PETN (9 ppq), 9,4 pg de NG (19 ppq), 23 de of EGDN (67 ppq) y 33 pg de RDX (67 ppq).

h) El aumento de sensibilidad promedio aportado por el tándem DMA + fragmentador es de un factor de 100, confirmándose la gran selectividad aportada por el análisis en tándem. Para llegar a este resultado se compararon los fondos atmosféricos obtenidos con la arquitectura GC-DMA-F-DMA, con los obtenidos al trasformar dicho equipo en un GC-DMA.

i) El GC-DMA-F-DMA se probó con explosivos comerciales ocultos en palés, siendo capaz de detectar con éxito EGDN, NG, TNT y PETN. No obstante, la PETN sólo se detectó indirectamente a través de trazas de NG y TNT. En esos análisis se utilizó de manera paralela el detector de explosivos ACES E2.1, con el objetivo de correlacionar y validar los resultados entre ambos instrumentos.

j) En un ensayo posterior la PETN se detectó con facilidad (detección directa) en el interior de una caja de 64 L de volumen, tras 11 minutos de espera una vez depositado el explosivo en la caja y a una temperatura ambiental de 10 ºC. Este ensayo confirma la existencia de notables diferencias en la tasa de emanación del mismo explosivo bajo diferentes preparaciones (cordón, escamas, polvo, masa).

k) La tecnología tándem IMS con fragmentación intermedia de iones a presión ambiente, ha sido recientemente demostrada por tan sólo otro grupo de investigación (grupo de investigación del profesor G. Eiceman, New Mexico State University, USA, resultados publicados en 2019), lo que ilustra el grado de novedad de ésta tecnología. Su potencial queda demostrado por el hecho de que el gobierno del Reino Unido ha financiado su desarrollo a través de tres proyectos consecutivos (EffeX,

EffeX II and HITEX), al igual que el Programa Marco de Investigación de la Unión Europea Horizonte 2020, a través del el proyecto COSMIC.

OTHER CONTRIBUTIONS

Mention of the DMA-F-DMA technology in a scientific book

Section 6.3 titled "*Tandem Differential Mobility Analysers*" of the book "*Advances in Ion Mobility-Mass Spectrometry: Fundamentals, Instrumentation and Applications*" reports the successful demonstration of DMA-F-DMA (tandem DMA), filtering explosive precursor ions in the DMA_1, decomposing them by thermal means and analyzing the product ions in the DMA_2.

Book reference: W. Alexander Donald, James S. Prell, G. A. Eiceman; P.E. Flower and Others. "Advances in Ion Mobility-Mass Spectrometry: Fundamentals, Instrumentation and Applications". *Elsevier Science & Technology*, Oxford, **2019**.

Mention of the DMA-F-DMA technology (Effex project) in the news section of the official website of United Kingdom Government (www.gov.uk)

Website: https://www.gov.uk/government/news/detecting-explosives-by-vapor-in-air-cargo-and-cabin-baggage

Article title: "Detecting explosives by vapor in air cargo and cabin baggage"

Other related scientific articles published during the doctoral studies:

1. Juan Fernandez de la Mora, Luis Javier Perez-Lorenzo, Gonzalo Arranz, **Mario Amo-Gonzalez** & Heinz Burtscher. Fast high-resolution nanoDMA measurements with a 25 ms response time electrometer. *Aerosol Science and Technology*. **2017**, 51(6), 724-734.

2. R. McCulloch, A. Alvaro, A. M. Astudillo, J. C. del Castillo, M. Gómez, J. M. Martín, M. Amo-González. A novel atmospheric pressure photoionization – Mass spectrometry (APPI-MS) method for the detection of polychlorinated dibenzo P- dioxins and dibenzofuran homologues in real environmental samples collected within the vicinity of industrial incinerators. *International Journal of Mass Spectrometry*. **2017**, 421, 135-143.

3. R. McCulloch and, **M. Amo-González**. Rapid Detection of Explosive Vapors by Thermal Desorption – Atmospheric Pressure Photoionization – Differential Mobility Analysis – Tandem Mass Spectrometry. *Rapid Communications in Mass Spectrometry*. **2019**, 33 (18), 1455-1463.

4. M. Piñero, **M. Amo-Gonzalez**, R. Delgado Ballesteros, L. Ruíz Pérez, G. Fernandez De La Mora, L. Arce. Chemical Fingerprinting of Olive Oils by Electrospray Ionization-Differential Mobility Analysis-Mass Spectrometry: A New Alternative to Food Authenticity Testing. *Journal of the American Society for Mass Spectrometry*. Just Accepted Manuscript DOI: 10.1021/jasms.9b00006.

5. L. Perez-Lorenzo, R. O'Mahony, **M. Amo-Gonzalez**, J. Fernandez De La Mora. Instant Acquisition of High Resolution Mobility Spectra in a Differential Mobility Analyzer with 100 Independent Ion Collectors: Instrument calibration. Submitted to the *Aerosol Science & Technology* on January 27, **2020** (under revision).

Oral presentations in international conferences

1. **Amo-González M**., Álvaro A., McCulloch R., del Castillo J.C., Martín J.M., Gómez M., Cuesta R. Evaluating a Rapid Atmospheric Pressure Photoionization - Mass Spectrometry (APPI-MS) Method for the Detection of Polychlorinated Dibenzodioxins (PCDD) and Furans (PCDF) in Real Environmental Samples Collected within the Vicinity of Industrial Incinerators. Oral Presentation at the *36th International Symposium on Halogenated Persistent Organic Pollutants,* Firenze, Italy, August 28th - September 2nd, **2016**

2. G. Fernández de la Mora, D. Zamora, **M. Amo**, J. Fernández de la Mora. A further step towards a vapor sensitivity of 0.01 part per quadrillion (10^{-17} atm) in the screening of large volume freight. *Workshop on Trace Explosives Detection TED* **2017**, April 24-28th 2017, Santa Fe, New Mexico, USA.

3. **M. Amo**, C. Barrios, J.C. del Castillo, J.F. de la Mora, A.G. Konstandopoulos, P. Baltzopoulou and N.D. Vlachos. Half-mini DMA modification for high temperature aerosols and evaluation on various combustion exhausts. *European Aerosol Conference,* August 27th - September 1st, **2017**, Zurich, Switzerland.

4. **M. Amo-González**, C. Barrios, R. Delgado, J. Fernandez de la Mora. A DMA operating at 200 ºC for the analysis of engine exhaust nanoparticles. *Aerosol Technology* (*AT2018),* Bilbao, España. June 18-20, **2018**.

5. Gonzalo Fernández de la Mora, César Barrios-Collado, **Mario Amo-González.** Fast carry-on luggage screening method for explosive detection. *Spectrometry for Security Applications - First International Workshop*. Dornbirn, Austria. February 10-13, **2019**.

6. S. Zinola, M. Leblanc, L. Chasapidis, D. Deloglou, P. Baltzopoulou, A. Melas, A.G. Konstandopoulos, T. Rüggeberg, M. Fierz, H. Burtscher, A. Tejero, **M. Amo**, D. Zamora. SUREAL-23 Project: Measurement of sub-23 nm particles on Gasoline Direct Injection Engine Under Various Conditions. *23rd ETH-Conference on Combustion Generated Nanoparticles*. Zürich, Switzerland. June 19, **2019**.

7. L.J. Perez-Lorenzo, **M. Amo-Gonzalez**, J. Fernandez de la Mora. Multi-Electrometer Detector for Real-Time High-Resolution Measurements in Planar Differential Mobility Analyzers. *37th AAAR Annual Conference.* Portland, Oregon, USA. October 16, **2019**.

Poster presentations in international conferences

8. **Mario Amo-Gonzalez,** Juan Fernandez De La Mora. Limits to the mobility-selected current transmitted and to the chemical background in a Differential mobility analyzer (DMA). *62nd ASMS Conference on Mass Spectrometry and Allied Topics* – Baltimore MD, MN, USA. June 5-19, **2014**.

9. **Mario Amo-Gonzalez**, Arturo Álvaro, Ross McCulloch, Juan Fernandez De La Mora. Development of a High Dynamic Range Differential Mobility Analyzer (DMA) Coupled with a Mass Spectrometer and nano-ESI Source. *63rd ASMS Conference on Mass Spectrometry and Allied Topics*. St.Louis MD, Missouri, USA. May 31-June 4, **2015**.

10. A. Alvaro, R. Mc Culloch, J.C. Del Catillo, **M. Amo-Gonzalez**, M. Gomez, J. Marroquin, R. Cuesta. Tracking Polychlorinated Dibenzodioxin (PCDD) and Furan (PCDF) Concentrations within the Environment Surrounding Incineration Facilities using Atmospheric Pressure Photoionization-Mass Spectrometry (APPI-MS). *12th International Conference and Exhibition on Emissions Monitoring*. Lisbon, Portugal. June 18-20, **2016**.

11. Ross McCulloch, **Mario Amo-Gonzalez**. Fast Detection of Environmental Vapors by Thermal Desorption - Atmospheric Pressure Photoionization Differential Mobility Analysis - Mass Spectrometry (TD-APPI-DMA-MS). *64th ASMS Conference on Mass Spectrometry and Allied Topics.* San Antonio, Texas, USA. June 5-9, **2016**.

12. **Mario Amo-Gonzalez**, Sergio Pérez, Juan Fernández de la Mora. Supercritical Planar DMA P5 Working at Resolving Power of 110 ($1cm^2/V/s$) Coupled with a Mass Spectrometer and nano-ESI Source. *65th ASMS Conference on Mass Spectrometry and Allied Topics*. Indianapolis, Indiana, USA. June 4-8, **2017**

13. **Mario Amo-Gonzalez**, Irene Carnicero, Rafael Delgado, Sergio Perez, Gary A. Eiceman, Gonzalo Fernández de la Mora, Juan Fernández de la Mora and Rafael Cuesta Barbado. Planar DMA: A unique instrument for high resolution nanoparticles analysis below 4 nm and tandem DMA analysis. *Aerosol Technology*, AT2018, June 18-20, **2018**, Bilbao, España.

14. Gonzalo Fernández de la Mora, **Mario Amo-González,** Juan Fernández de la Mora. New GC / Two Stage Differential Mobility Analyzer for the Screening of Explosives in Cargo (Poster). *Spectrometry for Security Applications - First International Workshop.* February 10-13, **2019**, Dornbirn, Austria.

Oral presentations in national conferences

15. M.Y. Piñero-González, **M. Amo-González**, L. Ruiz, R. Delgado, R. Cuesta, G. Fernández de la Mora. Coupling D-LFSESI-DMA-MS for Olive Oil Characterization: a Novel Application in Food Analysis. *XXII Reunión de la Sociedad Española de Química Analítica.* Valladolid, Spain, July 18-19, **2019**.

16. Zamora Pérez, Daoíz; Piñero González, María Ysabel; Pérez Velasco, Sergio; Delgado Ballesteros, Rafael; **Amo-González, Mario**. Nuevas soluciones para la Detección de Compuestos NRBQE en Contenedores (COSMIC). *VII Congreso Nacional de I+D en Defensa y Seguridad*. San Fernando, Spain, November 19-21, **2019**.

Poster presentations in national conferences

17. R. Cuesta, **M. Amo-González**, J.C. del Castillo, R. McCulloch, M. Gómez, J.M. Marroquín. A Novel APPI-MS Method for the Detection of PCDF/PCDDs Homologues in Real Environmental Samples Collected within the Vicinity of Industrial Incinerators. *V Reunión Nacional de Dioxinas, Furanos y Compuestos Orgánicos Persistentes Relacionados & VIII Reunión de la Sociedad Española de Espectrometría de Masas*. Barcelona, Spain. June 12-16, **2017**.

18. I. Carnicero, R. McCulloch, M.V. Martínez, M.Y. Piñero, **M. Amo-González**. Photoionization and Ion Mobility–Mass Spectrometry of Atmospheric Contaminants. *XXII Reunión de la Sociedad Española de Química Analítica.* Valladolid, Spain, July 18-19, **2019**.

BIBLIOGRAPHY

The bibliography below corresponds to the references cited in the introduction section of the thesis. All the references cited in the papers or in the patent (chapters 1-6) are detailed in the reference section of each publication.

1. Srebalus, C. A.; Li, J.; Marshall, W. S.; Clemmer, D. E. *Anal.Chem.* **1999**, 71, 3918−3927
2. Asbury, G. R.; Hill, H. H. *J. Microcolumn* Sep. **2000**, 12, 172.
3. Dugourd, Ph.; Hudgins, R. R.; Clemmer, D. E.; Jarrold, M. F. *Rev. Sci. Instrum.* **1997**, 68, 1122−1129.
4. Merenbloom, S. I.; Glaskin, R. S.; Henson, Z. B.; Clemmer, D. E. *Anal. Chem.* **2009**, 81 (4), 1482−1487.
5. Adams, K. J.; Montero, D.; Aga, D.; Fernandez-Lima, F. Int. *J. Ion Mobility Spectrom.* **2016**, 19, 69−76.
6. Purves, R. W.; Guevremont, R.; Day, S.; Pipich, C. W.; Matyjaszczyk, M. S. *Rev. Sci. Instrum.* **1998**, 69, 4094−4104.
7. Schneider, B. B.; Covey, T. R.; Coy, S. L.; Krylov, E. V.; Nazarov, E. G. *Anal. Chem.* **2010**, 82 (5), 1867−1880.
8. Shvartsburg, A. A. Differential Ion Mobility Spectrometry: Nonlinear Ion Transport and Fundamentals of FAIMS; CRC Press: Boca Raton, FL, **2008**.
9. Shvartsburg, A. A.; Seim, T. A.; Danielson, W. F.; Norheim, R.; Moore, R. J.; Anderson, G. A.; Smith, R. D. *J. Am. Soc. Mass Spectrom.* **2013**, 24, 109.
10. Vidal-de-Miguel, G.; Macía, M.; Cuevas, J. *Anal. Chem.* **2012**, 84, 7831−7837.
11. Vidal-de-Miguel, G.; Macía, M.; Barrios, C.; Cuevas, J. *Anal. Chem.* **2015**, 87 (3), 1925−1932.
12. Gillig, K. J.; Chen, C. H. *Mass Spectrom.* **2014**, 3, S0032.
13. Kurulugama, R. T.; Nachtigall, F. M.; Lee, S.; Valentine, S. J.; Clemmer, D. E. *J. Am. Soc. Mass Spectrom.* **2009**, 20 (5), 729−737.
14. Knutson, E. O.; Whitby, K. T. *J. Aerosol Sci.* **1975**, 6, 443−451.
15. Labowsky, M.; Fernandez de la Mora, J. J. Aerosol Sci. **2006**, 37 (3), 340−362.
16. Rus, J.; Moro, D.; Sillero, J. A.; Royuela, J.; Casado, A.; Estevez-Molinero, F.; Fernández de la Mora, J. *Int. J. Mass Spectrom.* **2010**, 298, 30−40.
17. Fernandez de la Mora, J.; Perez-Lorenzo, L. J.; Arranz, G.; Amo- Gonzalez, M.; Burtscher, H. *Aerosol Sci. Technol.* **2017**, 51 (6), 724−734.
18. Eiceman. G.A. (2013, August 1). Tandem Mobility Spectrometry - Chemical orthogonality in tandem differential mobility spectrometry at ambient pressure. Retrieved from: https://ionmobility.nmsu.edu/. Accessed January 13, 2020.
19. Hogan, C.J., Ruotolo, B., Robinson, C., Fernandez de la Mora, J.: Tandem differential mobility analysis-mass spectrometry reveals partial gas-phase collapse of the GroEL complex. *J. Phys. Chem. B*, **2011**, 115(13), 3614–3621.
20. Larriba-Andaluz, C., Fernandez de la Mora, J.: Gas-phase structure of Coulombically stretched polyethylene glycol ions. *J. Phys. Chem. B*, **2012**, 116, 593–598.
21. Criado, E., Fernández-García, J., Fernández de la Mora, J.: Mass and charge distribution analysis of large polyethylene glycol chains by negative electrospray ion mobility mass spectrometry (NES-IMS-MS). *Anal. Chem.* **2013**, 85(5), 2710–2716.

22. Fernández-García, J., Fernández de la Mora, J.: Measuring the effect of ion-induced drift-gas polarization on the electrical mobilities of multiplycharged ionic liquid nanodrops in air. *J. Am. Soc. Mass Spectrom.* **2013**, 24, 1872–1889.
23. Javaheri,H., Le Blanc,Y., Thomson, B.A., Fernandez de laMora, J., Rus, J., Sillero-Sepúlveda, JA.: Evaluation of the Analytical characteristic of a differential mobility analyzer coupled to a triple quadrupole system (DMA-MSMS), poster 061, in: proceedings of the Annual ASMS Conference. Denver, 1–6 June (**2008**) Available at: http://www.seadm.com/wp-content/uploads/2016/03/ASMS_2008_DMA_Poster_Bruce_V3.pdf
24. Eiceman, G.A.; Stone, J.A. Ion Mobility Spectrometers in National Defense. Anal. Chem. **2004**, 76 (21):390A-397A.
25. R.G. Ewing, D.A. Atkinson, G.A. Eiceman, G.J. Ewing. A critical review of ion mobility spectrometry for the detection of explosives and explosive related compounds. *Talanta*. **2001**, 54, 515-529.
26. Karpas, Z. Ion Mobility Spectrometry: A tool in the war against terror. *Bulletin of the Israel Chemical Society*, **2009**, Issue No. 24.
27. Martínez-Lozano, P. Rus, J. Fernández de la Mora, G. Hernández, M. Fernández de la Mora, J. Secondary Electrospray Ionization (SESI) of Ambient Vapors for Explosive Detection at Concentrations Below Parts Per Trillion. *J. Am. Soc. Mass Spectrom.* **2009**, 20 (2), 287-294.
28. Whitehouse, C. M.; Levin, F.; Meng, C. K.; Fenn, J. B. Proceedings of the 34th ASMS Conference on Mass Spectrometry and Allied Topics; Cincinnati, OH, June 8 –13, **1986**; p 507.
29. Fuerstenau, S.; Kiselev, P.; Fenn, J. B. Proceedings of the 47th ASMS Conference on Mass Spectrometry Allied Topics; Dallas, TX, June, **1999**; ThOE 3:00
30. Martínez-Lozano, P.; Fernández. de la Mora, J. Electrospray Ionization of Volatiles in Breath. *Int. J. Mass Spectrom.* **2007**, 265, 68–72.
31. Fernandez de la Mora, J.: Ionization of vapor molecules by an electrospray cloud. *Int. J. Mass Spectrom*. **2011**, 300, 182–193.
32. Vidal-de-Miguel, G., Macia, M., Pinacho, P., Blanco, J.: Low-sample flow secondary electrospray ionization: improving vapor ionization efficiency. *Anal. Chem.* **2012**, 84(20), 8475–8479.
33. Ewing R.G.; Waltman M.J.; Atkinson D.A.; Grate J.W.; Hotchkiss P.J. The vapor pressures of explosives. *TrAC, Trends Anal. Chem.* **2012**, 42, 35-48.
34. Eiceman, G. A.; Shoff, D. B.; Harden, C. S.; Snyder, A. P. *Int. J. Mass Spectrom. Ion Processes* **1988**, 85 (3), 265−275.
35. Ewing, R. G.; Eiceman, G. A.; Harden, C. S.; Stone, J. A. *Int. J. Mass Spectrom.* **2006**, 255−256, 76−85.
36. An, X. Eiceman, G.A. Rodriguez, J.E. Stone, J.A. *Intern. J. Mass Spectr*. **2011**, 303 (2-3), pp 181-190.
37. An, X. Eiceman, G.A. Stone, J.A. *Int J Ion Mobil Spectrom*. **2010**, 13 (1), 25-36.
38. Rajapakse, M.Y.; Stone, J.A.; Eiceman, G.A. *Intern. J. Mass Spectr*. **2014**, 371, 28-35.
39. Rajapakse, M.Y.; Fowler, P.E.; Eiceman, G.A.; Stone, J.A. *J. Phys. Chem. A*, **2016**, 120(5), pp 690-698.
40. Rajapakse, R.M.Y.; Stone, J.A.; Eiceman, G.A. *J. Phys. Chem.* A. **2014** 118 (15), 2683-2692.
41. Menlyadiev, M.R.; Eiceman, G.A. *Anal. Chem*. **2014**, 86(5), 2395-2402.
42. Menlyadiev, M.R.; Tarassov, A.; Kielnecker, A.M.; Eiceman, G.A. *Analyst*, **2015**, 140(9), 2995-3002.
43. Stimac, R.M.; Wernlund, R.F.; Cohen, M.J.; Lubman, D.M.; Harden, C.S., Initial studies on the operation and performance of the tandem ion mobility spectrometer, Pittcon. **1985** New Orleans, LA, March 1985.
44. Stimac, R.M.; Cohen, M.J.; Wernlund, R.F., Tandem ion mobility spectrometer for chemical agent detection, monitoring and alarm, Contractor Report on CRDEC Contract DAAK11 84 C 0017, PCP, Inc., West Palm Beach, FL, May **1985**, AD B093495.
45. S. L. Koeniger, S. I. Merenbloom, S. J. Valentine, M. F. Jarrold, H. R. Udseth, R. D. Smith and D. E. Clemmer. *Anal. Chem.*, **2006**, 78, 4161–4174.
46. S. I. Merenbloom, S. L. Koeniger, S. J. Valentine, M. D. Plasencia and D. E. Clemmer. *Anal. Chem.*, **2006**, 78, 2802–2809.